Hybrid Syntactic Foam Core Based Natural-Glass Fibre Sandwich Composite

A thesis submitted in fulfillment of the academic requirements for the degree of

Doctor of Engineering

Durban University of Technology

Faculty of Engineering and Built Environment

Mechanical Engineering

By

Olusegun Adigun Afolabi

Date: March 2023

Supervisors: Prof. K. Kanny

Dr. T.P. Mohan

Hybrid Syntactic Foam Core Based Natural-Glass Fibre Sandwich Composite

A thesis submitted in fulfillment of the academic requirements for the degree of

Doctor of Engineering

Durban University of Technology

Faculty of Engineering and Built Environment

Mechanical Engineering

By

Olusegun Adigun Afolabi

Student no: 21751997

MSc, The University of Ibadan, Nigeria

BTech, LAUTECH, Nigeria.

DECLARATION

The thesis is being submitted to the Durban University of Technology for the award of the degree of Doctor of Engineering (Mechanical Engineering). I declare that the thesis entitled “Hybrid Syntactic Foam Based Natural -Glass Fiber Sandwich Composites” is a record of research work carried out by myself. The content of this thesis, in full or in parts, has not been submitted to any other institute or university for the award of any degree. I further declare that the only part of this work that has been published is in the form of peer-reviewed manuscripts with details provided in “Publications and Conference Presentations.”

24/03/2023

Signature of Student — Date

Olusegun Adigun Afolabi

3/4/23

Signature of Supervisor I — Date

Professor Krishnan Kanny

3/4/2023

Signature of Co-supervisor — Date

Dr. Mohan Turup Pandurangan

ACKNOWLEDGEMENTS

Firstly, I would like to appreciate God Almighty, the creator of heaven and earth, the maker, sustainer, the giver of life, the omnipotent, omniscience, and omnipresent, the unchanging changer that changes situations, my Father and Lord for His grace, divine enablement, and love towards me during this academic journey.

Many people have shown immeasurable help and support to me in the process of this Doctoral study as such I would like to appreciate them. To my supervisors, I want to say thank you for the opportunity to undertake this study under your supervision.

I wish to appreciate the Durban University of Technology, for their financial support. My appreciation also goes to the staff of the Mechanical Engineering Department, especially Ms. Adele (the secretary) for her consistent support all through my study, my fellow CRG members, and postgraduate students: Dr. Ajay, Dr. Joseph, John, Moyo, Ayo, and Edwin.

My gratitude goes to Dr. and Mrs. Bunmi Oyekunle, Dr (Mrs) Yemisi Oyegbile, Dr. Kunle Oparinde, and Mr Wole Olatunde, for your assistance and support towards securing my PhD admission. I also appreciate Rev (Dr) and Pastor (Mrs) Samuel Bunmi Olajire, Pastor Olu Victor, and Prophet Ajala, for their prayers, words of encouragement, and support.

My heartfelt gratitude goes to my parents, siblings, Mr. Richard & Yemisi Olusegun, Shola Afolabi, Pastor Kayode & Ajoke Afolabi, Pastor Femi & Bose Afolabi, the Ilori family – my mother-in-law, Mr Sunday, Mrs Bose, Mr Biodun and Mrs Grace, my Aunties, and Uncles. Thank you for your prayers, support, and for believing in me.

Finally, I sincerely appreciate my lovely wife and friend Dr. Felicia Omolara Afolabi and my princesses Oluwatoni, Oluwatomisona, and Oluwatofunmi. Thank you for your immeasurable love and understanding. You have made this possible. Thank you for standing by me. I love you!

DEDICATION

This research work is dedicated to God Almighty for His mercies and faithfulness over my life. I also dedicate this work to my parents Pastor & Mrs. David-Funmilayo Afolabi.

PUBLICATIONS

Some publications have resulted from this study which are in the form of peer-reviewed journal articles and peer-reviewed conference papers.

Published Journal Articles

1. Afolabi O.A., Kanny K., Mohan T.P.: Processing of low density with high specific properties of HGM filled epoxy-syntactic foam composites for marine application. Material (Basel) – 16-01732, https://doi.org/10.3390/ma16041732

2. Afolabi O.A., Kanny K., Mohan T.P (2023): Investigation of Mechanical Characterization of Hybrid Sandwich Composites with Syntactic Foam Core for Structural Applications: Composites and Advanced Materials. vol 32: pp. 1-14, https://doi.org/10.1177/26349833221147539

3. Afolabi O.A., Kanny K., Mohan T.P (2022): Analysis of particle variation effect on flexural properties of hollow glass microspheres filled epoxy matrix syntactic foam composites. Polymers, 14, 4848. https://doi.org/10.3390/polym14224848.

4. Afolabi O.A., Kanny K., Mohan T.P: (2021): Processing of hollow glass microspheres (HGM) filled epoxy composites with improved Structural Characteristics. Science and Engineering of Composites Materials.; 28:116–127, https://doi.org/10.1515/secm-2021-0011.

5. **Afolabi O.**A., Kanny K., Mohan T.P (2021): Loading Effect of Hollow Glass Microsphere (HGM) and Foam Microstructure on the Specific Mechanical Properties and Water Absorption of Syntactic Foam Composite. International Journal of Engineering Research in Africa, vol. 56, pp. 34-56, https://doi.org/10.4028/www.scientific.net/JERA.56.34

6. **Afolabi O.**A., Kanny K., Mohan T.P (2018). Characterization of Tensile and Flexural Properties of Syntactic Foam Filled with Hollow Glass Microsphere (HGM). Third International Conference on Composite, Biocomposites, and Nanocomposites. Nelson Mandela Bay Stadium, Port-Elizabeth South Africa. ISBN: 978-1-919858-30-2.

7. Afolabi O.A., Kanny K., Mohan T.P: Effect of Composition on Impact and Flexural Properties of High-Density Hollow Glass Microsphere/Neat Epoxy filled Syntactic Foam Composites. (***Under Review***).

Conferences:

i. **Afolabi O.**A., Kanny K., Mohan T.P: Effect of Hollow Glass Microsphere (HGM) on Impact and Flexural Properties of High-Density Syntactic Foam Based Epoxy Composite. IMPLAST 2022: The 13th International Symposium on Plasticity and Impact Mechanics. Indian Institute of Technology Madras, Chennai, Tamil Nadu, India

ii. **Afolabi O.A.,** Kanny K., Mohan T.P: Effect of size Distribution and Characterization of Hollow Glass Microsphere/Epoxy Matrix on Flexural Properties of Syntactic Foam Composite. Conference of the South African Advance Material Initiative (COSAAMI), 18-21 October 2021.

iii. **Afolabi O.A.,** Kanny K., Mohan T.P, Rane Ajay: Effect of Dispersion of Epoxy/Hollow Glass Microsphere Filler-Matrix and Density in Predicting the Interphase Characteristics of Syntactic Foam Composite. 2nd Online International Conference on Material Science and Nanomaterials 12-13 August 2021.

iv. **Afolabi O.A.,** Kanny K., Mohan T.P: Loading effect of HGM and foam microstructure on the specific mechanical properties and water absorption of syntactic foam composite. 4th Interdisciplinary Research and Innovation Conference, Global Trends and Challenges in Research and Innovation 17-20 September 2019, Durban, South Africa

v. **Afolabi O.A.,** Kanny K., Mohan T.P.: Compression properties of heated matrix resin on hollow glass microsphere syntactic foam. 3rd Interdisciplinary Research and Innovation Conference, 18-20 September 2018, Durban, South Africa.

vi. **Afolabi O.A**., Kanny K., Mohan T.P.: Dynamic mechanical analysis of syntactic foam composite on the effect of hollow glass microspheres (HGM) loading. 2018 UKZN Nanotechnology Platform Symposium, October 2018.

vii. **Afolabi O.A.**, Kanny K., Mohan T.P: Data Characterization of tensile and flexural properties of hollow glass microsphere syntactic foam composite. Third International Conference on Composites, Bio-composites and Nanocomposites, 7-9 November 2018

ABSTRACT

Composite materials comprised of two separates with different properties to form a single material that reflect the properties of the combined materials. Syntactic foam composites (SFC) are made from the combination of hollow glass microspheres and epoxy resin. They are lightweight and used as a core in the hybrid sandwich composite. Hollow glass microspheres (HGM) are high strength microballoons that provide closed cell porosity and help to reduce material weight. SFCs made of HGM, and resin matrix are used as the core in sandwich composite material and reinforced with natural or synthetic fiber materials. The sandwich syntactic foam composite (SSFC) has a wide range of applications in the marine, aerospace, structural, and automobile industry. Therefore, it is important to investigate their physical, mechanical, thermal, and morphological properties to achieve high strength and low density. Most of the previous work in literature employed the use of different fillers and core materials in sandwich composite but are limited in strength because of their high density. In this study, a single HGM filler was employed as heterogeneous and homogenous by varying into four different particle sizes to investigate the effect of these particle sizes on the mechanical and physio-mechanical properties of the SFC used as the core in the SSFC. The effect of wall thickness and radius ratio of the HGM on the microstructural properties of SFC was also determined.

The heterogeneous and homogeneous SFC was fabricated by degassing method mixing the epoxy matrix with HGM filler, the filler was varied into five-volume fractions of 5, 10, 15, 20, and 25%. The functional group of the HGM filler and the neat epoxy was determined and compared with that of the SFCs fabricated using Fourier Transform Infrared Spectroscopy (FTIR). The results showed that the filler contain various functional groups such as hydroxyl group, phenol-OH, aldehyde C-H group, aromatic proton, epoxy group, which enhanced the bonding process. It was determined that the intensity of the SFCs for all the volume fractions increased more than the neat epoxy due to the shifts in the peaks representing the filler and the matrix groups. The physical (density, water absorption, buoyancy) properties and the mechanical (hardness, tensile, flexural, and impact) properties of the SFCs improved significantly compared with the neat epoxy. The Scanning Electron Microscopy (SEM), Dynamic Mechanical Analysis (DMA), and Thermo-gravimetric Analysis (TGA) were also used to determine the morphological structure, the viscoelastic properties, and degradation temperature of the HGM and the neat epoxy and compared with the fabricated SFCs. The surface of the HGM showed the microballoons in their different sizes before separation. The surface of the SFCs showed the epoxy matrix, matrix porosity, microballoons porosity, and

microballoons structure in their mixed state. It was an indication of good interaction between the epoxy matrix and the HGM filler using degassing processing method. The DMA showed improved storage and loss modulus values by 9% and above 100% respectively compared to the neat epoxy and the TGA showed better glass transition T_g values of 4.5% and 2.7% at 20% and 55% weight loss respectively compared to the neat epoxy. This indicated that good interaction and interfacial bonding existed between HGM and the epoxy matrix and because of lower density and void content.

The SFC was used as the core to fabricate a lightweight sandwich syntactic foam composite (SSFC). The SSFC was made into four different orientations (kenaf-SFC-kenaf, as KK; glass –SFC-glass, as GG; glass/kenaf – SFC – kenaf/glass, as GK; and kenaf/glass –SFC- glass/kenaf, as KG) using kenaf and glass fibers as reinforcement. The physical properties (density, water absorption capacity, and buoyancy), mechanical properties (hardness, tensile, compression, and flexural), morphological properties (SEM), and acoustic properties were determined. The porosity of KK increased by 21.6% because the kenaf fiber is less dense and more porous in terms of water absorption which makes it require higher buoyancy force to stay afloat. The mechanical properties results showed that GK and KG have the highest hardness, flexural and compressive strength of 70.2%, 74.4%, and 42.7% respectively, while GG has improved tensile strength of 210.96% increase than KK. The acoustic properties results showed that GG improved in sound level (P) dB by 24.1% compared to KK, while the sound pressure (L_p) dB does not show a significant difference in the SSFC.

In conclusion, the degassing processing method of SFCs improved its physical and mechanical properties by reducing the density using particle distribution analysis (PSA) and particle variation analysis (PVA) with the aid of a gas pycnometer, and porosity values thereby making it a suitable core material for the sandwich composite. A novel sandwich syntactic foam composite (SSFC) material was fabricated by hybridizing the face-sheets in different layering pattens. The SSFC physical and mechanical properties improved significantly with the use of hybrid fibers. Hence, this study has demonstrated that for structural and marine purposes, hybrid fibers can perform better as reinforcement in the sandwich composite than using a single fiber.

TABLE OF CONTENTS

Table of Contents

LIST OF TABLES

LIST OF FIGURES

GLOSSARY AND ACRONYMS

ASTM	American Standard Test Method
ATR-FTIR	Attenuated Total Reflectance- Fourier Transform Infrared Spectroscopy
CMC	Ceramics Matrix Composites
CSFC	Ceramic Syntactic Foam Composites
CTE	Coefficient of Thermal Expansion
DGEBA	Diglycidyl Ether of Bisphenol-A
DR	Degradation Rate
DSC	Differential Scanning Calorimetry
DMA	Dynamic Mechanical Analysis
DTA	Differential Thermal Analysis
EP	Epoxy Resin
FRP	Fiber Reinforced Polymer/Plastic
FRPC	Fiber Reinforced Polymer Composites
GF	Glass Fibers
GG	Glass-glass face sheets
GK	Glass-kenaf face sheets
HDPE	High-Density Polyethylene
HGM	Hollow Glass Microspheres
HSFC	Hybridized Syntactic Foam Composites
IPDT	Integral Procedure Decomposition Temperature

KF	Kenaf Fibers
KK	Kenaf-kenaf face sheets
KG	Kenaf-glass face sheets
MMC	Metal Matrix Composites
MSFC	Metallic-based Syntactic Foam Composites
NSSFC	Nano-Synthesized Syntactic Foam Composites
PET	Polyethylene Terephthalate
PMC	Polymer Matrix Composites
PPC	Particulate Polymer Composites
PSFC	Polymer Syntactic Foam Composites
PSA	Particle Size Analysis
PSD	Particle Size Distribution
PU	Polyurethane
PVA	Particle Variation Analysis
PVC	Polyvinyl Chloride
SEM	Scanning Electron Microscopy
SF	Syntactic Foam
SFC	Syntactic Foam Composite
SSFC	Sandwich Syntactic Foam Composites
TEM	Transmission Electron Microscopy
TGA	Thermo-Gravimetric Analysis

LIST OF NOTATIONS

T_g	Transition Temperature	(^oC)
V_c	Volume of composite	(cm^3)
v_c	volume fraction of composites	(%)
m_c	mass of composite	(g)
ρ_c	density of composites	(g/cm^3)
δ	void fraction of composite	(%)
ω	wall thickness	(µm)
a	aspect ratio	(%)
r_{op}	outer radius	(µm)
r_{ip}	inner radius	(µm)
η	radius ratio	(%)
ρ_{MB}	microballoons density	(g/cm^3)
P_w	water absorbed	(%)
$M_{(s)}$	maximum water measured	(%)
$M_{(t)}$	initial water measured	(%)
$M_{(d)}$	diffusion coefficient	(%)
F_b	buoyancy force	(N)
V	volume of submerged object	(m^3)
D	density of the fluid	(Kg/m^3)
F_o	force of gravity	(N/kg)
σ_f	flexural stress	(MPa)

ε_f	flexural strain	(mm/mm)
P_f	load	(N)
L	span length	(mm)
b	specimen width	(mm)
d	specimen thickness	(mm)
D	midpoint deflection	(mm/mm)
IS	impact strength	(Kj/m^2)
AE	absorbed energy	(J)
T	specimen thickness	(m)
W	remaining width at notch	(m)
P	Sound level	(dB)
Lp	Sound Pressure	(dB)

CHAPTER 1

1.0 INTRODUCTION

1.1 Background and Problem Statement

Syntactic foam composite (SFC) has a wide range of acceptability in engineering materials due to its lightweight, valuable mechanical properties, and improved structural characteristics. SFC, according to the American Society for Testing and Materials (ASTM), is defined as a material consisting of hollow glass microsphere (HGM) fillers in a resin matrix that has gained considerable attention over the past several years due to mechanical and thermal properties that are advantageous for use as a core material in naval and aerospace applications (ASTM 2012). Nowadays, hybrids SFCs are increasingly being used in different industries because of their properties. Various metallic-based syntactic foam composites (MSFC), polymer syntactic foam composites (PSFC), ceramic syntactic foam composites (CSFC), nano-synthesized syntactic foam composites (NSSFC), and hybridized syntactic foam composites (HSFC) are gaining popularity in the market. They find applications in thermal insulation, marine, and subsea applications – buoyancy, acoustic and sound because of their high hydrostatic and hygroscopic strength, high stiffness at low density and impact absorption, aeronautic and aviation industries – as a guide insulator to transducers because the dielectric properties remain constant at high depth, due to their isotropic character and randomness of their microstructure. SFC generates a cellular structure that is fundamentally different from the regularly used foams for core materials such as polyvinyl chloride (PVC) and polyurethane (PU), geopolymer foam, and so on (Sankaran *et al.* 2006; Le *et al.* 2020). However, because of their mechanical properties, SFCs are utilized as the core material in sandwich panels, making them an excellent material for load-bearing structural applications. The sandwich syntactic foam composites (SSFC) structure with SFC core can be employed in construction projects, particularly where habitable housing is scarce.

Housing challenge is one of the major problems globally due to inadequate shelter. Since 1994, the government of South Africa has been concerned about this issue, particularly in informal settlement, where there are over 1.5 million housing backlogs (Housing 1995; Report 2014; Prof-Emeka-E-Obioha-Emeka-Obioha 2019). To mitigate the impact of a scarcity of housing, an alternative method of construction is necessary. To this end, a sandwich panel with an SFC core and natural/glass fiber face-sheet is expected to meet the challenge and at low cost. Properties such as thermal stability, good acoustic resistance, fire retardant, and stiffness make it a suitable replacement.

This research anticipates several outcomes based on low weight, high strength materials, with SFC serving as the core in a sandwich panel for structural applications and being characterized for physical, mechanical, structural, morphological, thermal, acoustic, and water absorption properties. Previously, most investigations on the processing and use of syntactic foam as a core material in sandwich composites used various types of fillers (cenosphere or HGM) in generating the SFC by altering the volume fraction or weight fraction of the filler used (Gupta 2003; Ren *et al.* 2017b; Salleh 2017a) (Jayavardhan *et al.* 2017), (Bharath Kumar *et al.* 2016a). Also, different core materials such as nomax honeycomb, kraft honeycomb and syntactic foam have been hybridized with glass face-sheet to produce sandwich composite material (Kumar and Ahmed 2013). However, hybridizing different face-sheets by interchanging their sequences on SFCs is not yet studied. Therefore, it is important to produce a SFC of superior mechanical properties, reduced density, wall thickness, and radius ratio of the HGM that will be appropriate as the core. The effect of HGM particle sizes on wall thickness and radius ratio is also essential in understanding the effects of mechanical properties on syntactic foam. As a result, there is a knowledge gap in the field of understanding the impact of particle sizes on HGM, matrix and hybrid natural/glass fiber adhesion. The natural fibers serve as an alternative to the glass fiber because of their availability, their recyclability and reducing environmental pollution sometimes caused by the synthetic fibers. For the manufacturing of the syntactic foam core in this work, a single type of HGM with a density ($0.6 g/cm^3$) was used. The HGM was employed as a full filler in this investigation, and it was divided into four different particle sizes and employed at varying volume fractions. One of the advantages of HGM that was not immediately recognized was its lightweight, which aids in guarding against compound sagging on the material's vertical surfaces and makes it ideal for use as a core in SSFC structures (Kumar and Ahmed 2013; Daniel *et al.* 2018).

SSFC structures consist of two facial skin sheets, an upper and a lower layer, separated by the SFC core material. They are low in weight, with high flexural rigidity, and provide superior thermal insulation. They possess very lightweight, high flexural rigidity and good thermal insulation characteristics. Therefore, the property of SSFC is a function of the properties of the upper and lower face-sheet (hybrid kenaf/glass in this study) and the core (SFC).

Some of the materials employed in literature for the fabrication of SFC and SSFC include, but are not limited to: epoxy resin, hardener, glass fiber, kenaf fiber, silicone mold, foam core, poly-vinyl chloride PVC foam (R55), and polyurethane (PU) foam cores (Amran Alias. 2007; Yalkin, Icten and Alpyildiz 2015; Yalkin, Icten and Alpyildiz 2017; Balıkoğlu *et al.* 2018; Ding *et al.* 2018), metallic foam, polymeric foam, phenolic foam (Awad, Aravinthan and Zhuge 2012), corrugated lattice truss (Hu *et al.* 2016), balsa (ProBalsa, DIAB) and polymer foams (DIAB) (Katarzyna Greń* 2016),

ceramic foam, agglomerated cork (Sadeghian, Hristozov and Wroblewski 2016, 2018; Prabhakaran *et al.* 2019), honeycomb (aramid and cellulose) (Katarzyna Greń* 2016; Vitale *et al.* 2017; Sadeghian, Hristozov and Wroblewski 2018; Ashraf *et al.* 2019), 3-D integrated core (Safari, Karevan and Nahvi 2018), polyethylene terephthalate (Garay, Souza and Amico 2016), etc. However, there are certain drawbacks to using these foams as an SSFC, which includes:

- Difficulty in joining metallic structures.
- Poor water absorption capabilities of honeycomb and open-cell foam compositions.
- Low recyclability of ceramics and honeycomb foams.
- Poor fire resistance and high manufacturing costs, and;
- Degradation of the interface

With all the drawbacks of present foams used as core materials in SSFC, the development of a new foam material called 'SFC' was unavoidable, which will be beneficial in structural applications, cost-effective, and environmentally acceptable. Therefore, there is a need to develop a new SFC that will be lightweight, low density, and high strength which will give it good acceptability.

1.2 Aim

This research work focuses on developing a low-weight, high-mechanical-strength SFC and SSFC using natural fibers with low density and improved strength that can be applied for structural purposes.

1.3 Objectives of the Study

i. develop HGM filled SFC material with low weight and high strength.
ii. determine the process of making SFC out of HGM (based on concentration and particle size variations).
iii. determine the process of fabricating an
iv. SSFC panel with a hybrid fiber face-sheet and an SFC core.
v. evaluate the density, foam microstructure, mechanical, and physio-mechanical properties of SFCs.
vi. evaluate the density, mechanical properties, and physio-mechanical of SSFC.

1.4 Assumptions

Based on their usage and calibration time at the university and other institutions, data collection equipment, testing methods, and instruments were declared valid and trustworthy.

1.5 Limitations

Even though numerous natural fibers are available in the market, this study solely employs kenaf fiber, this was because of its readily availability and being in mat orientation than other natural fibers available during the time of this research work. Although there were many different types of filler

microspheres on the market, only a hollow glass microsphere (HGM) was employed in this investigation.

The conclusions obtained from this study's findings are exclusively relevant to the materials used in manufacturing and preparation under identical conditions. As a result, the findings cannot be applied to all syntactic/epoxy foam composites produced using various techniques, but the findings of this study may be useful in the development of structural and functional composites.

1.6 Thesis Layout

Table 1.1 below shows the thesis layout for this study.

Table 1.1: Thesis layout

Chapters	Contents
Chapter One: Introduction	This includes the introduction, background, problem statement, aim, objectives, preliminary study, pilot study, main study, limitations, delimitations, and structure of the thesis.
Chapter Two: Literature Survey	This includes a literature survey of syntactic foam composites, and sandwich foam composites enumerating the previous works done on them.
Chapter Three: Materials and Methods	This includes the raw materials used in the study, the characterization methods used to determine mechanical, morphological, structural, and thermal properties of syntactic foam composite, the step-by-step procedure of fabrication, mechanical testing conducted, and test configurations used in this study.
Chapter Four: Materials	This focuses on the characterization of

Characterizations.	materials
Chapter Five: Density Properties	This is titled the study of density in predicting the interface characteristics of Syntactic foam Composite and the sandwich syntactic foam composites
Chapter Six: Tensile Properties	Tensile properties of the homogeneous and heterogeneous syntactic foam composite, morphological properties of the syntactic foam composites for both heterogeneous and homogeneous tensile fracture surfaces
Chapter Seven: Flexural Properties	This discusses the flexural properties of the homogeneous and heterogeneous syntactic foam composites and the morphological properties of the syntactic foam composites for both heterogeneous and homogeneous flexural fracture surfaces
Chapter Eight: Sandwich Properties	This discusses the tensile, flexural, compressive, shear, and morphological properties of sandwich syntactic foams.
Chapter Nine: Structural and Thermal Properties	This discusses the structural and thermal properties of the syntactic foam composites and the sandwich syntactic foam. Detailing the effects of the attenuated total reflectance Fourier transform infrared spectroscopy (ATR-FTIR), thermal gravimetric analysis, and dynamic mechanical analysis.
Chapter Ten: Physio- Mechanical	This discusses the physio-mechanical

Properties	properties such as hardness property, water absorption, buoyancy property, impact property and acoustic property of syntactic foam composites, and sandwich syntactic foam composites.
Chapter Eleven: Conclusion and General Recommendations	This is titled general conclusions and recommendations, and future work. The general conclusion, recommendations, and suggestions for future work are drawn from the entire set of experiments, observation of results, and discuss the directions for the future study.

CHAPTER 2

2.0 LITERATURE REVIEW

2.1 Introduction

This part was divided into three sections. The first section discusses the material selection, the second section talks about the syntactic foam composite materials, and the third section talks about the hybrid sandwich material. Figure 2.1 shows the schematic structure of the syntactic foam composites, with hollow glass microballoons and epoxy matrix embedded in it. Figure 2.2 shows the schematic structure of the sandwich syntactic foam with kenaf-glass fibers face-sheets.

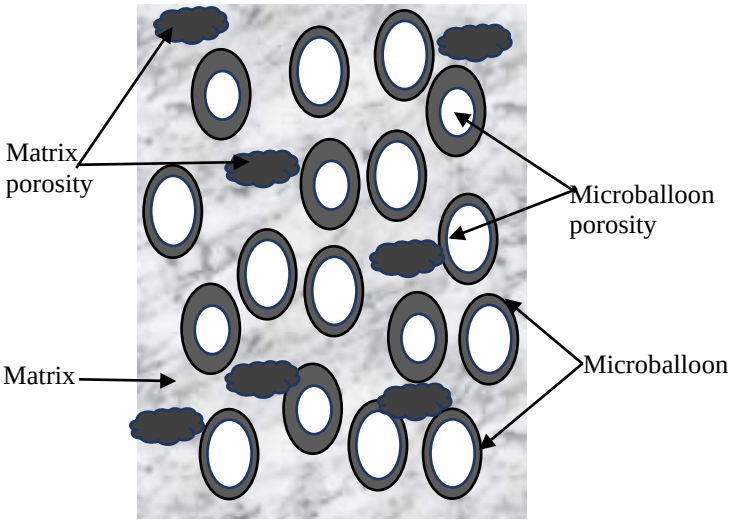

Figure 2.1: Schematic structure of microballoons and matrix porosities in the syntactic foam composite.

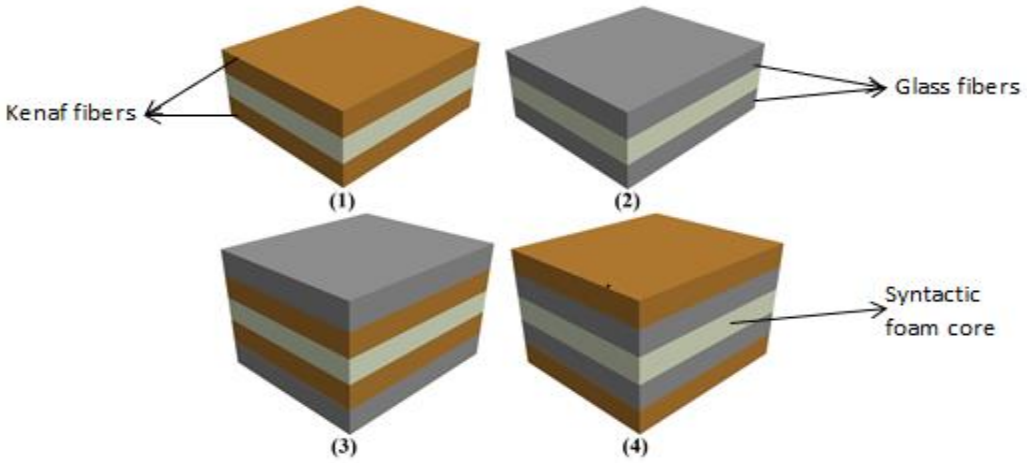

Figure 2.2: Schematic structure of hybrid sandwich syntactic foam composites, showing the kenaf fibers and glass fibers face-sheets, and the syntactic foam core.

2.1.1 Review of the Material Selection

2.1.1.1 Hollow Glass Microspheres

Hollow glass microspheres (HGM) are tiny spheres with high ball type rate (or their glass bead nature and ball bearing effect) that can improve their mobility and reduce viscosity, and internal stress of the resin mixture. They can be used to give reflectivity and a smooth surface. They are widely used in consumer goods, medicine, research, aerospace, automobile, and appliances. The use of HGM as the particulate filler in this research work was due to its low-density characteristics which is one of the major focus areas of this project.

2.1.1.1.1 Overview of Hollow Glass Microspheres

In 1963, Beck created a material called hollow beads which were later called hollow glass microsphere by 3M after reheating the particles to form a single wall. The HGM was patented in collaboration with the Standard Oil of Ohio (Sohio) which was later sold to Philadelphia Quartz (PQ) now known as PQ Corporation. Hollow glass microsphere (HGM) are microscopic spheres of glass manufactured for a wide variety of uses in research, medicine, consumer goods, and various industries. The use of HGM has extensively revolutionized the applications of polymer matrix with glass microspheres which are usually between 1 and 1000 micrometers in diameter, although the sizes can range from 100 nanometers to 5 millimeters in diameter (Stephen E Amos 2015).

Hollow glass microspheres, sometimes termed microballoons or glass bubbles, have diameters ranging from 10 to 300 micrometers. They are used as lightweight filler in composite materials such as syntactic foam and lightweight concrete. Microballoons give syntactic foam its lightweight, low thermal conductivity, and resistance to compressive stress that far exceeds that of other foams. These properties are exploited in the hulls of submersibles and deep-sea oil drilling equipment, where other types of foam would implode. Hollow spheres of other materials create syntactic foams with different properties: ceramic balloons e.g. can make a light syntactic aluminum foam (Erikson 2002).

Hollow spheres also have uses ranging from storage and slow release of pharmaceuticals and radioactive tracers to research in controlled storage and release of hydrogen. Microspheres are also used in composites to fill polymer resins for specific characteristics such as weight, wettability, and sealing surfaces. When making surfboards, for example, shapers seal the EPS foam blanks with epoxy and microballoons to create an impermeable and easily sanded surface upon which fiberglass laminates are applied.

2.1.1.1.2 Synthesis and Production of Hollow Glass Microspheres

Microspheres are spherical particles that can be divided into two groups: solid or hollow (Lee *et al.* 2017). Both the solid and the hollow microspheres can be produced from glass, ceramic, carbon, or plastic. According to Watkins and Prado (2015); Lee *et al.* (2017); Bobkova *et al.* (2020), solid glass microspheres are usually made from soda-lime glass due to the low melting point and chemical inertness of soda-lime glass. Glass microspheres can be obtained from several methods, and the product properties will be based on the production process adopted. Watkins and Prado processed glass microspheres using the In Flame Spherodization Method (IFSM) where irregular glass particles were fed into a flame with a temperature over the vitreous temperature (T_g). The obtained microspheres traveled through the cool region of the flame into a cyclone system where all the spheroid particles were collected (Watkins and Prado 2015). It was important to know the fundamentals of dispersion to understand the possibility of handling and mixing HGM because complications arise from simple vigorous mixing of materials with very fine particles (sometimes microscopic) as they still maintain electrical, molecular, and/or mechanical bonding after mixing (Shira and Buller 2015).

2.1.1.1.3 Structure-Property Relationship of Hollow Glass Microspheres

HGM are made from glass, carbon, ceramics, or plastics depending on the application. They can be distinguished into two categories, solid or hollow. The advent of HGMs has made a couple of generations of formulating chemists and polymer scientists go back and relearn the difference between volume and weight filling in composite systems. Determination of constituent materials volume in the composite is important when adding HGM and resin together, failure to do so may remove important filler or dilute too much resin and affect the entire composite (Stephen E Amos 2015; Lee *et al.* 2017). Warren Beck, a 3M scientist was the first person to discover the possibility of creating hollow beads called “HGMs” after much experimentation. In 1963, he patented the unique structures by formulating glass frit, milling it into specific particle size and particle size distribution before reheating the particles to form single-wall HGM (Stephen E Amos 2015). Physiochemical properties of HGM such as the surface free energies, thermal properties, glass transition temperature, electrical, and mechanical interfacial are important studies to understand the structure-property relationship of HGM. Interest in HGM as fillers are mostly due to their low density, high stiffness, low thermal conductivity, and electrical properties (Park, Jin and Lee 2005; Li *et al.* 2011). The heat insulation properties of HGM concerning density and thermal conductivity were extensively studied by Li *et al.* (2011), the mechanism of heat transfer in HGM was analyzed and thermal conductivity was proved to be the main heat transfer. It was discovered that HGM with hollow

structures can be used in the insulation areas due to its low thermal conductivity and the conduction of heat transfer in the most important means by a simple mechanism. Hollow glass is employed for this research work because of its ability to reduce material density (Lee *et al.* 2017), better than solid glass which is one of the major focus areas of this work.

2.1.1.1.4 Degradation and Stability of Hollow Glass Microspheres

HGM material has a very low coefficient of thermal expansion (CTE), low thermal conductivity, and low dielectric constant (D_k) (Yung *et al.* 2009) which prevents it from shrinkage, and the wall joint material is very hard after curing and required a significant amount of work to sand to a smooth surface. HGMs glass transition (T_g) temperatures are typically around 600^{o}C or less. When the temperature is above the T_g, the material behaves as liquid thermodynamically, metastable and of high viscosity (~10^7, - 10^{13} dPa x s). Differential thermal analysis (DTA) is a common method to determine glass transition, crystallization, and melting temperatures of glass materials. Differential scanning calorimetry (DSC) is another technique to measure the degradation of HGM by combining three DTA scans (baseline, standard of unknown heat capacity, and sample) to enable quantification of thermodynamic quantity, C_p, which is the heat capacity at constant pressure (Stephen E Amos 2015). The thermal conductivity of HGMs is a function of their hollow volume and wall thickness and it is mostly estimated using theoretical models. It can also be measured as a product of thermal diffusivity, specific heat, and density (Yung *et al.* 2009).

2.1.1.1.5 Applications of Hollow Glass Microspheres

HGM's various applications were promoted in the early days of its patent such as in plastics, resinous materials, rubber, for weight reduction, thermal insulation, concrete, synthetic, wood, gas storage, and transport, as flow aid, and in drywall joint sealer (Yung *et al.* 2009; Tall *et al.* 2012; Stephen E Amos 2015). One of the major applications of HGM was as a functional filler for plastics to enhance properties and /or reduce costs. It was employed for explosives and some resin applications (e.g., autobody filler, grout, potting compound, marine applications, extruded, bulk molding compound, and plastisol). Watkins et al reported the use of HGM as applicable for medical appliances, cancer radiotherapy treatment, drug delivery, propellants for the oil industries and in nuclear industries (Watkins and Prado 2015). According to Tall *et al.* (2012), the HGM is used to adjust the rheological properties, reduce part weight, and also reduce the warpage and shrinkage of materials. Most of the applications of HGM are also done together with some reinforcement such as kenaf and glass fibers, as used in this project.

2.1.1.2 Fiber Form

Fibers are additional strong, stiff, and lightweight reinforcement elements used in composite materials, they are classified into two: natural or artificial (synthetic) fibers. Due to their preferential orientation of the molecules, they are much stronger compared to their bulk counterparts. They are protected from damage that can happen in the process of contacting other fibers or equipment by covering them with a material called sizing, this helps to limits moisture absorption (Carey 2017). Fibers are often presented in terms of “Tex”, which is a unit describing the linear density (grams per 1000 m) of fibers, filaments, tows, and yarns.

2.1.1.2.1 Classification of Fiber Form of Fillers

Fibers are generally classified as natural and synthetic fibers (or man-made fibers) (Carey 2017; Erden and Ho 2017). The natural fibers are of the form: plant (cellulose-based such as hemp, jute, flax, cotton, etc.), animal (protein-based e.g., hair, cashmere), or mineral-based such as asbestos while the synthetic fibers, there are two subcategories (organic and inorganic), the organic polymers are natural polymer-based, which are in the form: acetate and rayon, while the synthetic polymers are the aramid and polyethylene. Inorganic synthetic fibers include carbon, boron, silicon carbide, stainless steel, glass, aluminum, etc. The fiber form of fillers is represented in Table 2.1 below.

Table 2.1: Classification of fibers (Ashik and Sharma 2015; Pickering, Efendy and Le 2016; Carey 2017; Erden and Ho 2017; Ramu, Jaya Kumar and Palanikumar 2019)

Fibers					
Natural			Synthetic		
Animal	Mineral	Plant	Organic	Inorganic	Metallic
Silk, hair	Asbestos	Short fibers, long fibers	Nylon, acrylic, aromatic, polyester, polyethylene, aramid	Glass, carbon, boron, silicon carbide etc.	Stainless steel, aluminum, copper, silver etc.

Table 2.2: Nature and types of different plant fibers (Faruk *et al.* 2012; Ashik and Sharma 2015; Pickering, Efendy and Le 2016; Carey 2017; Erden and Ho 2017; Ramu, Jaya Kumar and Palanikumar 2019)

Plant fibers							
Short fibers		Long fibers					
Wood		Nonwood					
Softwood	Hardwood	Cane, grass & reed	Fruit	Bast	Leaf	Stalk	Seed
		Bamboo, bagasse, Corn, Grass, wheat, etc.	Coir, Oil palm	Kenaf, Rattan, Roselle, Ramie, Stem, Jute, Flax, Hemp, etc.	Hard, Sisal, Banana, Abaka, Manila, Date palm, Pineapple, Mengkuang, etc.	Rice, Wheat, Maize, Oat, etc.	Cotton, Kapok, Oil palm Seed, Alfalfa

Fiber types are commonly categorized based on their origin: plant, animal, or mineral as listed above. Cellulose can be identified as the major structural component of all plant fibers while protein is identified with the animal fiber. Mineral fibers exist within the asbestos group and are avoided due to associated health issues (carcinogenic through inhalation/ingestion) caused by them (Pickering, Efendy and Le 2016). Good strength and stiffness with higher performance are obtainable mainly from the plant fibers, this makes plant-based fibers most suitable for use in composites with structural applications. Kenaf fiber is one of the natural fibers with higher performance having higher cellulose content that is applicable for structural requirement, which is one of the reasons why we chose kenaf fiber as the natural fiber in this project. But because the strength and stiffness of natural fibers are generally lower than that of glass fiber, hybridizing glass-kenaf fiber is then considered to achieve the strength and stiffness required for the desired purpose in this project.

2.1.1.2.1.1 Glass Fibers

2.1.1.2.1.1.1 Overview of Glass Fibers

Glass fibers are largely used in reinforced composites on an individual, commercial, and industrial scale. They are mostly classified into two: E-glass and S-glass. Glass fiber is one of the synthetic inorganic fibers, the use of glass fiber in polymer composites offers many potential advantages with to longer lifetimes, reduction of weight, and cost in industries such as transportation, infrastructure and structural applications (Schutte 1994). Understanding the mechanisms responsible for the loss of mechanical properties of glass fiber is complex but can be done with each constituent having the capability of being the weak component in the structure. It is mostly used as the reinforcement for many commercial composites, thereby making their durability be subjected to environmental exposure to determine the retention capability of their mechanical properties. The fundamental behavior of glass fiber in polymer composite can be understood better through the mechanism of crack growth and time-dependent fracture in bulk glasses.

2.1.1.2.1.1.2 Synthesis and Production of Glass Fibers

The process of manufacturing glass fibers is by drawing molten glass such as quarry products (e.g., sand, kaolin, limestone, and colemanite) or spinning the glass from an inorganic product of fusion into a fine thread and thereafter cooled to a rigid condition without crystallization by ensuring that they are not exposed to the atmosphere or hard surfaces so that they can be sheltered from the drawing process defect. Glass fibers are inorganic fibers that are responsible for their good strength but their properties change when the chemical composition (e.g. silicon+ sodium + carbonate + calcium carbonate under temperature >1000^{o}C) in the glass is altered and their lack of rigidity is due to their molecular structure (Gay Daniel 2003). The two major types are S-glass and E-glass, S-glass is common in France and possesses good properties such as high thermal stability and strength but of the high cost of purchase which factored their minimal account in usage. E-glass was preferred in this study because of its excellent thermal stability, strong resistance to water, good tensile and compressive strength, good electrical and insulation properties, excellent rigidity properties, and relatively low cost with very good reinforcement capability (Kamal 2017). Though their impact resistance is relatively poor, they remain the most common form of reinforcing fiber used in polymer matrix composites or reinforced medium for plastic as well as for textile fiberglass product applications (HILLI 2006). Numerous glass compositions have been developed, but few are available in commercially used to create continuous glass fibers. The E-glass is of good electrical grade while the S-glass is of high chemical resistance and strength.

2.1.1.2.1.1.3 Properties of Glass Fibers

Glass fiber composites have high specific strength and good environmental resistance (humidity, heat, cold, corrosion). They are easy to fabricate and are low in cost, compared to other fiber composites. The representative chemical compositions and inherent properties of these two types of glass fiber, namely, S-Glass, for high strength glass and E-Glass, for electrical glass are shown in Table 2.3 and Table 2.4. S-glass is employed for high-end structural applications, such as aerospace, for example, while E-glass fibers are most commonly used in continuous fibers (Carey 2017).

Table 2.3 Typical properties of glass fiber used in composite materials (Carey 2017)

Fiber Glass	Elastic modulus (GPa)	Tensile strength (Gpa)	Shear modulus (Gpa)	Failure strain (%)	Density ρ (g/cm^3)	Poisson ratio	Thermal conductivity (W/mK)
E-Glass	75	3.5	30	4.4 – 4.8	2.54 – 2.60	0.2	1.3
Commercial fiberglass used in the present work							
S-Glass	85	4.6 – 4.8	35	5.3 – 5.7	2.48	0.22	

Table 2.4 Glass composition of E-glass and S-glass (HILLI 2006)

	Material, percentage weight (%)							
Glass type	Silica	Alumina	Calcium oxide	Magnesia	Boron oxide	Soda	Calcium fluoride	Minor oxides
E-glass	54	14	20.5	0.5	8	1	1	1
Commercial fiberglass used in the present work								
S-glass	64	25	-	10	-	0.3	-	0.7

Table 2.5 Glass fibers inherent properties (HILLI 2006)

Glass type	Specific gravity	σ_{ult} (MPa)	E_t (GPa)	α (10-6/K)	Dielectric constant (a)	Liquidus temperature ^oC
E-glass	2.58	3450	72.5	5.0	6.3	1065
Commercial fiberglass used in the present work						
S-glass	2.48	4590	86.0	5.0	5.1	1454

2.1.1.2.1.1.4 Degradation and Stability of Glass Fibers

The properties of glass fibers are affected by the properties of their constituent polymer, the structure, assembly, and interactions of the changing environment. The characteristics of glass fiber are lightness, a novel appearance, and superior warmth because of the inclusion of air, compared with natural fibers of the same linear density, they are stiffer and more resistant to bending and torsion and have a more opaque appearance, caused by the diffused reflection of light (Wada 1992). The durability of glass fibers/polymer composites is determined by the durability of the constituent components: glass fiber, matrix, and the interface. The strength of glass fiber can be degraded by the environmental attack of the moisture, and by the chemical or mechanical attack. The degradation process of glass fiber is relatively a function of the chemistry of the matrix, length of time of exposure, temperature, degree of stress (whether cyclic or static), chemistry and morphology of coupling agent on the glass fiber, and the type of glass fiber used (Schutte 1994).

2.1.1.2.1.1.5 Applications of Glass Fibers

They are good electrical insulators. Glass fiber composites have good dimensional stability (Carey 2017). The application of glass fiber in structural material was dated as far back as the 17th Century before it became widely known in the 20th Century. They are used as a replacement for metals in commercial and military materials such as weapons of war and aerospace (Defence 2002). Many researchers have applied glass fiber in one form or the other either as a composite material or as reinforcement. They are mostly used as a hybrid fiber either with a co-synthetic fiber e.g. carbon (Badie, Mahdi and Hamouda 2011; Pandya, Veerraju and Naik 2011; Zhang *et al.* 2012; Kimiyoshi Naito 2017), or natural fibers such as jute (NALLUSAM and Majumdar 2016), sisal (Arpitha and Sanjay 2014), kenaf (Ramesh, Nijanthan and Palanikumar 2015; Dhar Malingam *et al.* 2018), sisal,

and ceramic fiber (Bharat, Abhishek and Palanikumar 2017), banana and rice husk (Gupta *et al.* 2016), Kevlar-149 (Yiping Qiu 1993). This is done to improve the mechanical strength and biodegradable property of synthetic fiber, facing off synthetic fibers cannot be actualized at once, there is need to hybridize them with natural fibers for the purpose of enhancing their biodegradability. Also, when considering the cost of using more expensive high performing fiber, glass fiber can be added as reinforcement to reduce the cost and maintain the mechanical property desired (Gupta *et al.* 2016). Arpitha and Sanjay (2014) investigated the use of glass and sisal fibers as a hybrid reinforcement with Silicon carbide (SIC) filler. They reported an increase in tensile, flexural and impact strength because of glass fibre addition as reinforcement. In another report, orientation of glass fibre was studied as it affect the carbon/epoxy reinforced composites using finite element model predictions (Badie, Mahdi and Hamouda 2011), Kimiyoshi Naito (2017) used carbon/glass hybrid to develop a novel thermoplastic composite rod. Also, Ramesh, Nijanthan and Palanikumar (2015); Dhar Malingam *et al.* (2018) stated that the hybrid of kenaf/ glass fiber was a good combination for tensile, flexural, and impact strength when placed at different orientations and configurations. In another report by Nallusamy and Majumdar (2016), inclusion of glass fiber through stacking sequence helps to increase the tensile and flexural strength of the jute-glass fiber composite material and also contributed to the increase in hardness and impact properties. In all the natural fibers used as a hybrid with glass fiber, kenaf fiber is not commonly used despite its good mechanical property (Ashik and Sharma 2015; Pickering, Efendy and Le 2016; Saba *et al.* 2017). This accounted for the usage of kenaf natural fiber with glass synthetic fiber as a hybrid at different stratifications for reinforcement and face-sheet in the composite sandwich structure for structural application in this present research work. In the composite sandwich panel, glass fiber has been used alone as the skin (both upper and lower face-sheet) with syntactic foam as the core (Alberto Corigliano 2000; Baedella Lorenzo 2001; Karthikeyan, Sankaran and Kishore 2007; Carrera Giovanni 2013; Salleh *et al.* 2016; Daniel Paul. 2018; Ahmadi and Liaghat 2019), with phenolic core material foam (Awad, Aravinthan and Zhuge 2012), with poly-vinyl chloride foam core (Garay, Souza and Amico 2016; Balıkoğlu *et al.* 2018), together with kenaf fiber as a reinforcement and an Aluminium honeycomb core (Sharba *et al.* 2016a; Ashraf *et al.* 2019), together with flax fiber and agglomerated cork and polypropylene honeycomb as the core (Sadeghian, Hristozov and Wroblewski 2016, 2018; Prabhakaran *et al.* 2019). Glass fiber possess high internal damping factor, resulting in their ability to reduced vibrations and transmission of noise to the external environment, thereby making them suitable for acoustic application in structural panel (Mallick 2007). This high damping capacity of glass fiber makes it suitable as reinforcement together with kenaf fibre in making composite sandwich structure for structural application desired in this study.

2.1.1.2.1.2 Kenaf Fiber

2.1.1.2.1.2.1 Overview of Kenaf Fibers

Kenaf fiber is from the family of genus Hibiscus with about 300 species. They are a new crop in the United States with good potential as raw material in the field of composite. The recent decortications of equipment by separating the core from the bast fiber has led to fiber shortage, thereby increasing the interest in the use of kenaf fiber (Zatta 2009; Ramu, Jaya Kumar and Palanikumar 2019). Kenaf fiber is an annual or short-lived perennial herbaceous fiber plant in the combination of bast and core, and they are also a dicotyledonous plant with three layers of the stalk: an outer cortical (bast), tissue layer (called phloem), and an inner woody core tissue layer (called xylem) (Ramesh 2016). Kenaf fibers as a form of natural fiber are alternative to synthetic fibers which have gained the attention of researchers in recent times for composite material application. They can be distinguished by their source either from the plant, animal, or mineral source and consist of mainly cellulose, lignin, and pectin (Elanchezhian 2015). Kenaf fibers as plant natural fibers are made of cellulose. They can be used alone for composite preparation with the matrix polymer, as hybrid fiber with synthetic fiber, or as reinforcement on sandwich materials. They are nowadays preferred to the synthetic ones because of their biodegradable nature as they take a major role in the emergence of the green economy to reduce carbon emissions and to minimize waste. Over the years, they have been renewed by nature and human inventions on them because they are less toxic to the environment as they absorb the same quantity of carbon dioxide that was produced by them (Faruk *et al.* 2012; Arpitha and Sanjay 2014; Ashik and Sharma 2015; Jauhari, Mishra and Thakur 2015). Kenaf fibers are easily accessible, processible, and cost-effective which is why they are been employed in day-by-day applications such as automobile industries. Due to the abundance of these kenaf fibers, they are gaining usage in traditional reinforcement as a replacement for synthetic fibers in composite materials most especially where weight reduction is required and because of their low density and high toughness ability (Ashik and Sharma 2015; Ramu, Jaya Kumar and Palanikumar 2019). Jauhari, Mishra and Thakur (2015) stated that for kenaf fibers to be used effectively, their physical and mechanical properties must be put into consideration because there is variation in their characteristics and component. Kenaf fibers have been used with other fibers/materials to make composite materials. Kenaf fiber was reinforced with Al_2O_3 using the epoxy matrix to experiment the effect of the mechanical properties of the composite. The Kenaf fiber enhances the increase in the mechanical properties such as flexural and tensile strength, hardness, and modulus of the composite (Swain 2014). Hybrid kenaf/banana fiber was studied by Alavudeen *et al.* (2015), where it was discovered that the strength of the composite increased due to hybridization of the natural fiber. Also, banana/kenaf hybrid fiber was studied to ascertain their resistance to water absorption unlike

the un-hybrid composite (Samivel 2013; Ashik and Sharma 2015). The combination of sisal/kenaf composite was discovered to possess better tensile properties than aloe vera /sisal combination in the work reported by Kumar, Sekaran and Pitchandi (2017). This is further proof that kenaf fibers improve the mechanical properties of composite materials which is one of the main reasons for employing it as the plant natural fiber in this present project.

2.1.1.2.1.2.2 Synthesis and Production of Kenaf Fibers

The plant origin/family of kenaf is called Malvaceae and Hibiscus. cannabis species, obtained from the stem part known as genus hibiscus. The production of kenaf fiber is done by using a small amount of water on the seed plant and they are mainly cultivated in India and China. The extraction process involves soaking the stalks (the retting process) and manual removal of the fibers. This method gives superior reinforcement quality (Hamidon *et al.* 2019). Kenaf is a valuable fiber plant and a high potential industrial crop cultivated in the tropical climate and a source of raw materials for fiber-based industries (Aziz, Halim and Othman 2018). Due to their easy to cultivate characteristics, they are one of the most widely used natural fibers because of their rapid growth. This makes them contribute about 40% to the useful fibers which are approximately twice compared to other fibers and the yield percentage makes the fiber more economical compared to that of other plants (Zatta 2009; Dhar Malingam *et al.* 2018; Hamidon *et al.* 2019). Kenaf fiber is rated third (3^{rd}) largest producing natural fiber in the world production ranking in tons (970×10^3 ton) (Faruk *et al.* 2012). Figure 2.3 shows the selection of kenaf fiber as separated from bast fiber to bundle fiber and finally to single fiber using Waltex magnifying glass (Mohd Yussni Hashim 2017). The growth and environmental conditions of kenaf fiber are presented in Table 2.6 (Zatta 2009).

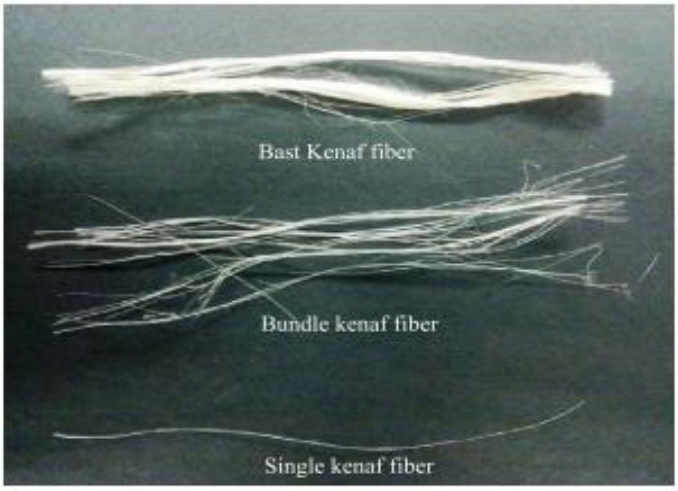

Figure 2.3: Selection of kenaf fiber from bast to bundle and to single fiber (Mohd Yussni Hashim 2017)

Table 2.6: Growth and environmental conditions of kenaf fiber (Zatta 2009)

Parameter	**Average range**
Base T- emergence (^oC)	9 – 10
Base T – growth (^oC)	12 – 14
Optimum T (^oC)	20 – 27
Cycle length (d)	75 – 105 (short cycle); 105 – 120 (mid cycle); 120 – 140 (long cycle)
Photoperiod	Flowering occurs when day-length is < 12.5h
Transpiration efficiency (L Kg^{-1})	400 – 600
RUE (g MJ^{-1})	2.4
Needed rainfall (mm)	500 – 600 (in 5 months)
Soil	Drained sandy-loamy soil

2.1.1.2.1.2.3 Properties of Kenaf Fibers

The tensile and impact strength of kenaf/glass, kenaf/banana, and kenaf/neem hybrid fibers was studied by Elanchezhian *et al.* (2015); Dhar Malingam *et al.* (2018), it was reported that the hybrid configuration gave the highest impact strength than the single configuration of an individual fiber. Different orientations of the fibers ($0^o/90^o$ and $\pm45^o$) also constituted impact and tensile strength. High flexural strength and hardness were also observed from the hybrid kenaf/glass and kenaf neem composite which is highly applicable for automobile application. Kenaf fiber possesses good impact and hardness properties Elanchezhian *et al.* (2015) , they also possess a good reinforcement and face-sheet to syntactic foam core in sandwich composites.

Alavudeen *et al.* (2015) in their study on the mechanical properties of woven banana fiber, kenaf fiber, and hybrid of banana/kenaf fiber composites discovered that the mechanical strength of the hybrid banana/kenaf fiber composites increase relative to the hybridization of kenaf with banana fiber. The tensile, flexural, and impact strengths increased in the woven banana/kenaf fiber hybrid composites than the individual fibers.

Aziz, Halim and Othman (2018), studied the effect of Sodium Hydroxide [NaOH] of different concentrations on the properties of kenaf sandwich structures. It was discovered that the chemical treatment of kenaf fiber with NaOH increases the hydrogen bonding between the fibers and removes

impurities from the kenaf fiber for efficient behavior. The treated kenaf fiber shows less impurity than the untreated kenaf fiber. The mat kenaf fibers used for this study were also surface treated to improve their reinforcement properties. Faruk *et al.* (2012), investigated the use of the compression molding process on the mechanical properties of chopped kenaf fiber and polypropylene (PP) matrix. Kenaf fiber reinforcement increases the strength of the PP matrix and exhibited superior tensile and flexural strengths compared to other compression molded natural fiber composites like sisal, coir, etc. This also contributed to the choice of kenaf fiber as the natural fiber employed in this project.

2.1.1.2.1.2.4 Degradation and Stability of Kenaf Fibers

The degradation process of kenaf fiber does not only influence the structure but also the chemical composition. The major chemical component of a living tree is water, but, on a dry basis, all plant cell wall consists of mainly sugar-based polymers (cellulose, hemicellulose) that are combined with lignin with a lesser number of extractives, proteins, starch, and inorganics. The major chemical and mechanical composition of kenaf fiber is shown in Table 2.7 and Table 2.8 (Faruk *et al.* 2012; Hamidon *et al.* 2019).

Table 2.7 Chemical composition of kenaf fiber (Faruk *et al.* 2012)

Fiber	Cellulose (wt%)	Hemicellulose (wt%)	Lignin (wt%)
Kenaf	72	20.3	9

Table 2.8 Mechanical properties of kenaf fiber (Hamidon *et al.* 2019)

Fiber	Density (g/cm^3)	Elongation (%)	Tensile strength (MPa)	Young's modulus (GPa)
Kenaf	1.50	1.6	930	52

Mohd *et al.* (2017) , studied the effect of alkali treatment on the physical properties of kenaf fiber such as density, weight loss, diameter, cross-sectional, and fiber morphology. The treated kenaf fiber was found to increase in density compared to the untreated fiber and likewise the weight loss. While the diameter and cross-sectional area decline in pattern after being treated with alkali. The

three variables considered during the alkali treatment process are alkali solution concentration, immersion duration, and immersion temperature.

Fiore, Di Bella and Valenza (2015); Akhtar *et al.* (2016), in their study, detailed the effect of alkaline treatment on the kenaf/polypropylene (PP) composite on the structural, thermal, and mechanical properties. The three properties of kenaf/PP treated with alkaline improved because of the surface roughness, adhesion, and strong bonding between the fiber and the matrix.

Ghani *et al.* (2012), experimented with the effect of three different aqueous solution environments: distilled water, seawater, and acidic solution at room temperature on the mechanical properties of kenaf/fiberglass polyester hybrid composite. The tensile properties decreased due to longer immersion and the formation of hydrogen bonding between the water molecules and cellulose of the fiber. This result guided the water absorption process studied for the hybrid kenaf/glass fiber in this project.

2.1.1.2.1.2.5 Applications of Kenaf Fibers

Kenaf fiber is produced for various applications, including paper products, absorbents, building materials, and livestock feed, the combination of kenaf/E-Glass fiber is good for the textile and industrial applications (Hamidon *et al.* 2019). Kenaf reinforced polymer composite has the huge possibility and potential usage in industrialized applications due to their low cost and lightweight property, such applications include automobile, aerospace (high-performance component), interior and exterior panels and gas tanks, construction (building section and structural panels), food packaging (plastic carrier, wrapping films and containers), and electrical and electronics (printed circuit boards and integrated components) (Sreenivas, Krishnamurthy and Arpitha 2020). Elsaid *et al.* (2011), stated that kenaf reinforced composite can be used in the production of impact resisting members and also to enhance the durability of concrete at a relatively low cost compared to other fibers. A combination of kenaf/ramie hybrid composite has been studied to be applicable for automotive headliners (Thiruchitrambalam 2012). Globally, kenaf fiber has been used as a suitable biological resource and potential substitute for fossil fuels and wood pulp because of its wide and extensive adaptation, strong resistance, large biomass, and rich cellulose (Ramesh 2016). Other possible applications of kenaf fiber and its composites are listed below (Cheung *et al.* 2009; Zatta 2009; Pang, Shanks and Daver 2015; Ramesh 2016).

Rope, twine, cordage, etc.; Bags and fabrics, hamburger wrappers, fast food containers, wallpaper; Engineering wood, Animal bedding, poultry, and cat litter; Oil and liquid-absorbent materials; Substrate for mushroom production; Materials for blending with resins for bioplastic composites; Bio-

medical applications such as drug/gene delivery, tissue engineering, orthopedics, and cosmetic orthodontics; Sails; Coarse cloth (similar to that made from jute); Energy (both electrical/heat and generation of biofuels); Insulated panels; Black liquor, a by-product of making paper from kenaf, is burned for fuel or chemical recovery in the USA; Seed oil, and several other.

2.2 Composites

Composites are materials made of two constituents that are at a microscopic scale and have chemically distinct phases, they are different from heterogeneous material but comprises of strong fibers, with continuous or noncontinuous layers, and are surrounded by a weaker matrix material. They are made up of at least two separate elements coming together to form a material that will possess different properties from the properties of the separate parent materials (Gurit ; Gay Daniel 2003). Practically speaking, most composites consist of a bulk material known as matrix, and a reinforcement of some kind, which is to give an addition to the strength, and stiffness of the matrix which is usually in the fiber form. According to Kamal (2017), composite materials was described as a major class of advanced elements and are either used or being considered as an alternative to metals/traditional materials in aerospace, automotive, civil, mechanical, and other industries because of their lightweight, flexibility, impact strength, fatigue strength, and high corrosion resistance. Some of the excellent performance of composite can be seen in their high strength, high specific stiffness, and controlled anisotropy, which make them very attractive materials. The specific characteristics feature of composites is in their ability to tailor their finished product towards a unique engineering requirement by careful consideration of the matrix and filler. Such characteristics make them useful for different applications (Kamal 2017).

2.2.1 Classification of Composites

There are three main classifications of composites material which include: Polymer Matrix Composites (PMCs), Metal Matrix Composites (MMCs), and Ceramic Matrix Composites.

2.2.1.1 Polymer Matrix Composites (PMCs)

Development of materials needs to be accompanied by the understanding of cost-effectiveness and structural functionality of the materials. Materials form the basis of human endeavors with more emphasis given to PMCs. PMCs are the most common type of composites material and are also referred to as Fiber Reinforced Polymer/Plastic (FRP). PMCs used polymer-based resin as the matrix, and a variety of fibers such as glass, carbon, natural fibers, and aramid as the reinforcement. In this section of the review, we describe the role of fillers in enhancing the properties of PMCs with principles governing their distribution and interaction within polymer composites materials.

2.2.1.2 Metal Matrix Composites (MMCs)

They are most common in the automotive industry, and they employ materials with metals such as aluminum as the matrix, and fibers or particles, such as silicon carbide as the reinforcement.

2.1.2.3 Ceramic Matrix Composites (CMCs)

They use ceramics as their matrix with reinforcement such as short fibers, or whiskers such as those made from silicon carbide and boron nitride and are mostly used in the high-temperature environment.

2.2.2 Advantages of Composites

Composites materials are applicable in different ways and structures because they can be tailored to meet the specific functional requirements such as the following (Kamal 2017):

- Sports: composite material provides new materials for the sporting goods market as well as the commercial mode of operation. Some of the materials produced from composite materials in sport include golf sticks, hockey sticks, bicycle stands, baseball bat, marine hull, and fishing rods.
- Transportation**:** Composite materials are formed into automotive, bus, camper and vehicle components, engine and body panels, truck, rail and other vehicle components and fittings, land and sea containers, railway track and signaling components, traffic signs, seating, window masks, and partitions, etc.
- Engineering and Industrial Applications**:** Composites materials are used for assemblies and fittings, sundry enclosures, pallets, safety helmets, trays, bins, profiles, medical items, assemblies, and equipment components, etc.
- Infrastructures**:** composite materials are used to produce more durable infrastructure. Fiber-reinforced composite designs with unique properties are now being used for many infrastructure applications.
- Electrical and Electronics**:** Composites materials are used for internal and external aerial components and fittings, circuit boards, generation and transmission components, insulators, switch boxes and cabinets, distribution posts and pylons, telegraph poles, fuse tubes, ladders and cableways, transformer elements, etc.
- Marine Applications: Composites materials are advantageous in the manufacturing of canoes and boats, yachts, surf and sailboards, lifeboats and rescue vessels, buoys, boat accessories and subassemblies, window masks, and internal moldings and fittings for ferries and cruise liners, workboats, and trawlers, etc.

- Building and Construction**:** Composites materials are good alternatives to wood and planks in building external and internal cladding, permanent and temporary formworks and shuttering, structural and decorative building elements, fencing and walkways, etc.
- Defense: Composite materials are used in the defense industry for the manufacturing of aircraft vehicles, aerospace and satellite components, enclosures and containers, pipes and ducts, personnel armor, rocketry and ballistics items, shipping and transit containers, simulators and allied, etc.
- Aerospace and Aircraft**:** Composites materials have wide applications in the aerospace industry such as the construction of containers, gliders, galley units and trolleys, satellite components, structural members, ground support equipment components, enclosures, etc.

2.2.3 Disadvantages of Composites

Despite the numerous advantages of composite materials, there are some unavoidable disadvantages associated with them some of which are (Kamal 2017):

- Manufacturing difficulties: The manufacturing costs of composite materials are high because of the technology involved in manufacturing high-quality composite, thereby increasing the product cost.
- The cost of production of consumer goods at competitive pricing is high: for example, in the aerospace and automotive sector, the equipment, tooling, and running costs are so high that the production of general-purpose items is not economical.
- The Source of material economy and functions are scarce and most often not easily assessable.
- The full potential of composite materials cannot be utilized unless there is a technology for the competitive production of items in place.
- The problem arises in composite materials if the product has a complex geometry like flat, flat with a curve, and flat with a curve to the cone.
- Application of high pressure to minimize the void content in composites material products having a complex geometry and getting high volume percent of fiber is not feasible.

2.2.4 Polymer Matrix Composites

The selection of materials for the matrix and reinforcement, the form of reinforcement, and the manufacturing process in PMC are very critical for obtaining a composite product with desired results.

2.2.4.1 Processing of Polymer Matrix Composites

The syntheses of polymer are generally manufactured by polymerization, polycondensation, or polyaddition. The polymers are combined with different agents to enhance or in a way change the material properties (Masuelli 2013). Most composite materials used the same method as matrix processing for fabrication some of which include compression molding, injection molding, and extrusion. Some methods are mainly applicable for composite processing such as filament winding, pultrusion, and hand lay-up. The operational condition of all the processes available for the processing of PMC differs and as such, it is important to understand the differences for careful consideration. For this research, the hand lay-up method was mostly employed. This method involves laying down the fabrics made of reinforcement and painting with the matrix resin layer by layer until the desired thickness is obtained. This method can be time and labor-consuming in PMC processing, but it is mostly used in aerospace composite products. It is also advantageous because it can accommodate irregular-shaped products, long fibers can be aligned with controlled orientations such as fiber-glass and some natural fibers (Park and Seo 2011).

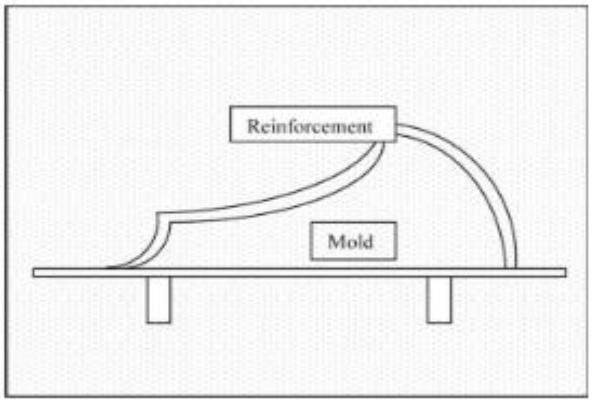

Figure 2.4: Schematic diagram of hand lay-up process (Park and Seo 2011)

2.2.4.2 Advantages of Polymer Matrix Composites

The advantages of PMCs can be seen in their various applications which varied from different sectors of human endeavors, these include (Kamal 2017):

- Business and Appliance Equipment: molded items like enclosures, frameworks, covers, fittings, and assemblies for internal use, switchgear bodies, associated electrical and insulation components, etc.

- Agriculture: PMCs are applicable in the agricultural sector in the production of feed troughs, fencing, partitions, staging, containers and enclosures, equipment components, flooring, silos, tanks, etc.
- Building and Construction: PMCs are applicable for external and internal cladding, permanent and temporary framework and shuttering, partitions, polymer concrete, prefabricated buildings, kiosks, cabins and housing, structural and decorative building elements, bridge elements and sections, quay facings, staging, fencing, signposts and street furniture, and walkways, etc.
- Aerospace and Aircraft: PMCs application is very wide in the aerospace industry such as the construction of containers, gliders, control surfaces, and light aircraft, internal fittings, window masks, partitions and floors, structural members, aerials and associated enclosures, galley units, and trolleys, ground support equipment components and enclosures, satellite, etc.
- Consumer Product Components**:** For domestic and industrial furniture, sanitary ware, sporting goods, caravan components, archery and playground equipment, garden furniture, etc.
- Corrosion –Resistance Equipment**:** Chemical plant, linings, oil industry components, pipes and ducts, chimneys, grid flooring, etc.

2.2.4.3 Disadvantages of Polymer Matrix Composites

The manufacture of PMCs involves the preparation of a network of fibers according to the desired shape of the component, impregnating this fiber network with the resin, and curing the resin while the part is being supported. Due to this reason, the PMCs are the disadvantage in that:

- There are challenges in efficiently handling the fibers and application of uniform pressure during the curing of the resin.
- Resin is supplied into the mold under pressure and makes the fiber wet.
- The fibers are stiff and do not flow.
- The continuous fibers are stacked in layers and kept in the mold.
- It is difficult to get a high-volume percent of fibers in the composites.

2.2.4.4 Classification of Polymer Matrix Composites

2.2.4.4.1 Particulate Filler Filled Polymer Composites

Particulate fillers are a form of reinforcement in composite materials; they are employed in matrix resins for a variety of reasons such as density control, optical effects, cost reduction, thermal conductivity, improved processing, electrical properties, control of thermal expansion, magnetic

properties, flame retardancy, and improved mechanical properties such as hardness and tear resistance (Park and Seo 2011). The properties of filler differ from one to another and are influenced by their particle size, shape, and surface chemistry, with their characteristics also differing from cost to particle morphology. The properties of composite materials involving particulate fillers can be determined by their critical factor as in the carbon black, natural mineral filler, and synthetic mineral filler types. Surface modification of fillers is another important factor to consider when considering them in composite materials (Park and Seo 2011).

2.3.4.4.1.1 Processing of Particulate Filler Filled Polymer Composites

Most particulate filler polymer composite (PPC) materials used the same method as matrix processing for fabrication some of which include compression molding, injection molding, and extrusion. Some methods are mainly applicable for composite processing such as filament winding, pultrusion, and hand lay-up. The operational condition of all the processes available for the processing of PPC differs and as such, it is important to understand the differences for careful consideration. For this research, the hand lay-up method was mostly employed. This method involves laying down the fabrics made of reinforcement and painting with the matrix resin layer by layer until the desired thickness is obtained. This method can be time and labor-consuming in PMC processing, but it is mostly used in aerospace composite products. It is also advantageous because it can accommodate irregular-shaped products, long fibers can be aligned with controlled orientations such as fiber-glass and some natural fibers (Park and Seo 2011). Composite materials offer the widest range of high-strength skins with the ability to change the fiber type (fiberglass, carbon, and aramid) in addition to the fiber volume and orientation.

2.2.4.4.1.1 Advantages of Particulate Filler Filled Polymer Composites

Particulate fillers for polymer composite differ in chemical structure, shape, size, and inherent properties. The interactions between the filler/matrix interfaces can be improved by employing a compatibilizer or grafting agents. The effect of good interface interaction can also be felt in their applications. Some of the advantages of particulate filler polymer composites include (Petrucci and Torre 2017; Khan, Srivastava and Gupta 2020):

- Low cost of producing fine particles of low aspect ratio and high purity
- Ease of compatibilization through surface modification
- Untreated clay minerals are widely used as fillers in elastomers.
- They are used to reduce the effect of petrochemical waste disposal on the environment.

- They possess suitable mechanical and barrier properties required for food packaging containers.
- Good flexibility and conductivity make them applicable for electronics industries.

2.2.4.4.1.2 Disadvantages of Particulate Filler Filled Polymer Composites

Some of the main disadvantages of particulate filler polymer composites are (Petrucci and Torre 2017):

- Reduction in toughness
- Anisotropic composite properties during shrinkage
- Increase in equipment wear due to abrasive nature.
- Quick surface damage during the handling operations

2.2.4.4.2 Fiber Reinforced Polymer Composites

Fiber Reinforced Polymer Composites (FRPs) are materials that are generally classified based on the geometry of their reinforcement used, which could be in the form of fibers or particles.

2.2.4.4.2.1 Processing of Fiber Reinforced Polymer Composites

Composite materials are well suited for large deflection applications where high strain capability and fatigue are required and they are more corrosive and environmentally resistant than metals. For the FRPC using hand lay-up, it can also be processed by spraying resin solubility on the material or poured and brushed into a mold. The reinforcement is then wet with resin and placed into the mold. Depending on the thickness or density of the reinforcement, it may receive additional resin to improve wet out and allow better drape-ability into the mold surface. Thereafter, the reinforcement can be rolled, brushed, or applied using a squeegee to remove entrapped air and compact it against the mold surface (Park and Seo 2011).

Most fiber-reinforced polymer composite (FRPC) materials used the same method as matrix processing for fabrication some of which include compression molding, injection molding, and extrusion. Some methods are mainly applicable for composite processing such as filament winding, pultrusion, and hand lay-up. The operational condition of all the processes available for the processing of FRPC differs and as such, it is important to understand the differences for careful consideration. For this research, the hand lay-up method was mostly employed, and degassing method was used to overcome the challenges of void propagation on the surface of the composites before solidification and ensure uniform/homogenous dispersion during the experiment. This method involves laying down the fabrics made of reinforcement and painting with the matrix resin layer by

layer until the desired thickness is obtained. This method can be time and labor-consuming in PMC processing, but it is mostly used in aerospace composite products. It is also advantageous because it can accommodate irregular-shaped products, long fibers can be aligned with controlled orientations such as fiber-glass and some natural fibers (Park and Seo 2011).

2.2.4.4.2.2 Advantages of Fiber Reinforced Polymer Composites

Due to the outstanding performance features of FRPCs, they are widely used for different purposes such as pulp and paper, semiconductors, metal refining, waste treatment, petrochemicals, power, pharmaceutical, and several other industries.

- Some of the products made from FRPs includes: hoods, ducts, pressure vessel, pumps, pipes, hoppers, valve bodies, heat-exchanger, scrubbers, fans, elevator buckets, mist-eliminator blades, tank lining system, shells and tube sheets, floor coatings, etc. (Kamal 2017)

2.2.4.4.2.3 Disadvantages of Fiber Reinforced Polymer Composites

FRPC can be disadvantageous in the forms like:

- Reduction in toughness
- Anisotropic composite properties during shrinkage
- Increase in equipment wear due to abrasive nature.
- Quick surface damage during the handling operations

2.3 Syntactic Foam Composites

Syntactic foams composites (SFC) are the product of the interaction between the polymer matrix and filler components, the filler (hollow glass microsphere) is directly mixed with the binder and the process can also be regarded as micro-capsulation. They are plastic-like foam due to their heterophase shape with a structure related to those of gas-blown cellular plastic unlike other foams (Hong 2015; Kamal 2017). They are called ‘syntactic’ (in Greek, “syn” means ‘same’ and “taktos” means ‘ordered’) because of the high order of regularity controlled by the size of the particles in them. The presence of continuous shells of the microsphere filler is responsible for the absence of an anisotropic and closed-cell structure of the syntactic foam. Also, the material in making the shells of the filler of the syntactic foams differs from that of the matrix making them a ternary system instead of the binary one common in the other plastic foams. The density is sometimes reduced by introducing air into the binder during the formation process. The process consists of mixing the hollow glass microsphere filler with the binder and then pouring the mixture into the mold structure

for proper curing at room temperature and post-curing at a certain required temperature. Different types of microballoons which could be spherical, chemical resistant, non-cohesive are employed some of which are glass, phenolic, carbonized, and metal-coated microballoons (Kamal 2017).

2.3.1 Processing of Syntactic Foam Composites

Several methods have been adopted in the past by different researchers in fabricating syntactic foam. These include:

2.3.1.1 Extrusion Technique

This technique was done by allowing the 5-10%wt of microballoons comprising of PE powder to pass through the heated zone in a laboratory for about one minute with a temperature of about 170^{o}C. Low-density polyethylene (PE) was used as a matrix with a melting point of 102^{o}C. The particle size for such a technique range between 6-9um and a starting temperature of 98-104^{o}C (Salleh 2017b) .

2.3.1.2 Firing Technique

The firing method is done by bonding the microballoons with an inorganic binder solution of $Al(H_2PO_4)_3$ and mono-aluminum phosphate in water. The solution is heated to lose water and to form a complex hydrate. The hydrates then decompose to an amorphous substance with formula $Al_2O_3.3P_2O_5$ at temperatures above 300^{o}C. The mixture of the microballoons/mono-aluminum slurries is then molded and vacuum-filtrated, dried at 50-90^{o}C, and heated for 24 hours at 230^{o}C. Thereafter, the syntactic foams are made by firing the microballoons with spherical intergranular cavities shape for 3 hours at 600^{o}C (Salleh 2017a).

2.3.1.3 Coating Technique

Syntactic foams can be fabricated via coating techniques by either resin coating, vacuum filtration, or polymer precipitation. The resin coating brings about agglomeration that is not required caused by a thin film of the polymer leading to the slurry solution which is vacuum filtered and rinsed on the filter. A molding powdery form of the discrete particles is then obtained after the coated spheres were vacuum dried. Then, the desired amount of the microballoons coated by drying is pressed into the preferred volume by mold charging and then cured at room temperature.

2.3.1.4 Stir Mixing Technique

This is the most common method of all the techniques which has been adopted by many researchers in the past for the fabrication of syntactic foam (Kim Ho Sung . 2001; Kim and Plubrai

2004; Wouterson *et al.* 2005, 2007; Salleh, Islam and Epaarachchi 2015; Salleh 2017a). This consists of mixing manually the hollow glass microballoons and the resin i.e., the filler and the matrix. The filler was added gradually into the matrix and gently stirred together to prevent the breakage of microballoons. This can be done in a beaker and the thorough mixture poured into a pre-designed mold made either from steel, aluminum, copper, or plastic PVC materials. The mold can be in any shape depending on the desired outlook of the syntactic foams to be produced. Mostly, a rectangular mold is used and then, the syntactic foam is machined to desired shapes after curing. A new system of conservative mixer is used nowadays with the help of a stir mixing machine by using a glass rod and a magnetic bar which most time perform better. This method can be shaken manually for gelatinizing the starch as microballoons are in the container. The conservative mixing method must be performed carefully to avoid microballoons breakage or container breakage. The desired quantity of microballoons and the matrix resin to be mixed must be measured on a weighing scale inside a beaker. The mixture is then mixed thoroughly until a slurry solution is formed to remove or reduce the viscosity.

This study also employed the use of stir mixing techniques because of their ability to control and give a better quality of the specimens. Degassing method was used to overcome the challenges of stir mixing and to ensure uniform/homogenous dispersion during the experiment. Molds of different shapes and sizes are designed for the fabrication of syntactic foam. Many researchers have used rectangular and cylindrical mold made from copper, steel, aluminum, and plastic PVC materials for compressive, tensile, and flexural test samples yielding excellent performance, according to specific test standards as given in Table 2.9.

Table 2.9 Mechanical testing shapes and standard for syntactic foam (Rizzi, Papa and Corigliano 2000; Kim Ho Sung . 2001; John *et al.* 2007; John, Nair and Ninan 2010)

Shape	Test Method	Size (mm^3)	Testing Machine	ASTM Standard
Cylindrical	Compression	10 x10	-	-
Cylindrical	Compression	30 x 75	MTS 329.10S	
	Tensile	14 x 74		D-638
	Three Point Bending	14 x 60	Instron 8652	E-399

Rectangular	Tensile Flexural Compression	5 x 13 x 69 5 x 12 x 100 12 x 12 x 24	Universal Testing Machine (Instron 4202)	D-3039 D-790 D-695
Rectangular	Compression	25 x 25x 12.5	-	C-365 M-91
Rectangular	Flexural	125 x 10 x 6	Shimadzu 5000	D 790M-92

Preparation of the specimens was done accordingly in line with each standard applicable for each test. But before that, molds used for the fabrication of the specimens were properly cleaned with acetone and white tissue paper was used to wipe and dry the mold. Thereafter, the mold was coated with wax for easy removal of the specimen without sticking to the mold due to the heat generated during the mixture. Stir mixing is the most common method used for the fabrication of syntactic foam because it helps in controlling the porosity generated during mixture and the release agent often used is silicone gel. Other forms of mixing can be adopted where applicable such as conventional mixer using a glass rod, stir mixer using machine, using a stir magnetic bar as a mixer. During mixing, a careful observation must be made in order not to break the microballoons.

2.3.2 Properties of Syntactic Foam Composites

Syntactic foam has a special structure between the filler and the binder resulting in some valuable properties, such as low coefficient of thermal expansion, high strength-to-weight ratio, low density, good acoustic property, low moisture absorption, and good resistance to hydrostatic pressure. Most of these special properties are caused by some factors such as the filler sizes, type of binder used, volume fraction considered, void fraction, filler/matrix interface, and condition of manufacturing which allows unique applications (Wouterson *et al.* 2005). Syntactic foams are lightweight which makes them good material for marine, submarine, and floating devices. Their mechanical properties are better than that of other foams with porosity in the matrix material making them a good choice in reinforcement. When reinforced, their properties change from that of plain syntactic foam, and this is mostly done with a matrix such as epoxy, phenolic, and vinyl ester resins (Nikhil Gupta 2013; Kamal 2017). Nanomaterials have been of recent advantages to the reinforced composite in science and technology, especially in the field of multiscale reinforced composites. The structure, physical, and morphological properties of nano and micro-scale reinforced syntactic foam manufactured with

polymer matrix can be analyzed to identify the trend at which their properties might likely affect the design and the application of the composite. In this study, the micro filler (hollow glass microsphere) material is taking into consideration for use in the processing of the syntactic foam. The increasing use of different types of reinforcement in syntactic foams requires knowing and understanding the structure and property correlations for the various types of reinforced syntactic foams to understand the trends that can help in designing lightweight composites for engineering structures (Nikhil Gupta 2013). Syntactic foams can multi-function in that they can be used to perform different purposes and can be tailored for the specific application. For such applications to be unique, their properties such as tensile, flexural, acoustic, compressive, and thermal properties must be known. All these properties are considered and experimented with within this study which is tailored to several studies on such in the literature. The structural application of syntactic foams is controlled by the density and volume fraction of the constituent materials in accordance with their mechanical properties. Compressive property of the syntactic foam is responsible majorly for their structural applications most especially when reinforced with other materials such as warp knitted spacer fabric (SF-WKSF) (Chao Zhi. 2015), carbon fabrics (Omar *et al.* 2015; Yaseer Omar *et al.* 2015; Lamanna *et al.* 2017), carbon nanofibers (Poveda, Dorogokupets and Gupta 2013), glass-fiber/polymeric matrix (Alberto Corigliano 2000; Baedella Lorenzo 2001; Karthikeyan, Sankaran and Kishore 2007; Salleh *et al.* 2016; Daniel Paul. 2018), and resin impregnated paper honeycomb (RIPH) (Kumar and Ahmed 2013). The compressive strength and modulus of syntactic foam very generally with different types of foam composite in respect to their density, this can either be epoxy syntactic foam (Gupta *et al.* 2006; Yung *et al.* 2009; Ghamsari, Zegeye and Woldesenbet 2013; Huang *et al.* 2016; Bardella *et al.* 2018; Daniel Paul. 2018), vinyl ester syntactic foams (Adel Shams 2017), polyetherimide (PEI) syntactic foams, magnesium alloy syntactic foam (Anbuchezhiyan *et al.* 2017), cyanate ester syntactic foam (B. John 2010), high-density polyethylene (HDPE) syntactic foams (Bharath Kumar *et al.* 2016b; Cosse *et al.* 2019b), A356 aluminum alloy syntactic foam (Taherishargh *et al.* 2015) and more were studied in the literature.

2.3.2.1 Physical Property

The physical properties of SFC such as density and water absorption are discussed in this section as they affect the functionality of the composite material.

2.3.2.1.1 Relative Density

Relative density (i.e., physical magnitude) is a quick, efficient, and important factor in determining the structure and quality of hollow and solid materials. Such properties in polymer composites tend to increase, decrease, or both with density. Determining and analyzing the density of SFC thus

becomes important for the tracking and identification of physical changes in the polymer composite (Rane *et al.* 2021). Relative density is mostly studied in terms of the difference between the theoretical and experimental densities. The theoretical density is calculated based on the rule of the mixture while the experimental density is measured by dividing the weights of selected samples by their respective volumes (Qiao *et al.* 2015, 2016; Manakari *et al.* 2017; Ozkutlu, Dilek and Bayram 2018; Patil, Kubade and Kulkarni 2020; Afolabi, Kanny and Mohan 2021a; Afolabi, Kanny and Mohan 2021b).

2.3.2.1.2 Water Absorption

Water absorption is a means of testing the capacity of the syntactic foam in an aqueous environment. Water is considered to remain in a single free phase driving to penetrate the resin by the water concentration gradient. Water absorption can cause swelling and plasticization of SFC (Mortensen 2007). Under most conditions, water can penetrate the materials in several directions. In general, the coefficient of diffusivity varies with the direction so edge effects can become important and should be considered in any analysis of water uptake of SF structures that present more than one surface to water diffusion. It must also be noted that water penetration into resin matrix composites can lead to changes in mechanical properties. Water absorption of SFC can be performed on different water conditions such as freshwater, saltwater, and deionized water at room temperature (Tagliavia, Porfiri and Gupta 2012). The absorption of moisture or water absorption can change the density and mechanical properties of the SFC, which causes a change in the attenuation coefficient (Gupta and Woldesenbet 2003).

Moisture absorption is used to identify the sustainability of syntactic foam when different conditions are applied. The ASTM standard that will be applicable to this test are ASTM D570 or ASTMD 5229-92, or another as specified in the literature. Water absorption has been used to test the final product in marine applications such as the buoyancy effect, which is due to the degradation mechanism of syntactic foam and the combined effect of pressure, temperature, and water ingress (Tagliavia, Porfiri and Gupta 2012). Moisture absorption is increased when the void is present, and porosity breakage from glass microballoons in a specific direction occurs (Gupta N 2003;). Two types of water conditions have been used during this testing: deionized water (D.I. water) and saltwater (S.W. water), in two different temperature conditions, room temperature and 70oC - 80oC. The unit to determine the water absorption content is in weight percentage (%).

2.3.2.2 Mechanical Properties

It is important to understand the functionality of SFC by considering its applicability through the examination of its mechanical properties. Modern engineering practice makes continual demands upon the material and many of the time-honored approximations made by designers. When an engineer specifies the use of a particular material for use in each application, he does so from the consideration of the mechanical properties of the material.

The mechanical properties of an SFC are not governed by reinforcement alone but by a synergy between the reinforcement and the matrix. Along with several other factors, the mechanical performance of an SFC is expected to depend on the following factors:

- wettability and interfacial bonding,
- the volume fraction of the fillers,
- thermal stability,
- the aspect ratio of the reinforcements,
- dispersion of the fillers in the matrix,
- fiber orientation,
- the crystallinity of the matrix
- density of the filler material

SFCs generally possess good stiffness and tensile characteristics.

2.3.2.2.1 Hardness Test

Hardness is a measure of the resistance to localized plastic deformation induced by either mechanical indentation or abrasion. In general, different materials differ in their hardness; for example, hard metals such as titanium and beryllium are harder than soft metals such as sodium and metallic tin, or wood and common plastics. Macroscopic hardness is generally characterized by strong intermolecular bonds, but the behavior of solid materials under force is complex; therefore, there are different measurements of hardness: scratch hardness, indentation hardness, and rebound hardness. Manakari *et al.* (2017), studied the microhardness measurement of pure magnesium (Mg) and SFC, where it was reported that the progressive addition of HGM particles resulted in a steady rise in the hardness of pure Mg.

2.3.2.2.2 Tensile Test

The tensile properties of syntactic foam measure the ability to which the composite can withstand longitudinal stress before breakage or without breakage. Tensile properties are very useful,

especially for the structural application of syntactic foam for sandwich purposes, to characterize their behavior and failure mode in structural core modifications (Salleh *et al.* 2016; Yalkin, Icten and Alpyildiz 2017). The nature of syntactic foam under uniaxial tension is much less desirable, with brittle fracture occurring often. Tensile strength for uniaxial loading varies between 25-55% of the compressive strength depending on the type of HGM used, but the modulus in tension is much less than the compressive modulus (Gupta and Nagorny 2006; Young 2007; Hu and Yu 2011). Tensile strength has been reported to increase with a decrease in microballoons volume fraction and increased with microballoons density (Gupta and Nagorny 2006; Hu and Yu 2011).

An ASTM D 638 standard will be used in this study for the dog bone shapes, with an appropriate range of relative dimensions. It is easy to grip and has comfortable workability in a universal testing machine, and axisymmetric bars with tapered cross-sections were preferred. Figure 2.5 shows the dog-bone specimen and its geometry diagram and the sample specification of the tensile test.

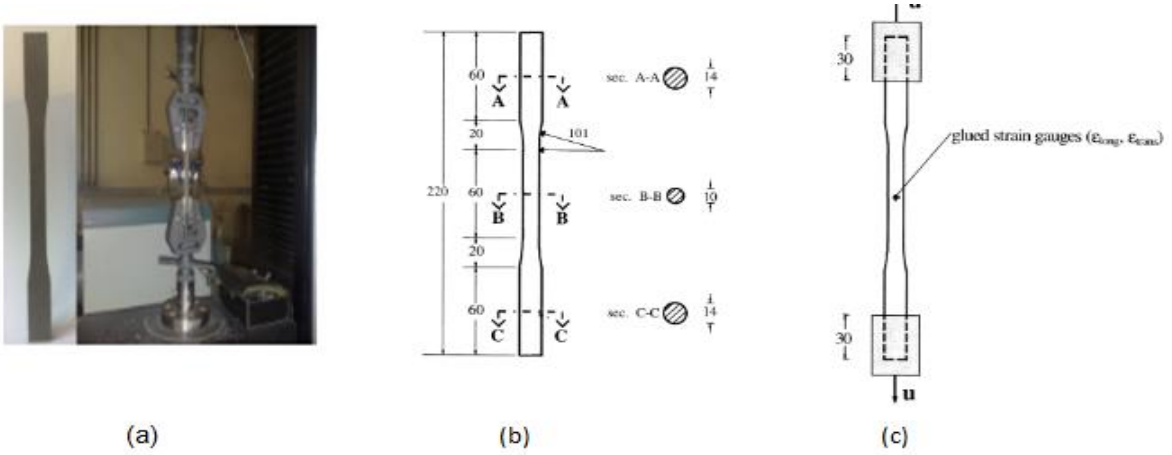

Figure 2.5 Syntactic foam tensile test sample: (a) sample and test machine, (b) geometry and dimension of specimen, (c) displacement control (Rizzi, Papa and Corigliano 2000).

An increase in the volume fraction of microballoons leads to a reduction in the tensile strength of syntactic foams, this simply shows that the tensile strength of syntactic foams is significantly influenced by the microballoons content (Ahmadi H 2016). The tensile strength of other materials reinforced with syntactic foams has also been investigated. Dimchev, Caeti and Gupta (2010); Colloca, Gupta and Porfiri (2013) reported that the tensile properties were enhanced by the presence of nanofibers because of the role played by the matrix during fracture under tensile loading of the composites. In other work, the glass-bead filled polypropylene composite tensile properties increases with an increase in glass bead concentration but with a difference in toughness between

the two types of bead used (Liang J.Z. 2000). Wouterson *et al.* (2007) reported a significant increase in the ultimate tensile strength of fiber reinforcement on the syntactic foam composite which is an improvement considered impressive in polymer composites. This study examines the tensile strength of syntactic form both in the plain form and when reinforced with hybrid glass and natural fibers.

2.3.2.2.3 Flexural Test

Flexural testing is performed using a three-point bend or four-point bend configuration apparatus on a machine. Flexural strength or bending strength or transverse rupture strength is the property of a material, defined as the maximum stress in bending in the outermost layer of the SFC just before its yield point. This is calculated at the surface of the specimen on the convex or tension side of the SFC. The flexural modulus of SFC is calculated from the slope of the stress against the deflection curve. Flexural modulus of SFC is important because it enables the fracture test procedure used to be validated using the specimen deflection and maximum load to failure and it also determines the strain energy release rate of the fracture specimen (Young 2007). Several studies have been done on the flexural properties of SFC with different methods, fillers, and matrices. Bharath Kumar *et al.* (2016b) used injection-molded cenosphere/HDPE to study the surface treatment of the flexural properties of SFC. The study shows that the flexural strength of SFC increases with the cenosphere content. Likewise, Doddamani *et al.* (2015) used functionally graded fly ash cenosphere and epoxy resin in their study of SFC flexural property. Moreover, Karthikeyan, Sankaran and Kishore (2005) studied the effect of fiber reinforcement on the flexural behavior of syntactic foam, using epoxy resin, HGM, and chopped strands of E-glass fiber. Also, Liang (2005) in his study used hollow glass beads and ABS matrix in the composite for flexural properties using a twin-screw extruder. And recently, Patil, Kubade and Kulkarni (2020) examined the properties of hybrid HGM/fly ash cenosphere filled vinyl ester SFC using the hand layup method to avoid the breakage of the microballoons. This same hand layup method was adopted in this present study.

2.3.2.2.4 Impact Test

Charpy impact test are used to identify the fracture resistance of the SFC, it is mostly done at room temperature using a Houndsfield Impact tester. Few studies have been done on the impact test of composite material. Jefferson Andrew *et al.* (2015) reported that the impact stiffness between repaired composite and unrepaired composite, the impact stiffness of the repaired was more consistently higher than the unrepaired composite which acknowledges a good impact resistance between the bonding of the composite materials. Also, Davies *et al.* (2004), studied the impact behavior of sandwich panels with carbon epoxy skins and aluminium honeycomb core. The robust

panel were more energy absorber than the thin skins because the impactor forced the back-face of the skin to debond massively. Moreover, Patil, Kubade and Kulkarni (2020), in their own study discovered that the absorbed impact energy decreases inversely to the volume % of the HGM in vinyl ester matrix syntactic foam and rises with an increase in wall thickness of HGM. SFC generally possesses good stiffness and can absorb impact resistance when subjected to impact test.

2.3.2.2.5 Hardness Test

The hardness property of the syntactic foam composite is a measure of the resistance to localized plastic deformation induced by either mechanical indentation or abrasion. In general, different materials differ in their hardness; for example, hard metals such as titanium and beryllium are harder than soft metals such as sodium and metallic tin, or wood and common plastics. Macroscopic hardness is generally characterized by strong intermolecular bonds, but the behavior of solid materials under force is complex; therefore, there are different measurements of hardness: scratch hardness, indentation hardness, rebound hardness, and microhardness (Manakari *et al.* 2017).

2.3.2.3 Structural Properties

2.3.2.3.1 Attenuated Total Reflectance Fourier Transform Infrared Spectroscopy (ATR-FTIR)

The Fourier Transformed Infrared Spectroscopy (FTIR) helps in investigating the relationship existing between the structure of polymer composites and their structure sensitive properties by determining molecular interactions. It also helps in surface modification of SFC and good interface formation. Mutua *et al.* (2012), investigated the importance of surface modification in ensuring an excellent interfacial adhesion between polymer and HGM. A strong interfacial bonding between the reinforcement and the matrix enhances the properties of the resultant composites by facilitating good load transfer between the matrix and the HGM filler. Huang *et al.* (2016), used FTIR to detect the chemical bonding between the hollow glass microspheres and coupling agent groups.

2.3.2.4 Thermal Properties

2.3.2.4.1 Thermal Gravimetric Analysis

Thermal gravimetric analysis [TGA] was used to determine the thermal stability and decomposition characteristics of extracted nano-cellulose fibers, i.e., decomposition temperature and residue. Lightweight structural thermal insulating SFC has a limited number of applications in space and deep-sea exploration, as well as aerospace, marine, and civil infrastructure. Designing SFC with both high strength and thermal insulating properties is difficult because the two properties contradict each other. Therefore, selecting the materials such as the matrix and the volume fraction of HGM

will affect the results of the thermal properties (Salleh 2017a). The application to a thermal insulator is based on the subject of high temperatures, resulting in thermal properties such as glass transition temperature, T_g using TGA testing. For this study, TGA was performed from 30℃ to 500℃, with a heating rate of 10℃/minute. Thermal characterizations form part of the main study of this research work. The thermal conductivity of the SFC can be evaluated according to effective thermal conductivity models. Qiao *et al.* (2015), studied that the thermal conductivity of the composite decreased with the increase in HGM volume fraction.

2.3.2.4.2 Dynamic Mechanical Analysis

The behavior of syntactic foam is quite like the behavior of metal matrix composite combined with features of conventional foams. Dynamic mechanical analysis (DMA) is most useful for studying the viscoelastic behavior of polymers. Sinusoidal stress is applied and the strain in the material is measured, allowing one to determine the complex modulus. It can simply be described as applying an oscillating force to a sample and analyzing the material's response to that force. The amplitude of the deformation of the composite materials at the peak of the sine wave is measured and the lag between the stress and strain sine waves, thereby, given the measurement to quantities like modulus, viscosity, and damping coefficient (Peroni *et al.* 2012; Steven Eric Zeltmann 2018; Menard 2020).

2.3.2.5 Morphological Properties

2.3.2.5.1 Scanning Electron Microscopy (SEM)

The micrograph characterization of SFC was used to study the effect of the distribution of HGM in the matrix composition. Micrographs reveal different particle size distributions of HGM filler, secondary phase particles, and the presence of micro-voids at the HGM/matrix interface. The HGM is noted to be having an outer diameter between 36-120um due to its particle size variation (Afolabi, Kanny and Mohan 2021a) and exhibited good morphology variations within the microstructure (Manakari *et al.* 2017).

2.3.2.5.2 Transmission Electron Microscopy (TEM)

Transmission electron microscopy is a method of characterization used to investigate the distribution of particles in composite materials. The distribution can be done at different specifications. This technology reveals the structure, crystallization, morphology, and stress of the filler substance whereas scanning electron microscopy can only provide information about the morphology of a

specimen. However, TEM requires very thin specimens that are semi-transparent to electrons, which can mean sample preparation takes longer (Hu and Yu 2011)

2.3.3 Advantages of Syntactic Foam Composites

SFC is lightweight composite material applicable in different sectors and organizations or industries. Some of these applications include:

1. Aircraft: currently a large variety of SFC components are used in aircraft e.g. as primary structural components such as wing box, empennage box, fuselage, the control components, interior components, and exterior components (Gay Daniel 2003), Boeing (Chicago, IL) and Airbus Americas (Herndon, VA) have both used SFC as reinforcement in the hollow arrears within the aircraft (Gupta *et al.* 2013).
2. In Helicopters: SFC is used for the blade of the helicopter which consists of an envelope or a box that assures an aerodynamic profile and a stiffener for torsion, a filler material that prevents the deformation of the profile. The blade is molded by two shells under pressure and helps to control the stiffness and torsion.
3. Yoke rotor: this is a mechanical assembly that allows the rotation of the blades and the small amplitude angular displacements of the blades during rotation (Gay Daniel 2003).
4. Automobiles: SFC is applicable for automobile manufacturing components such as the roof, doors, seat frames, side panel, hatchback door, motor cap, headlight supports, oil tanks, transmission shaft, chassis parts, etc.
5. In marine structures: SFC is applicable naturally in the marine world for buoyant behavior because of its low moisture absorption and high hydrostatic compressive strength. Marine structures are still the primary application sector for SFC, they are used as blocks in the forward and aft free-flood areas of the Trelleborg Emerson & Cuming (TEC) and Trelleborg Offshore (Gupta *et al.* 2013).
6. Oil and gas industry: the thermal insulation properties of SFC have been used in insulation for oil pipelines.
7. Consumer Products: The sports industries have employed the usage of SFC to produce the soccer ball. The ball used for the 2006 World Cup was produced by Adidas Inc., from a polyurethane SFC. The SFC layer helped in regaining the spherical shape of the ball immediately after being kicked, thereby enabling it to travel further and in the precise trajectory (Gupta *et al.* 2013)
8. Furniture Industry: Synthetic wood is produced from the combination of polyvinylidene chloride saran microballoons mixed with epoxy or polyester. The product has a similar feel to

real wood and can accept machine screws, nails, and staples. Unlike natural wood, synthetic wood is highly resistant to moisture exposure and is used in small boats, synthetic marble bathroom fixtures such as bathtubs (Gupta *et al.* 2013).

9. Food container: SFC is used to produce the Eccolite food product line, approved by the U.S. Food and Drug Administration for usage in food and beverage containers. SFC with the thermoplastic matrices is capable of withstanding repeated thermoforming, allowing the containers to be recycled repeatedly.
10. Composite Tooling and Vacuum-Forming Plug Assists: SFC is used as composite materials tooling boards and plug assists because of their thermal stability, low weight, low conductivity, and easy machining (Gupta *et al.* 2013).

2.3.4 Disadvantages of Syntactic Foam Composites

The main disadvantage of syntactic foams comprising glass-based microspheres is that they are stiff, brittle and are prone to damage when they are exposed to large strains and are therefore not recoverable (Yousaf *et al.* 2020).

2.4 Sandwich Foam Composites

The sandwich foam composites construction is a form of sandwich structure that is widely used in many applications mainly because of its concept that is suitable for lightweight structures.

2.4.1 Processing of Sandwich Syntactic Foam Composites

Processing of sandwich foam composites is majorly in two forms: firstly, the preparation of the face sheets and secondly, the joining together of the core and the face sheets. Cores are the middle part of the sandwich composites which are based on the performance requirements and applications to be used for. The core material must have adequate shear stiffness to absorb applied shear forces, distributing them over a large area, and low specific weight, being joined to the faces mechanically or by adhesive bonding (Garay, Souza and Amico 2016). Three main categories of popular core materials are: low density solid materials-open and closed-cell structured foams, expanded high-density materials in the cellular form: honeycomb, web core, and expanded high-density materials in the corrugated form: truss, corrugated sheets. Some of the cores mostly used are wood, polyurethane, polystyrene, polyethylene terephthalate (PET), and polyvinyl chloride (PVC) foam core. Using syntactic foam as core materials enhances weight saving in the marine application and contributes to improving the performance of the sandwich structure which is not common in use (Tagliavia, Porfiri and Gupta 2010; Salleh *et al.* 2016).

The skin or face-sheet of the sandwich composites is known to be the carrier of the compressive, tensile, shear, and flexural strength resultants acting parallel to the sandwich panel while the thicker core provides the reinforcement and ensure adequate shear stiffness with low specific weight to absorb applied shear forces. Adhesive is used to connect the core and the face-sheets to ensure a structural continuity across the sandwich panel depth. When the combined weight of the skin (face-sheet) is almost as that of the core, an efficient sandwich composite structure is produced (Amran Alias. 2007; Vitale *et al.* 2017).

2.4.2 Properties of Sandwich Syntactic Foam Composites

The properties of sandwich foam composites depend upon the properties of the core and skins, their relative thickness, and the bonding characteristics between them. Sandwich foam composites typically consist of two materials, the face sheets, and the thicker lightweight core. The face sheets is the one carrying the bending and the in-plane loads while the core provides the flexural stiffness and the out-of-plane shear and compressive strength (Kanny and Mahfuz 2005). Sandwich structured composites are a special class of composite materials that have become very popular due to their high specific strength and bending stiffness. Sandwich panels are known for their good reliability and applicability in different sectors and industries such as automobile, marine, wind turbine, aerospace, railway system, and structural application. The low density of these materials makes them especially suitable for use in aeronautical, space, and marine applications (Gupta 2003). A sandwich composite comprises two stiff panels or face-sheet which are light materials are joined with a thick form core. This is done to provide the composite material with high bending stiffness and a low density.

The concept of sandwich structure has been in use for more than two decades with several methods of processing. Many core and skin layers have been used in the past by researchers for the sandwich panels but nowadays, syntactic foam core is most preferred for the composite sandwich panels because of their high bending rigidity, good thermal insulation, better acoustic damping characteristics, and lighter weight (Salleh *et al.* 2016; Ahmadi and Liaghat 2019).

2.4.2.1 Physical Property

2.4.2.1.1 Mechanical Properties

2.4.2.1.1.1 Hardness Test

The hardness property of the sandwich foam composite is a measure of the resistance to localized plastic deformation induced by either mechanical indentation or abrasion. In general, different materials differ in their hardness; for example, hard metals such as titanium and beryllium are harder

than soft metals such as sodium and metallic tin, or wood and common plastics. Macroscopic hardness is generally characterized by strong intermolecular bonds, but the behavior of solid materials under force is complex; therefore, there are different measurements of hardness: scratch hardness, indentation hardness, and rebound hardness.

2.4.2.1.1.2 Tensile Test

The tensile properties are a very useful characterization method, especially for the structural syntactic foam of the sandwich type, to understand their behavior and failure mode. Presently, few studies are available on the behavior of tensile properties of sandwich foam composite (Salleh 2017a). An ASTM C297 standard will be used in this study to evaluate the tensile properties of the sandwich foam composite. Enhancement in the tensile strength of sandwich foam composite can be achieved by using high-density microballoons for the core material, however, this may lead to a reduction in fracture strain and may damage tolerance properties. Hence, there is a need to determine the low cost and efficient methods to increase tensile characteristics of sandwich foam composite without degrading their damage tolerance properties (Salleh 2017a). Tensile properties of sandwich foam composite with skin paper were studied by (Islam and Kim 2011) where the tensile strength and modulus of the paper skin increased by 0.6% and 8.3%, respectively, as a result of fast-drying adhesive. Salleh *et al.* (2016), studied the effect of tensile properties on the sandwich composite made of syntactic foam and glass fiber reinforced plastics, the results showed that the tensile strength of the syntactic foam sandwich composite decreased when the glass microballoons content increased.

2.4.2.1.1.3 Flexural Test

Islam and Kim (Islam and Kim 2011), studies the flexural properties of sandwich foam composite where the properties of both syntactic foams panels appear to be similar with the same volume fraction of starch. Three-point bending test was carried out on the sandwich fiber-reinforced syntactic foam composite by Karthikeyan, Sankaran and Kishore (2007), where the flexural modulus values of the fiber-reinforced syntactic foams increased with fiber content. The increase was attributed to the increase in the load-bearing capacity of the fibrous reinforcement and density, despite the void level. Also, Gupta and Woldesenbet (2005), investigated flexural properties of glass micro-balloons/epoxy-based syntactic foam core sandwich composite for different radius rations, the results showed that the flexural strength increased with a decrease in the radius ratio. Moreover, Salleh *et al.* (2016), studied the effect of flexural properties on the sandwich composite made of syntactic foam and glass fiber reinforced plastics, they observed an increase in the flexural modulus for all the test coupon influenced by the thickness of the skin. Other investigations on the flexural properties of sandwich

composites are on fiber-reinforced composite of synthetic and natural fiber (Sadeghian, Hristozov and Wroblewski 2016), square sandwich panel of mild steel and PU core sheets (Amran Alias. 2007), flax fabrics as face sheet and cork core materials (Sadeghian, Hristozov and Wroblewski 2018), and PVC and E-glass fabrics (Yalkin, Icten and Alpyildiz 2015).

2.4.2.1.1.4 Compression Test

The compressive failures of sandwich composite have been studied by several researchers. Balıkoğlu *et al.* (2018), studied the flatwise compressive performance of marine sandwich composite, it was reported that the compressive strength and modulus increased by increasing the quantity of the resin pins in the foam core. Gupta, Woldesenbet and Mensah (2004), studied the flatwise compressive properties of cenospheres/epoxy-based sandwich foam composites for different radius ratios of cenospheres. The results showed that there is an increase in the compressive strength due to a decrease in the radius ratio of cenospheres. Also, Kumar and Ahmed (2013), conducted two compressive tests flatwise (to determine properties under out-of-plane) and edgewise (to determine properties under in-plane load) on the sandwich foam composite. They reported that the flatwise compressive properties show a sudden drop in the stress-strain curve. The edgewise compression was seen to show a complete failure of the coupon by vertically splitting the core.

Moreover, Salleh *et al.* (2016), studied the effect of compressive properties on the sandwich composite made of syntactic foam and glass fiber reinforced plastics, they observed that the compressive modulus of elasticity reduced with an increase in the glass microballoons content in the syntactic foam cores. However, the compressive maximum yield stress and the maximum yield strain were observed to decrease with an increase in the glass microballoons content in the syntactic foam core.

2.4.2.1.1.5 Impact Test

The impact test has been used to investigate the fracture resistance of composite materials using either Charpy impact or Izod impact test method. Resistance to impact on aluminum matrix syntactic foam was studied by Altenaiji *et al.* (2014); Ahmadi and Liaghat (2019), where the velocity of the impact loading was used to evaluate the effectiveness of the mechanical performance of the aluminum sandwich syntactic foam. The ability of sandwich composite material to withstand sudden external forces has been studied via impact testing (Altenaiji *et al.* 2014). Also, Li and Muthyala (2008), studied the impact characterization on sandwich structures with an integrated stiffened syntactic foam core where the residual impact strength of the sandwich was on the positive side.

Effect of impact strength as it affects the face-sheets of the sandwich composite is of importance which will be the focused area during this experiment.

2.4.2.2 Buoyancy Properties

Buoyancy or upthrust is an upward force exerted by a fluid that opposes the weight of a partially or fully immersed object. Buoyancy force arises because of variations of density in a fluid subject to gravity and produces a wide range of phenomena of importance in many branches of fluid mechanics. This force acts on an object and it is directly proportional to the volume for the object that is submerged i.e. the more the weight of the solid object that is submerged, the greater the force of buoyancy that acts on it (Bess Ruff 2022). Ren *et al.* (2016); Ren *et al.* (2017a) developed buoyancy material with hollow glass microsphere and SiO_2 and studied its characteristic for high-temperature resistance application. The HGM bonded by borosilicate glass produced good compressive and thermal properties of 14.46 MPa, and 0.15 W/m K respectively, and are potentially applicable in deep-sea exploration.

2.4.2.3 Acoustic Properties

Acoustic is done to measure the sound absorption capacity of sandwich composite, the extent to which a sandwich material can emit or retain external noise. Cosse *et al.* (2019a), studied the sound absorption coefficient on the neat HDPE and the syntactic foam composite using frequencies between 250Hz to 3150Hz. The syntactic foam was found to perform a better sound absorption coefficient than the neat HDPE. Also, Prabhakaran *et al.* (2019) investigated the effect of sound and vibration responses on natural-based composite sandwich material with flax and agglomerated cork face-sheets. It was discovered that flax fiber-reinforced sandwich composites have a higher sound absorption capacity of 45-96% than the glass fiber reinforced sandwich composite with no reference to core density. Most of the acoustic absorption was done on a single face-sheet sandwich composite, there is a need to test the absorption capacity of hybrid face-sheet in the sandwich composite. Hashimoto (2001), reported the measurement of sound radiation efficiency by discrete calculation method which gave a considerable high precision sound radiation capacity for the vibration of an object. Conta, Santoni and Homb (2020), studied the benchmarking of the vibration velocity based measurement method to determine the sound power of a room using three different approaches: the Rayleigh Integral Method (RIM), the Discrete Calculation Method (DCM) (Hashimoto 2001), and the Integral Transform Method (ITM). The three methods were found to be in good agreement with the sound power obtained from the sound pressure measurement. The present study evaluates the acoustic vibration measurement in sandwich composites for structural application based on the existing literature. The frequency of vibration is ~200Hz.

2.4.2.4 Morphological Properties

2.4.2.4.1 Scanning Electron Microscopy (SEM)

Fractured surfaces for each hybrid sandwich composite were examined under scanning electron microscopy (SEM) by gold coating each of them and placed under the Zeiss EVO 1 HD 15 Oxford instrument X-max SEM machine. SEM is done on hybrid sandwich composites to describe the microstructural pattern of the fractured impact on the SSFC during mechanical testing. Karthikeyan, Sankaran and Kishore (2007), investigated the bending modulus of fiber-reinforced syntactic foams for the sandwich and structural applications where the strength was reduced because of the accumulated voids entrapped in the fibers. This further led to the clustering and bunching of fibers. Gupta, Woldesenbet and Kishore (2002), investigated the response of syntactic foam sandwich structured composites in three-point bending such that the skin failed due to micro-bulking due to the integral bonding of the syntactic foam core to the skins and large aspect ratio used for the test. Such that the shear stresses at the skin-core interface were not enough to cause de-bonding at the skin-core interfacial fracture. This is one of the r set-back of this report. Also, Prabhakaran *et al.* (2019) reported through SEM images that the glass fibers prevented the sound waves from entering into the structure thereby reducing the sound absorption capacity. This is a setback in this report which we shall be improving upon in this research by using hybrid face-sheets.

2.4.3 Advantages of Sandwich Foam Composites

Some of the advantages and applications of sandwich foam composites include:

- The possibility of tailoring properties by choosing appropriate constituting materials and their volume fractions.
- Large availability choice of constituents for core and skins
- Low density leads to saving of weight.
- High bending stiffness
- Higher damage tolerance
- In-situ fabrication
- Good vibration damping capacity.
- Low density leads to saving of weight.
- Structural applications in aircraft, spacecraft, submarine, ships, and boats, surface transport vehicles, building materials, etc.

2.4.4 Disadvantages of Sandwich Foam Composites

Some of the disadvantages associated with sandwich foam composites are:

- Higher thickness of sandwich foam composite
- Higher cost of preparation and processing
- Difficult to join.
- Difficult to repair if damaged.

2.5 Conclusion

From the above information on syntactic foam composite and sandwich foam composites, it was clear that its application well suits the fabrication of structural applications. Hence through our research study, we propose a technique, wherein the processing and shape of fillers are considered.

Further, **Chapter 3** discusses in detail the materials, methods, and processing techniques adopted in this study to fabricate syntactic foam composite and sandwich syntactic foam composite.

CHAPTER 3

3.0 MATERIALS AND METHODS

3.1 Introduction

This chapter focuses on the research materials, manufacturing procedures, and characterization methods. Let's start with the materials that are utilized to make the syntactic foam composite (SFC) and sandwich syntactic foam composites (SSFC). The physical, tensile, flexural, impact, hardness, and fracture mechanisms of hollow glass microballoons/epoxy SFC were characterized. The effect of the volume percentage and wall thickness of microballoons on the mechanical properties of the SFC is very important to be investigated. All the specimens were prepared using the open mould method and are tested using an MTS 793 servo-hydraulic machine. A single type of hollow glass microballoons (T60) was used as heterogeneous (unvaried) particle filler and separated into four different homogeneous (varied) particle sizes AA, BB, CC, and DD (20-24µm, 25-44µm, 45-49µm, and 50-60µm respectively). This particle sizes were based on the sieve size available and the output HGM that came out from the mesh and the closeness of the size ranges as retrieved from the mesh were named accordingly (there was no specific mechanism for choosing the sieve apart from their availability). Particle distribution analysis (PDA) was thereafter performed on the HGM using particle size analyzer, to authenticate the sizes gotten from the sieves. Each size was separated into five volume fractions of the microballoons (5, 10, 15, 20, and 25 vol%), and designated as EPT60-5 to EPT60-25, and the neat epoxy (NE) as EPT60-0. The five-volume fractions were chosen for the purpose of experimental comparison and the structural applications of the study. The syntactic foams fabricated were characterized based on their various mechanical properties like tensile, flexural, compression, and hardness, including strength, modulus of elasticity, strain, fracture features, and thermal properties. The effect of the five-volume fractions was also taking into consideration on each particle size variation of the microstructural analysis, mechanical and thermal properties of the syntactic foams. All the specimens were prepared by open resin casting method and poured into silicon mold under room temperature for curing and post-curing before testing with a universal MTS machine. The scanning electron microscope (SEM) and the dynamic mechanical analysis were used to characterize the fracture mechanism and the microstructural analysis of the syntactic foam.

3.2 Materials

Table 3.1 shows the properties of hollow glass microsphere (HGM) specifications from the manufacturer.

Table 3.1 Hollow glass microsphere (HGM) specifications from the manufacturer

Material	Appearance	True density	FRA			Crush strength	Melting point	Floating ratio	pH
		g/cm^3	10th%	50th%	90th%	Psi/MPa	^{o}C	%	
T60	White powder	0.6	18	40	60	10000/69	625	94	8-9.5

Table 3.2 shows the materials that were used for the fabrication of syntactic foam composites (SFC)

Table 3.2: Materials that were used for the fabrication of syntactic foam composite (SFC).

Materials	Supplier
Diglycidyl ether of bisphenol „A" (DGEBA) epoxy resin (LR 20)	AMT Composite, Durban. South Africa
Cycloaliphatic amine-based hardener (LH281)	AMT Composite, Durban. South Africa
Hollow glass micro balloons (HGM T60)	Anhui Industrial Cop, Limited, Hong Kong Elite Industrial Group Limited, China.

Table 3.3 shows the materials that were used for the fabrication of sandwich syntactic foam composite.

Table 3.3: Materials for SSCF

Materials	Supplier
SFC core	Manufactured (Table 3.1)
Kenaf fiber (KF)	CSIR, Port Elizabeth, Durban
Glass fiber (GF)	AMT Composite, Durban.
Diglycidyl ether of bisphenol „A" (DGEBA) epoxy resin (LR 20)	AMT Composite, Durban. South Africa
Cycloaliphatic amine-based hardener (LH281)	AMT Composite, Durban. South Africa

Table 3.4 shows densities of constituent materials used in the fabrication of sandwich composites**.**

Table 3.4: Densities of constituent materials used in the fabrication of sandwich composites**.**

Constituent material	Density (g/cm^3)
Kenaf fiber[1]	0.73
Glass fiber[1]	2.50
Syntactic foam[2]	1.096
Matrix epoxy[1]	1.15

(1) from manufacturer; (2) calculated

3.3 Methods of Fabrication

3.3.1 Syntactic Foam Composites (SFC)

The open resin casting method was used to fabricate SFC for both heterogeneous and homogeneous particle sizes (see Figure 3.1), and degassing method was used to eliminate voids in the composites. The method of fabrication adopted in this study is the stir mixing technique because of its common control style which is one of the main focuses of this study [1]. The syntactic foam composites were fabricated by measuring the matrix resin to be used per specimen in a beaker on a weighing scale and then heated. Figure 3-1 (a) shows the schematic representation and (b) shows the practical procedure of the fabrication process and the viscosity of the matrix were lowered by heating it to 60^{o}C for 1 hour. Then, cooled at room temperature (RT) and volume fraction (5, 10, 15, 20, and 25 vol%) of the HGM filler was added. The composite was manually stirred for 10 minutes thoroughly before hardener was added in ratio 10:3 of the epoxy resin. The composite was transferred to the magnetic stirrer for another 5 minutes to obtain uniform slurry and a homogenous solution to reduce agglomeration. The mixture was poured into the silicon mould and left to cure for 24hours at RT (27^{o}C). The SFC slab was then post-cured for 4hrs at 80±5^{o}C.

Figure 3.2 shows the Retsch magnetic shaker used for the separation of HGM into the four homogeneous particles sizes.

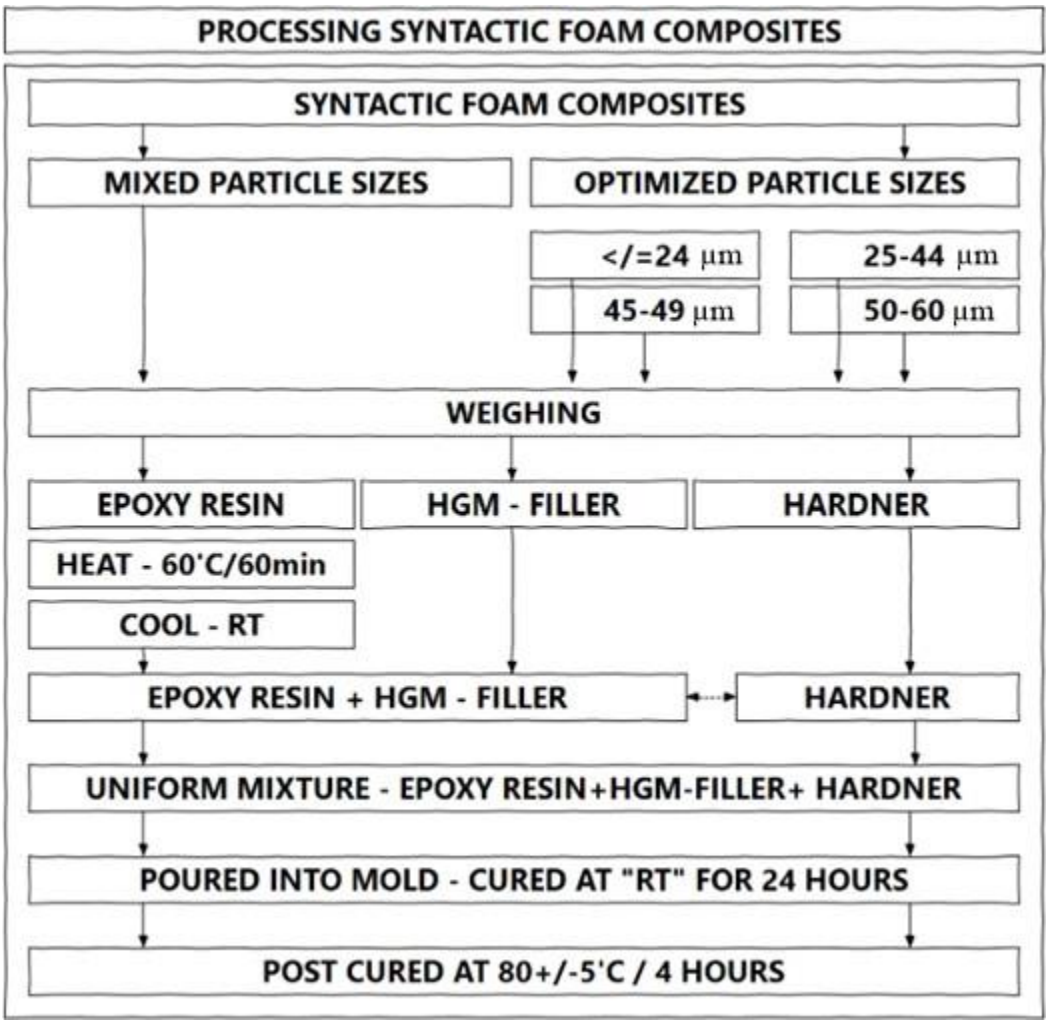

Figure 3.1(a): Schematic representation of open resin casting method for fabrication of syntactic foam composite for both heterogeneous and homogeneous HGM filler particle concentration.

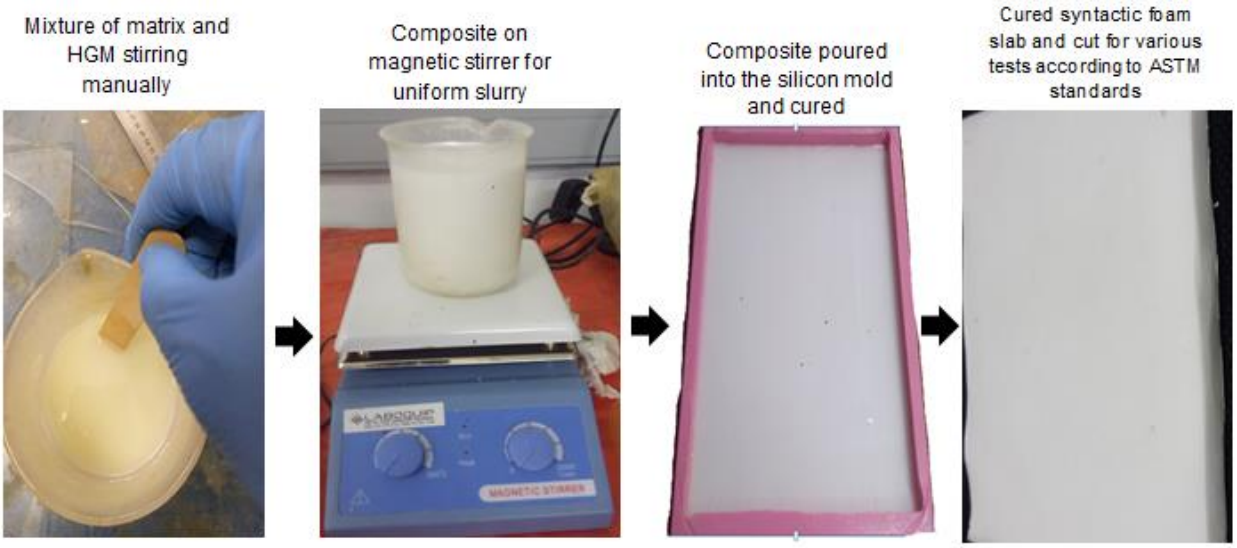

Figure 3.1 (b): Processing sequence of syntactic foam composite

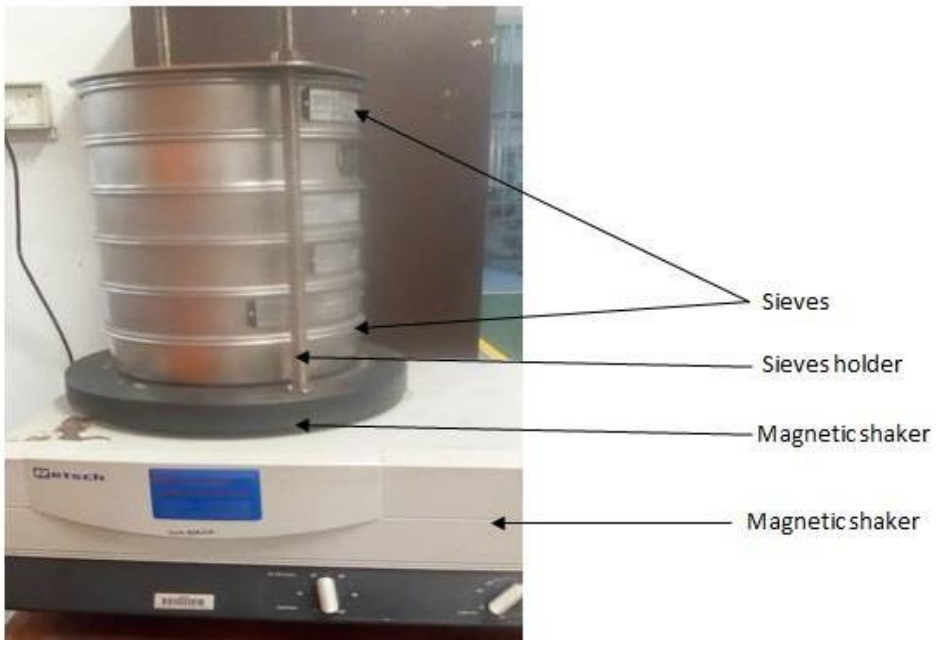

Figure 3.2: The Retsch magnetic shaker used for the separation of HGM into four different particle sizes (i.e., 0-24µm; 25-44µm; 45-49µm and 50-100µm).

3.3.2 Sandwich Syntactic Foam Composites (SSFC)

Figure 3.3 (a) shows the schematic representation and (b) practical process involved in the fabrication of SSFC for the four types of orientations which are: kenaf fiber-syntactic foam-kenaf fiber

(designated as KK), glass fiber- syntactic foam-glass fiber (GG), kenaf/glass fiber- syntactic foam-glass/kenaf fiber (KG), and glass/kenaf fiber-syntactic foam-kenaf/glass fiber (GK). The method adopted was hand lay-up for proper stacking of the face-sheet to the core (i.e., SFC) material. 12 plies of woven glass fiber "6mm" in thickness (6 uppers (3mm) and 6 lower (3mm) layers) were used for GG, 4 plies (two upper (3mm) and two lower (3mm)) of mat kenaf fiber were used for KK, 6 plies of glass fiber (3mm) + 2 plies of kenaf fibers (3mm) were used interchangeably for both GK and KG (3plies glass/1 plies kenaf as upper and lower face-sheet) respectively, (**see Figure 3.3(b) and Appendix 13.1**). The dimension of the slab made for each sample is 320 x 195 x 26 mm^3.

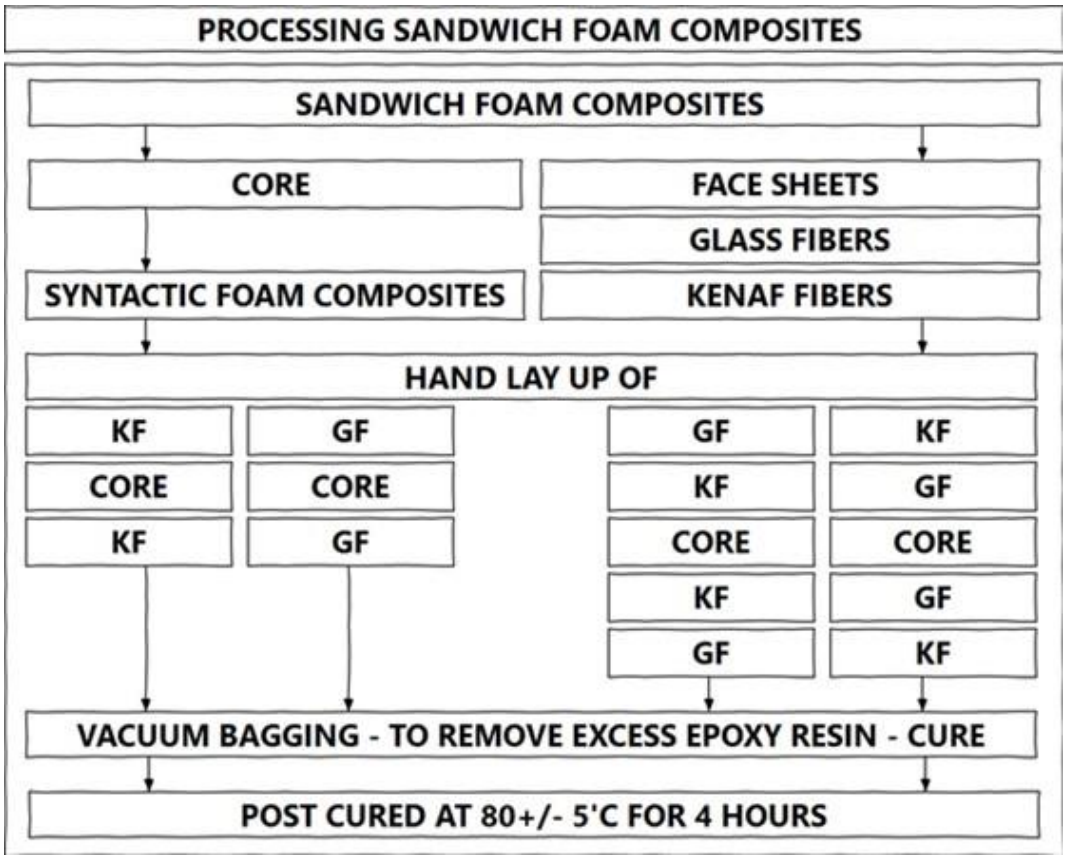

Figure 3.3 (a): Schematic representation of SSFC fabrication process for the four types of orientations which are: kenaf fiber-syntactic foam-kenaf fiber (designated as KK), glass fiber-syntactic foam-glass fiber (GG), kenaf/glass fiber- syntactic foam-glass/kenaf fiber (KG), and glass/kenaf fiber-syntactic foam-kenaf/glass fiber (GK).

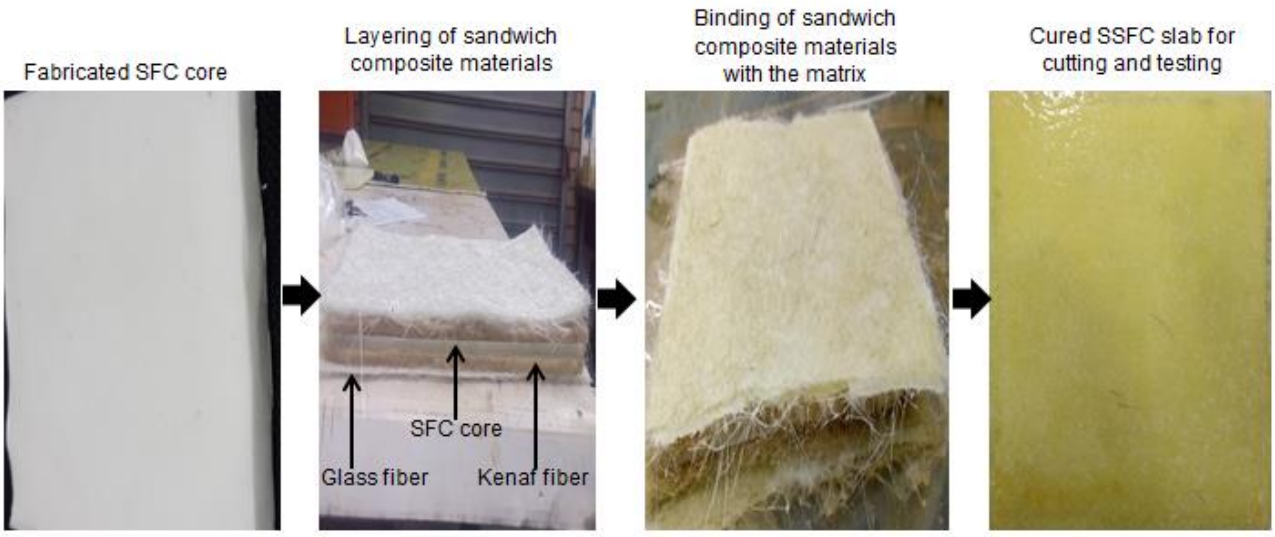

Figure 3.3(b): Practical processes involved in the fabrication of sandwich syntactic foam composites.

3.4 Characterizations

3.4.1 Characterization of HGM, KF, GF, SFC, and SSFC

Table 3.4 presents the characterizations done on the raw materials, syntactic foam composites (SFC) and sandwich syntactic foam composites (SSFC) used in this study.

Table 3.5: Characterization of HGM, KF, GF, and SFC

Material/ Standard	Characterization type	Purpose	Equipment	Number of specimens
	Particle Size			
ISO 13320	Particle Size Analysis of HGM	To measure the diameter of the size ranges of HGM that was collected via sieve	Anton Paar PSA 1190 Particle size analyzer	Five (5)
	Thermal Property			

ASTM D4065	Thermal Gravimetric Analysis (TGA)	It was used to determine the thermal stability	TA Model Q800 V20.6 instrument from the USA.	Three (3) specimens each
		and decomposition characteristics of HGM, KF, and GF (performed from 30^{o}C to 500^{o}C, with a heating rate of 10^{o}C/minute)		
	Morphological Property			
	Scanning Electron Microscopy (SEM)	It was used to study the microstructure of HGM, KF, and GF and the size variation of HGM.	Zeiss EVO 1 HD 15 Oxford Instrument X. The gold coated with Quorum Q 150R ES machine	Three (3) specimen each

3.4.2 Characterizations of Composites

3.4.2.1 Syntactic Foam Composites

3.4.2.1.1. Physical Property

3.4.2.1.1.1 Relative Density

The density of SFC was obtained as measured and theoretical densities. The measured density was determined using ASTM C271-94. The theoretical density was determined using rule of mixture and calculated using equations 3.1- 3.9:

$$V_C = V_f + V_e \qquad 3\text{-}1$$

or

$$v_f + v_e = 1 \qquad 3\text{-}2$$

Also, from

$$V = \frac{m}{\rho} \qquad 3\text{-}3$$

then, $$m_c/\rho_c = m_f/\rho_f + m_e/\rho_e \quad (3\text{-}4)$$

where V, v, m, and ρ are the volume, volume fraction, mass, and density respectively, likewise the subscripts 'c,f, and e' represent composite, filler (HGM), and the epoxy matrix respectively. The density of the syntactic foam composite can therefore be calculated from $\rho_c = \frac{m_c}{V_c}$, the mass of the HGM measured using weighing scale. The pressure applied in forming the specimens is augmented through the volume fraction of the HGM, this is calculated from mass fraction relationship, and the volume of the composite is given as the sum of the matrix and the filler (HGM) volume.

$$\rho_{SF} = \rho_f V_f + \rho_e V_e \quad (3\text{-}5)$$

But V_f was calculated using equation (3.6) or (3.7) while V_e is calculated using equation (4)

$$V_f = \frac{v_f}{v_T} \quad (3\text{-}6)$$

$$V_f = \frac{w_f}{w_f + (1 - w_f)\frac{\rho_f}{\rho_e}} \quad (3\text{-}7)$$

$$V_e = 1 - V_f \quad (3\text{-}8)$$

Where ρ_{SF} is the density of syntactic foam composite, ρ_f and ρ_e are the densities of the HGM and epoxy resin, respectively. Also, V_f and V_e are the volume fractions for the HGM and epoxy resin respectively, w_f, v_f and v_T are the weight and volume of filler and total volume of composite respectively. The value for the void/porosity volume fraction also known as matrix porosity was calculated by estimating the difference between the theoretical or calculated density (ρ_t) and the experimental density (ρ_m) using Equation (3.9) (Karthikeyan, Sankaran and Kishore 2005; Liang 2005; Colloca, Gupta and Porfiri 2013; Qiao *et al.* 2016). The theoretical density was calculated using the rule of mixture. Density is an intensive property, meaning that it does not depend on the amount of material present in the sample. The density is the same irrespective of the particle sizes involved. Therefore, the theoretical density is the same for all the particle size variation because it is not affected by the grain or particle size of its constituent (Fadhil 2015; Farid 2015; Khakbiz 2015; Lund 2022)

$$\delta = \frac{\rho_t - \rho_m}{\rho_t} X\ 100 \qquad 3\text{-}9$$

3.4.2.1.1.2 Radius Ratio Concerning Porosity

The porosity of microballoons affects their radius ratio which can be characterized based on their particle wall thickness (w_t). The radius ratio is the relationship between the outer radius r-out (r_{op}) and inner radius r-in (r_{ip}) of the particle given as η, Equation 3-10. (Gupta and Nagorny 2006; Zhia and Long 2015).

$$\eta = \frac{r_{ip}}{r_{op}} \qquad 3.10$$

The report from Gupta and Nagorny (2006) shows extensively discussion regarding the relationship between the radius ratio and the hollow glass microballoons density (ρ_{MB}), the relationship is shown in Equation 3-11:

$$\eta = \left(1 - \frac{\rho_{mb}}{\rho_g}\right)^{1/3} \qquad 3.11$$

where ρ_g represents the density of the microballoons material which is glass, and it is given as 2.54g/cm^3. The radius ratio is said to be connected to the microballoons and the wall thickness by inverse proportionality ratio. Therefore, if η is the same due to a single type of microballoons used, there will be a difference in the inner radius and wall thickness, but the same microballoons cavity volume as shown in Figure 3-4. The density, wall thickness, particle size, and radius ratio for the single type of HGM used in the fabrication of the syntactic foam are listed in Table 3.5.

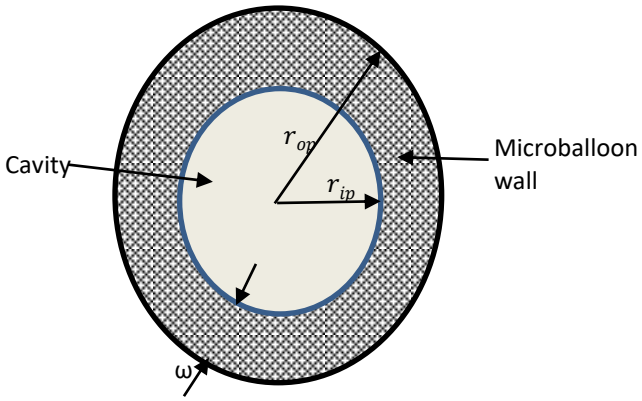

Figure 3.4: Schematic representation of inner radius (r_{ip}), outer radius (r_{op}), and wall cavity (ω) of HGM.

Table 3.6: Particle size (from the specification of the manufacturer), radius ration, wall thickness, and cavity size of the microballoons used for the fabrication of syntactic foam.

HGM size distribution (µm)	Microballoons density ρ (g/cm^3)	Radius ratio η	Outer radius (µm)	Inner radius (µm)	Wall thickness (µm)	Microballoons cavity volume η 3
10	0.6	0.9142	18	16.46	1.54	76.4
50	0.6	0.9142	40	36.57	3.43	76.4
90	0.6	0.9142	60	54.85	5.15	76.4

In the present study, changing the volume fraction (V_{mb}) and particle size variation of the HGM was the primary consideration as it affected different properties of the syntactic foam. Using high-density microballoons at different concentrations produced HGM-matrix interface changes. Since the strength of a composite depends on the interfacial strength between the particles and the matrix, an approach must be derived to keep the interfacial area between the syntactic foam and microballoons properties constant. This present research adopted a scenario of having a constant radius ratio, same cavity volume but different wall thickness (Afolabi, Kanny and Mohan 2021a). The strength and microballoons density ρ_{mb} at various concentrations is affected by the difference in the inner radius and radius ratio. This can also affect the stress concentration generated because of different curvature in the particles. The higher the stress concentration in the syntactic foam with high microballoons V_{mb}, the more the effect of the failure caused (Gupta and Woldesenbet 2003; Li, Luo and Lin 2013). The porosity of the syntactic foam

can be classified into two major categories, which are the matrix porosity $V_{m,p,}$ and the microballoons porosity $V_{mb,p}$. The density of the syntactic foam material is reduced by the closed cell porosity which was caused by the rise in microballoons porosity because of the hollow volume enclosed within the microballoons. The cavity volume fraction in the microballoons structure ($V_{mb,c}$) is given as, Equation. 3-12 (Gupta and Nagorny 2006)

$$V_{mb,p} = \eta^{3} \qquad (3\text{-}12)$$

3.4.2.1.1.3 Water Absorption Capacity of SFCS and SSFCS

Water absorption was used to determine the amount of water the SFCs and SSFCs can absorb under specified conditions. The specimen used were dried in an oven for 3 hours at 60^{0}C and then transferred into a desiccator to cool. Five different specimens were prepared for each composition according to ASTM D570-98. They were weighed immediately after cooling before immersing into a beaker of 200 ml water. The values of the weighed specimen measured were recorded as the initial value (dry weight) for all the specimens. The specimen was left inside the water for a period of 24, 48, 120, 192, 336, and 720 hours at room temperature. Specimens are removed thereafter, dry cleaned with tissues, and weighed. The second values were recorded as the final values (wet weight). The percentage water absorption was calculated using the formula.

$$\%\, water\ absorbed\ (P) = \left({(wet\ weigth\ (W_f) - dry\ weigth\ (W_i))} \Big/ {dry\ weight\ (W_i))} \right) X100 \qquad 3\text{-}13$$

At saturated *water* absorption, i.e when the variation in weight gained after 30days (720hours) is less than 0.1%, the value of the maximum weight gained $M_{(s)}$ was measured for this study. The first measurement taken after the specimens were immersed in the distilled water for over 24 hours is given as $M_{(t)}$. The diffusion coefficient $M_{(d)}$ at maximum moisture absorption of the syntactic foam composites is expressed as

$$M_{(d)} = M_{(s)} - M_{(t)} \qquad 3.14$$

3.4.2.1.1.4 Buoyancy Force Determination of SFC and SSFC

Buoyancy is a measure of an upward force exerted by a fluid that opposes the weight of a partially or fully immersed object. The neat epoxy, SFCs, and the SSFCs samples were

submerged in a test-tube containing water of 400ml. The submerged SFCs and SSFCs were of the same weight for proper comparison. Three specimen each was submerged in the test-tube filled with water shown in Figure 3.5. The force of buoyancy arises because of variations of density in the fluid subject to gravity. The force of buoyancy is given by the Equation 3.15:

$$F_b = V_o \times D \times F_g \qquad 3.15$$

where F_b (N) is the buoyancy force acting on the object, V_o (m^3) is the volume of the submerged object, D (Kg/m^3) is the density of the fluid the object is submerged in, and F_g is the force of gravity (N/Kg).

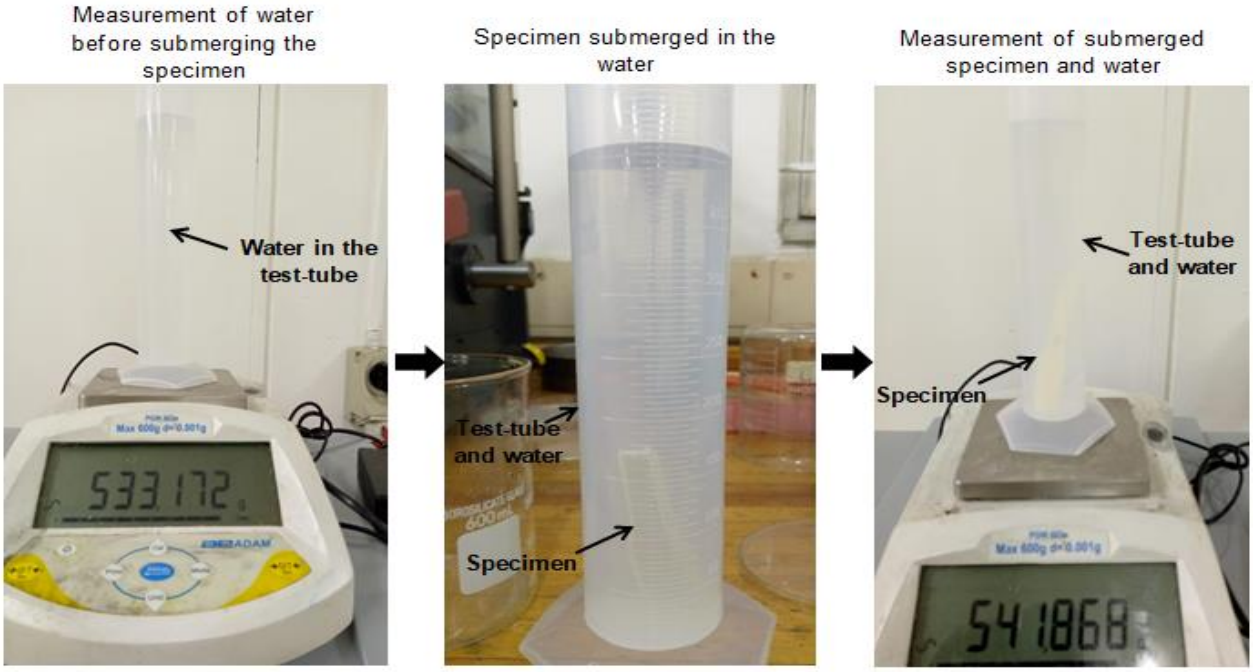

Figure 3.5: Buoyancy measurement procedure for the SFCs and SSFCs

3.4.2.1.2 Mechanical Properties

Mechanical characterizations are an integral part of the study which helped in corroborating the results of mechanical strength of syntactic foam composites. Results from the study related to the mechanical characterization has been published (Afolabi, Kanny and Mohan 2021a; Afolabi, Kanny and Mohan 2021b; Afolabi, Kanny and Mohan 2023) .

3.4.2.1.2.1 Hardness Test

A hardness test was conducted on the syntactic foam composites using Barber Colman GY2J 934.1 Barcol impressor hardness tester. The test was conducted as per ASTM D 2583

test specification. Hardness tests describe the level of indentation the composites can withstand, and this was done by gauging the depth of the indenter point penetration on the specimen shown in Figure 3. 6. The truncated cone of the impresser (6.82 heights and a tip diameter of 0.55 mm) which is hardened steel indentable was placed on each of the samples, at an angle of 260^{o} with a flat tip of 0.157 mm in diameter. Twenty readings were taken per sample and the mean value was recorded.

3.4.2.1.2.2 Tensile Test

Tensile strength and modulus of syntactic foam composites were performed for dog-bone shape specimens as per ASTM D638 test standard specifications, respectively. MTS 793 servo-hydraulic machine with a load cell of 30 KN was used with a strain rate of 50mm/mm and a test speed of 2 mm/min; five specimens were tested for each sample and mean value is considered for analysis. The standard deviation for each round of experiment was considered and reported to validate the accuracy of the test results. Figure 3.6 shows the test set-up for tensile specimen with extensometer on Figure 3.6(a) Tensile test specimen and broken specimen on Figure 3.6(b).

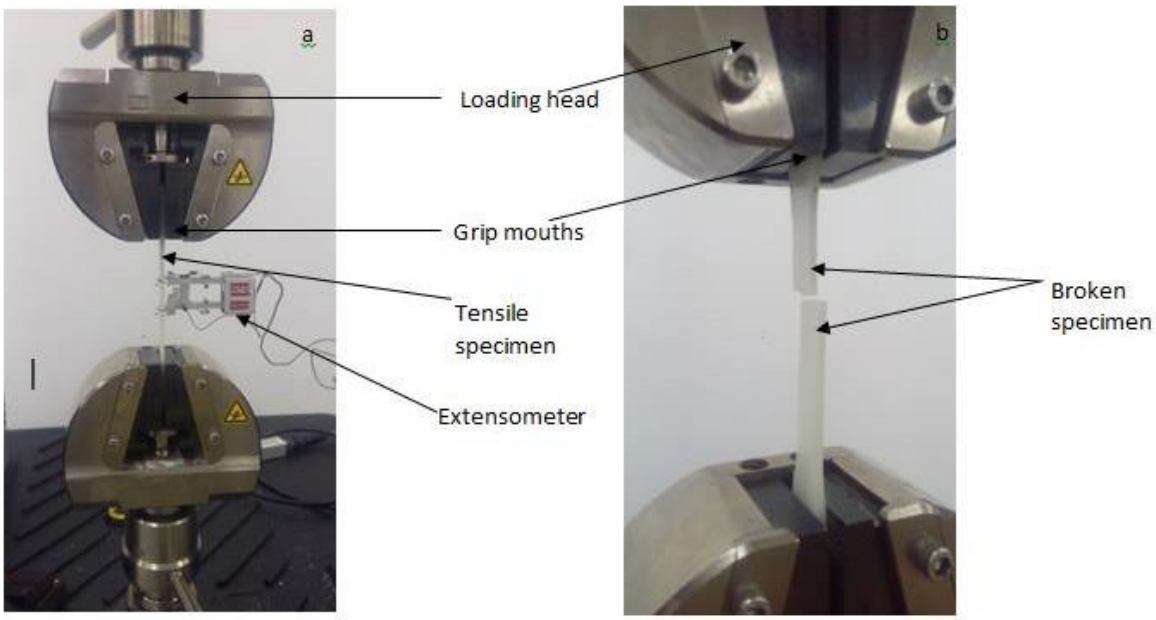

Figure 3.6 (a) shows the tensile test specimen set-up with the extensometer and (b) shows the broken specimen after strain measurement.

3.4.2.1.2.3 Flexural Test

Flexural strength and flexural modulus of syntactic foam composites performed on five specimens using MTS 793 servo-hydraulic machine were performed as per ASTM D790-02 with a load cell of 30 KN and a test speed of 2 mm/min as shown in Figure 3.7. Figure 3.7a shows the specimen at loading while Figure 3.7b shows the broken specimen after testing. A constant span length of 48mm (which represents the standard ratio of span length to thickness e.g., 16:1) was maintained during the test for all the samples. The crosshead was maintained at a strain of 5mm/mm and values for maximum flexural stress (σ_f) and strain (ε_f) were calculated using equations (3-16) and (3-17)

$$\sigma_f = \frac{3PL}{2bd^2} \qquad 3\text{-}16$$

$$\varepsilon_f = \frac{6Dd}{L^2} \qquad 6\text{-}17$$

Where, σ_f and ε_f are the flexural stress and strain at the midpoint; respectively, and P, L, b, d, D are the load, span length, specimen width, specimen thickness, and midpoint deflection; respectively. The flexural strength was determined using the maximum stress value recorded before sample fracture and flexural modulus was determined by the slope of the initial linear region of the stress-strain curve.

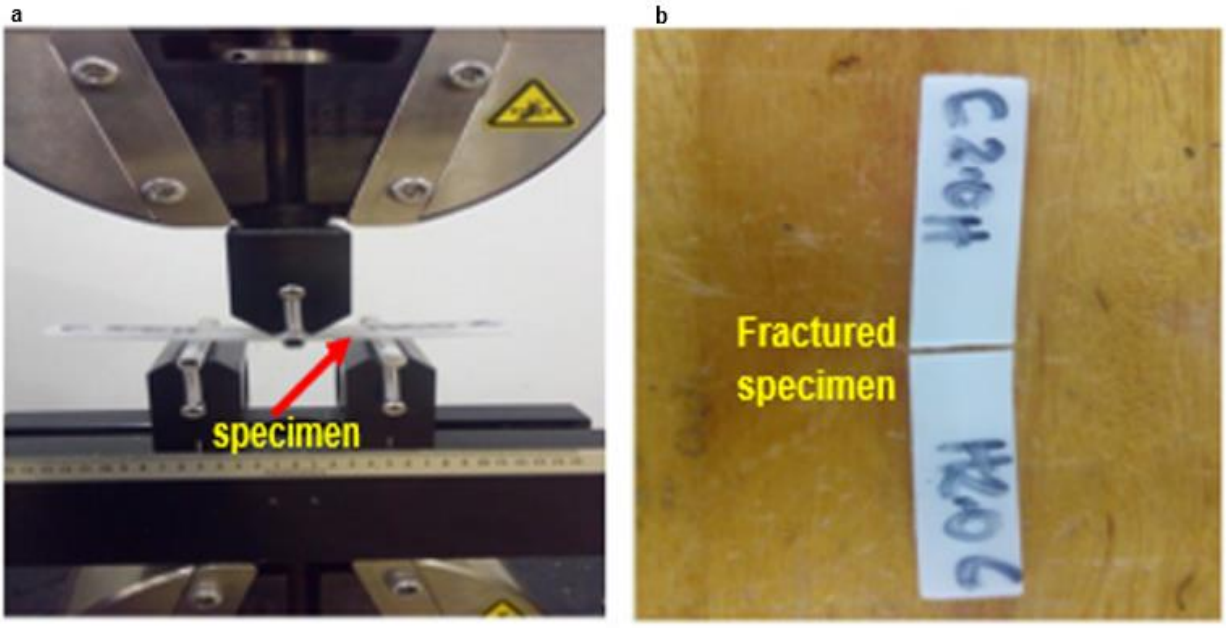

Figure 3.7: Flexural experimental three-point bending test setup for a) specimen at the point of loading, and (b) fractured specimen.

3.4.2.1.2.4 Impact Test

Charpy impact tests are also known as the Charpy V-notch test carried out on the syntactic foam composite material and the neat epoxy were performed at room temperature. The test has been a high strain-rate involves striking a standard notched specimen with a controlled weight pendulum swung from a height. This was done to identify the fracture resistance and energy absorbed by the syntactic foam composites compared to the neat epoxy using a Hounsfield Balanced Impact Tester from Tensiometer Ltd., Croydon, England. The Hounsfield Impact Machine was loaded in a three-point impact manner to that created by a Charpy apparatus as per ASTM D6110 – 04. This test method permitted a variation in the width of the specimens for many materials, either a brittle or a ductile will occur. All impact specimens were notched 2 mm deep, leaving the impact width to be 8 mm. The impact velocity of the Hounsfield balanced impact tester was approximately 6.7 m/s. Five specimens were tested. Figure 3.8 revealed the experimental set-up for the V- notched Charpy test. The test values were obtained, and the average was used to determine the energy absorption using Equation 3-18.

$$IS = \frac{AE}{TW} \qquad 3.18$$

where: IS = the impact strength (kJ/m^2), AE= absorbed energy (Joule), T= specimen thickness (m), and W= width at notch (m).

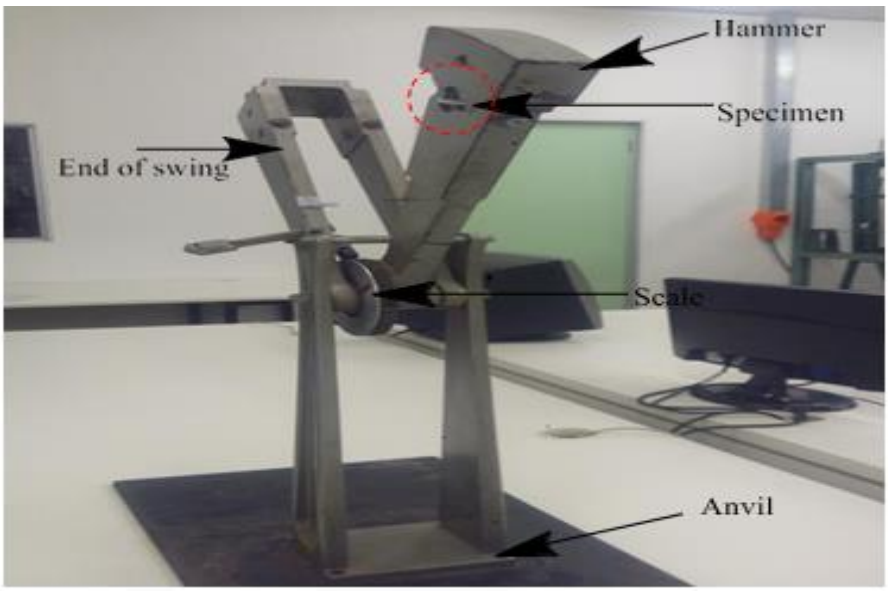

Figure 3.8: Charpy impact set up for the syntactic foam test showing the specimen with the red dashes.

3.4.2.1.3 Dynamic Mechanical Analysis (DMA)

Dynamic mechanical analysis of SFC and SSFC was done to study and characterize the viscoelastic behavior of the materials. This was done by applying sinusoidal stress to measure the behavior of the strain and determine the complex modulus. The TA (Model Q800 V20.6) instrument was used as per ASTM D4065 test standard to perform the dynamic mechanical analysis. Three test runs were conducted per sample and the mean value was computed. The tests were run on a 3-point bending mode on a support span length of 50mm with heating temperature ranges from 20^0C to 200^0C at a frequency of 10Hz, at a rate of 3^0C/min and amplitude of 20 µm.

3.4.2.1.4 Morphological Properties

3.4.2.1.4.1 Scanning Electron Microscopy

Scanning Electron Microscopy (SEM) was used to study the microstructure of HGM, kenaf and glass fibers, SFC, and SSFC using a Zeiss EVO 1 HD 15 Oxford instrument X-max scanning electron microscope (SEM). Before SEM (Carl Zeiss) observation, the specimen was gold-coated for the flow of electrons using Quorum Q 150R ES machine for 6 minutes.

3.4.2.1.4.2 Transmission Electron Microscopy

The transmission electron microscopy resolution performed on the syntactic foam was used to transmit the bean of electrons of the hollow glass microscope to form an image. The image was formed because of the interaction between the electrons and the syntactic foam, was examined with the aid of a higher resolution transmission electron microscopy (HR-TEM) Joel 2100, from Japan.

3.4.2.2. Sandwich Syntactic Foam Composites

3.4.2.2.1 Density Measurement

The density of the sandwich foam composite was measured for tracking physical changes in polymer samples/ filled and reinforced composites. Measured density was calculated according to *ASTM C271-94. Annual Book of ASTM Standards* 1994). Since density is equal to mass/volume, Equation. 3.19, therefore, volume is equal to mass/density, Equation. 3.20. The volume of the sandwich composite was calculated by adding the volumes of all the constituent materials together using Equation.3.21.

$$\rho = \frac{m}{v} \tag{3.19}$$

$$v = \frac{m}{\rho} \tag{3.20}$$

$$v_c = v_k + v_g + v_{sf} + v_m \tag{3.21}$$

where v_c , v_k , v_g , v_{sf} , and v_m are the sandwich composite volume, kenaf fiber volume, glass fiber volume, syntactic foam volume, and matrix resin volume respectively (cm^3). The volume fraction of each constituent material is then calculated using Equation. 3.22.

$$V = \frac{v}{v_c} \tag{3.22}$$

where V is the volume fraction.

The sandwich composite density is therefore calculated using Equation. 3.23.

$$\rho_c = \rho_k V_k + \rho_g V_g + \rho_{Sf} V_{Sf} + \rho_m V_m \tag{3.23}$$

The percentage difference between the measured and theoretical density is taking as the matrix porosity (void) content using Equation. 3.24.

$$P_c = \left(\frac{\rho_t - \rho_m}{\rho_t} \right) * 100 \tag{3.24}$$

Where P_c is the sandwich composite porosity (void), ρ_t is the theoretical density and ρ_m is the measured density.

3.4.2.2.2 Characterization of Sandwich Syntactic Foam Composite

Table 3.7 below presents the mechanical, structural, and acoustic characterizations of SSFC.

Table 3.7 Mechanical, structural, morphological, and acoustic characterization of SSFC

Standard	Characterization type	Purpose	Equipment	Number of specimens
	Mechanical Property			
ASTM D 2583 (ASTM D 2583- 95 American Society for Testing and Materials 2001)	Hardness test	It was conducted to investigate the level of indentation the SSFC can withstand	Barber Colman GY2J 934.1 Barcol impressor.	Twelve (12) specimens
ASTM C297 (C297/C97M-04 2004)	Tensile test	Used to evaluate the SSFC strength, modulus, and strain ability	MTS 793 servo-hydraulic machine with a load cell of 100 KN	Twelve (12) specimens
ASTM C393-94 (C365/365M-11A 2011)	Flexural test	To investigate the bending strength and modulus of the SSFC.	MTS 793 servo-hydraulic machine with a load cell of 100 KN	Twelve (12) specimens
ASTM C365-94 (C365/365M-11A 2011)	Compression test	To investigate the compressive strength and strain of the SSFC	MTS 793 servo-hydraulic machine with a load cell of 100 KN	Twelve (12) specimens
ASTM D256	Notch Izod Impact test	To investigate the ability of the SSFC in withstanding impact strength.	Hounsfield Impact Tester	Twelve (12) specimens
	Scanning Electron Microscopy (SEM)	It was used to study the fracture surfaces of the SSFC	Zeiss EVO 1 HD 15 Oxford Instrument X. Gold-coated with Quorum Q 150R ES machine	Twelve (12) specimens
ASTM E1050-12	Acoustic test	To investigate the sound level	Digital Sound Level Meter:	Four (12)

(Cosse *et al.* 2019a)		absorption of the SSFC	CVHM-H65	specimens

3.4 Conclusion:

This chapter enumerates the materials, processing techniques, and characterizations involved in the manufacturing of SFC and SSFC composites. The detailed processes involved, and the ASTM standards used were highlighted in tables forms for easy accessibility and understanding.

Further, in **chapter 4,** characterization of the constituent materials relating to morphological properties and particle size analysis of T60-HGM was discussed.

CHAPTER 4

4.0 PROPERTIES OF MATERIALS

In this chapter, the characterization of the raw materials used as the constituent materials for the fabrication of SFC and SSFC is discussed. This was considered important because HGM, and epoxy resin formed the base materials (filler/matrix) used for the fabrication of SFC and it helps to compare the changes in the mechanical, morphological, and thermogravimetric compositions of the composite as discussed in **chapter 6, 7 & 9.**

4.1 Morphological Property

4.1.1 Scanning Electron Microscopy (SEM)

4.1.1.1 Hollow Glass Microspheres

The morphology of T60-HGM analyzed by SEM is shown in Figure 4.1. Different sizes of the T60-HGM may be seen on the micrograph ranging from 10µm to 90µm. The SEM shows the spherical shape of the HGM in their different sizes. Understanding the size range of HGM was important as it form part of the objectives of this study. The effect of the sizes on the syntactic foam composites was discussed further in **chapters 6 and 7.**

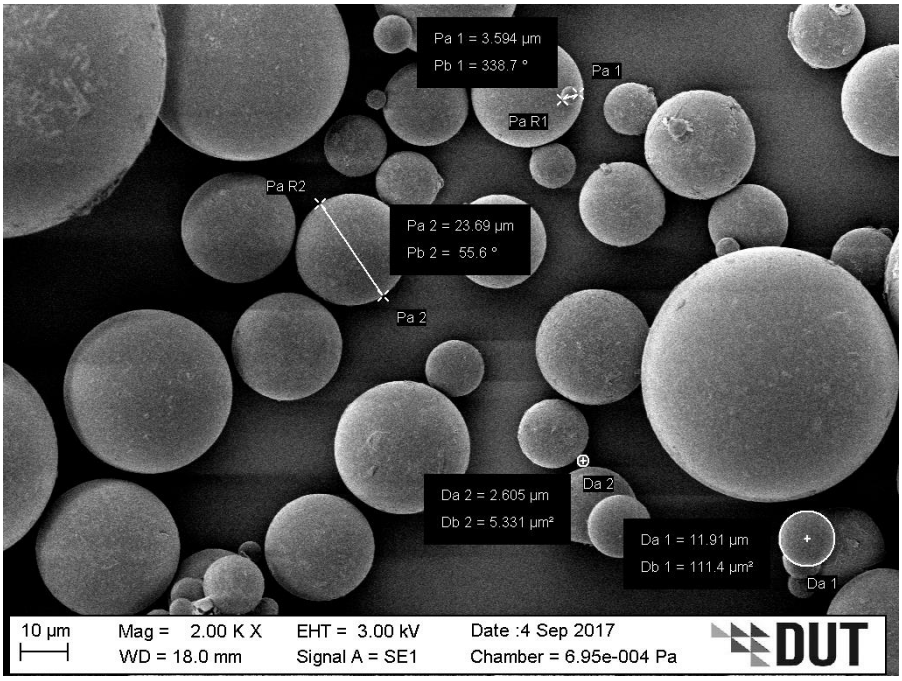

Figure 4.1 : SEM microstructure of Hollow Glass Microsphere showing different size range from 10µm to 60µm.

4.1.1.2 Glass fibers

The SEM image of the glass fiber mat is shown in Figure 4.2. The glass fiber strands ranges in diameter. Single fiber strand and clustered fibers can be observed on the surface of the morphology which aided the bonding with the matrix when used as face-sheet to determine the strength of hybrid kenaf-glass fiber reinforcement on the sandwich syntactic foam composite as part of the objectives in this study.

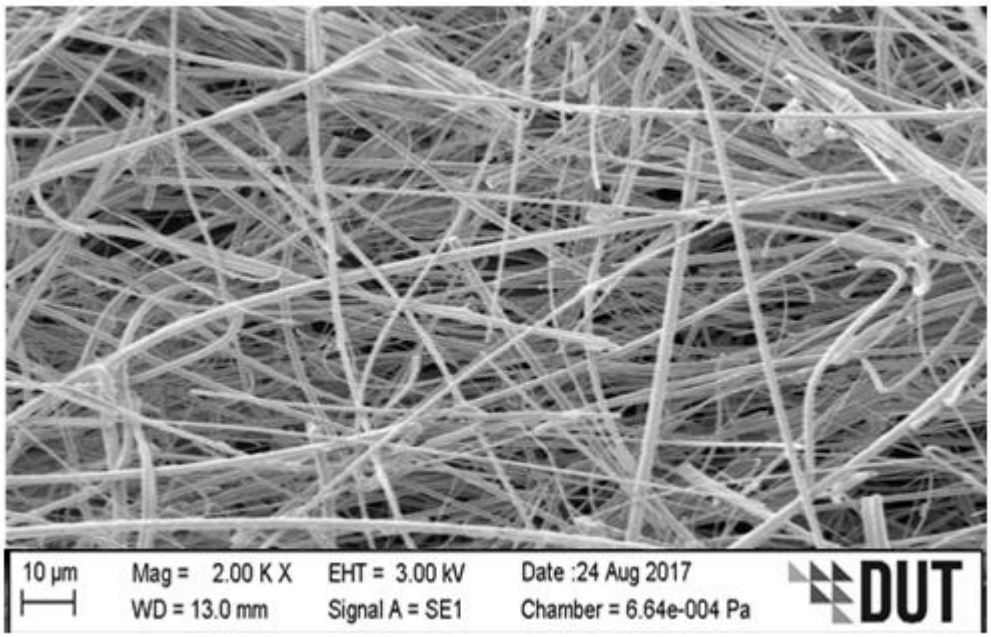

Figure 4.2: SEM image of glass fiber showing the strands of the fiber mats.

4.1.1.3 Kenaf fiber

The SEM image of the kenaf fiber is represented in Figure 4.3; the roughness observed on the surface of the fiber aided the bonding strength between the kenaf fiber and the matrix. The roughness can also create a gap for the formation of voids at the interface due to poor wetting. Kenaf fiber was also part of the face-sheet used as reinforcement for the sandwich syntactic foam composite, its micrograph surface gives an insight on its strength ability when bonded with other materials.

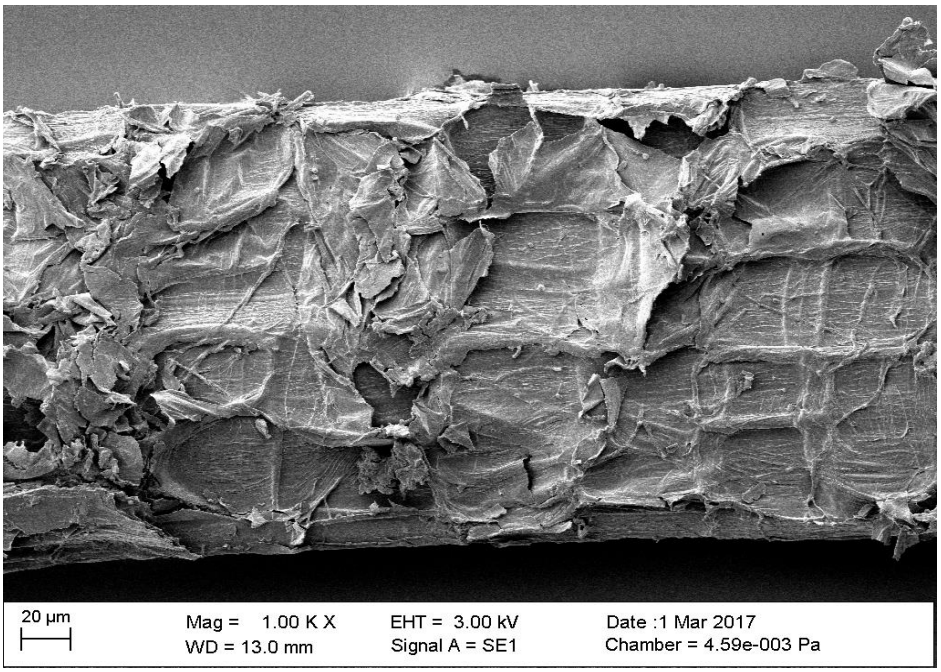

Figure 4.3: SEM micrograph of kenaf fiber showing the surface roughness.

4.2 Particle Size Distribution (PSD)

The unvaried/parent hollow glass microsphere (T60-HGM) filler (designated as “OO”) was varied into four different particle sizes (i.e., 0-24µm – as “AA”; 25-44µm – as “BB”; 45-49µm – as “CC” and 50-90µm – as “DD”) using different sieve ranges on a Retsch magnetic shaker. The varied size particles were further characterized by particle size analyzer “PSA” 1190 and discussed through particle size distribution (PSD) analysis. In dispersed system, the material bulk density and porosity is a function of the particle size (Wiacek and Stasiak 2018). Since the strength of the syntactic foam composites is largely dependent on the strength of the HGM, and a batch of HGM is often a composition of many individual glass microspheres with true densities, particle sizes, and wall thicknesses. Then, it resulted in variance of strength which mostly led to the dissimilarities in failure mechanism of syntactic foam composite (Wang *et al.* 2022). With this understanding, it is therefore important to study the influence of particle size distribution on a single HGM varied into four micro sizes and its effect on the tensile and flexural properties of syntactic foam composite. Density of the material also plays an important role in determining the effect of particle sizes on its mechanical, microstructural, and thermal properties of syntactic foam composites.

4.2.1 Procedure for particle size analysis

The background sound was checked and recorded to exclude the noise signal from the actual measurement. Then, the dry T60-HGM sample was poured into the sample holder are then dispersed by high pressure using compressed air in the venturi nasal as shown in Figure 4.4 (a, and b). The instrument thereafter detected the diffraction pattern caused by the sample through the laser beep. And the sample flow was adjusted in combination with the air pressure to achieve the desired obscuration. After the measurement, the samples are collected by a vacuum cleaner. Then, the Kalliope software (Paar 2022) was used to interpret the data and the results are displaced on the screen. The measurements were then collected, exported, recorded, and analyzed.

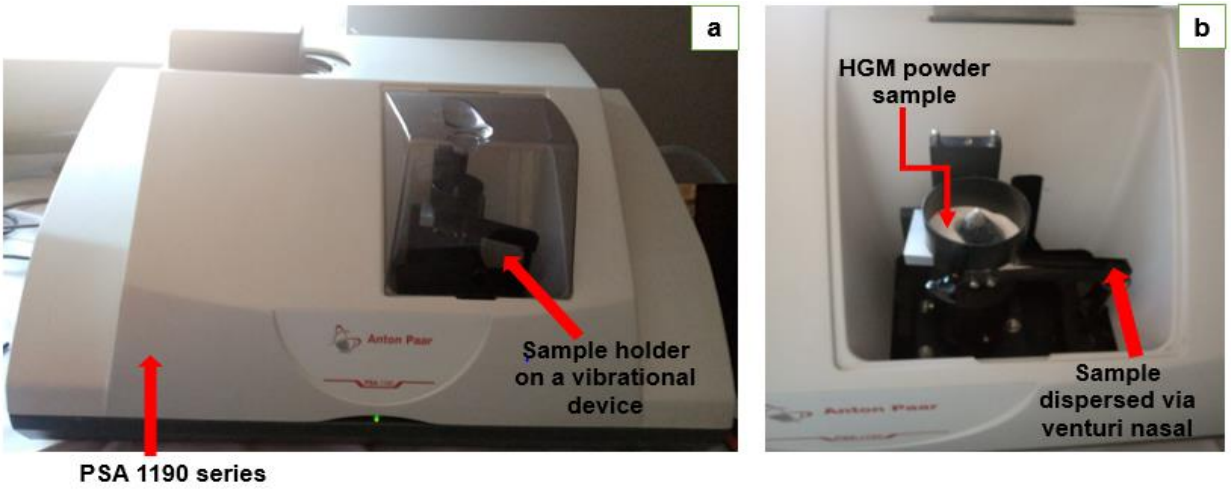

Figure 4.4. PSA 1190 particle size analyzer showing (a) the sample holder sitting on a vibrational device, and (b) T60-HGM sample inside the holder and dispersed through the venturi nasal.

Table 4.1 Particle size distribution conducted on the hollow glass microsphere to measure the particle diameter of the size ranges of the T60-HGM

HGM size variation	D10 volume (µm)	D50 volume (µm)	D90 volume (µm)
OO	8.26	36.97	64.42
AA	5.54	20.59	37.53
BB	5.72	29.39	45.30

CC	6.43	30.42	47.27
DD	14.18	56.07	77.97

The size distributions of the four particle ranges for T60-HGM are listed in Table 4.1. The D10 indicates that 10% by volume of the samples fall within the range of the values under it. Likewise, D50 and D90 indicates that 50% and 90% by volume of the samples fall within the ranges of the values under it. For example, at DD, the value of D10 was 14.18 µm, this shows the diameter of distribution for all the particle sizes between 50 – 60 µm. The density and the geometric properties of all the four-particle size variation are listed in Table 4.2. The ω and η defines hollow geometry of the HGMs, and it is important to note that particle sizes enclosure also play an important role in the severity of the borosilicate reaction (Bas, Jin and Gupta 2021).

Table 4.2 The parameters of particle size distribution of T60 - HGM samples

Particle size (µm)	OO	AA	BB	CC	DD
V_d (%)	6.86	9.66	31.02	9.80	12.16
d (µm)	39.26	29.62	30.86	29.40	55.04
ω (µm)	5.53	3.22	3.89	4.06	7.67
a	7.09	9.58	7.61	7.24	8.23
η	0.9141	0.9141	0.9141	0.9141	0.9141
r_o (µm)	64.42	37.53	45.30	47.27	77.97
r_i (µm)	58.89	34.31	41.41	43.21	71.27
ρ_d (g/cm^3)	0.6000	0.7548	0.7286	0.7083	0.5529

Table 4.2 shows the parameters of the particle size distribution of HGM-T60, the volume fraction of distribution (V_d), and the average particle diameter of the volume distribution (d) was measured by PSA 1190 laser particle size analyzer. In this analysis, the aspect ratio "**a**" given as (a=d/ ω, where ω are the average wall thickness of hollow particles) is one of the important factors influencing the strength of HGM particles in composite materials. HGM with higher **"a"** are thought to possess higher strength. In fact, a bigger **"a"** reflects the smaller particle size of HGM. Therefore, the strength of HGM increases with decreasing particle size. The average wall

thickness (ω), radius ratio (η), external radius (r_o), and inner radius (r_i) were all calculated from the formula previously explained (**in chapter 3, section 3.4.2.1.1.2, equations 3.10 and 3.11**).

The particle size distribution range of T60 samples consists of five parts: the volume fractions of OO is 6.86%, the volume fractions of AA, BB, CC, and DD, were 9.66%, 31.02%, 9.80%, and 12.16% respectively. It can be seen from Table 4.1 that as the particle size variation increases, the wall thickness and average particle diameter also increases gradually. However, the aspect ratio gradually decreases. It suggested that the wall thickness and aspect ratio of a batch of HGM is not uniform. HGM with smaller wall thickness showed higher strength in syntactic foam. The findings have been published by the author (Afolabi, Kanny and Mohan 2022; Afolabi, Mohan and Kanny 2023)

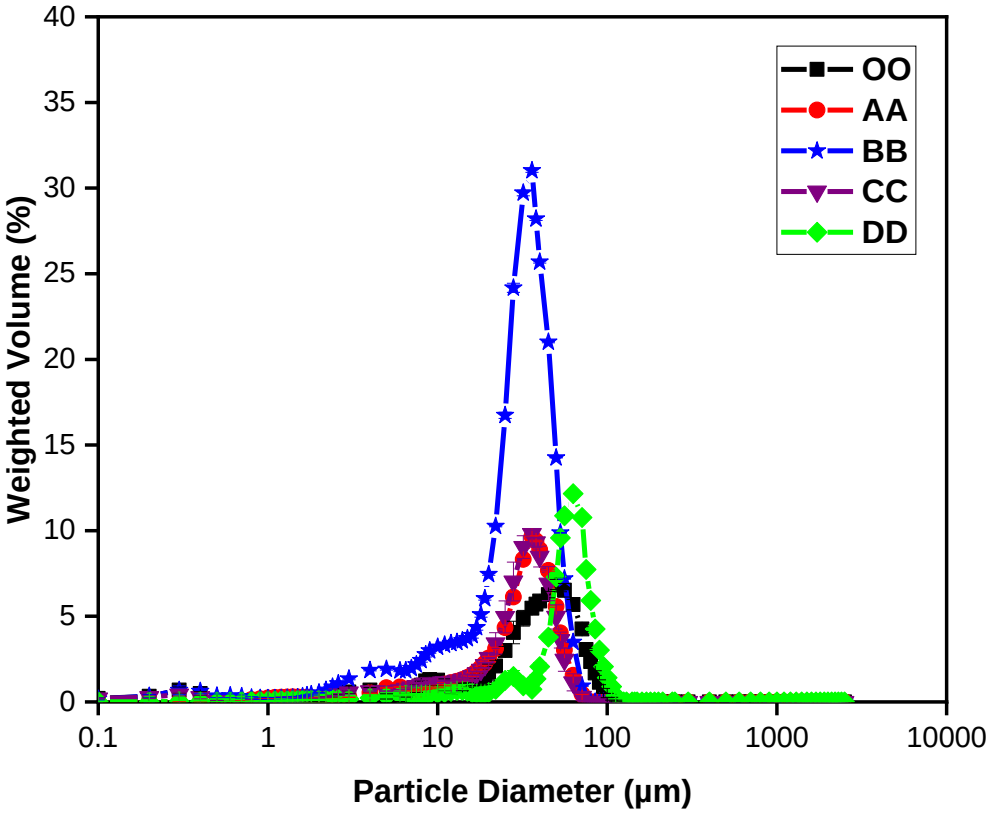

Figure 4.5. Particle size distribution (PSD) of T60-HGM variation

The volume fraction of distribution of BB shows the highest in the particle size variation and it is 77.9% increase than the OO (unvaried) T60-HGM. This feature can be clearly seen from the particle size distribution plotted in Figure 4.5. From Table 4.2, BB shows the highest V_d,of

31.02%. This implies that there is more level of uniformity in the HGM particles at that range than the others. It can be noted that the larger the particle size, the larger the wall thickness and the lower the strength (**see chapter 6 and 7**). The particle size distribution with size variation of AA, BB, CC, and DD were all consistent with this trend. While the unvaried/parent OO do not conform to this rule since it comprises of all the particle sizes. Therefore, the overall strength for a batch of HGM-SFCs can be improved by controlling the particle size and wall thickness.

Conclusion:

In chapter 4, the morphological properties of the raw materials and the particle size distribution of HGM were described to understand the bonding strength of the material with the matrix and effect of size distribution as a base reference for comparison in analyzing the density and mechanical properties of syntactic foam composite **chapters 5**. The wall thickness **"ω"** and aspect ratio **"a"** influence the size variation. The particle size variation of the T60-HGM is an important factor in determining the spreadability of the HGM as it is influenced by wall thickness and aspect ratio.

Further, in chapter 5, the physical properties i.e., density measurement as a function of the particle size variation and wall thickness on the SFCs are discussed.

CHAPTER 5

5.0 DENSITY PROPERTIES OF SYNTACTIC FOAM COMPOSITE

5.1 Introduction

The relative density of the syntactic foam composite (SFC) with respect to the microstructure of the hollow glass microsphere (HGM) is discussed in this chapter. The relative density [RD] of composite materials is used in composite materials to identify them, track physical changes, and ensure acceptable product quality. The concentration of HGM in epoxy varies according on particle size regularity and concentration. Density analysis is used to investigate the impact of concentration and particle size regularity on the microstructure of SFCs. The variation in SFCs density can be related to HGM packing efficiency within SFCs in terms of concentration and particle size regularity. The variance in theoretical (calculated from the rule of mixture) and experimental density values provides a thorough grasp of packing efficiency and inter-particle features.

5.2 Hollow glass microspheres microstructure for all the syntactic foam compositions

Figure 5.1 (a) to (e) with 20 - 24µm particle sizes, (f) to (j) with 25 - 44µm particle sizes, (k) to (o) with 45 - 49µm particle sizes, and (p) to (t) with 50-60µm particle sizes shows the microstructure of SFCs filled with homogeneous HGM particle sizes, while Figure 5.1(u) to (y) shows the microstructure of SFCs filled with heterogeneous HGM particle sizes. These microstructures show the effect of porosity as it relates to density of SFCs. Figure 5.2 show the graphically representation of density values of SFCs filled with heterogeneous particle size and varying volume concentration versus neat epoxy “NE” (EPT60-0). Also, the homogeneous particle sizes at varying concentration versus neat epoxy to gain better understanding of particle sizes versus concentration on the density of SFCs. Figure 5.2 (a) to (d) shows a drop in density values for SFCs with homogeneous sized HGM (irrespective of HGM volume concentration) when compared to NE, which may be attributed to a decrease in the vol% of epoxy, which corresponds to the substitution with equivalent vol% of HGM.

Furthermore, with increasing HGM vol%, density values for SFCs filled with homogeneous-sized HGM drop, which may be ascribed to a decrease in vol% of the epoxy matrix, which corresponds to substitution by equivalent vol% of HGM. The decrease in epoxy matrix vol% and

replacement with comparable vol% of HGM creates a porous structure, lowering the density of SFCs filled with homogeneous-sized HGM (Wypych 2010).

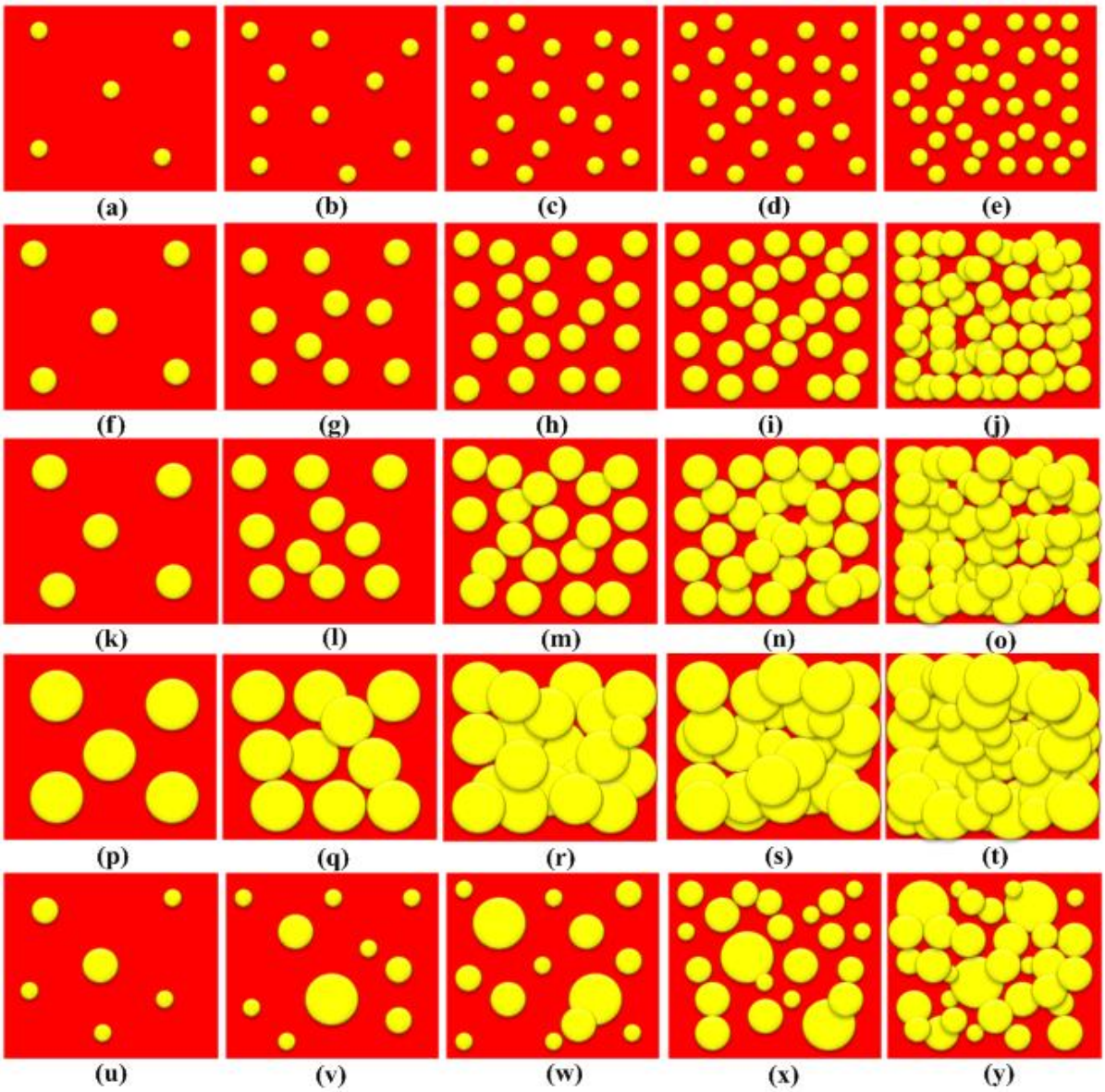

Figure 5.1. Schematic representation of microstructure for (a) EPT60-AA5 (b) EPT60-AA10 (c) EPT60-AA15 (d) EPT60-AA20 (e) EPT60-AA25 (f) EPT60-BB5 (g) EPT60-BB10 (h) EPT60-BB15 (i) EPT60-BB20 (j) EPT60-BB25 (k) EPT60-CC5 (l) EPT60-CC10 (m) EPT60-CC15 (n) EPT60-CC20 (o) EPT60-CC25 (p) EPT60-DD5 (q) EPT60-DD10 (r) EPT60-DD15 (s) EPT60-DD20 (t) EPT60-DD25 (u) EPT60-5 (v) EPT60-10 (w) EPT60-15 (x) EPT60-20 and (y) EPT60-25.

The density values of SFCs filled with heterogeneous sizes of HGM are graphically shown in Figure 5.2(e). There is little variation in density values for SFCs filled with heterogeneous sizes of HGM, which may be ascribed to the well disseminated HGM inside the epoxy matrix, where the gaps between the big-sized HGM are occupied by tiny sized HGM, preventing the spaces from being left empty. It was observed that the density decreased with an increasing volume fraction and particle sizes. Also, the increasing wall thickness of HGM tends to increase the density of the SFC. Meanwhile, Wiacek and Stasiak (2018); Wiacek, Stasiak and Kafashan (2020), in their study on granular assemblies of uniform spherical particles, reported that the density decreased with an increase in particle size. It was also discovered that there was a larger average coordination number in monodispersed samples with smaller particles, because the packing density affected the contact between the particles. Moreso, McGeary stated that the mixture of spherical particles with the same volume fraction of particle, but different sizes resulted in increased density with decreasing particles sizes. Packing density of samples decreased substantially when the particle size fractions increased from smaller to larger particles. In order word, for binary mixture, the packing density increase with volume fraction of smaller particles (Wi¸acek, Parafiniuk and Stasiak 2017).

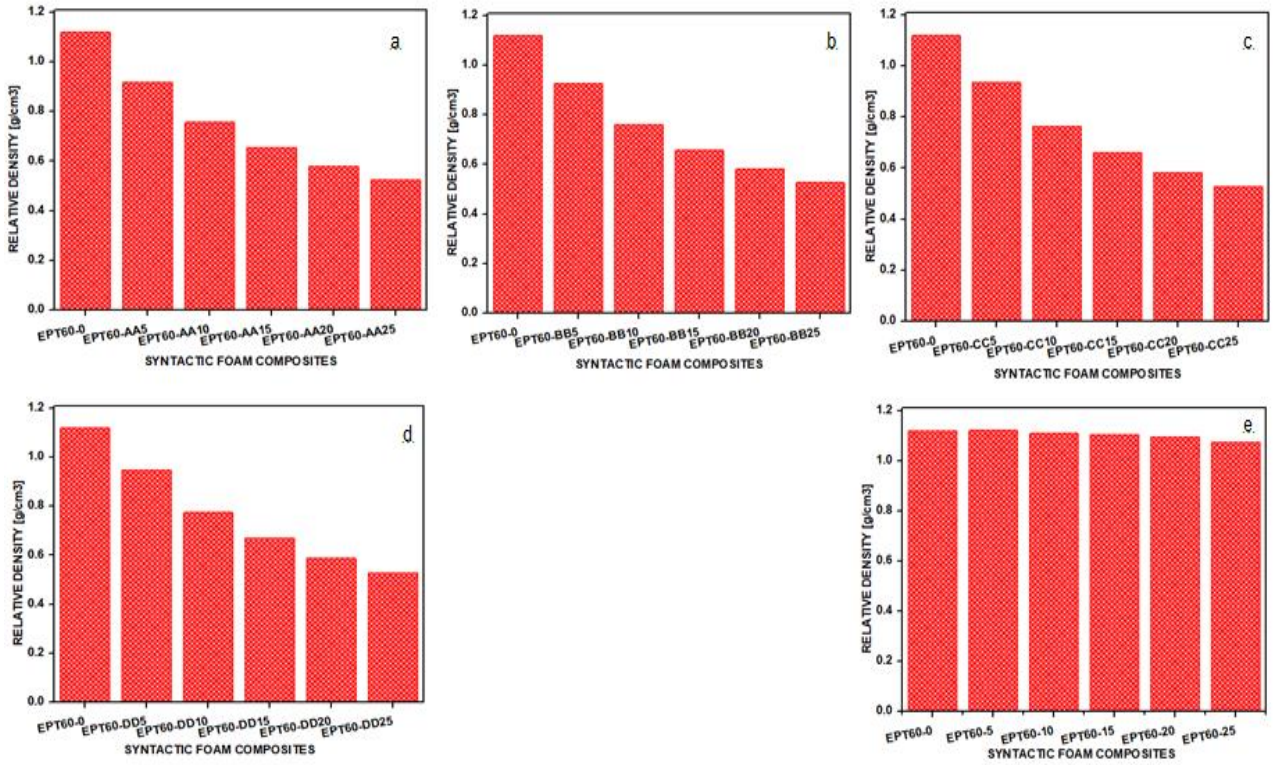

Figure 5.2. Graphical representation of density for (a) EPT60-0 vs. EPT60-AA5, EPT60-AA10, EPT60-AA15, EPT60-AA20, EPT60-AA25 (b) EPT60-0 vs. EPT60-BB5, EPT60-BB10, EPT60-BB15, EPT60-BB20, EPT60-BB25 (c) EPT60-0 vs. EPT60-CC5, EPT60-CC10, EPT60-CC15, EPT60-CC20, EPT60-CC25 (d) EPT60-0 vs. EPT60-DD5, EPT60-DD10, EPT60-DD15, EPT60-DD20, EPT60-DD25 (e) EPT60-0 vs. EPT60-5, EPT60-10, EPT60-15, EPT60-20 and EPT60-25

The graphical depiction of theoretical density versus experimental density is shown in Figure 5.3.(a) through (e). When SFCs filled with homogeneous sizes of HGM are compared to theoretical density, the experimental density drops; however, when SFCs filled with heterogeneous sizes of HGM are compared to theoretical density, the experimental density shows little variation. The discrepancy in real contact surface and theoretical contact surface predicted by the equations 3.1-3.9 (**chapter 3, section 3.4.2.1.1.1**) can be ascribed to the modest drop in experimental density for SFCs filled with homogeneous sizes of HGM. The highest packing efficiency, i.e., maximum real contact surface, which was not anticipated by the theoretical equation, can be related to the rise in experimental density for SFCs packed with heterogeneous sizes of HGM. This relates to the little variations between the theoretical and the

experimental density of the heterogeneous sizes of HGM. This findings have been published by the author (Afolabi, Mohan and Kanny 2023).

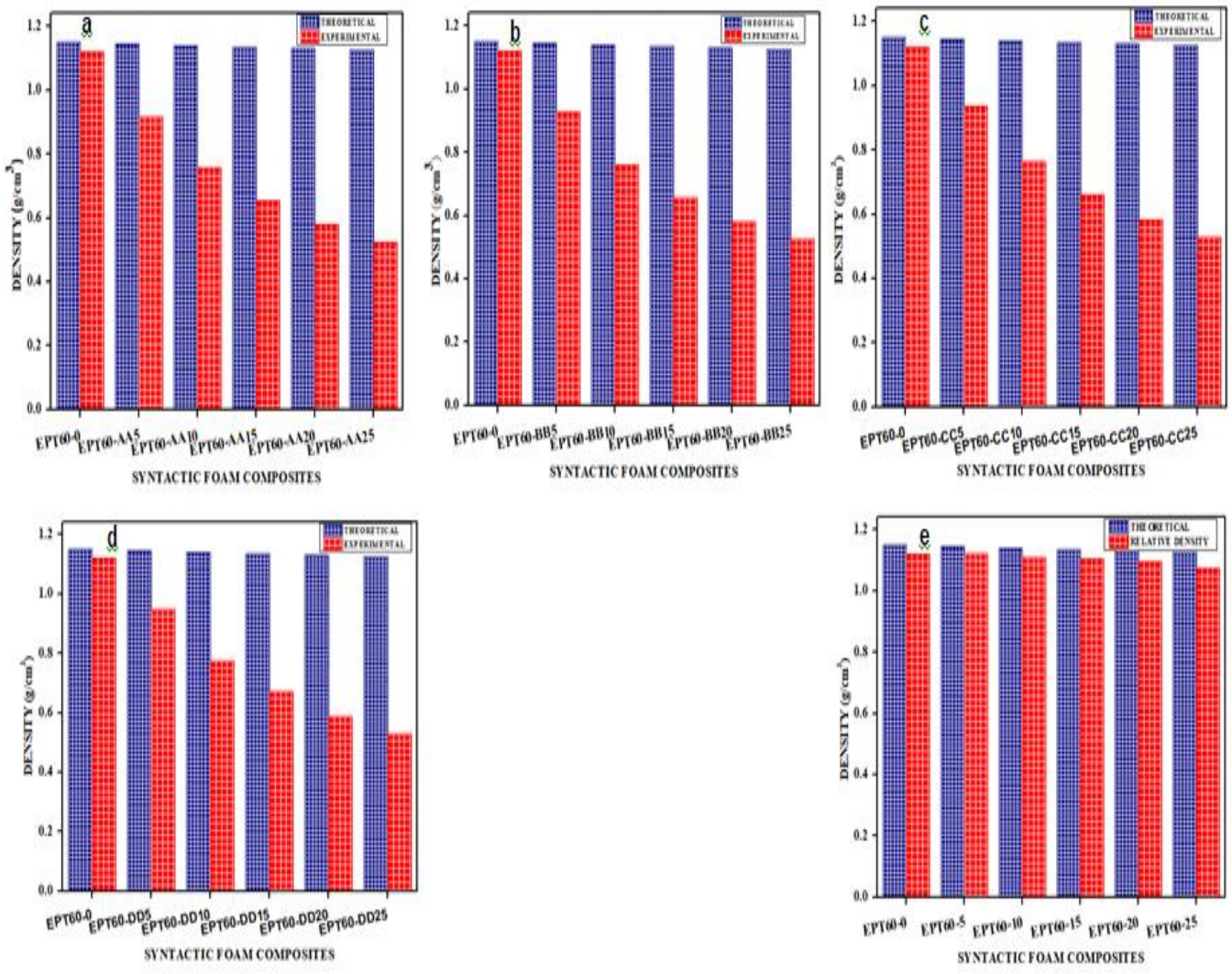

Figure 5.3. Graphical representation of experimental density versus theoretical density for (a) EPT60-0 vs. EPT60-AA5, EPT60-AA10, EPT60-AA15, EPT60-AA20, EPT60-AA25 (b) EPT60-0 vs. EPT60-BB5, EPT60-BB10, EPT60-BB15, EPT60-BB20, EPT60-BB25 (c) EPT60-0 vs. EPT60-CC5, EPT60-CC10, EPT60-CC15, EPT60-CC20, EPT60-CC25 (d) EPT60-0 vs. EPT60-DD5, EPT60-DD10, EPT60-DD15, EPT60-DD20, EPT60-DD25 (e) EPT60-0 vs. EPT60-5, EPT60-10, EPT60-15, EPT60-20 and EPT60-25

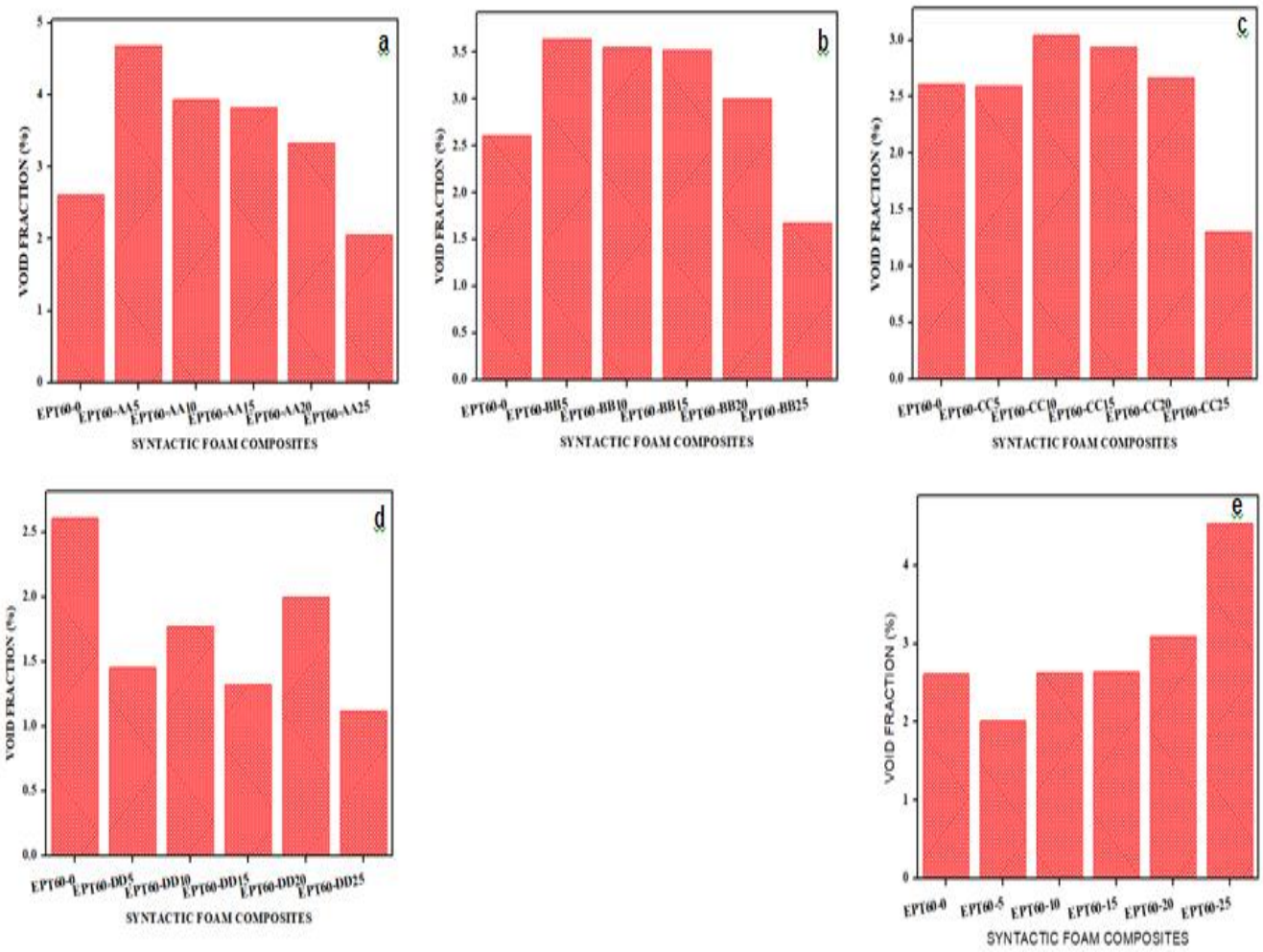

Figure 5.4. Graphical representation of void fraction for (a) EPT60-0 vs. EPT60-AA5, EPT60-AA10, EPT60-AA15, EPT60-AA20, EPT60-AA25 (b) EPT60-0 vs. EPT60-BB5, EPT60-BB10, EPT60-BB15, EPT60-BB20, EPT60-BB25 (c) EPT60-0 vs. EPT60-CC5, EPT60-CC10, EPT60-CC15, EPT60-CC20, EPT60-CC25 (d) EPT60-0 vs. EPT60-DD5, EPT60-DD10, EPT60-DD15, EPT60-DD20, EPT60-DD25 (e) EPT60-0 vs. EPT60-5, EPT60-10, EPT60-15, EPT60-20 and EPT60-25

Figure 5.4 (a) through (e) presents the graphical of void fraction of the density in the SFCs. In Figure 5.4 (a) and (b), the void fraction of the SFCs is decreased with an increase in the volume fraction of HGM, corresponding to their density pattern, Figure 5.4(c) also shows decreased void fraction with an increasing HGM vol% except at EPT60-5 which is the same value as the EPT60-0. At Figure 5.4(d), there is no uniform pattern with the void fraction of SFCs, but their values reduced to that of the EPT60-0. At Figure 5.4(e) with heterogeneous sizes of HGM, the

void fraction increased with an increase in the vol% of the HGM. This is possibly because of surface infiltration between the matrix and the HGM. This results corresponds to an earlier report by Zhu *et al.* (2012) where the void content also increased with an increasing volume fraction of HGM. Also, it was an indication that there is heterogeneity and entrapment of air bubbles during the mechanical mixing of the constituent elements (Yu, Zhu and Ma 2012).

5.3 Conclusion

The most fundamental qualities of matter are mass and packing, which determine the properties of any material. The foregoing findings show that the particle size of the HGM affects density in SFCs. The density of SFCs filled with heterogeneous sizes of HGM reduced as the concentration of HGM increased, which can be attributed to the interface organization, in which homogeneous-sized HGM are well dispersed and are more porous in the epoxy matrix. The density of SFCs with heterogeneous sizes of HGM was nearly constant regardless of HGM concentration, which can be attributed to long range of the HGM particles inside the epoxy matrix, where the gaps between the large-sized HGM are occupied by smaller sized HGM, preventing the spaces from being unoccupied.

In the next chapter 6, the tensile properties of the syntactic foam composites are discussed.

CHAPTER 6

6.0 MECHANICAL PROPERTIES OF SYNTACTIC FOAM COMPOSITE (SFC)

6.1 Tensile Properties

This chapter explains the tensile properties of syntactic foam composites (SFC) for the heterogeneous (whole HGM) volume% concentrations and homogeneous (size varied HGM) volume% concentrations. As part of the main objectives of this study to determine the process of making SFC from HGM based on concentration and particle size variation, the influence of HGM volume fractions and size variations of the SFC were elaborated. The chapter is divided into three sections: section 6.1 is based on the tensile properties of SFC with heterogeneous HGM, section 6.2 is on the flexural properties of SFC with homogeneous HGM, and section 6.3 describes the morphological properties of SFC fractured surfaces.

6.1.1 Tensile Results of SFC with Heterogeneous HGM sizes

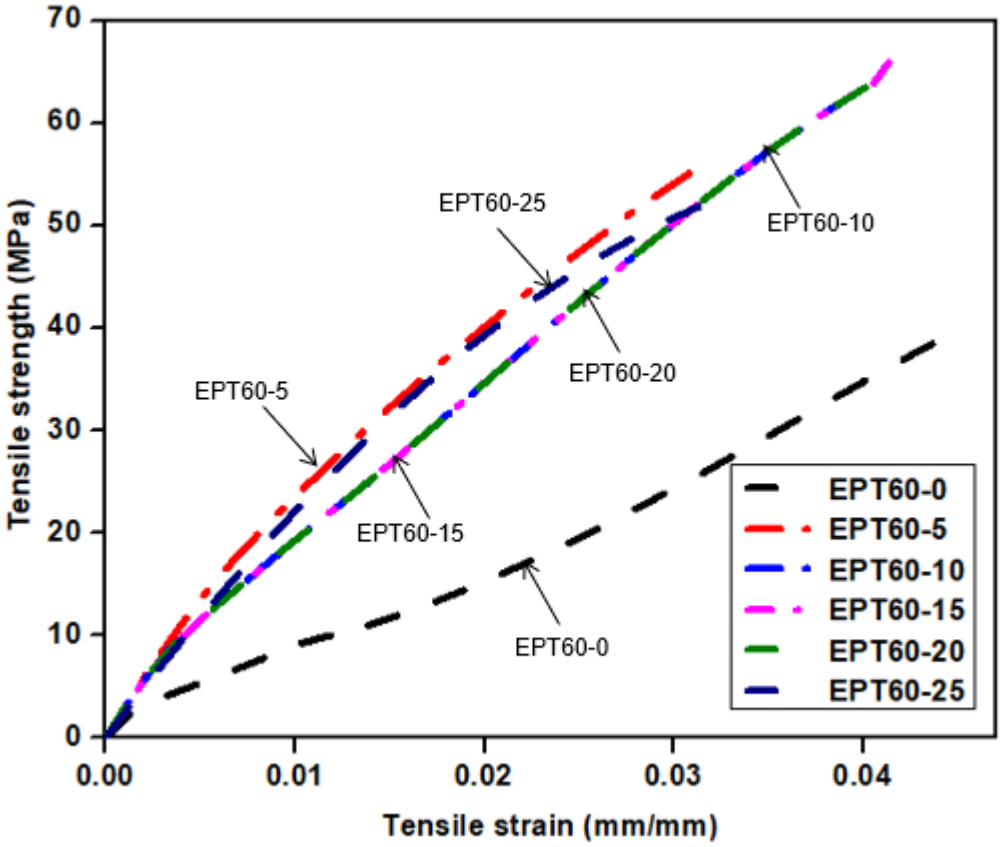

Figure 6.1 Tensile stress and strain relations of SFC compared with the neat epoxy.

Figure 6.1 shows the tensile stress-strain of the SFCs with heterogeneous HGM sizes compared with the neat epoxy "NE" (EPT60-0). The tensile properties of SFCs increased with the inclusion of HGM compared with the neat epoxy. It was observed that the addition of HGM increased the strength of all SFCs series, making these series have greater strength than EPT60-0. This performance may be attributed to the presence of HGM in the matrix which increased the adhesion capacity of the SFCs as seen in the SEM image in Figure 6.4. The strain shows that the elongation of neat epoxy was higher than the SFCs before failure because of the presence of void content at the zero loading.

Table 6.1: Tensile properties of SFC with heterogeneous HGM particle sizes

SFCs	Tensile Modulus	Sp. Tensile Modulus	Tensile Strength	Sp. Tensile Strength	Tensile Strain
	(GPa)	(GPa.cm^3/g)	(MPa)	(MPa.cm^3/g)	(mm/mm)
EPT60-0	2.14 ± 0.14	1.91	40.47 ± 0.64	36.13	0.0497 ± 0.0028
EPT60-5	2.81 ± 0.48	3.08	57.97 ± 2.37	63.49	0.0409 ± 0.0079
EPT60-10	2.48 ± 0.24	3.28	63.97 ± 6.62	84.73	0.0277 ± 0.0014
EPT60-15	4.63 ± 1.76	7.12	66.60 ± 8.48	101.52	0.0219 ± 0.0055
EPT60-20	4.57 ± 1.09	7.81	66.73 ± 8.57	114.00	0.0256 ± 0.0029
EPT60-25	3.78 ± 1.16	7.40	52.55 ± 5.54	102.84	0.0217 ± 0.0057

From Table 6.1, the SFCs show an increase in tensile modulus (TM) and the specific tensile modulus (STM) for all the compositions of HGM volume fraction compared to EPT60-0. The highest tensile modulus was at EPT60-15 (4.628 GPa) with an increase of 117% compared to the EPT60-0. The tensile modulus increased with increasing volume fraction of HGM from EPT60-5 to EPT60-20 (2.813 to 4.570 GPa) before it decreased at EPT60-25 (3.782 GPa). This indicates that the SFC resisted elastic deformation up to EPT60-20 before it reduced at EPT60-25. Similar results were observed by Liang (Liang 2005), where the tensile modulus of the composite increased linearly with an increase in HGB volume fraction. The highest specific tensile modulus was at EPT60-20 (7.81 GPa.cm^3/g), which was possibly due to variation in density values as reported in **chapter 5**.

The highest tensile strength and specific tensile strength are at EPT60-20 (66.7 MPa and 114 MPa.cm^3/g respectively), which was an increase of 65% compared to the EPT60-0. The tensile strength of SFC increased consistently with an increase in the HGM vol% due to the strength capacity of the glass material in HGM filler until EPT60-20 before it decreased at EPT60-25. This could be due to an increased void content caused by the agglomeration and reduced resin content at high vol% of HGM resulting in low bonding and load transfer stability between the filler and the resin. This result corresponded to the earlier report by Kumar *et al.* (2017); Gogoi *et al.* (2018) where the tensile strength of the Polypropylene increased with the inclusion of HGM as a result of improved interfacial adhesion with the matrix. The interfacial strength between the HGM and the matrix is essential for the SFC as it affects their overall tensile strength. The interfacial shear strength between the matrix and the HGM also contributed to the improved mechanical properties of the SFC. Also, adding HGM created a few imperfections leading to unwanted porosity and weak interfacial surfaces between the HGM and matrix as discussed in **chapter 5, Figure 5.4**. This resulted in crack propagation inside the SFC as shown in the SEM images in Figure 6.4 (b-f). The bond between the HGM and the matrix should be in good adhesion in a well-prepared SFC to enable the crack to propagate along with the matrix or possibly cause HGM fracture.

The strain of EPT60-0 “0.0497” mm/mm was higher than that of the SFCs (EPT60-5 to EPT60-25), showing that neat epoxy has more extended elongation period before failure than the SFCs, though with reduced strength. For the SFCs, EPT60-5 has the highest tensile strain of 0.0409 mm/mm. This performance corresponds to the report of Liang (Liang 2005), where the highest composite strain was observed at 5vol% of the filler.

Table 6.2: Comparison of tensile properties of SFCs for the present work to the existing literature

S/no	Matrix type	Composition of HGM and type	Tensile strength (MPa)	Tensile modulus (MPa)	Reference
1	Epoxy resin LR 20	_____	40.47	2135	Present work
2	Epoxy resin LR 20	5% HGM-T60	57.97	2813	
3	Epoxy resin LR 20	10% HGM-T60	63.97	2480	
4	Epoxy resin LR 20	15% HGM-T60	66.60	4628	
5	Epoxy resin LR 20	20% HGM-T60	66.73	4570	
6	Epoxy resin LR 20	25%HGM-T60	52.55	3782	
7	Epoxy resin DER 332	_____	57.2	2752	(Gupta and Nagorny 2006)
8	Epoxy resin DER 332	30% HGM-K46	25.1	3700	
9	Epoxy resin DER 332	40% HGM-K46	20.7	3641	
10	Epoxy resin	50% HGM-K46	15.6	3615	
	DER 332				
11	Epoxy resin DER 332	60% HGM-K46	12.8	3491	
12	Epoxy resin	_____	26.0	2700	(Colloca,

	DER 332						Gupta and Porfiri 2013)
13	Epoxy DER 332	resin	30% S22	HGM –	17.0	2200	
14	Epoxy DER 332	resin	50% HGM-S22		16.5	2100	
15	Epoxy DER 332	resin	30% HGM-K46		21.5	3200	
16	Epoxy DER 332	resin	50% HGM-K46		23.0	4100	

Table 6.2 shows a comparison of tensile properties to those in some existing literature. The present work tensile and modulus properties improved compared to the existing literature due to the modified processing method applied. In this method, degassing was introduced to remove excess void in the SFC resulting in good matrix/filler interaction. A high-volume fraction can result in agglomeration of HGM and cause low tensile strength and modulus in the syntactic foam composite, however, values are higher than neat epoxy. Also, a poor interfacial bond between the matrix and the microballoons resulting from a high-volume fraction of HGM can be responsible for the reduction in the tensile strength of the syntactic foam (Gupta and Nagorny 2006). However, good interfacial adhesion between the matrix and HGM volume fraction in the syntactic foam was responsible for increased in tensile strength in the present work as reported in Table 6.1. Published article on this part is in **Appendix 13.2 (A1-2)**

6.1.2 Tensile Properties of SFC with Homogeneous HGM sizes

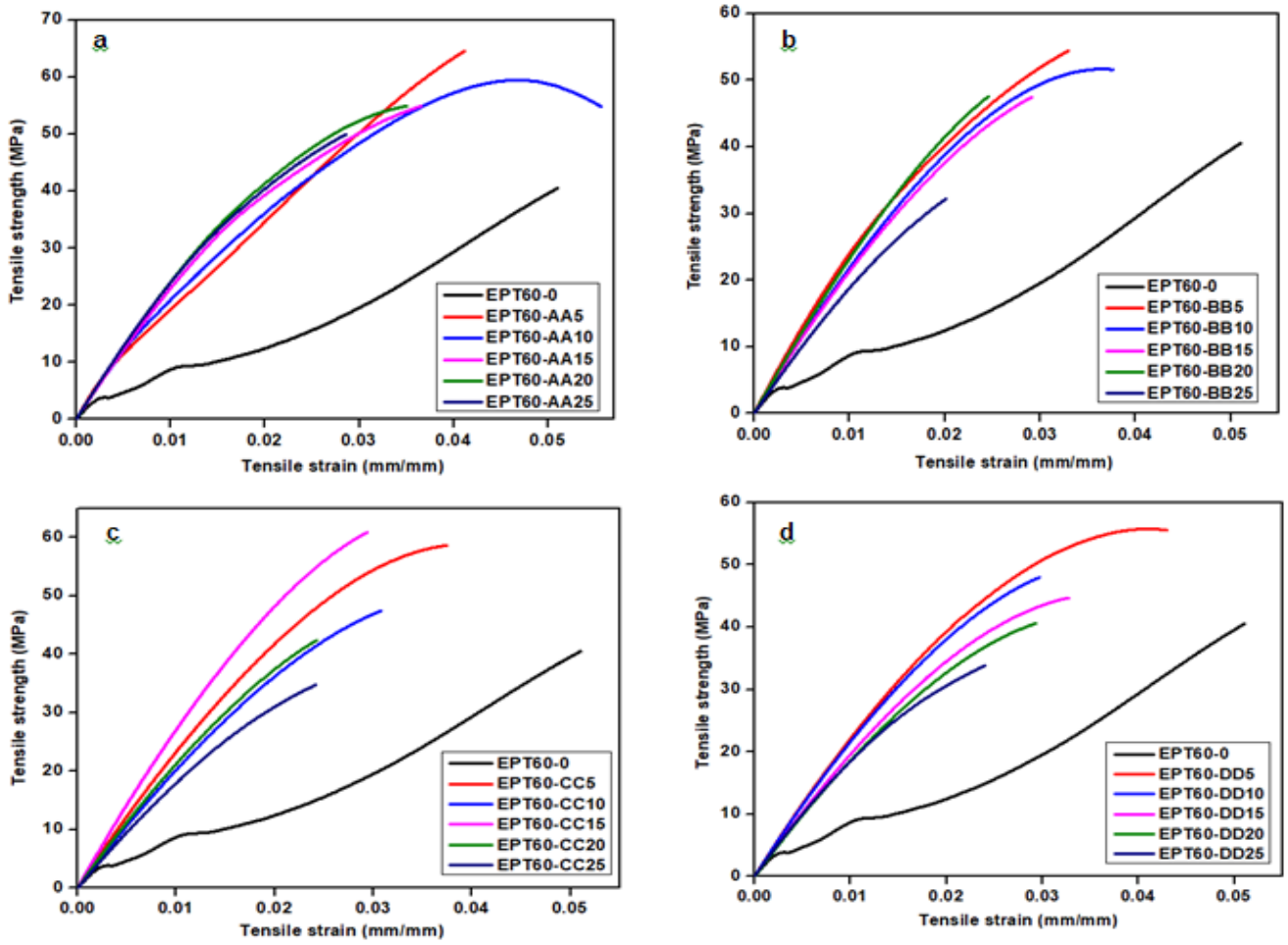

Figure 6.2 (a-d): Tensile stress and strain of SFC with homogeneous HGM particle size variations

Figure 6.2 (a-d) shows the tensile strength and strain relationship for the homogeneous HGM particle sizes of SFC. The curves show a similar stress-strain relationship consisting of a linear elastic region followed by the specimen's brittle fracture. It also indicated that the tensile properties of SFCs increased upon the inclusion of HGM compared to the neat epoxy-EPT60. With the addition of HGM, all the SFCs of the homogeneous HGM (EPT60-AA5-DD5 to EPT60-AA25-DD25) withstand more load before failure than the EPT60-0 because the presence of HGM and its synergistic effect as filler reduced the void content, gives lightweight, and increase

tensile strength of SFC as discussed in previous published article (Afolabi, Kanny and Mohan 2021b). This was because the presence of HGM in the matrix increased the adhesion capacity of the SFCs. The strain shows that the elongation of the SFCs and the neat epoxy could stretch before failure. The strain of the EPT60-0 for all the compositions has the highest elongation.

6.1.2.1 Tensile Modulus (GPa)

Table 6.3: Tensile modulus of SFC with homogeneous HGM particle size variations

Size variation	Volume fraction of HGM (%)					
Particle sizes	NE (GPa)	EPT60-5 (GPa)	EPT60-10 (GPa)	EPT60-15 (GPa)	EPT60-20 (GPa)	EPT60-25 (GPa)
AA (20-24µm)	2.14 ± 0.14	2.55 ± 0.46	2.48 ± 0.22	2.51 ± 0.03	2.65 ± 0.16	2.68 ± 0.10
BB (25-44µm)	2.14 ± 0.14	2.64 ± 0.25	2.35 ± 0.43	2.30 ± 0.34	2.44 ± 0.07	2.09 ± 0.18
CC (45-49µm)	2.14 ± 0.14	2.52 ± 0.48	2.14 ± 0.21	2.95 ± 0.70	2.33 ± 0.16	1.98 ± 0.15
DD (50-60µm)	2.14 ± 0.14	2.35 ± 0.50	2.31 ± 0.31	2.10 ± 0.32	2.00 ± 0.58	1.90 ± 0.31

Table 6.3 shows the tensile modulus of the homogeneous SFC. An increase in tensile modulus was observed for SFCs mostly for the particle sizes variations and volume fractions, which is higher than the NE except at EPT60-25BB, EPT60-25CC, and EPT60-15DD, EPT60-20DD, and EPT60-25DD. These results correspond to the earlier report by (Liang 2005); Gupta, Ye and Porfiri (2010), where modulus of several compositions of syntactic foams was higher than that of the neat resin. The highest tensile modulus of the SFCs was 2.95 GPa at EPT60-15CC. Meanwhile, the tensile modulus values of the SFCs decreased at EPT60-BB, EPT60-CC, and EPT60-DD with an increase in the volume fraction of the HGM except at EPT60-20BB. A Similar case was reported by Hu and Yu (2011), where the tensile modulus of the SFCs for various compositions reduced as the volume fraction of the microballoons increased. The lowest tensile modulus of the SFC was observed at EPT60-25CC and EPT60-25DD, this reduction can be attributed to the porous nature of SFC at higher loading of HGM in the matrix and related to their density values. For hollow particulate-filled polymer composites, the increase in modulus of the SFC compared to the EPT60-0 can be related to some crosslinking points generated by the movement of the molecular chains of the matrix. These crosslinking points blocked to some

extent by the addition of the HGM filler, resulting in improved stiffness of the SFC, thereby leading to decreased young modulus as the volume fraction of the HGM filler increased. In general, to get a better stiffness of the SFC, the viscosity reduction of the matrix and the interfacial bonding between the matrix and the HGM filler must be improved.

6.1.2.2 Tensile Strength (MPa)

Table 6.4: Tensile strength (TS) of homogeneous HGM particle size variations of SFC

Size variation	Volume fraction of HGM (%)					
Particle sizes	NE	EPT60-5	EPT60-10	EPT60-15	EPT60-20	EPT60-25
AA (20-24µm)	40.47 ± 0.64	64.51 ± 3.8	59.43 ± 5.8	54.86 ± 0.98	54.87 ± 3.5	49.91 ± 1.4
BB (25-44µm)	40.47 ± 0.64	54.38 ± 1.1	51.65 ± 9.2	47.45 ± 10.7	47.35 ± 4.3	32.18 ± 8.9
CC (45-49µm)	40.47 ± 0.64	58.62 ± 9.6	47.42 ± 7.7	60.84 ± 8.5	42.38 ± 8.3	34.79 ± 4.4
DD (50-60µm)	40.47 ± 0.64	55.74 ± 11.6	47.95 ± 4.7	44.68 ± 4.5	40.59 ± 7.2	33.84 ± 5.1

The tensile strength of the SFCs filled with homogeneous HGM particle sizes is shown in Table 6.4. The tensile strength results were compared in two steps. In the first step, a comparison of tensile properties of SFC containing HGM of different size variations (AA, BB, CC, and DD) and different volume fractions (EPT60-5 to EPT60-25 vol%) was compared with the EPT60-0. The second step discussed comparing the of tensile strength of SFC of different size variation and same volume fraction of HGM with the EPT60-0.

In the first step, it was observed that the SFC with AA at 5 volume fractions EPT60-5AA has the highest tensile strength of 64.51MPa, followed by EPT60-15CC, 60.84 MPa. A uniform trend of decreasing tensile strength with an increasing volume fraction of HGM was observed at EPT60-AA, EPT60-BB, and EPT60-DD. The tensile strength decreased with increasing volume fraction of HGM from EPT60-5 to EPT60-25 by 22.6%, 40.8%, and 39.3% at AA, BB, and DD respectively. A similar case was reported by (Gupta and Nagorny 2006); Ahmadi H (2016), where an increase in the content of HGM of the foams led to the decreased tensile strength of

SFCs. The tensile strength for most size variations (AA, BB, and DD) are highest at 5vol% of HGM except for CC which was at 15vol%. This can be ascribed to the fact that the inclusion of HGM in the EPT60-0 at small volume fraction led to homogeneity in the composite reactions and strong interfacial bonding between the matrix and the HGM, thereby increasing the tensile strength.

However, the tensile strength reduced in value than the NE at EPT60-25BB, EPT60-25CC, and EPT60-25DD by 20.5%, 14%, and 16.4% respectively. This means that the strength of SFC strongly depended on the matrix's content at a high-volume fraction of HGM which is the main constituent of load bearing. Also, it was noted that the addition of HGM created imperfections such as unwanted porosity and weak interfacial surfaces between the HGM and the matrix. Moreover, the matrix-HGM interface does not appear to be very strong in the composite as the presence of high-volume fraction of HGM reduces the volume fraction of the epoxy resin in the structure, thereby causing the tensile strength of the SFC to decrease. This corresponded to earlier report by Nikhil et al and Ahmadi et al (Ahmadi H 2016) results, where the strength of SFC decreased by 25-60% and 33-35%, by adding above 20% of microballoons to epoxy resin. It further revealed that for polymer composite with poor interfacial adhesion (or bonding) between the filler and the matrix, the tensile strength would decrease as the HGM filler volume fraction increases.

The reduction in their tensile strength can also be related to the fact that the density of SFC was reduced with increasing filler content as reported in chapter 5, which corresponds to the reduction of epoxy matrix and substitution by void equivalent volume fraction. This void results in quicker crack propagation resulting in lowered strength (**see chapter 5**).

The second step compared the different particle size variations against the same volume fraction. At EPT60-5, no peculiar trend was observed for the tensile strength of the SFC with the increase in particles sizes. The order here was AA > CC > DD > BB. However, the tensile strength for all the SFCs increased by 59.4%, 44.8%, 37.7% and 34.4% respectively than the EPT60-0 but decreased with an increase in particle size establishing the concept of better homogeneity of dispersion of HGM at lower size particles. Also, the decrease in aspect ratio with increasing particle size which invariably led to decrease in wall thickness with increasing particle size (**chapter 4, section 4.2**) contributed to its increased tensile strength. At EPT60-10, the tensile strength decreased with increasing particle sizes in the order AA >BB > DD > CC. However, all the SFCs exhibited more tensile strength with 46.8%, 27.6%, 18.5% and 17.2% than the EPT60-0. At EPT60-15, the highest strength was at CC, as there was no trend relating

to particle sizes and volume fraction. The order of tensile strength increase was CC > AA > BB > DD with increase of 50.3%, 35.6%, 17.2% and 10.4% respectively. At EPT60-20, the SFCs showed a trend of decrease in tensile strength with increasing particle sizes in the order AA > BB > CC > DD and greater than the NE by 35.6%, 17.5%, 4.7% and 0.3% respectively as discussed earlier. Lastly, at EPT60-25, the order of tensile concerning particle sizes was AA > BB > DD > CC. The comparison helped to understand the effect of varying and analyzing particle sizes at the same volume fraction of HGM on the tensile strength of SFC.

Tensile Strain (mm/mm).

Table 6.5: Tensile strain of homogeneous HGM particle size variations of SFC

Size variation	Volume fraction (%) of HGM					
Particle sizes	NE	5	10	15	20	25
AA (20-24µm)	0.050	0.041	0.056	0.037	0.035	0.029
BB (25-44µm)	0.050	0.033	0.038	0.029	0.025	0.021
CC (45-49µm)	0.050	0.038	0.031	0.029	0.024	0.024
DD (50-60µm)	0.050	0.043	0.03	0.033	0.029	0.024

Table 6.5 illustrates the influence of the HGM size variations and volume fractions on the tensile strain at the break of the SFC. Tensile strain at break was an important parameter for characterizing the tensile fracture relative to the tensile strength. The material fracture rate was relative to the strain as presented in Table 6.5. The chain mobility was responsible for the tensile break of SFC during tensile testing and is controlled by the volume fraction of the filler (Liang J.Z. 2000).

The tensile strain at break was lower for all the homogeneous SFCs compared to the EPT60-0, because during the cooling of SFC, the thermal energy associated with the SFC chains decreased, and the molecular mobility of the SFC chains was arrested as described by the TGA in chapter 9. The decrease in the tensile strain of SFC at break can be related to the presence of large aggregates and a strong cluster of HGM filler at higher volume fractions in the SFC. It

can also be said that the tensile fracture of SFC can be modified by the content of the HGM filler at a lower concentration. This can further influence the formation of stress concentration in the interfacial layer between the matrix and the HGM filler (Liang 2005).

The decreased tensile strain is relative to the density values and consistent with the tensile strength which also decreased with an increase in the volume fraction loading of HGM. This can be related to the weak molecular bonding observed in the mixture between the HGM filler and the matrix. It can further be attributed to the fact that when the concentration of HGM filler increases, ligament thickness will be smaller than the critical thickness, and agglomeration of HGM in the epoxy matrix will occur quickly, leading to a reduction in the toughness of the SFC thereby reducing the tensile strain (Liang J.Z. 2000).

6.2 Morphological Properties of Syntactic Foam Composites

6.2.1 Dispersion Characteristics of Syntactic Foam Composites –Transmission Electron Microscopy (TEM)

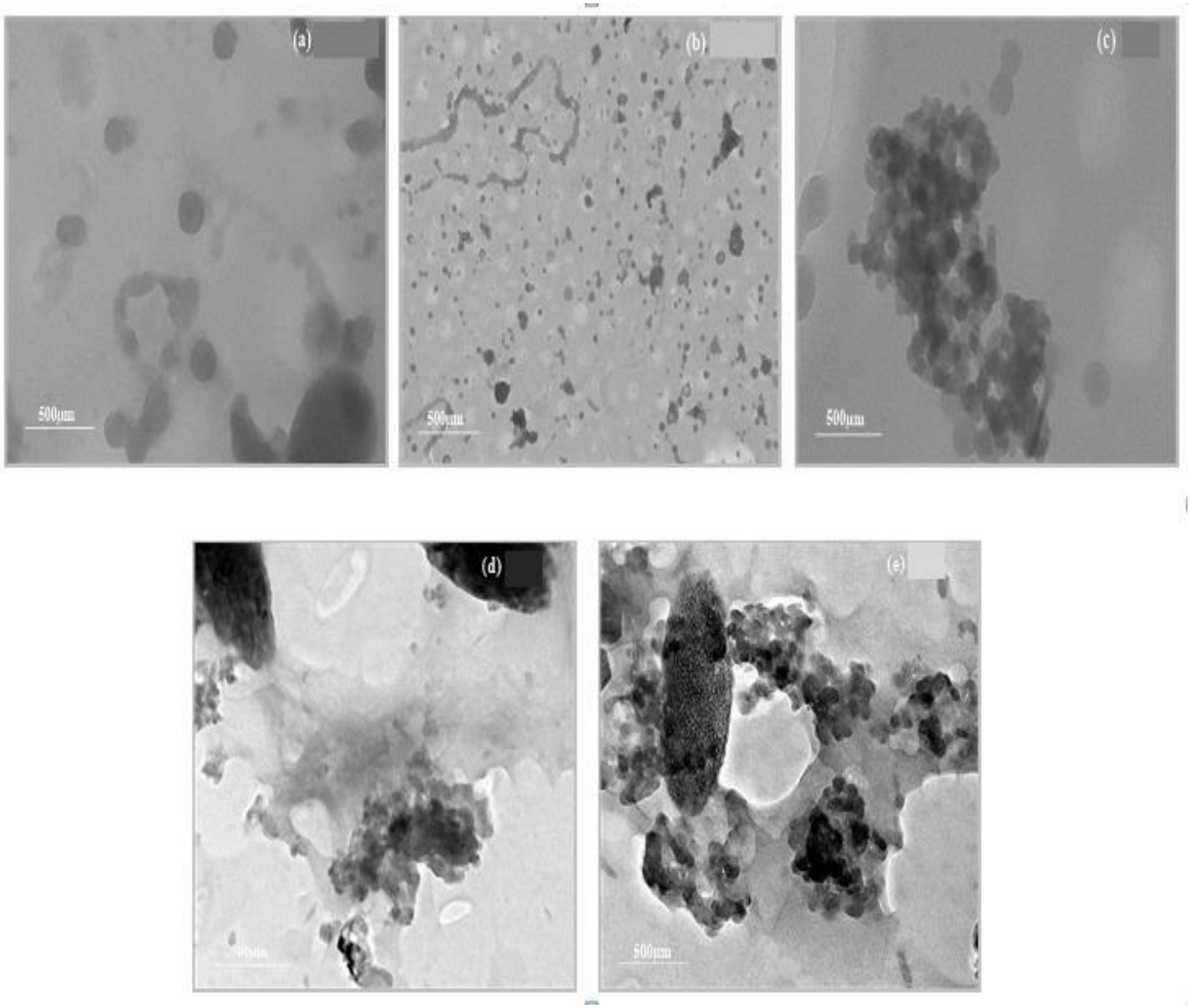

Figure 6.3: Transmission Electron Microscopy (TEM) of SFC at (a) EPT60-5, (b) EPT60-10, (c) EPT60-15, (d) EPT60-20, and (e) EPT60-25 showing the clustered particles of the hollow glass microspheres dispersed in the syntactic foam composite at each volume fraction.

The distribution of HGM filler in the SFC was investigated using transmission electron microscopy (TEM). Figure 6.3 (a-e) shows the TEM images of SFC at different volume fractions (EPT60-5 to EPT60-25) of HGM in the matrix for the heterogeneous form. There was an uneven distribution of HGM filler in the matrix as the concentration increased from EPT60-5 to EPT60-25. This affected the mechanical properties of the SFC and contributed to an increase in the matrix porosity level, especially with the high loading volume fractions. EPT60-5 and EPT60-10 show little agglomeration of the HGM due to lower concentration. The agglomeration increased as the concentration increased as seen in EPT60-15, EPT60-20, and EPT60-25 with much clustering and percolation of HGM at EPT60-25.

6.2.2 Scanning Electron Microscopy for Heterogeneous HGM Particle sizes

6.2.2.1 Tensile Fractured Surfaces

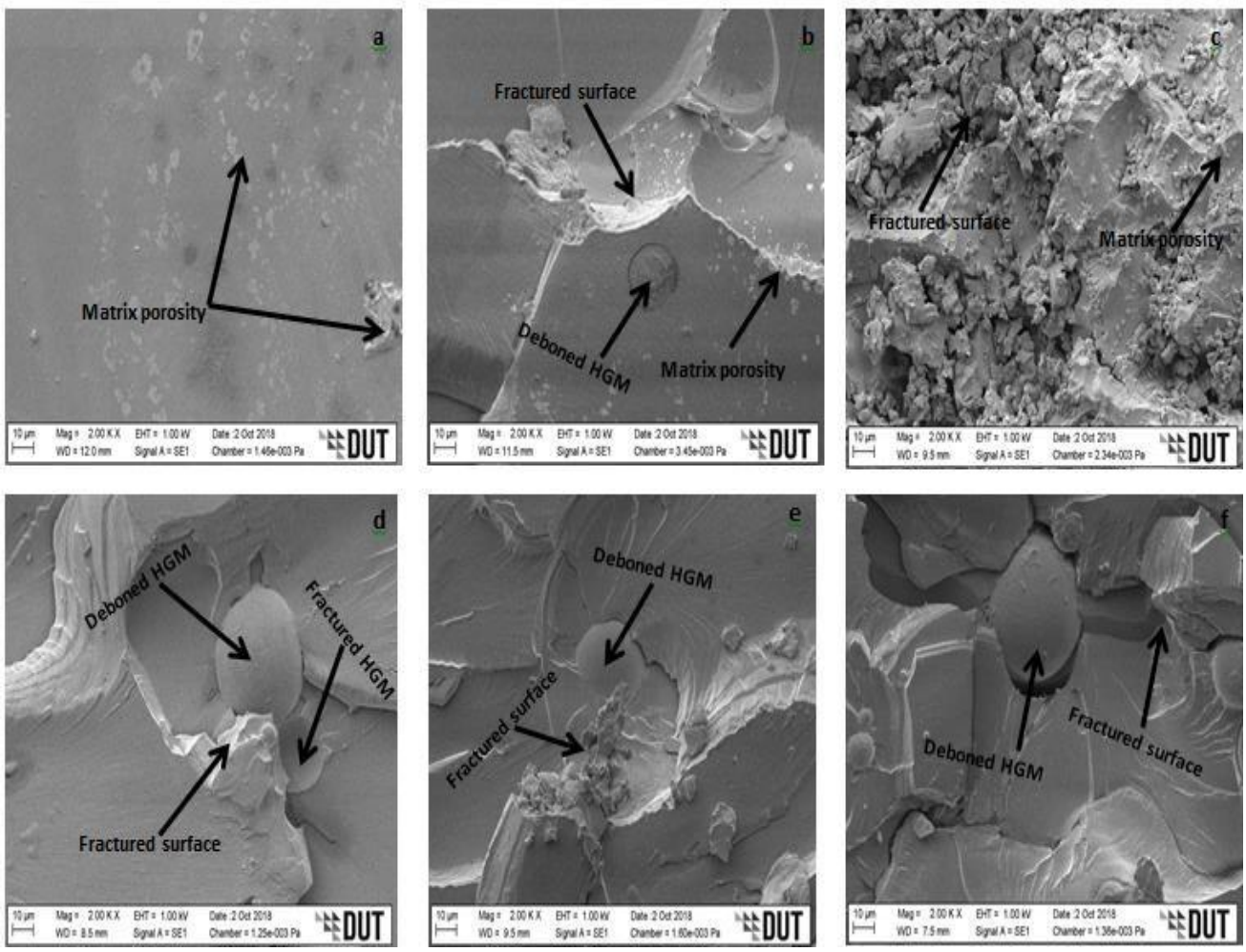

Figure 6.4: SEM images for tensile fractured specimens of SFC-heterogeneous HGM at (a) EPT60-0, (b) EPT60-5, (c) EPT60-10, (d) EPT60-15, (e) EPT60-20 and (f) EPT60-25

Figure 6.4 (a-f) shows the fractured surfaces for the plain matrix and SFCs with heterogeneous HGM at different volume fractions under tensile testing. Figure 6.4(a) shows portion of the plain matrix with a smooth surface morphology where the void could be seen freely propagating around the surfaces which are responsible for its brittle failure. Voids are air bubbles entrapped during the mixture of the HGM and the epoxy resin (see Figure 2.1). . The SEM images of the fractured surfaces of SFC filled with heterogeneous HGM show the interaction and the microstructural changes that occurred in the composites when HGM was added to the epoxy matrix as shown in Figure 6.4 (b-f). HGM of each volume fraction was distributed in the arrows show the fractured surfaces as deboned microspheres (un-fractured HGM), fractured microspheres, and matrix porosity surfaces on the SFC. The fractured microsphere and debonded microspheres increased with an increasing volume fraction of HGM in the SFC. Also, the surface smoothness reduced which resulted of good interaction on the interfaces between the epoxy matrix and the HGM. Moreover, it could be because of the restriction caused by the HGM spheres in the matrix flow causing changes in the surface morphology. Figure 6.4 (b) shows slight roughness and matrix porosity on the surface morphology which could be attributed to the large volume fraction of the matrix and possible increase in the strain value. The ductile fracture was observed in Figure 6.4 (c-e) due to their increased HGM vol% but with reduced matrix porosity, resulting in their increased tensile strength and reduced strain compared to the epoxy matrix. The extension of fractured surfaces in Figure 6.4 (f) EPT60-25 was responsible for its reduced tensile strength and strain values as described earlier in **Table 6.1 of section 6.1**.

6.2.2.2 Scanning Electron Microscopy for Homogenous HGM Particle sizes

6.2.2.2.1 Tensile Fractured Surfaces-Homogenous HGM

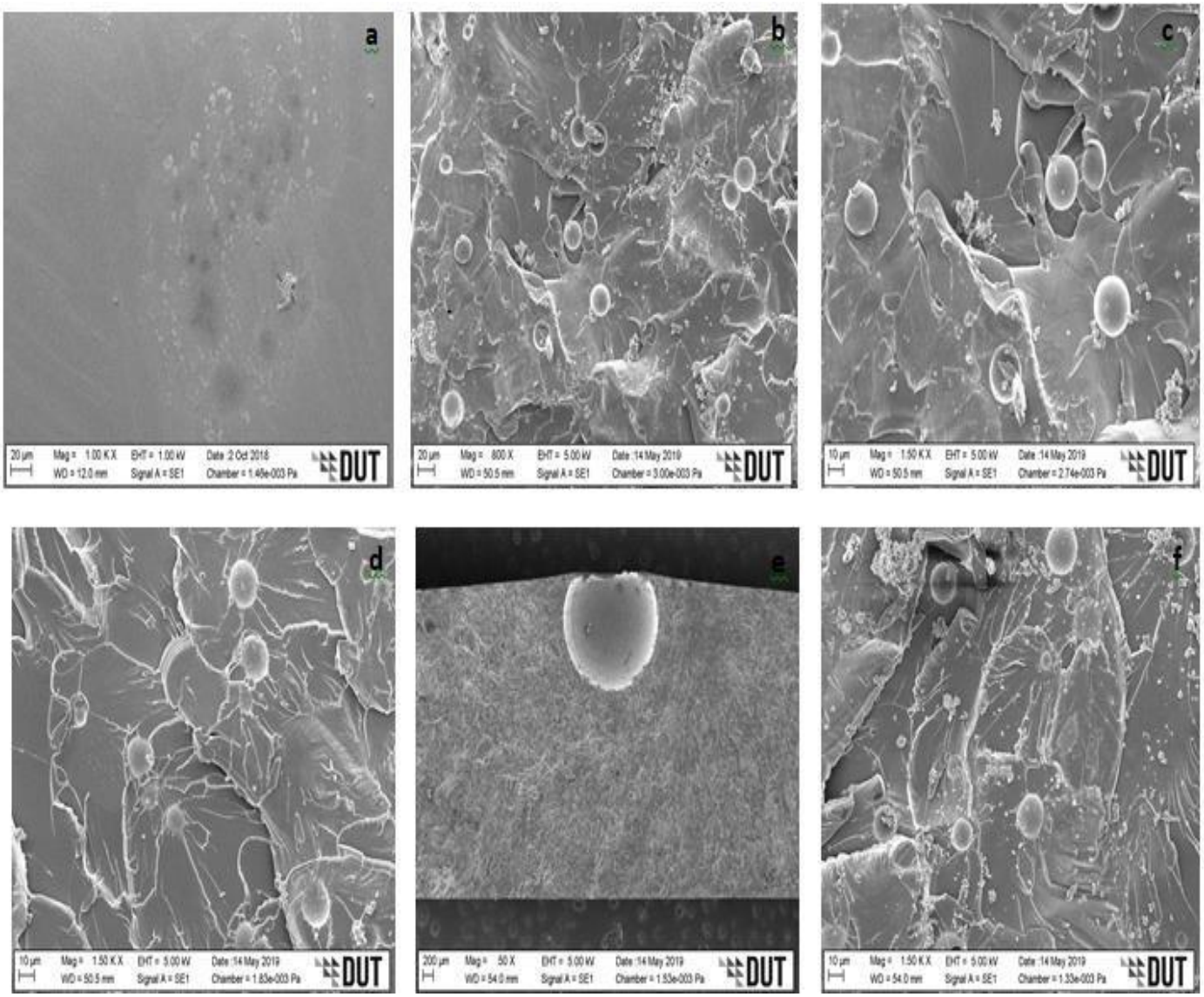

Figure 6.5: SEM images for tensile fractured specimens of SFC-homogenous HGM (20-24µm) at (a) EPT60-0, (b) EPT60-AA5, (c) EPT60-AA10, (d) EPT60-AA15, (e) EPT60-AA20 and (f) EPT60-AA25

.

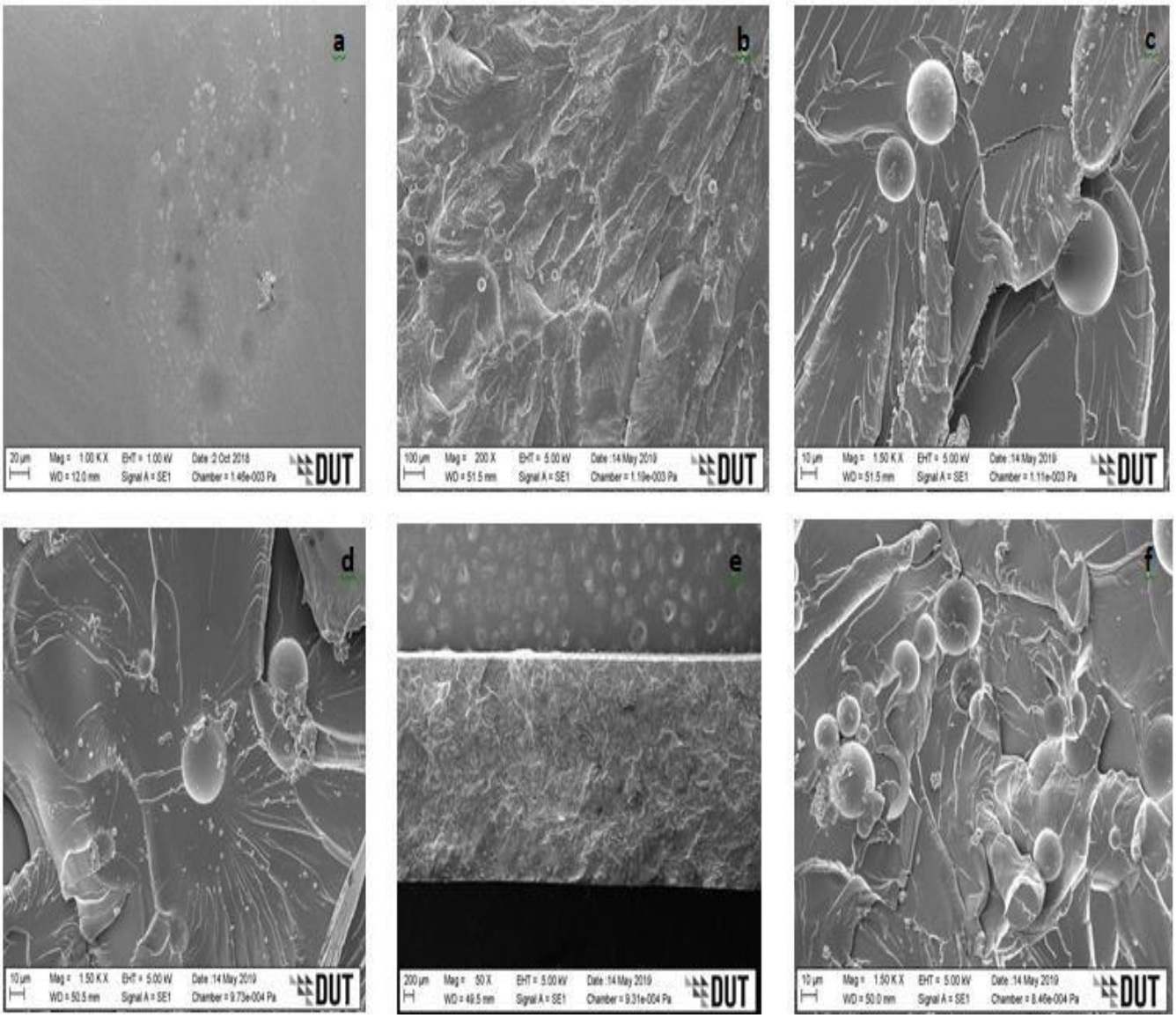

Figure 6.6: SEM images for tensile fractured specimens of SFC-homogenous HGM (25-44µm) at (a) EPT60-0, (b) EPT60-BB5, (c) EPT60-BB10, (d) EPT60-BB15, (e) EPT60-BB20 and (f) EPT60- BB25

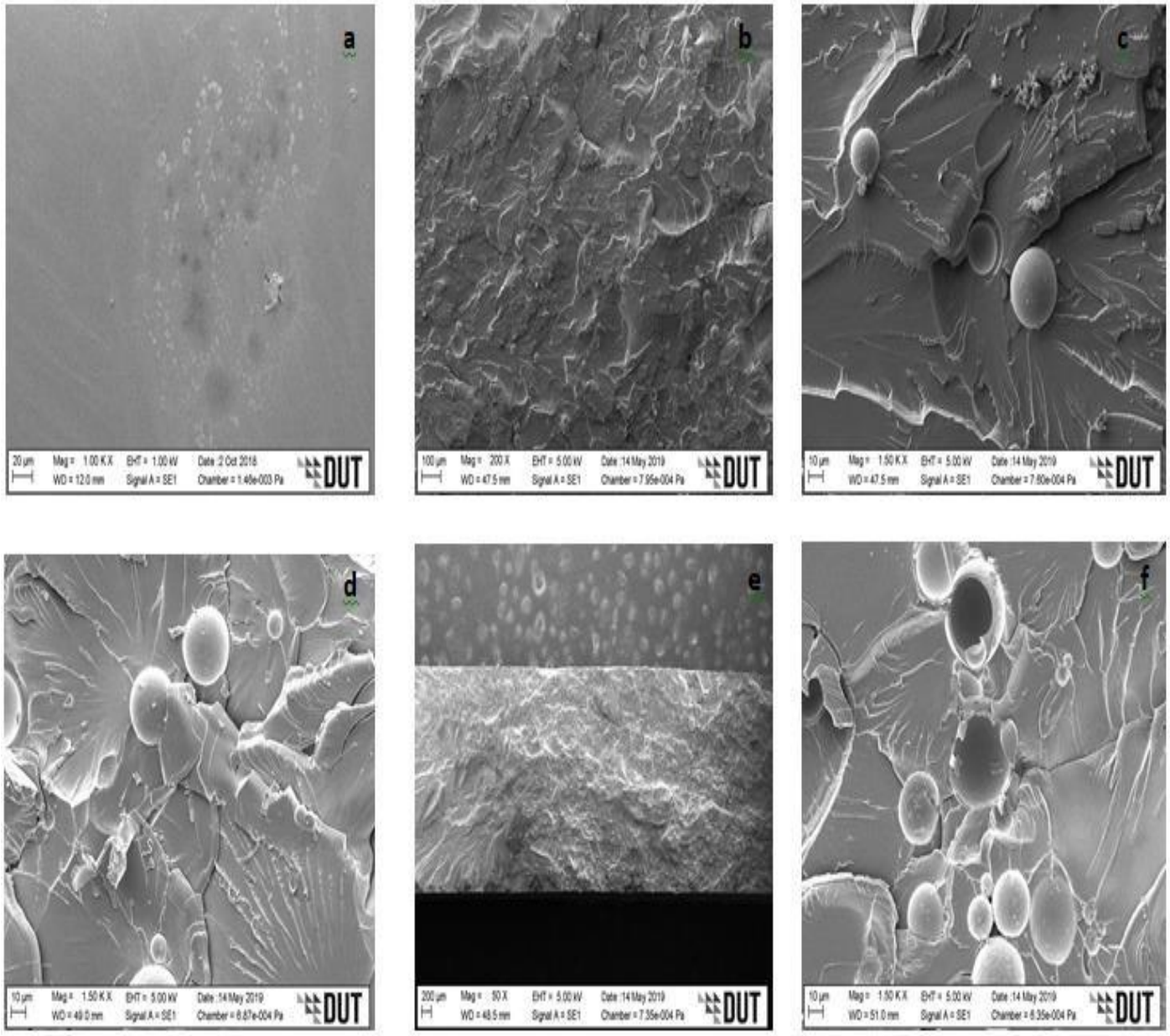

Figure 6.7: SEM images for tensile fractured specimens of SFC-homogenous HGM (45-49µm) at (a) EPT60-0, (b) EPT60-CC5, (c) EPT60-CC10, (d) EPT60-CC15, (e) EPT60-CC20 and (f) EPT60- CC25

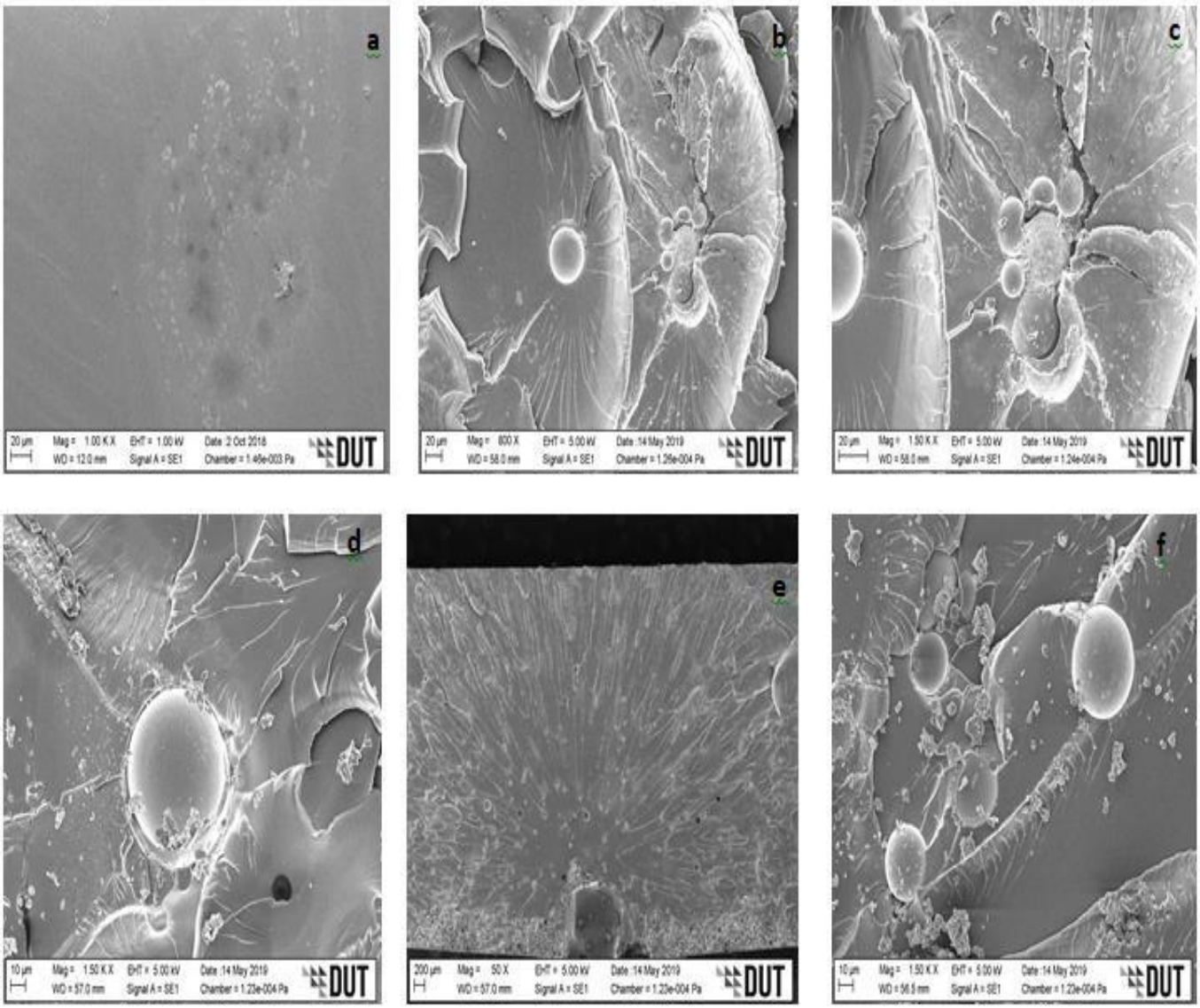

Figure 6.8: SEM images for tensile fractured specimens of SFC-homogenous HGM (50-60µm) at (a) EPT60-0, (b) EPT60-DD5, (c) EPT60-DD10, (d) EPT60-DD15, (e) EPT60-DD20 and (f) EPT60- DD25.

Figures 6.5 - 6.8 shows the surface morphology of tensile fractured surfaces for the homogenous HGM at different volume percentage in the SFC. Figures 6.5 (a) to 6.8(a) indicates the plain NE surface which has been previously discussed (Figure 6.4 (a)). The smooth surfaces suggest the typical brittle fracture characteristics of epoxy resin (Hu and Yu 2011). Figures 6.5(b-f) to 6.8(b-f) show the SEM fractured surfaces of the SFCs which shows the interaction between the epoxy matrix and the homogeneous HGM filler at different volume fractions. The SFCs through the micrographs showed resistance to tensile deformation as reflected in their increased tensile strengths and reduced strain values (**section 6.1.3, Table 6.4 – 6.5**).

The micrographs in Figure 6.5 (b) – 6.8(b), with 5vol% of HGM (i.e., EPT60-AA5 - EPT60-DD5) show rough surface morphology for each size of particle with little matrix porosity. This structure could indicate good adhesion between the HGM filler and the epoxy matrix at a small volume fraction of HGM. This was responsible for their improved tensile strength and strain values (**section 6.1.3, Table 6.4**). Also, from Figures 6.5 (c, and d) to 6.8 (c, and d), with 10vol% and 15vol% of HGM (i.e., EPT60-AA10, and AA15 to EPT60-DD10 and DD15), the micrograph structure surfaces exhibited roughness (which shows the entrapped air bubbles in the composites), matrix porosity, and deboned HGM because of ductile failure deformations experienced resulting in their reduced tensile strength compared to the 5vol%. These regions consisted of collapsed microballoons and matrix porosity with increasing agglomeration. This occurred due to particle deformation caused by the processed composites and exposed cavities (Hu and Yu 2011).

Moreover, Figures 6.5(e) – 6.8(e), with 20vol% of HGM (i.e., EPT60-AA20 – EPT60-DD20), exhibited clustered HGM, rough surface morphology, and deboned HGM. This corresponds to their failure mode and the fragmentation of the specimen with reduced tensile strength. Also, in Figures 6.5(f) – 6.8(f), with 25vol% of HGM (i.e., EPT60-AA25 – EPT60-DD25), there were unclear interfaces between the epoxy resin and the HGM leading to clustered HGM with rough surfaces and matrix porosity which could be seen spreading over the morphology surface with structures of debonded HGM. These observations showed that the toughening mechanism of SFCs at high vol% of HGM could not withstand tensile properties compared to when at smaller vol% of HGM. The reduction in the strain of the SFCs can be said to have resulted from the restriction of free molecular chain movement by the HGM during the mixture with epoxy resin (Awais *et al.* 2020). Also, it could be due to poor interaction between the intermolecular attraction forces between the matrix and the HGM hydroxyl group (Cunha *et al.*

2018).

Generally, adding HGM with varying particle sizes and volume fractions have contributed to better incorporation of the reinforcement by the polymer matrix. Moreover, it could be said that the tensile properties depend on the interfacial bonding characteristics to transfer load from the epoxy matrix to the filler particle (Bharat, Abhishek and Palanikumar 2017).

Conclusion:

Tensile properties of the SFCs with heterogeneous and homogeneous HGM particle sizes variation was discuss in this chapter. The tensile stress and strain for all the compositions shows an improvement in tensile stress than the neat epoxy- EPT60-0. In contrast, the neat epoxy has more extended elongation than the SFCs. The tensile modulus increased for all the SFCs for heterogeneous and homogeneous HGM particle sizes and volume fractions compared to the neat epoxy matrix. In contrast, the tensile strength for both heterogeneous and homogeneous particle size variation of SFC increased considerably for most of the composites compared to the neat epoxy except at some volume fraction variations of HGM, especially with high volume fraction (EPT60-25BB, EPT60-25CC, and EPT60-25DD). This is because the decrease in aspect ratio with increasing particle size which invariably led to decrease in wall thickness with increasing particle size (**chapter 4, section 4.2**) contributed to its increased tensile strength. Also, the EPT60-0 tensile strain was higher than all the SFCs at heterogeneous and homogeneous HGM particle sizes and volume fractions. The morphology of fractured surfaces validates these points.

In the next chapter 7, the mechanical properties of the SFCs are continued where the flexural properties for heterogeneous and homogeneous particle size variations are discussed.

CHAPTER 7

7.0 THE FLEXURAL CHARACTERISTICS OF SFC

In this chapter, the flexural (modulus, strength, and strain) properties of syntactic foam composites (SFCs) for the heterogeneous (whole HGM) volume% concentrations and homogeneous (size varied HGM) volume% concentrations are discussed.

In this chapter, findings from the effect of mixing HGM and the NE in heterogenous and homogenous volume fraction variation are elaborated. The chapter is divided into three sections; section **7.1** is based on the flexural properties of SFC with heterogenous HGM, section **7.2** is on the flexural properties of SFC with homogenous HGM, while section **7.3** is on scanning electron microscopy of the fractured surfaces of the SFCs.

7.1 Flexural Properties of SFC with Heterogeneous HGM

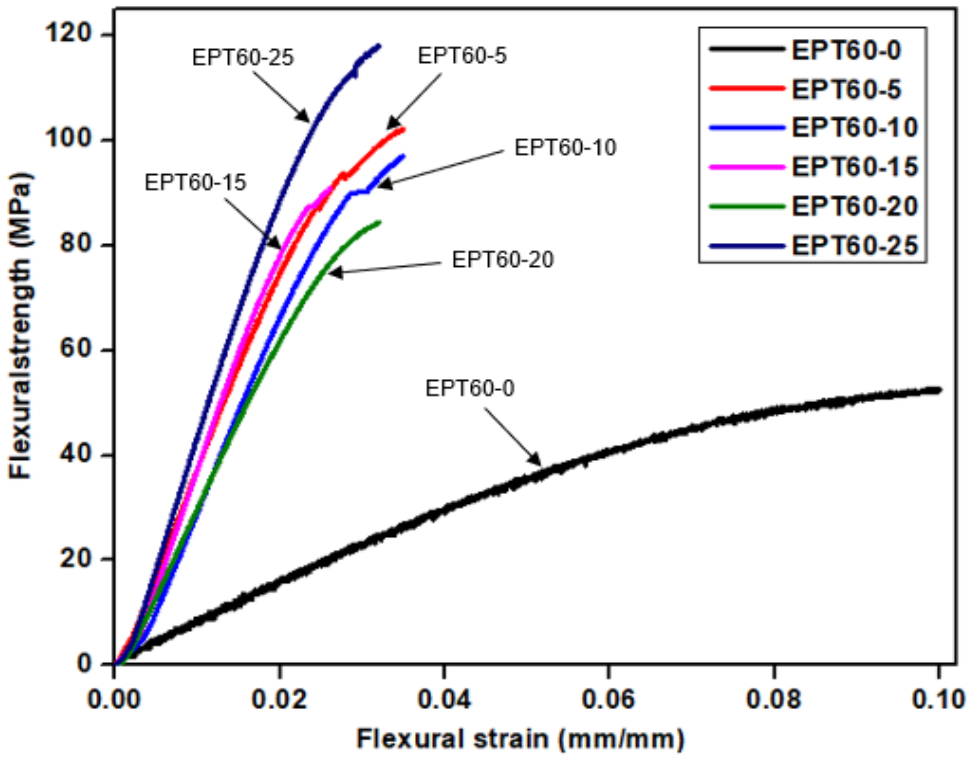

Figure 7.1: Flexural stress-strain of SFC with heterogeneous HGM filler.

Figure 7.1 and Table 7.1 shows the flexural stress-strain graph and flexural properties of SFC with heterogeneous HGM filler in epoxy matrix. The stress-strain graph in Figure 7.1 shows that the stress increases linearly for all the SFC with respect to the strain for all the volume fractions of the HGM filler before rupture. The trend for the stress-strain curve is similar for all the SFC and the neat epoxy matrix. The initial portion of the curve is elastic, while the latter part is non-linear. The flexural strength increases with an increase in the volume fraction of the HGM filler, and the flexural strain at the break of the SFC is close to that of the neat epoxy matrix except at EPT60-15. Similar observation was reported by Bharath et al Bharath Kumar *et al.* (2016b), where the strength of the syntactic foam increased with the filler content. The plastic deformation observed at the later parts of the stress-strain curve may be attributed to the increased strength of the SFC. Specimen are subjected to compressive stresses on the top part and tensile stresses on the lower part during flexural loading as shown in **section 3, Figure 3.8**. The load decreases after the end of the elastic region due to failure initiation in the SFC. The SFCs subjected to flexural loadings failed at the side under tensile stresses. The deformation increased with increasing HGM content which resulted from the amount of epoxy matrix fraction in each composition. These results have been published by the author (Afolabi, Kanny and Mohan 2021a; Afolabi, Kanny and Mohan 2021b)

Table 7.1: Flexural properties of SFC with heterogeneous HGM filler concentration

Specimen name	Volume fractionof HGM (%)	Flexural Modulus (GPa)	Flexural strength (MPa)	Flexural strain (mm/mm)
1	Neat epoxy	2.4	53.5	4.36E-02
2	EPT60-5	3.5±0.78	94.0±2.71	3.49E-02
3	EPT60-10	3.7±0.92	96.9±4.76	4.36E-02
4	EPT60-15	3.9±1.06	97.9±5.47	2.97E-02
5	EPT60-20	4.3±1.34	103.4±9.36	3.80E-02
6	EPT60-25	4.8±1.70	118.08±9.74	3.65E-02

From Table 7.1, it was observed that the SFC shows highest flexural modulus of 4.8 GPa at 25vol% of HGM. The flexural modulus increased with an increase in the HGM content in the SFC. This may be attributed to strong bonding and adhesion force exhibited by the interaction of the HGM and the epoxy. The result is consistent with the report by Tagliavia, Porfiri and Gupta (2010) where the flexural modulus also increased with increasing HGM filler concentration at a prescribed volume fraction.

The flexural strength of the SFCs increased in values for all the volume fractions of the HGM filler compared to the neat epoxy. The SFCs shows better resistance to flexural load with the ability to withstand the bending force. All the composition of the SFC increased in flexural strength compared to the neat epoxy. The flexural strength of SFC progressively increased with increasing volume fraction of HGM, with the highest flexural strength at EPT60-25 with an increase of 120.7% compared with the neat epoxy. This was possibly due to improved dispersion that occurred during interfacial bonding between the HGM-matrix which enhances the increased strength as shown in the micrograph of **Figure 7.3 (b-f)**. Similar observation was reported by Bharath Kumar *et al.* (2016b) and Liang (2005), that the flexural strength of the composites with increasing particle content.

However, the flexural strain of SFC shows decrease in values compared to the NE with increasing volume fraction of HGM. At EPT60-10, the strain of SFC shows the same values with that of NE as published by the author (Afolabi, Kanny and Mohan 2021b).

Table 7.2: Comparison of flexural properties of uniform HGM filler SFC with existing literature

S/no	Matrix type	Composition of HGM and type	Flexural strength (MPa)	Flexural modulus (MPa)	Reference
1	Epoxy resin LR20	_____	53.3	2359	Present work
2	Epoxy resin LR20	5% HGM-T60	94.0	3485	
3	Epoxy resin LR20	10% HGM-T60	96.9	3728	

4	Epoxy resin LR20	15% HGM-T60	97.9	3931	
5	Epoxy resin LR20	20% HGM-T60	103.4	4292	
6	Epoxy resin LR20	25% HGM-T60	118.1	5752	
12	Epoxy resin E51	47% HGM-S38	21.8	2120	Yingjie Q.Y et al [19]
13	Epoxy resin E51	49% HGM-S38	21.8	2090	
14	Epoxy resin E51	51% HGM-S38	18.3	2080	
15	Epoxy resin E51	53% HGM-S38	16.0	2050	
16	Epoxy resin E51	55% HGM-S38	14.4	1940	
17	Epoxy resin E51	57% HGM-S38	12.3	1794	
18	Epoxy resin araldite LY5052	S25 HGM	37.4		Karthikeyan C.S. et at [24]

Table 7.2 shows the comparison of flexural properties for the SFC with heterogeneous HGM filler compared to existing literature. The flexural strength and modulus of SFCs shows improved properties compared to the existing literature which can possibly be due to the good adhesion between the matrix and the HGM filler during mixture and the incorporation of a lower volume fraction of HGM. Degasification of the SFCs composites during mixture to reduce the void content also contributed to its improved properties as discussed in previous published article (Afolabi, Kanny and Mohan 2021b). Part of this has been published in **Appendix 13.2 (A1-2)**

7.2 Flexural Properties of SFCs Size Variation with Homogeneous HGM filler compositions

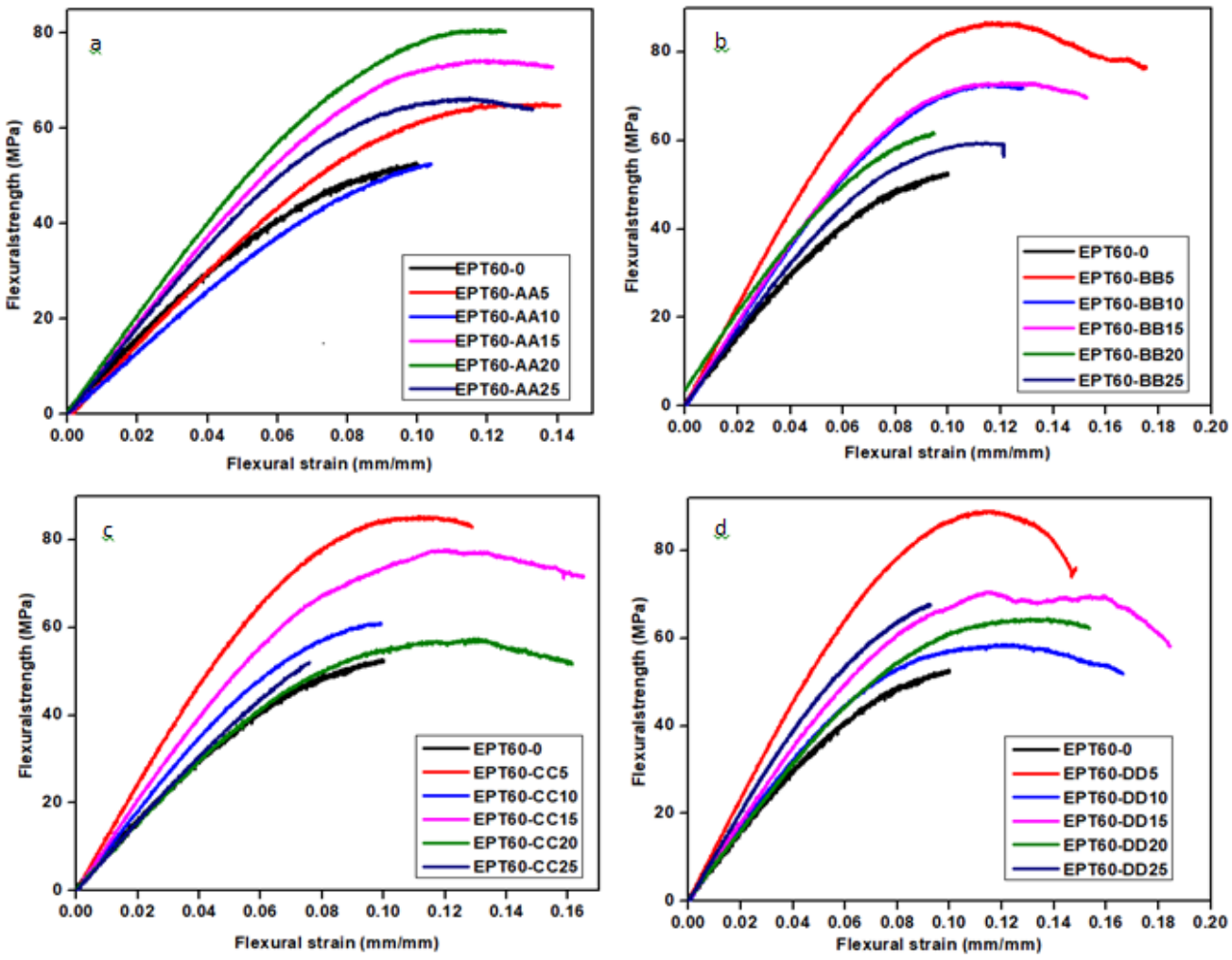

Figure 7.2 (a-d): Stress-strain graphs for SFCs with homogeneous HGM particle sizes compared to the neat epoxy (EPT60-0).

Figure 7.2 (a-d) presents the stress- strain graphs of the SFC with homogenous HGM particle sizes compared with the neat epoxy (EPT60-0). All the samples showed brittleness in nature by breaking after reaching maximum yield stress. They also possess good bending capacity than the EPT60-0 except EPT60-AA10 and EPT60-CC25 with little lower stress values. This can possibly be due to the either poor interation between the filler and the matrix during mixing leading to early breakage and reduced strain of the specimens. Also, it resulted from interface debonding and matrix cracking of the specimens. Figure 7.2 (a) shows that the highest stress is at EPT60-AA20, while in Figure 7.2 (b-d), the highest stress is at EPT60-BB5, EPT60-CC5, and EPT60-DD5 respectively. Increase in flexural stress at 5vol% of HGM as the size variation

increased can possibly be because of the fact that the addition of smaller quantity of filler particle is observed to give a better dispersion in the matrix during mixture resulting in high strength and stiffness.

Table 7.3: Flexural modulus of SFC filled with homogeneous HGM-epoxy resin (GPa)

Size variation	Volume fraction of HGM (%)					
Particle sizes	NE	EPT60-5	EPT60-10	EPT60-15	EPT60-20	EPT60-25
AA (20-24µm)	2.4	0.81	0.60	1.00	1.02	0.94
BB (25-44µm)	2.4	1.09	1.01	1.02	0.95	0.82
CC (45-49µm)	2.4	1.31	0.81	1.06	0.74	0.90
DD (50-60µm)	2.4	1.14	1.01	0.86	0.78	1.03

Table 7.3 shows the flexural modulus of SFCs for the homogeneous HGM filler. The neat epoxy being the base material for comparison has higher flexural modulus than all the homogeneous SFCs unlike the heterogeneous SFCs which has an increase of 100% in modulus than the NE. At AA, EPT60-20 has the highest flexural modulus of 1.02 GPa. At BB, the highest flexural modulus was 1.09 GPa at EPT60-5 and happens to be the highest for all the particle sizes and volume fractions. At CC and DD, the highest flexural modulus is 1.31 GPa and 1.14 GPa at EPT60-5 respectively. The increase in flexural modulus of the SFCs at higher particle sizes of HGM resulted from the followings: stiff particles in HGM, reduced wall thickness “ω”, and high aspect ratio “a” at lower volume fractions. It also occurred because of possible weak bonding that existed between the molecules of the homogeneous HGM and the neat epoxy. Moreover, it could be as a result of density reduction as the HGM volume fraction increases (Paul and Velmurugan 2018). Moreover, it shows that the particle sizes of HGM affected the mechanical properties of syntactic foam which correspond with the report by Kadhim Al-Sahlani (2018) where the varying sizes of the particles changes the microstructure and flexural modulus of glass-metal syntactic foam.

Table 7.4: Flexural strength of SFC filled homogeneous HGM-epoxy resin (MPa)

Size variation		Volume fraction (%)				
Particle sizes	NE	EPT60-5	EPT60-10	EPT60-15	EPT60-20	EPT60-25
AA (20-24µm)	53.5	65.3±8.3	52.6±0.6	74.4±4.8	80.7±9.2	66.3±9.1
BB (25-44µm)	53.5	86.7±3.5	72.7±3.6	70.7±2.2	62.8±6.5	59.5±4.2
CC (45-49µm)	53.5	85.5±2.6	61.2±5.4	77.8±7.2	57.6±2.9	52.1±0.9
DD (50-60µm)	53.5	89±5.1	58.6±3.6	70.5±2.0	64.5±7.8	67.8±1.1

Table 7.4 represent the flexural strength (MPa) of SFC for the homogeneous HGM filler. The flexural strength of the SFCs increased compared with the NE except at EPT60-10AA and EPT60-25CC with 1.7% and 2.6% decrease respectively due to possible machine error at that loading. At AA, the SFC increased in flexural strength for all the volume fraction of HGM, the highest flexural strength is 80.7 MPa at EPT60-20AA which is 50.8% increase compared to the neat epoxy. At BB, the SFCs show a trend of decreased flexural strength with increasing volume fraction of HGM. The highest been 86.7 MPa at EPT60-5BB which is 62.1% increase compared with the NE. The highest V_d at BB possibly influenced this trend. This implies that the uniformity of particles distribution reduced the flexural strength with increasing volume fraction. Also. it was because of the high aspect ratio "**a**" at higher concentration of filler particles in matrix components which reduces the adhesion interface between the filler and the matrix which in turn leads to poor strength and brittle structure (Qiao *et al.* 2016). At CC, the highest SFC was 85.5 MPa at EPT60-5CC which is 59.8% increase compared with the NE. However, at EPT60-25CC, the SFC strength is 52.1MPa which is 2.8% lower than the NE. At DD, the highest SFC flexural strength is 89 MPa at EPT60-5DD which is 66.4% increases compared with the NE. It doubles as the highest flexural strength of all the SFCs both at volume fraction variations and particle sizes variations. As the particle size increases, the highest flexural strength also increases for BB, CC, and DD which is at 5vol% fraction of HGM. This is because the addition of a smaller quantity of filler particles has been observed to give a better dispersion in the matrix, lower agglomeration and reduced porosity content resulting in high strength and stiffness and these findings has been published by the author (Afolabi, Kanny and Mohan 2022). Similar observation was reported by Bharath et al (Bharath Kumar *et al.* 2016b) where

the strength of syntactic foam increased with an increasing volume fraction of HGM compared to the neat matrix. It is also an indication that the flexural strength is reliant on the micro balloons volume fraction and particle sizes (Tagliavia, Porfiri and Gupta 2010).

Table 7.5: Flexural strain of SFC filled with homogeneous HGM-epoxy resin (mm/mm)

Size variation	Volume fraction (%)					
Particle sizes	NE	EPT60-5	EPT60-10	EPT60-15	EPT60- 20	EPT60- 25
AA (20-24µm)	0.044	0.141	0.104	0.139	0.125	0.133
BB (25-44µm)	0.044	0.175	0.128	0.153	0.114	0.212
CC (45-49µm)	0.044	0.129	0.099	0.165	0.193	0.076
DD (50-60µm)	0.044	0.148	0.167	0.225	0.154	0.093

Table 7.5 shows the influence of the HGM size variations and volume fractions on the flexural strain at the break of the SFC. Flexural strain or elongation at break is obtained during tensile testing. Flexural strain at break was an important parameter used in characterizing the flexural fracture toughness of SFCs. The flexural strain at the break of the homogeneous SFC relative to the tensile strength is presented in Table 7.5. The chain mobility is responsible for the flexural break of SFC during flexure testing and is controlled by the concentration of the filler and their forming network within the polymer formation of the matrix making them lower than that of the pure NE (Liang J.Z. 2000). In Table 7.1, lower values of flexural strain at break were observed for all the heterogeneous SFC, compared to the NE, because during cooling of SFC, the thermal energy associated with the SFC chains decreases, and the molecular mobility of the SFC chains arrested. The decrease in the tensile strain of SFC at break can be related to the presence of large aggregates and a strong cluster of HGM filler as shown by the SEM images at higher volume fractions in the SFC (Liang 2005).

7.3 Flexural Fractured Surfaces of SFC with Heterogeneous HGM

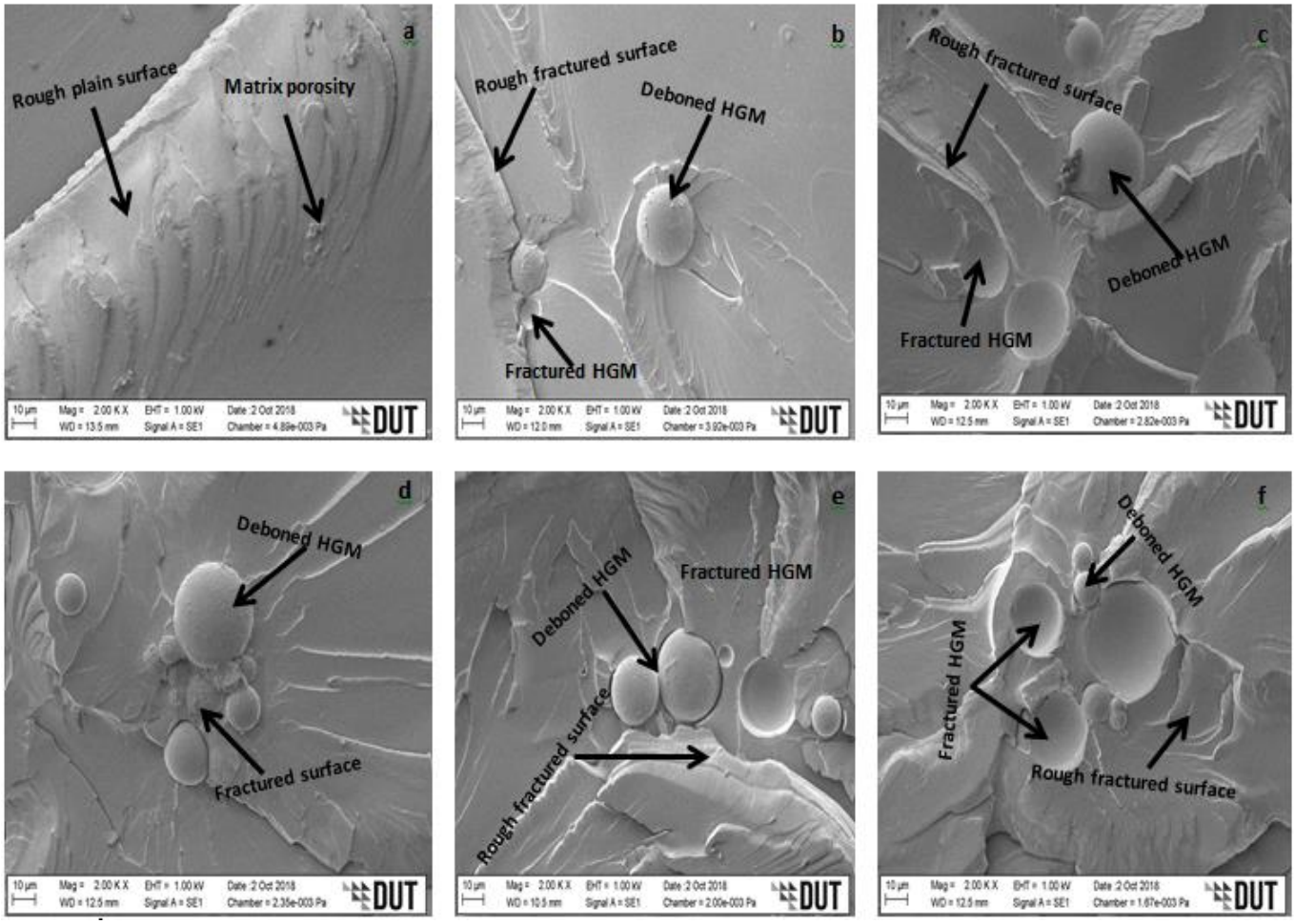

Figure 7.3: SEM images for flexural fractured specimens of SFC-heterogeneous HGM at (a) EPT60-0, (b) EPT60-5, (c) EPT60-10, (d) EPT60-15, (e) EPT60-20 and (f) EPT60-25, showing fractured HGM, deboned HGM and rough fractured surfaces.

Figure 7.3 (a-f) shows the fractured surfaces of the flexural samples of SFCs for the heterogeneous HGM vol% compositions. Figure 7.3 (a) shows the morphology of the NE, a rough plain surface with matrix porosity can be observed, resulting in its brittle failure and low flexural strength. At Figure 7.3 (b), the micrograph of the fractured SFC can be seen with debonded (unbroken) HGM from the matrix indicating lack of adhesion, leading to rough fractured surfaces with brittle failure. At Figure 7.3 (c), the morphology of the SFC with fractured HGM becomes obvious due to the increase in filler concentration in the epoxy matrix, the

fractured surface was also rough and deboned microsphere observed but improved adhesion with the matrix which resulted in increased flexural strength. The increased in the HGM vol% from Figure 7.3 (d-f) reveals resistance to fracture in their morphology; this could possibly be characterized with good adhesion of the HGM with the matrix, leading to improved flexural strength. The fracture was ductile with rough surfaces and deboned HGM. Strong interfacial bonding is desired in order to achieve good flexural strength in SFC (Bharath Kumar *et al.* 2016b).

7.4 Flexural Fractured Surfaces-Homogenous HGM

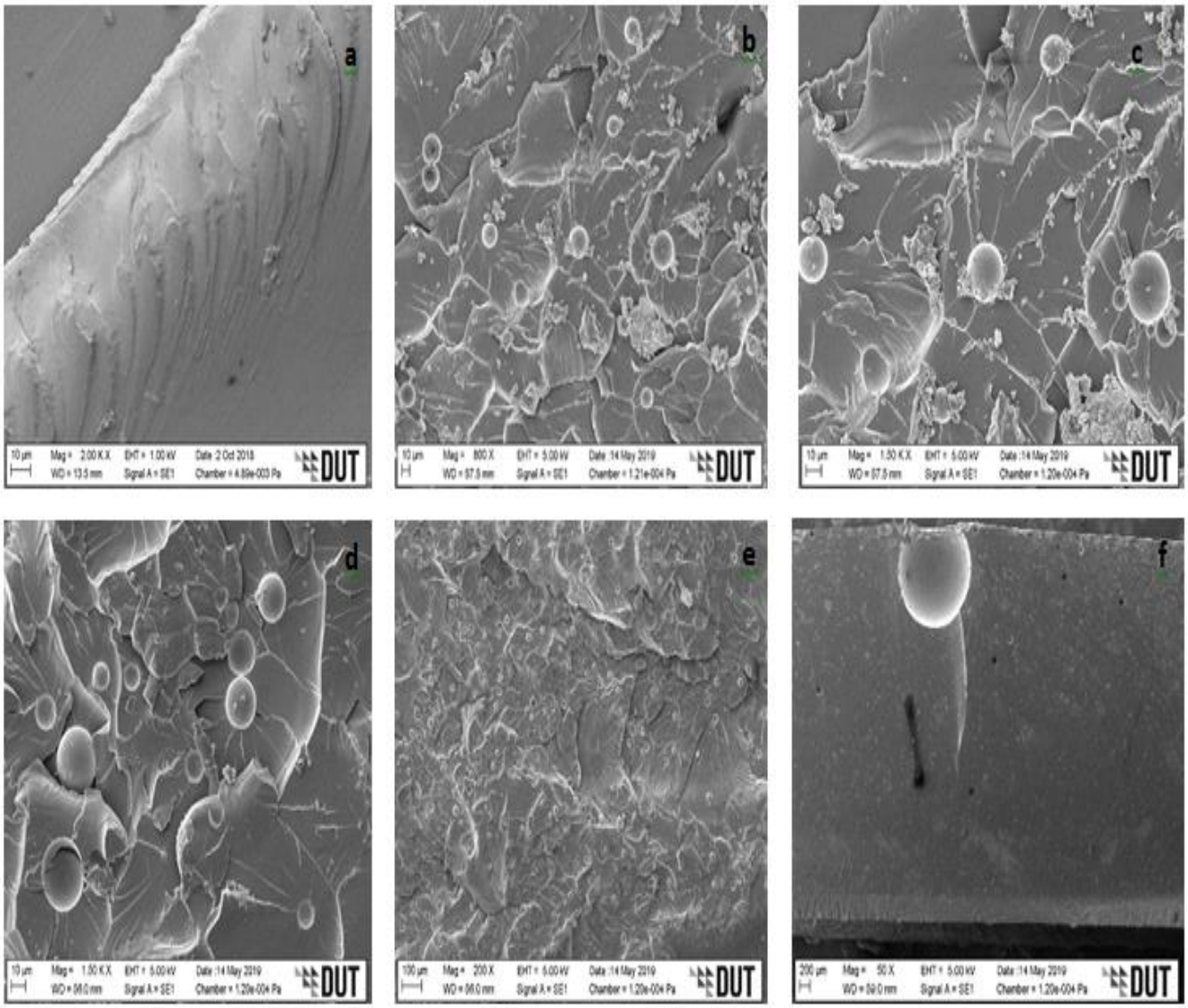

Figure 7.4: SEM images for flexural fractured specimens of SFC-homogeneous HGM at (a) EPT60-0, (b) EPT60-AA5, (c) EPT60-AA10, (d) EPT60-AA15, (e) EPT60-AA20, (f) EPT60-AA25

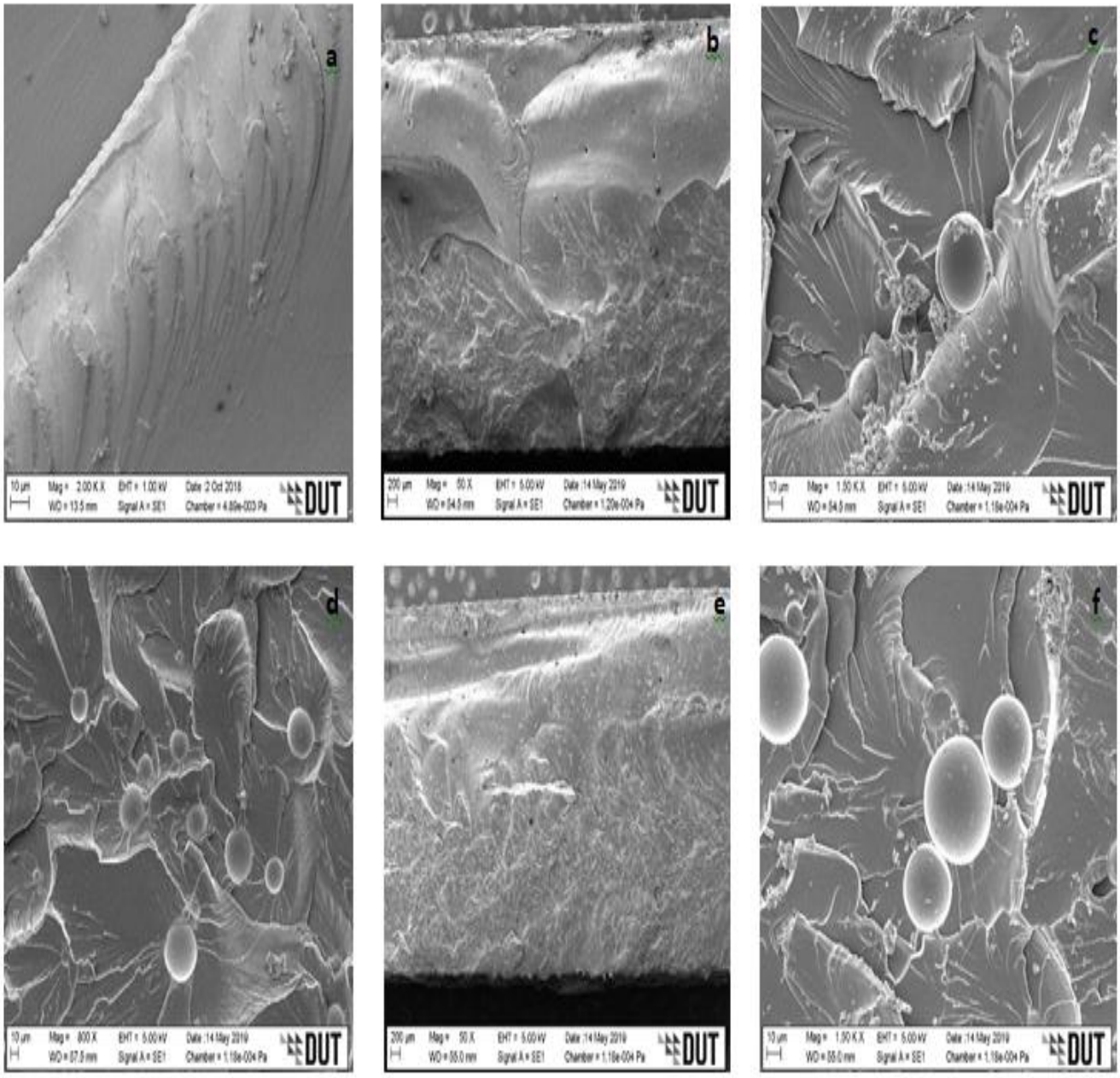

Figure 7.5: SEM images for flexural fractured specimens of SFC-homogenous HGM at (a) EPT60-0, (b) EPT60-BB5, (c) EPT60-BB10, (d) EPT60-BB15, (e) EPT60-BB20 and (f) EPT60-BB25.

Figures 7.4 (a) – 7.7(a) shows the plain fracture morphology of epoxy resin as earlier reported in Figure 7.3(a). it was necessary to show it because it serves as the base surface for comparison. Figures 7.4(b-f) – 7.7(b-f) shows the flexural fractured surfaces of SFC with homogeneous HGM filler. From Figure 7.4(b and c), the micrograph shows brittle fracture surfaces which occurred possibly due to agglomeration between the particles of the microspheres and the matrix.

The agglomeration occurred due to air entrapped during the mixture of HGM and the epoxy resin which are evident on the surface of the morphology by the smaller microspheres, but it does not affect the homogenous distribution of HGM in the matrix. It could also be due to their smaller sizes causing a smooth separation during fracture and in turn increased flexural strength (**see section 7.2, Table 7.4**).

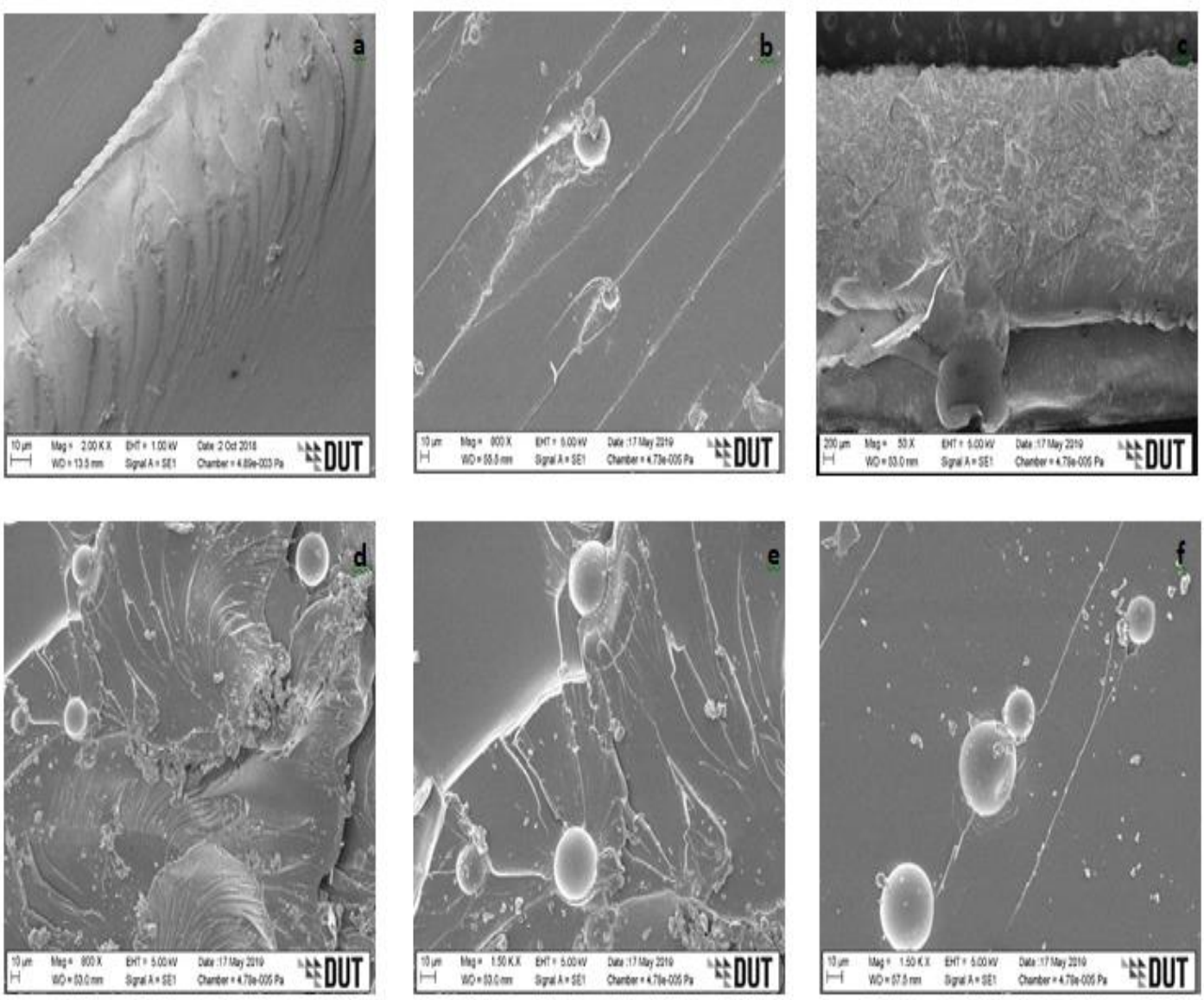

Figure 7.6: SEM images for flexural fractured specimens of SFC-homogenous HGM at (a) EPT60-0, (b) EPT60-CC5, (c) EPT60-CC10, (d) EPT60-CC15, (e) EPT60-CC20 and (f) EPT60-CC25.

From Figure 7.4 (d, e, and f), ductile fracture occur as a result of good adhesion and good interface interaction between the HGM and epoxy resin (Qiao *et al.* 2016). The fractured micrographs were seen on the rough morphology surface with some microsphere debris which could be attributed to the ductile fracture under flexural loading conditions and resulted in high flexural strength. From Figures 7.5(b) – 7.7(b), a rough morphology surface can be seen with little agglomeration, which can be possibly due to small vol% (5vol%) of HGM in the SFCs though with larger particle sizes (25-44µm), (45-49µm) and (50-60µm) respectively. It can also be said that good surface interaction occurred between the micrograph of the HGM and the epoxy resin with little agglomeration resulting in higher flexural strength **(**section **7.2, Table 7.4)**. Also, Figures 7.5(c-f)–7.7(c-f) shows surface morphology with fractured microspheres, deboned microspheres, matrix porosity, and agglomeration. There was an increase in the debris on their surfaces, which is possible due to an increase in the HGM vol% in the SFCs. They exhibited ductile fracture which correspond possibly to the fact that the adhesive force between the HGM and the epoxy matrix weakens during flexural loading, resulting in their reduced flexural strength.

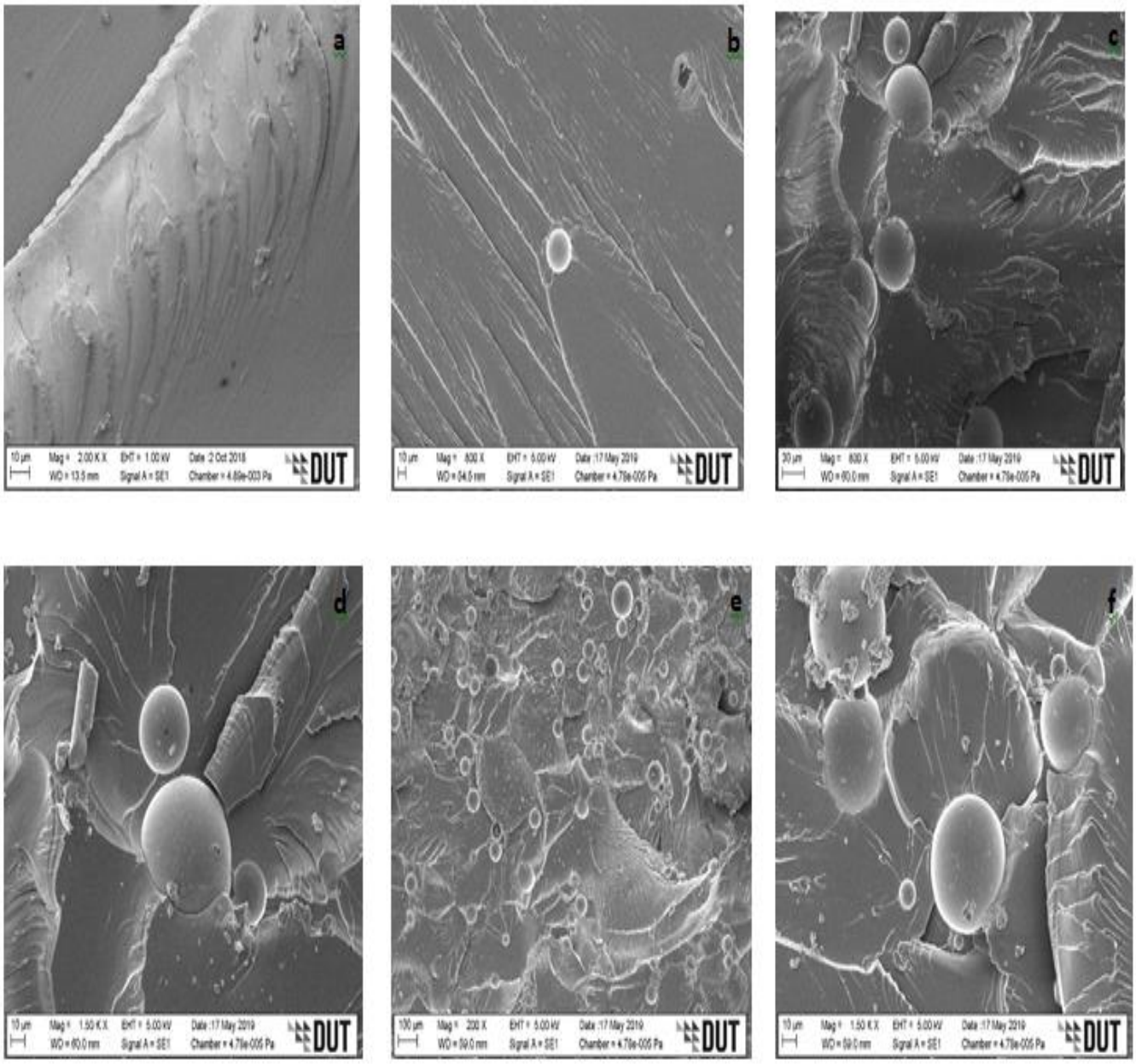

Figure 7.7: SEM images for flexural fractured specimens of SFC-homogenous HGM at (a) EPT60-0, (b) EPT60-DD5, (c) EPT60-DD10, (d) EPT60-DD15, (e) EPT60-DD20 and (f) EPT60-DD25.

7.5 Conclusion.

It can generally be said that a good interface interaction occurs between the HGM and the matrix for all the size variation but the bigger sizes at smaller volume fractions (5vol%) were able to withstand flexural loading than the smaller sizes and larger volume fractions (10vol%-25vol%), resulting in their improved flexural modulus, strength, and strain values (section **7.2, Tables 7.3-7.5**). This shows that at the smaller size of the HGM, there is more surface area available for bonding which increases the stiffness of the composite which caused decreased in flexural strength. Further observation shows that the ductile fracture experienced by the larger sizes is relative to the microsphere's nature. However, the flexural modulus, strength, and strain, decreased with increasing volume fraction of microsphere due to a stronger interfacial strength experienced during flexural loading, because flexural properties are known to strongly require the interfacial bonding characteristics to transfer the load from the matrix to the HGM particles (Karthikeyan C.S. 2000b; Karthikeyan, Sankaran and Kishore 2005; Dong, Ranaweera-Jayawardena and Davies 2012; Bharath Kumar *et al.* 2016b; Qiao *et al.* 2016).

In the next chapter 8, SFC was used as core for fabricating sandwich syntactic foam composite (SSFC) and its mechanical properties and density characteristics were discussed.

CHAPTER 8

8.0 MECHANICAL PROPERTIES AND DENSITY MEASUREMENT OF SANDWICH SYNTACTIC FOAM COMPOSITES (SSFC)

In this chapter, the mechanical properties of sandwich syntactic foam composite (SSFC) discussed. The mechanical tests performed are tensile, flexural, and compression (edgewise), and the results were analyzed accordingly. Been part of the objectives to fabricate sandwich syntactic foam composite (SSFC) using SFC core and hybrid kenaf-glass fibers face-sheet, the mechanical test of the SSFC was carried out to study the effects of different fiber layering of the face-sheet on the core syntactic foam composites (SFC). The fiber layering was performed in four methods; kenaf – SFC – kenaf, designated as (KK), glass – SFC – glass, designated as (GG), glass-kenaf – SFC -kenaf-glass, designated as (GK), and kenaf-glass- SFC -glass-kenaf, designated as (KG) respectively.

This chapter is divided into three sections: section **8.1** focused on the mechanical properties of SSFC (tensile, compression, and flexural), section **8.2** is on the theoretical modelling to validate the experimental results and section **8.3** is on morphological properties to study the fractured surfaces of the SSFC.

8.1 Density measurement for SSFC

ASTM standard C271-94(*ASTM C271-94. Annual Book of ASTM Standards* 1994) was employed to calculate experimental densities of the sandwich composites. Rule of mixtures (Equation 1) was adopted to calculated theoretical densities and it is relatively higher than measured density (Zhu *et al.* 2012). Table 8.1 shows the comparison between the theoretical and experimental densities. The experimental density was used to normalize the mechanical properties to calculate the specific properties as reported in Tables 8.2-8.4.

$$\rho_c = \rho_k V_k + \rho_g V_g + \rho_{Sf} V_{Sf} + \rho_m V_m \qquad (8.1)$$

The matrix porosity (void) which is the difference between the theoretical and experimental densities was calculated using Equation 8.2 and reported in Table 8.1.

$$P_c = \left(\frac{\rho_t - \rho_m}{\rho_t}\right) * 100 \qquad (8.2)$$

Where P_c is the sandwich composite porosity (void), ρ_t is the theoretical density and ρ_m is the measured density.

Table 8.1 Density measurement of hybrid sandwich syntactic foam composites

Composite notation	Composite sandwich weight (g)	Volume of sandwich composites (cm^3)	Theoretical density (g/cm^3)	Experimental density (g/cm^3)	Porosity (void) (%)
KK	695.0	777.1	0.894	0.865±0.006	4.03
GG	771.2	884.8	0.912	0.872±0.001	4.42
GK	1013.3	972.1	1.042	0.908±0.031	3.13
KG	951.6	975.6	0.975	0.883±0.059	2.94

8.2 Mechanical Properties

8.2.1 Tensile properties

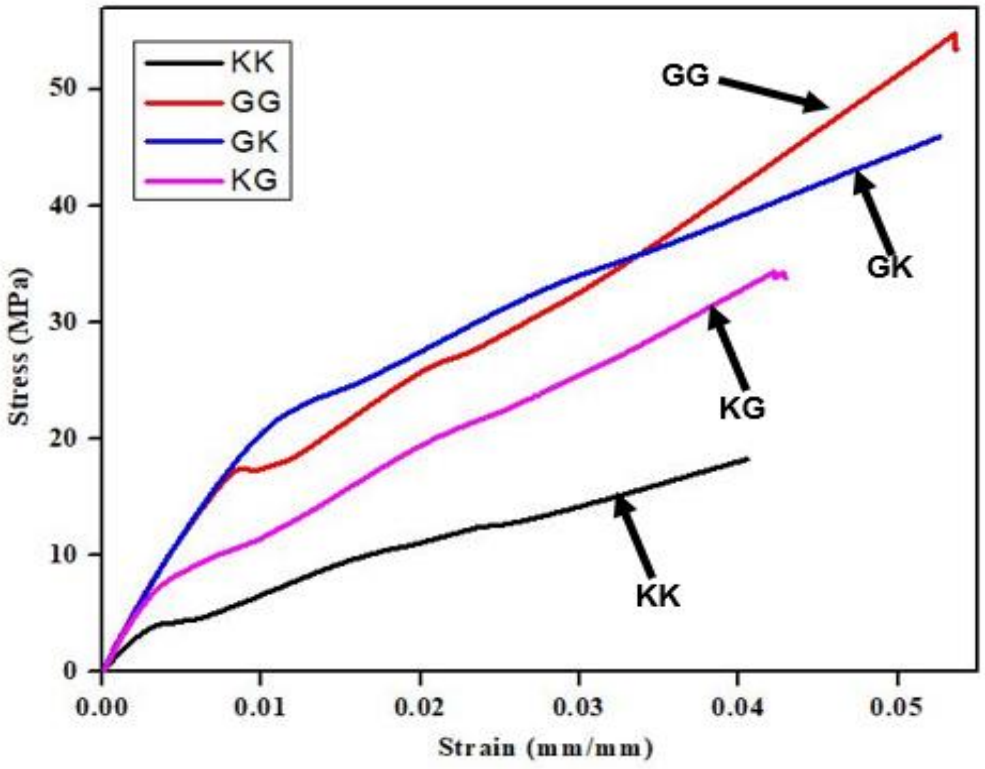

Figure 8.1: Tensile stress-strain graph of SSFC for (kenaf fibre-syntactic foam core-kenaf fibre) “KK”, (glass fiber-syntactic foam core-glass fiber) “GG”, (glass-kenaf fiber-syntactic foam core-kenaf-glass fiber) “GK” and (kenaf-glass fiber-syntactic foam core-glass-kenaf fiber) “KG” hybrid composites.

Figure 8.1 shows the relationships of the tensile stress-strain graph for the four different structures SSFC. Table 8.2 shows the tensile properties of the SSFC. The tensile stress-strain of the SSFC shows linear curves for the entire hybrid composite. From Figure 8.1, a trend of stiffness change behavior of the entire sandwich composites up to rupture with a transition zone at a strain ranging from 0.02 to 0.05mm/mm was observed. The strain rate of KK was lower compared to other sandwich composites. Sharba *et al.* (2016a) reported a similar case where both the stress and strain of the kenaf-based composite were lower than the corresponding glass and hybrid glass/kenaf composite.

Table 8.2: Tensile properties of hybrid sandwich syntactic foam composites

Sandwich Composites	Tensile Modulus (GPa)	Sp. Tensile Modulus ($GPa.cm^3.g^{-1}$)	Tensile Strength (MPa)	Sp. Tensile Strength ($MPa.cm^3.g^{-1}$)	Tensile Strain (mm/mm)
KK	1.42 ± 0.182	2.02	16.42 ± 1.65	23.41	0.038 ± 0.003
GG	2.48 ± 0.124	2.84	51.06 ± 3.18	58.58	0.053 ± 0.002
GK	2.14 ± 0.315	2.35	40.39 ± 4.81	44.49	0.058 ± 0.011
KG	2.23 ± 0.105	2.52	32.95 ± 1.91	37.32	0.048 ± 0.007

Table 8.1 shows that the maximum tensile strain rates of the sandwich composites range from 0.038 at KK to 0.058 at GK. The KK hybrid composite exhibited the lowest tensile strength and modulus of 16.42 MPa and 1.4 GPa respectively, due to a facing tensile failure experienced (i.e brittle behavior) and total fracture of specimens which was responsible for its reduced tensile strength. The GG hybrid composites exhibited the highest tensile strength and modulus of 51.06 MPa and 2.477 GPa respectively. This corresponds to an earlier report by (Sharba *et al.* 2016a) where the glass sandwich composite exhibited the highest strength and modulus. There was however significant improvement in the overall mechanical properties of the hybrid composites

compared to the kenaf fiber composite. The specific tensile strength and modulus of all the SSFC increased from 9% to 30% respectively. The increase in specific values was an indication that the results were consistence and shows the effect of density (**section 8.1**) on the SSFC was significant. This results has been published by the author (Afolabi, Kanny and Mohan 2023).

Based on observation from Table 8.2, the tensile strength, specific tensile strength, modulus, and specific tensile modulus were highest at GG and lowest at KK respectively. However, GK and KG exhibited little difference in their results but shows the same form of facing tensile failure because of the delamination that occurred between the core and the face-sheet as presented in Figure 8.2 (c and d).

Figure 8.2 Fractured surfaces of SSFC for (a) adhesive failure at KK, (b) cohesive failure at GG, (c) facing tensile failure at GK, and (d) facing tensile failure at KG composites.

From Figure 8.2, based on ASTM C297 and according to Salleh *et al.* (2016), four types of standard failure mode properties can be observed from the tensile testing: (a) core failure, (b) cohesive failure, (c) facing tensile failure, and (d) adhesive failure. Based on this finding, it was revealed from testing in this study that only failure modes (b), (c), and (d) were detected. In Figure 8.2(b), GG experienced failure conditions between the core and the face-sheet in the form of cohesive failure which was possibly responsible for its ability to withstand the maximum tensile strength. In general, based on the peak stress values of the stress strain curves, it can be observed that the GG shows better tensile properties compared to other hybrid sandwich composites. The order of tensile strength and specific tensile strength increase is GG > GK > KG > KK while that of tensile modulus and specific tensile modulus increase is GK > GG > KG > KK.

8.2.1.1 Scanning Electron Microscopy for Tensile SSFC

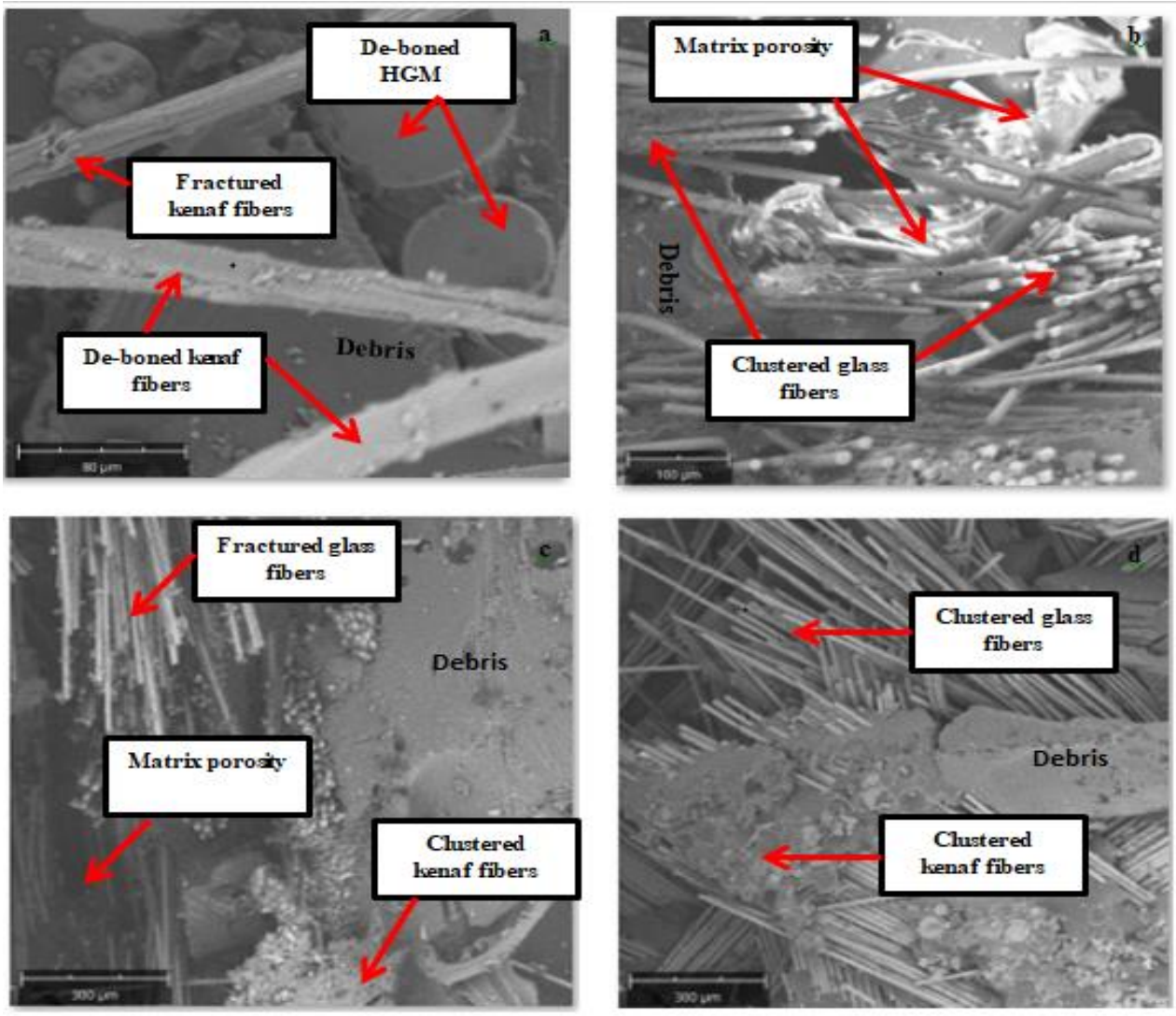

Figure 8.3: SEM images for the tensile SSFC at (a) kenaf-SF-kenaf (KK), (b) glass-SF-glass (GG), (c) glass/kenaf-SF-kenaf/glass (GK), and (d) kenaf/glass-SF-glass/kenaf (KG) orientations fractured surfaces, respectively.

Figure 8.3 (a-d) shows the SEM images of the hybrid sandwich composites which described the microstructural results of the fractured surface of the SSFC during tensile loading. Figure 8.3a shows the KK fractured micrographs where clustered kenaf fibers can be noticed which possibly led to its early breakage (brittle) and low strength values as discussed above in **section 8.2.1, Figure 8.1, and Table 8.1** because they bear the load individually before the core fracture (Alberto Corigliano 2000; Sharba *et al.* 2016a). The GG (Figure 8.3b) also revealed clustered fractured surfaces with the roughness of glass fiber around the syntactic core and matrix porosity. This resulted in foam cracking and skin failure but was able to bear more loads during testing before fracture resulting in its higher tensile strength and modulus series more than other orientations. The micrograph is shown in Figure 8.3 (c and d) exhibits the fractured features of GK and KG. Clustering of fibers can be seen on the morphology of GK and KG, especially with kenaf fibers, this can be related to the fact that kenaf fibers were not completely wetted by the resin matrix, hence, they were less effective in bearing the load transferred from the matrix to the core during testing (Karthikeyan, Sankaran and Kishore 2007). Crack generation is restricted by the presence of the glass fiber but resulted in skin failure and matrix cracking with face wrinkling (Kumar and Ahmed 2013).

8.2.2 Flexural Test

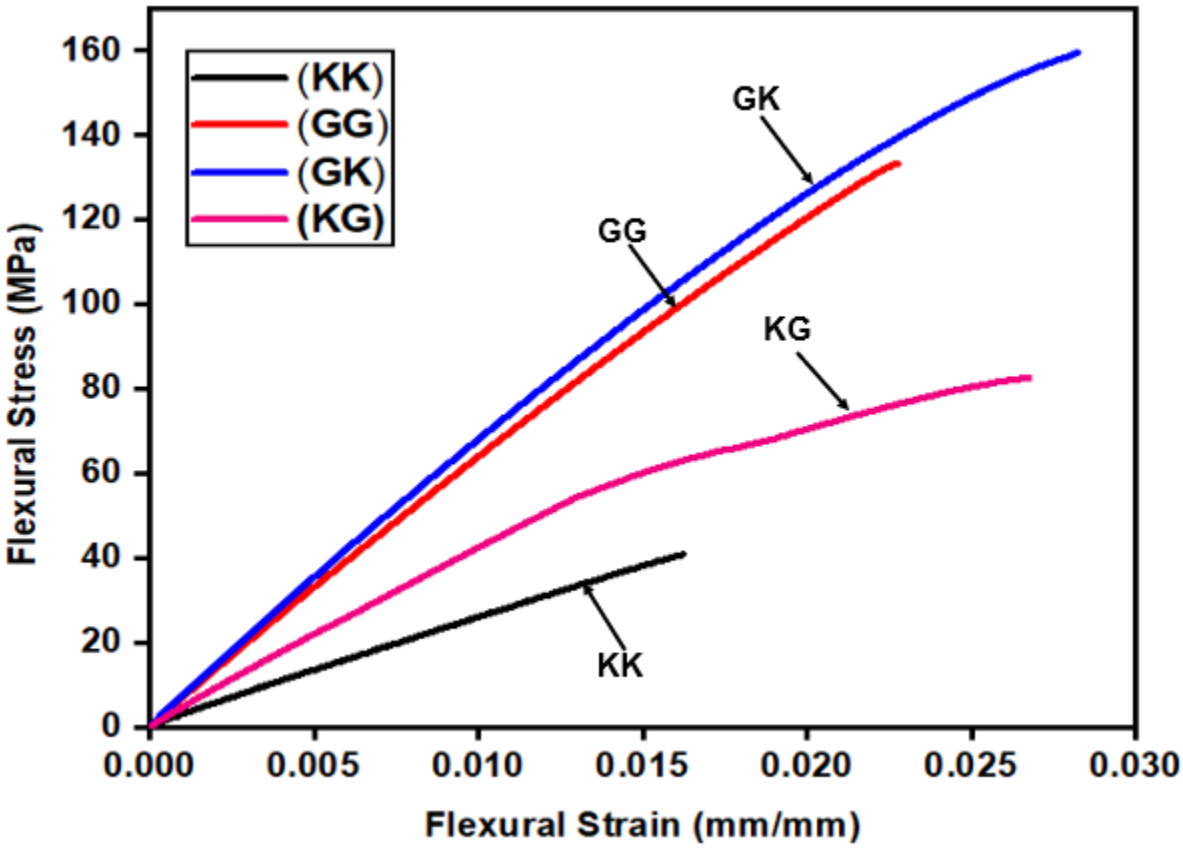

Figure 8.4: Flexural stress-strain graph of SSFC for kenaf-syntactic foam-kenaf "KK", glass-syntactic foam-glass "GG", glass/kenaf-syntactic foam-kenaf/glass "GK", and kenaf/glass-syntactic foam-glass/kenaf "KG" hybrid composites

Figure 8.4 shows the flexural stress-strain curves for the SSFC showing the four layering methods "KK", "GG", "GK", and "KG" at the three-point bending test.

The following can be deduced from the stress-strain graphs in Figure 8.4

i. All the hybrid composites exhibited linear behavior to a certain point before failure.

ii. The load carried by KG decreased sharply after the end of the elastic region due to failure initiation on the core of the SSFC. The elastic region can be divided into three parts in this curve and the slope calculated showing three Moduli but only Modulus I was recorded in Table 8.3 because such region is not common to other curves.

Nikhil Gupta (2003) had earlier reported similar observation where the stress-strain curve for syntactic foam experienced elastic regions in three parts.

iii. KK completely failed during testing while KG shows plateau region after there was a decrease in load which caused sudden fracture.

iv. The difference in the displacement value at which the peak load is observed for KK, GG, GK, and KG is considered.

v. The failure was initiated from the tensile point of the test in the form of crack initiation as the displacement increases (Figure 8.5b), and tensile cracks of the core were observed at the bottom of the specimen (Figure 8.5 c and d)

vi. The failure of GG and GK are ductile in nature which influenced their strength and modulus.

The summary of the 3-point bending results for the flexural test is listed in Table 8.4. It can be observed that all the four SSFC exhibited stress-strain with ultimate individual stress above 40 MPa. The flexural test shows that the core shear differs in failure mode, there were tensile cracks on the SFC-core at the bottom of the specimen, also, compressive failure was noticed between the face-sheets and the SFC-core due to de-bonding and unsymmetrical shear failure. Salleh *et al.* (2016), reported similar case of crack originating from the bottom of tensile skin and progressing with load application using glass fiber reinforced plastic sandwich composite. The stiffness of the SSFC was used to calculate the modulus of elasticity and was obtained from the slope of the stress-strain curve. The stiffness generally varied when the thickness and width of the SSFC had different sizes for a fixed span length. All the four orientations exhibited a smooth linear stress-strain curve before breakage as observed from Figure 8.4. Most of the test specimens exhibited core shear failure of the SFC during flexural testing. The curve of KG revealed sudden ruptures as the load increases before the final failure. This contributed to the reduced strength of the KG compared to GK and GG as shown in Table 8.3.

Table 8.3: Flexural properties of hybrid sandwich syntactic foam composites

Sandwich Composites	Flexural Modulus (GPa)	Sp. Flexural Modulus ($GPa.cm^3.g^{-1}$)	Flexural Strength (MPa)	Sp. Flexural Strength ($MPa.cm^3.g^{-1}$)	Flexural Strain (mm/mm)
KK	2.74 ± 0.20	3.91	40.87 ± 3.94	58.29	0.0162 ± 0.0001
GG	6.70 ± 0.44	7.69	133.35 ± 15.99	153.01	0.0229 ± 0.0007
GK	7.16 ± 0.68	7.87	159.51 ± 26.18	175.32	0.0283 ± 0.0022
KG	4.52 ± 0.96	5.12	82.59 ± 10.48	93.55	0.0424 ± 0.0086

From Table 8.3, the flexural modulus, specific flexural modulus, flexural strength, and specific flexural strength of SSFC are shown. The KK has the lowest flexural modulus and strength of 2.74 GPa and 40.87 MPa respectively, because the skin could not withstand the bending load for long. The gradient of the linear graph of the stress-strain provides the modulus of elasticity for the skin. The maximum flexural modulus and strength of the SSFC was 7.16 GPa and 159.51 MPa respectively as observed at GK. The differences in the maximum flexural values are due to the ability of each sandwich structure to withstand the bending force. The influence of the skin thickness in this study only slightly affects the higher modulus of elasticity at GK and GG. Although the highest flexural strength is at GK with hybrid face-sheets, it is higher than KG which is also with a hybrid face-sheet. Therefore, the variation of fiber layering in hybrid sandwich composite has an influence on the flexural strength. The GG shows the flexural strength lower than the GK, but higher than KG and KK. This reflected the ability of glass fiber to better absorb bending stress than kenaf fiber (Sadeghian, Hristozov and Wroblewski 2016; Salleh *et al.* 2016; Sadeghian, Hristozov and Wroblewski 2018).

The highest flexural modulus and strength at GK indicates that good bonding existed between its core and face sheets. The order of increase for the flexural modulus and strength is GK>GG>KG>KK and percentage increase of GK to KK is 161% and 290% in flexural modulus and strength respectively. The highest flexural strain is at KG, which means that the extension exhibited by KG before the failure is more than the other composite. This implies that their strain properties vary due to slight variation in their thickness (Salleh *et al.* 2016; Sharba *et al.* 2016b).

Salleh *et al.* (2016) had earlier reported that the thickness of the face sheets has a lower impact on the maximum strength and modulus of elasticity of the SSFC.

The density of the SSFC (section 8.1) was used to normalize the flexural modulus and strength, resulting in the specific flexural modulus and strength. The effect of the specific properties increased for both flexural modulus and strength at 30%, 13%, 9%, and 12% for “KK, GG, GK, and KG” respectively. The uniformity in the percentage increase of the specific properties for both flexural modulus and strength is possibly an indication of the reliability and validity of the results. The highest percentage increase is at KK, 30% though, with the lowest values of flexural modulus and strength, this is possibly because of their lower density value which indicated that the density of the composites affects the overall performance of the SSFC. Moreover, it can be expressed that the bonding strength of SSFCs showed appreciative changes with foam density and that the flexural strength and bending modulus increased with foam density (Shen *et al.* 2013).

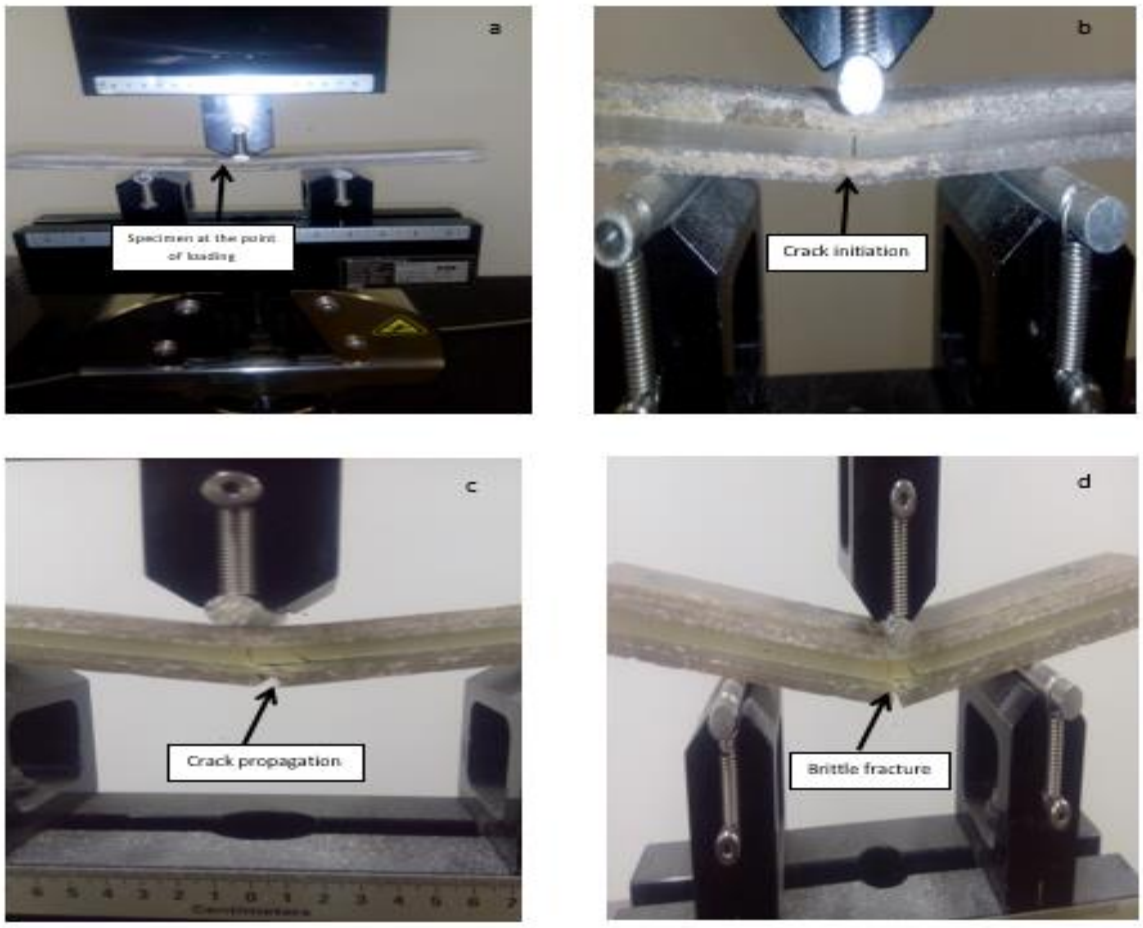

Figure 8.5: Flexural fractured samples of SSFC showing (a) specimen at the point of loading, (b) crack initiation after loading the specimen, (c) crack through the core, and (d) fracture propagation at the end of the loading.

Figure 5 (a-d) shows different failure modes observed from the experiment which are, (i) de-bonding between the core and the face sheets, (ii) local buckling of the top face sheet, which was attributed to the in-plane forces caused by the rounded surface of the anvil making contact with the top face sheets, (iii) unsymmetrical shear failure in the core, (iv) symmetrical shear failure in the core and (v) local de-bonding between the top face sheet and the core. Daniel Paul. (2018), had earlier reported a similar situation where three failure modes were observed in the sandwich structure. The first mode is the core failure (cracking), this was because of the lower strength of the core compared to the skin. The second failure was the fiber breakage, followed by the skin-core de-bonding.

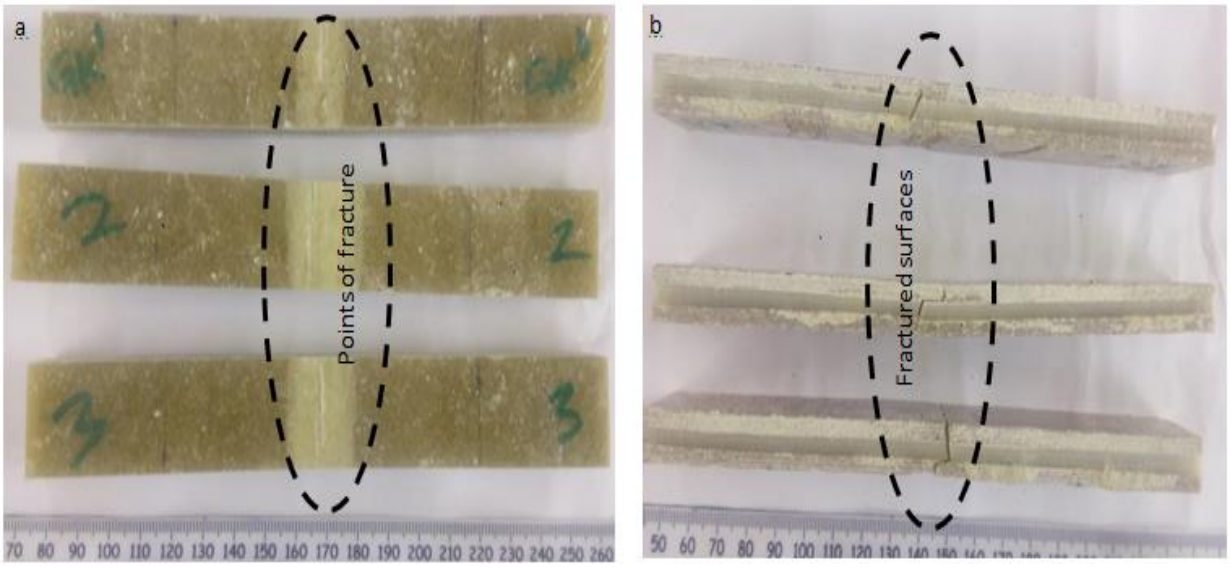

Figure 8.6: Flexural fractured samples of SSFC showing (a) points of fractured on the flatwise position and (b) fractured surfaces on edgewise position.

From Figure 8.6, the points of fracture shown in (Figure 8.6a) indicates that interface shear stresses can also be responsible for the fracture between the core and the face-sheets. Therefore, the location of the crack origination can assist in finding the types of stresses that caused the specimen failure with skins fracture (Figure 8.6a). Figure 8.6b shows the edgewise direction of the failure showing the propagation of cracks and failure modes from the skin to the core. Meanwhile, the occurrence of the un-symmetrical factsheets of the SSFC caused premature failure of the KK leading to brittle failure mode as observed in Figure 8.6 (b).

8.3.2 Scanning Electron Microscopy for Flexural SSFC

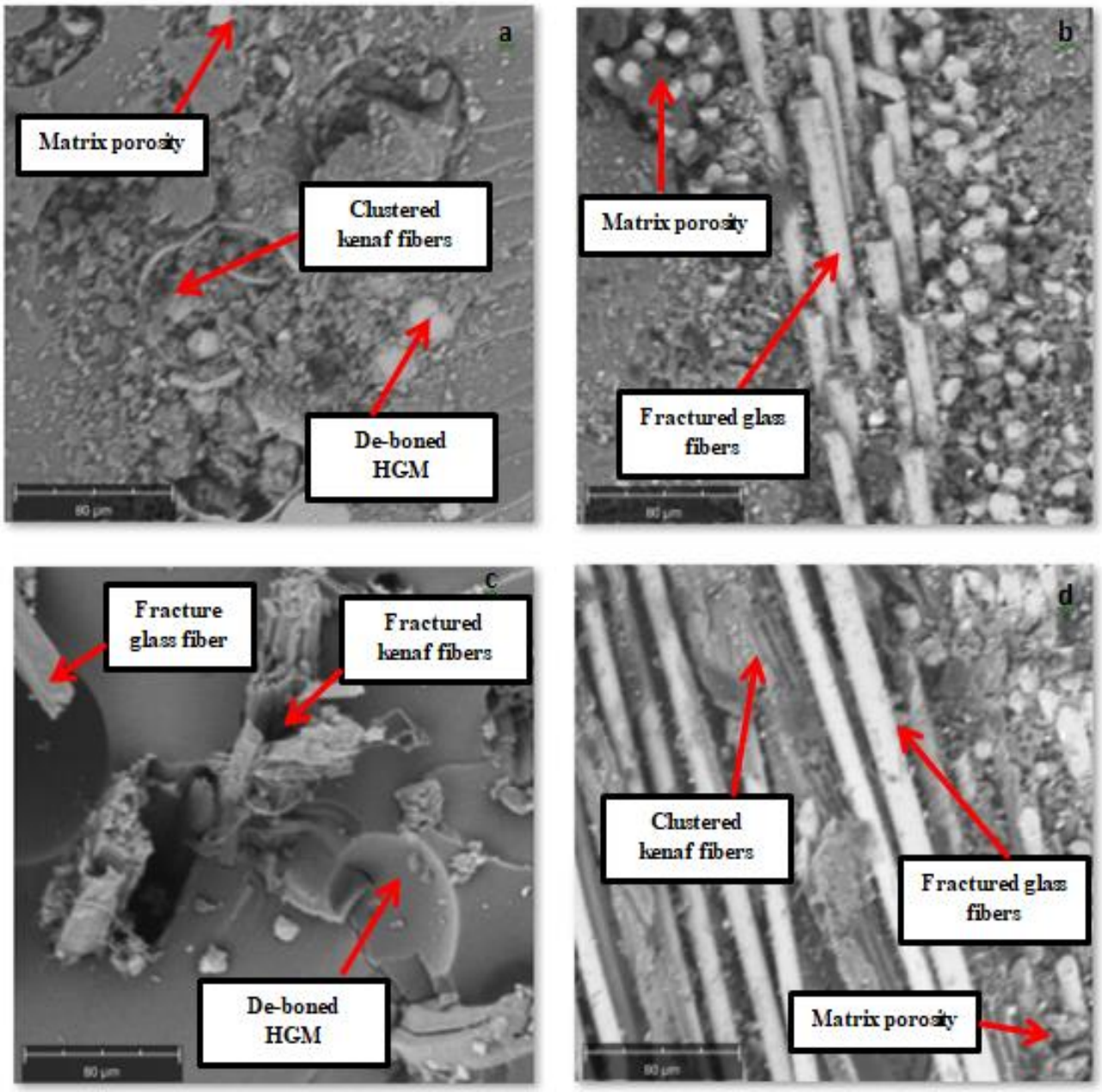

Figure 8.7: SEM images for the flexural SSFC at (a) kenaf-SF-kenaf (KK), (b) glass-SF-glass (GG), (c) glass/kenaf-SF-kenaf/glass (GK), and (d) kenaf/glass-SF-glass/kenaf (KG) orientations fractured surfaces, respectively.

The flexural specimens were used to examine the crack and fracture nature of the SSFC under flexural loading. The thickness of the core for the hybrid face sheets serves as an advantage for the SSFC specimens, resulting in arresting crack propagation between the core and the face sheets and having less of an impact during flexural loading. Figure 8.7 (a-d) presents the morphology structure of the flexural fractured surfaces during flexural loading. Figure 8.7(a) shows clustered kenaf fibers (KK), matrix porosity, and de-bonded HGM. There was a sudden fracture caused by the delamination of the face sheets, thereby causing the flexural strength to reduce due to the inability of the composite to withstood higher load-bearing force. Figure 8.7 (b) shows the fractured glass fibers (GG), matrix porosity was evident due to degradation in matrix material during deformation and fracture processes. However, a good interaction occurred between the face-sheets and the core, resulting in an improved flexural strength, modulus, and strain. Figure 8.7 (c) shows the GK sandwich composite flexural fractured surface, the interaction between the core SFC and the hybrid face-sheets shows adhesion and good boundary stiffness resulting in the highest flexural strength and modulus better than other orientations as shown in **Table 8.3**. Shen *et al.* (2013), reported an improvement in the stiffness boundary condition of the sandwich when the thickness of the face sheets is controlled. Such incidence was also noticed in GK and can possibly occur due to the degradation of matrix material during deformation and fracture processes in flexural testing (Salleh *et al.* 2016). This phenomenon possibly occurred because during flexural loading, the SSFC withstood the stresses by the matrix material and the core, leading to flexural cracking as shown in the composite failure (Figure 8.5c).

In Figure 8.7 (d), kenaf fiber being the first layer of the hybrid face-sheets contributed to its reduction in flexural strength because of its early delamination and deprived wetting with the resin fiber. Also, the incomplete wetting of the resin on the kenaf fiber could cause the interface region to be filled with voids, which opens during flexural loading condition. Based on the load deformation images and micrographs images shown in Figure 8.7, it can be potted that the failure mechanism of SSFC with KK, and KG orientations deformed plastically before the core shear occur. The glass fiber structure cells were deformed, but the strength increased to a certain point. Such that the cell collapsed initially after loading and then their deformation was stopped in the hidden parts of the core. Moreover, elastic deformation was observed during the flexural and shear loading until a vertical crack in the core and de-bonding at the interface of the face sheets where the crack appeared. The direction in which the crack was propagated is an indication that a significant number of bending stresses happened in the samples.

8.2.3 Compression Test

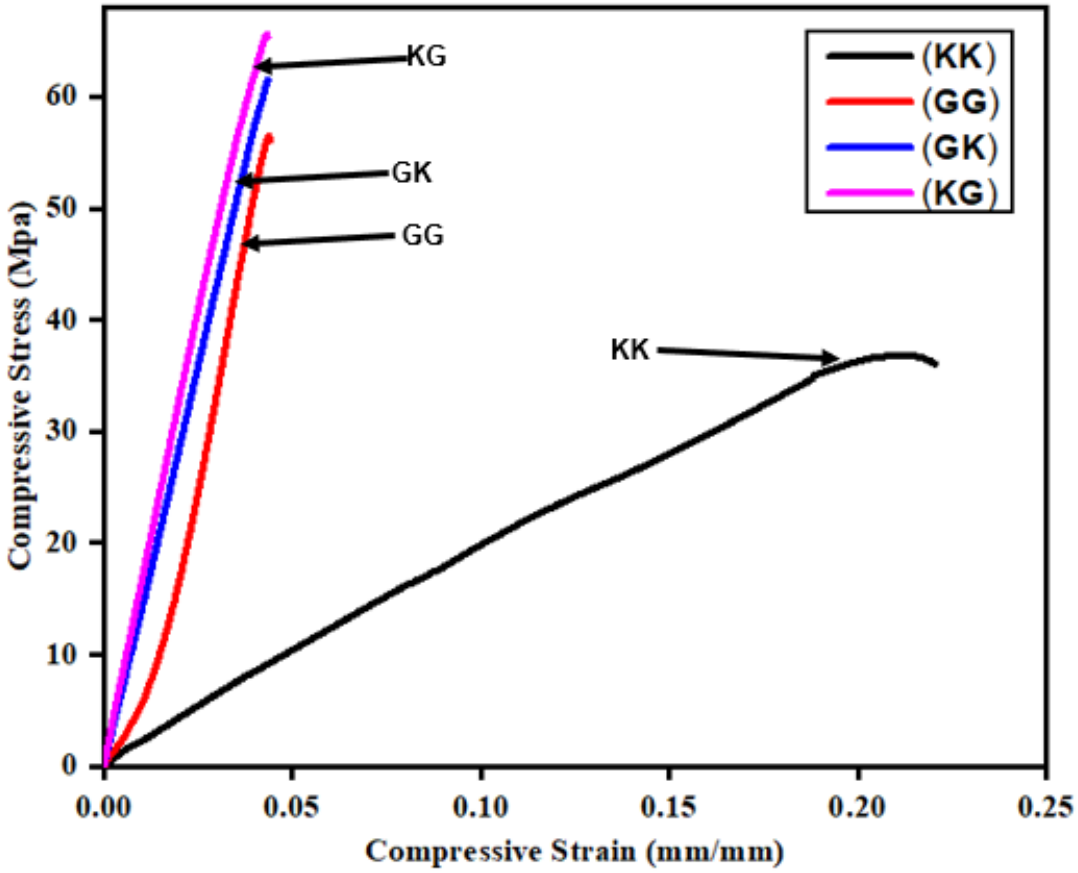

Figure 8.8 Compressive stress-strain graph of SSFC for kenaf-syntactic foam-kenaf “KK”, glass-syntactic foam-glass “GG”, glass/kenaf-syntactic foam-kenaf/glass “GK” and kenaf/glass-syntactic foam-glass/kenaf “KG” hybrid composites.

Figure 8.8 shows the compressive stress-strain curves for a few specimens of the SSFC for KK,GG, GK, and KG. The strain value was taken as the strain rate at the intersection of tangents drawn in the plateau and densification regions of the stress-strain curve. All the specimens showed a linear elastic phase leading to the yield stress. The elastic behaviour of the SSFC was caused by the deviation at the cross-section that occurred before the final rupture. The elastic region of KK can be divided into two parts while GG, GK, and KG shows single elastic region. The slope of the two regions at KK is calculated and presented Figure 8.8 as Modulus I and Modulus II, though only Modulus I was reported in Table 8.3 because Modulus II is not common to all the specimens. It could be observed from the stress- strain curve that the

compressive result for the SSFC indicates an initial linear elastic region accompanied by plateau plastic region and a desification stage at the end of loading.

Table 8.4: Compression properties of hybrid sandwich syntactic foam composites

Sandwich Composites	Compressive Modulus (GPa)	Specific Compressive Modulus ($GPa.cm^3.g^{-1}$)	Compressive Strength (MPa)	Specific Compressive Strength ($MPa.cm^3.g^{-1}$)	Compressive Strain (mm/mm)
KK	1.28 ± 0.18	1.28	37.50 ± 8.78	43.65	0.278 ± 0.185
GG	2.11 ± 0.59	2.42	53.95 ± 6.70	61.90	0.058 ± 0.046
GK	1.61 ± 0.23	1.77	61.41 ± 0.16	67.65	0.043 ± 0.001
KG	1.65 ± 0.26	2.05	65.50 ± 3.67	72.38	0.083 ± 0.013

Table 8.4, shows the compressive modulus (GPa), specific compressive modulus ($GPa.cm^3.g^{-1}$) compressive strength (MPa), specific compressive strength ($MPa.cm^3.g^{-1}$), and compressive strain (mm/mm). Highest compressive modulus and specific modulus is 2.11 GPa and 2.48 $GPa.cm^3.g^{-1}$ at GG while highest compressive strength and specific strength is 65.5 MPa, $72.38MPa.cm^3.g^{-1}$, at the KG. This can possibly indicate that the hybrid of natural fiber and glass fiber can be of better strength as face-sheet in sandwich composite with syntactic foam core. The compressive strengths for the hybrid fiber face sheets (GK and KG) are higher than the separate face-sheets (GG and KK) which shows that for compressive strength, hybrid face-sheets will perform bettter as reinforcement than separate face-sheet. Sharba *et al.* (2016a), reported similar results where the compressive strength of kenaf fiber was smaller compared to the hybrid sandwich composites. Although in using glass fiber, kenaf or sisal fibers alone, as face-sheet with syntactic foam core, the glass fiber has been found to have the highest compressive strength (Amico, Angrizani and Drummond 2008; Sharba *et al.* 2016a). The order of increase for the compressive strength and specific compressive strength of the SSFC is KG > GK > GG > KK.

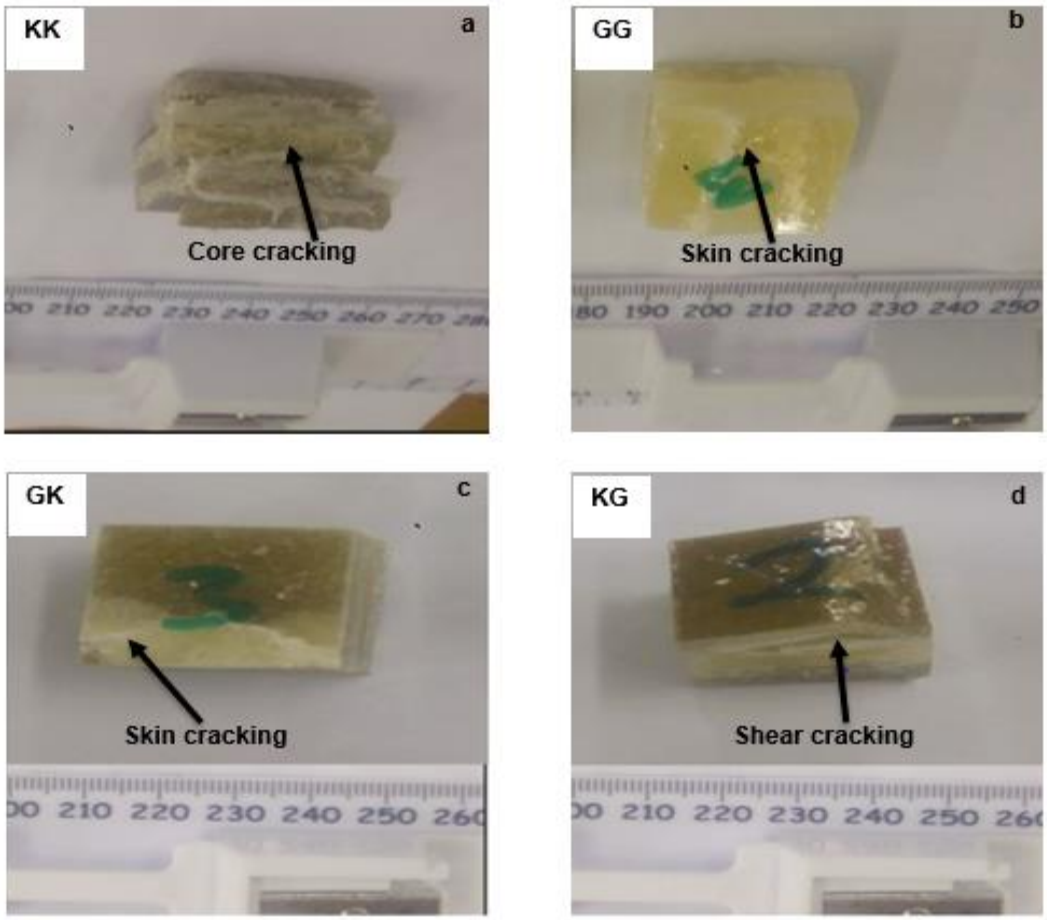

Figure 8.9: Fractured surfaces of SSFC composite for (a) core cracking at KK, (b) skin cracking at GG, (c) skin cracking at GK and (d) shear cracking at KG, under compression loading.

From Figure 8.9 (a-d), different type cracks and failures occured in the SSFC which are core crack at KK (Figure 8.9a), skin crack at GG and GK (Figure 8.9 b and c), shear crack at KG (Figure 8.9d). It was observed that the face-sheets bear less load than the core resulting in their early failure, but core shows better failure strain compared to the face-sheets. Nikhil Gupta and Kishore (1999) has earlier observed that the skins (face-sheets) are the first to fracture during compression of sandwich composite because the fracture direction is usually normal to the applied load. Failure of the face-sheet could also be caused by the combined effect of true compression and shear stress component of the applied load. The high compressive strength and stiffness of KG and GK shows that the cores were able to withstand more load than the face-sheet. When the load is applied during testing, the composite is strain until break before attaining peak stress (Kumar and Ahmed 2013). The crack initiation takes place on the skin of the GG, GK and KG as shown in Figure 8.9 (b, c, and d) which led to their increased

compressive strength than the KK as shown in Table 8.4. The KK experienced propagation of crack in the core before the sudden drop in the stress-strain curve as a result of the plateau of the composite (Ahmadi and Liaghat 2019). Similar observation was reported by Kumar and Ahmed (2013) where the only test conducted on syntactic foams was noticed to have exhibited plateau failure because the RIPH core cannot sustain the edgewise compression load. Karthikeyan C.S. (2000a) also reported similar trend for the reinforced foam, the reinforced foam has a peak which was followed by a drop in the curve and a plateau region which led to a gradual decrease up to a point before a steady increase on the stress-strain curve.

The percentage increase of the specific properties on compressive modulus of SSFC are 30%, 13%, 9%, and 20% and that of compressive strength are 30%, 13%, 9%, and 12% for “KK, GG, GK, and KG” respectively. The closeness in the percentage increase for both specific compressive modulus and strength is an indication of the reliability and validity of the results. The highest percentage increase is at KK, 30%, due to its lowest values of compressive strength and modulus, this indicated that the density of the composites affects the overall performance of the SSFC. Moreover, it can be observed that the bonding strength of SSFCs showed appreciative changes with foam density and that the flexural strength and bending modulus increased because of foam density (Shen *et al.* 2013). The increased in percentages are consistence for the specific tensile, flexural, and compressive strength and moduli.

8.3.4 Scanning Electron Microscopy for Compression SSFC

The specimens under compressive are used to analyze the fracture microstructure mechanism of the SSFC under compressive loading. The micrograph in Figure 8.10 (a-d) revealed the fractured surface morphology of the four-sandwich layering using the same SFC core. Salleh *et al.* (2016) used SFC core with different weight fraction to explain the fracture mechanism of the SSFC compressive testing. Delamination between the face-sheets and the core SFC was observed for the four-sandwich layering before the failure but was faster with the KK in Figure 8.11 which led to its early face-sheet and core rupture than other compositions. This led to its reduction in the compressive strength of KK (Kumar and Ahmed 2013). The high porosity value of KK resulted in its weak compressive load bearing capacity as reported in **Table 8.1**. In Figure 8.10(b), clustered glass fiber and debris can be observed on the GG fractured surface. The surface fracture of face sheets observed in Figure 8.9 (c-d) contributed to the improved load bearing capacity of GK and KG with less agglomeration because of the strong bond that existed between the hybrid face-sheet and the core. This resulted in their higher compressive strength and modulus as discussed above. Figure 10 (c-d) shows fiber clustering of kenaf and glass

fibers, the clustered hybrid fibers could be responsible for their improved compressive properties. It can also be noted from Figure 8.9 (d) that KG withstand greater force of failure during deflection resulting in high strength of 65.5 (MPa) and strain of 0.083 (mm/mm) more than the other sandwich composite as reported in **Table 8.4**.

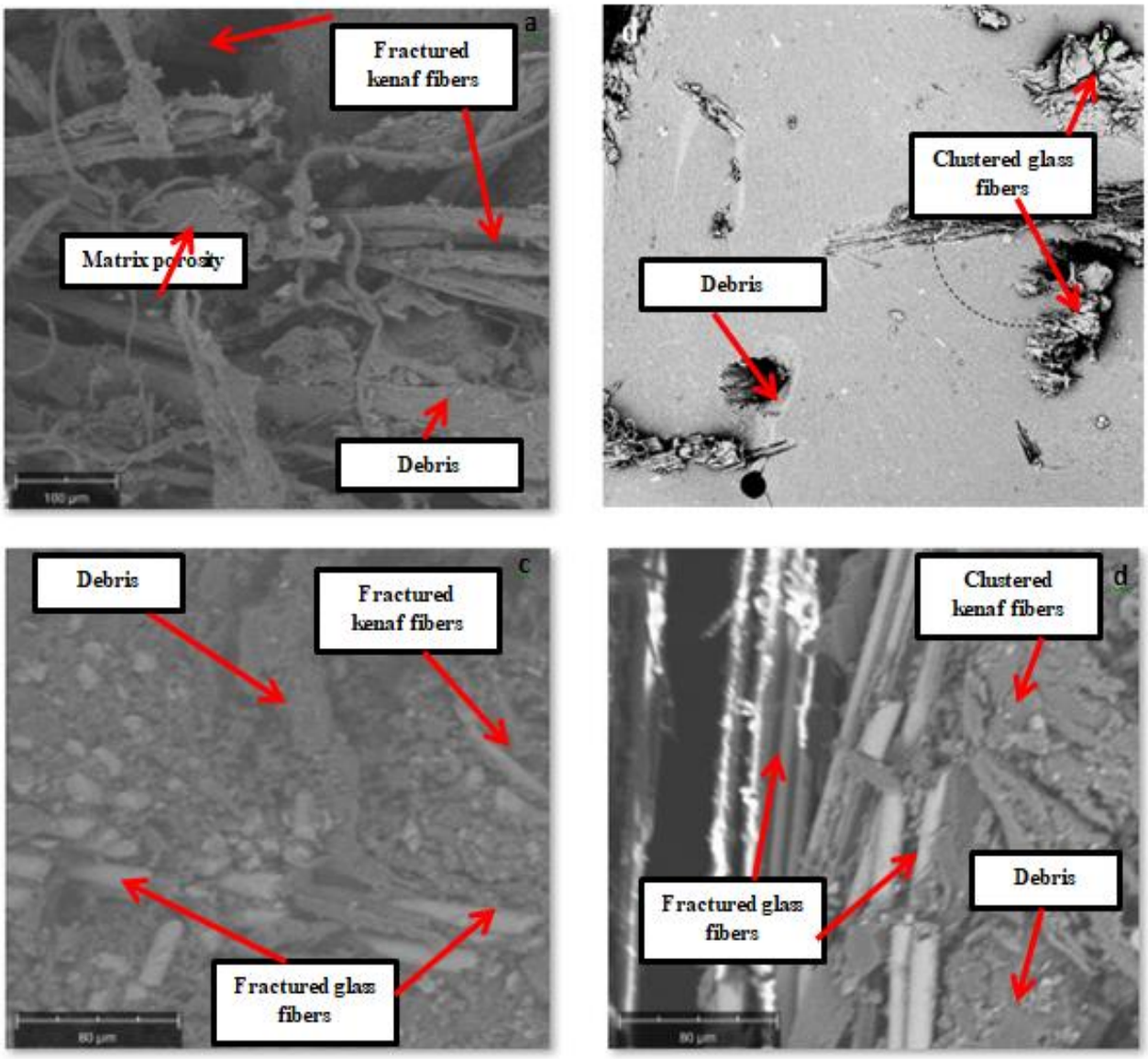

Figure 8.10: SEM images for the compression SSFC at (a) kenaf-SFC-kenaf (KK), (b) glass-SFC-glass (GG), (c) glass/kenaf-SFC-kenaf/glass (GK), and (d) kenaf/glass-SFC-glass/kenaf (KG) fractured surfaces, respectively.

8.2.4 Shear Properties of Sandwich Syntactic Foam Composite

Table 8.5: Shear properties and specific shear properties of the sandwich syntactic foam composite

Syntactic Foam Sandwich Composites	Shear Strength (MPa)	Specific Shear Strength ($MPa.cm^3.g^{-1}$)
KK	2.733 ± 3.058	3.898
GG	4.967 ± 4.877	5.699
GK	3.567 ± 5.212	3.929
KG	4.667 ± 2.915	5.287

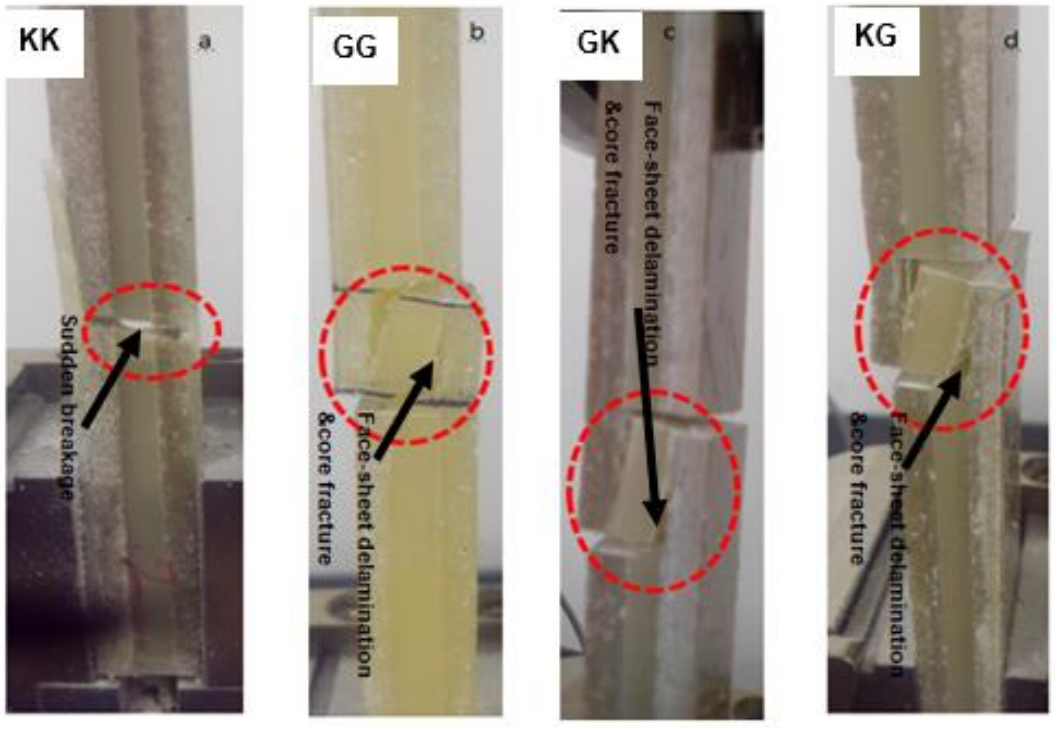

Figure 8.11: Shear fractured surfaces for sandwich syntactic foam composites for (a) kenaf-SFC-kenaf, (b) glass-SFC-glass, (c) glass/kenaf-SFC-kenaf/glass and (d) kenaf/glass-SFC-glass/kenaf orientations, under compression loading.

Figure 8.11 (a-d) shows the fractured surfaces due to shear load for hybrid sandwich composites of KK, GG, GK, and KG respectively. Different types of failures were observed as shown in Figure 8.11. KK exhibited sudden plastic deformation, breaking early after load application. The GG, GK, and KG experienced core shear, lap shear, buckling, delamination and interfacial de-bonding (Castanie 2004; Ding *et al.* 2018) as shown by the dotted circles of Figure 8.8 (b-d). Table 8.5 shows the shear properties of the SSFC, all the specimens were subjected to a shear resistance under the MTS machine. The laminates bonding strength were observed under shear loading. Both the face-sheets have a quasi-linear response to sandwich deflection and load. The highest shear strength was observed at GG, 4.967 MPa, which is 50% more than KK with the lowest shear strength of 2.733 MPa. This possibly means that the use of syntactic foam as core in sandwich composite can significantly affect the average change of the shear strength unlike the report of Ding *et al.* (2018), where there was no significant change in the average shear strength due to PVC foam deterioration. The early breakage at KK could possibly be due to either the core or the stabilizing face-sheets breaks before the failure of the working face-sheet (Castanie 2004). The analysis of the shear properties shows that hybrid sandwich composites can undergo failure with high intrinsic resistance at a static load up to a shear breaking point with little deterioration. The shear strength is in order GG > KG > GK > KK. From Table 8.5, the percentage difference between the specific shear strength and the shear strength are 30%, 3%, 9%, and 12% for KK, GG, GK, and KG respectively. This is consistence with other mechanical test (tensile, flexural, and compression) results above, which is an indication of good interfacial bonding that existed between the hybrid composites.

8.3 Theoretical Modeling:

The mechanical properties of sandwich composites can be derived from various experimental verifications and be ascertained by different mathematical models. Mathematical modeling is used to predict experimental results; they are a time saver and cost-friendly compared to experimental investigation. Modeling reduces stress on the part of the engineer during composite manufacturing (Kalaprasad 2014; Yashwant S. Munde 2015; Dong and Davies 2018; Xu *et al.* 2018). The mathematical model can be used to predict the best combination of constituent materials to be used for composites manufacturing and to satisfy design consideration for the materials most especially in the area like sandwich panel structures where multiple materials were involved. These models can yield information on the fundamental mechanisms of reinforcement.

Mathematical model was used in this study to validate the experimental results by using two existing models. Micromechanical composites models are derived based on the properties of the individual components of the sandwich composites and their arrangement. These include the volume fractions of the constituent materials (which was calculated from the rule of mixture), the modulus of constituent materials, tensile strength of constituent materials, and matrix component materials.

Nomenclature	
M_{sc}	Tensile modulus of sandwich composite
M_m	Tensile modulus of the matrix
M_f	Tensile modulus of fibers (kenaf and glass)
M_{sf}	Tensile modulus of syntactic foam
T_{sc}	Tensile strength of sandwich composite
T_m	Tensile strength of the matrix
T_f	Tensile strength of fibers
T_{sf}	Tensile strength of the syntactic foam
V_m	Volume fraction of matrix
V_f	Volume fraction of fibers
V_{sf}	Volume fraction of syntactic foam.

The different theories used to model the mechanical properties of sandwich composites are:

(i) Series and parallel model: According to these models, the tensile modulus and tensile strength are calculated using Equation. 8.3-8.8. (Yashwant S. Munde 2015).

For series model:

$$M_{sc} = M_f V_f + M_m V_m + M_{sf} V_{sf} \quad (8.3)$$

$$T_{sc} = T_f V_f + T_m V_m + T_{sf} V_{sf} \quad (8.4)$$

For parallel model:

$$M_{sc} = \frac{M_m M_f M_{sf}}{M_m V_{sf} + M_f V_m + M_{sf} V_f} \quad (8.5)$$

$$T_{sc} = \frac{T_m T_f T_{sf}}{T_m V_{sf} + T_f V_{sf} + T_{sf} V_f} \quad (8.6)$$

ii. Hirsch's model: It is the combination of series and parallel models. The equation for calculation of tensile modulus and strength are as follows:

$$M_{sc} = x(M_f V_f + M_m V_m + M_{sf} V_{sf}) + (1 - x).\frac{M_m M_f M_{sf}}{M_m V_{sf} + M_f V_m + M_{sf} V_f} \quad (8.7)$$

$$T_{sc} = x(T_f V_f + T_m V_m + T_{sf} V_{sf}) + (1 - x).\frac{T_m T_f T_{sf}}{T_m V_{sf} + T_f V_m + T_{sf} V_f} \quad (8.8)$$

x is a parameter that determines the stress transfer between fiber, syntactic foam, and matrix which is taken as 0.5 for both equations (5) and (6). And it is a function of the difference between the densities of the SFC and the HGM.

Series, parallel, and Hirach's model equations used for the modeling are functions of the volume fractions of all the constituent parameters used for each sandwich composite fabrication.

Table 8.6: Volume fractions of fiber, matrix, and syntactic foam composite used for the model.

SSFC	V_f	V_{sf}	V_m
KK	0.08	0.65	0.27
GG	0.09	0.58	0.34
GK	0.15	0.52	0.33
KG	0.14	0.52	0.34

Table 8.7: Experimental and theoretical modulus (GPa) values for sandwich syntactic foam composites model

SSFC	**M_{exp}**	M_{matrix}	M_{fiber}	M_{sf}	**M_{series}**	**$M_{parallel}$**	**$M_{hirsch's}$**
KK	1.42	2.14	0.64	4.57	3.60	3.24	3.42
GG	2.48	2.14	1.14	4.57	3.48	5.46	4.47
GK	2.14	2.14	1.28	4.57	3.27	5.64	4.46
KG	2.23	2.14	1.50	4.57	3.31	6.48	4.90

Table 8.8: Experimental and theoretical tensile strength (MPa) values for sandwich syntactic foam composites model

SSFC	**T_{exp}**	T_{matrix}	T_{fiber}	T_{sf}	**T_{series}**	**$T_{parallel}$**	**$T_{hirsch's}$**
KK	16.42	40.47	2.82	66.73	54.53	235.011	144.77
GG	51.06	40.47	20.72	66.73	54.33	1532.06	793.20
GK	40.39	40.47	15.59	66.73	50.40	1163.08	606.74
KG	32.95	40.47	26.44	66.73	52.16	1813.35	932.76

Table 8.6 shows the values of the volume fractions of fiber, matrix, and syntactic foam composites used for the theoretical calculations of the model. Also, Table 8.7 shows the theoretical modulus values (GPa) of SSFC in series, parallel, and hirsch's compared with the experimental values. While Table 8.8 shows the theoretical tensile values (MPa) of SSFC in series, parallel, and hirsch's compared with the experimental values used for the model.

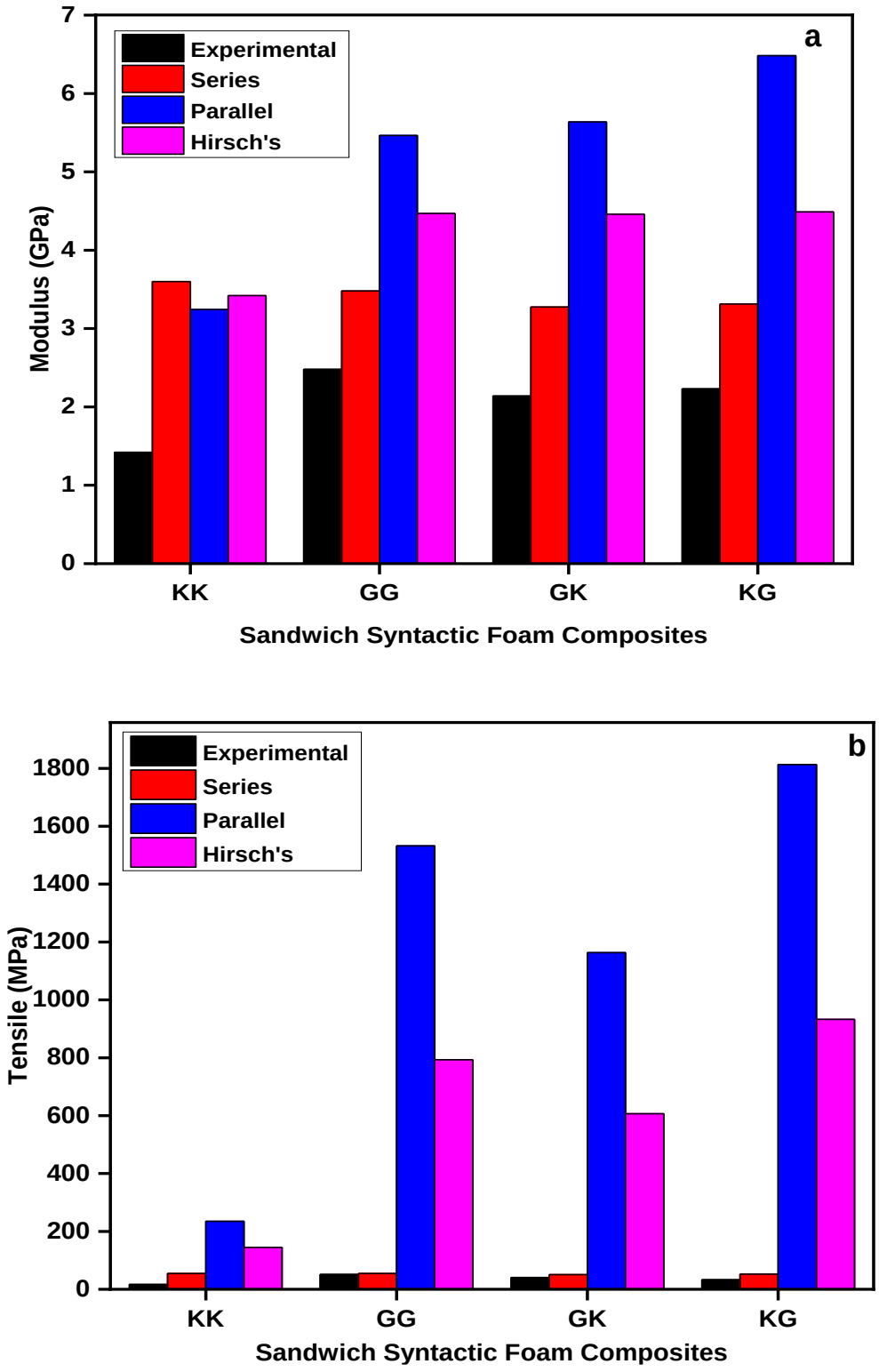

Figure 8.12 Variation of (a) theoretical vs experimental modulus and (b) theoretical vs experimental tensile strength values as a function of sandwich composite orientations compared with the experimental values.

Figure 8.12 (a, and b) shows the variation of the theoretical models (tensile modulus, and tensile strength) as a function of sandwich composite compared with the experimental results. From Figure 8.12(a), the three models show an increase of theoretical modulus values compared to the experimental result, the highest modulus (GPa) values for the models are at GK and KG, which shows that the model predicted better result for the combination of glass and kenaf fibers reinforcement. From Figure 8.12 (b), the theoretical tensile strength values for series model shows a closer range of results compared to the experimental while parallel and Hirach's models are more than the experimental values possibly because of the additional parameters considered in the model. This indicated that in comparison generally, the values of the series model for tensile modulus and tensile strength are closer to the experimental investigation than the parallel and Hirach's model.

8.4 Conclusion:

From this chapter, the focus was on the density properties and the mechanical characterization of sandwich syntactic foam composite as it affects the physical behavior of the hybrid composite. The percentage increase between the theoretical and experimental densities resulted in the porosity of the sandwich composites. Comparing the mechanical results and observing the fracture surfaces by SEM leads to the conclusion that the tensile, flexural, and compressive properties are dependent of the face-sheets of the sandwich composites. The following conclusion can be drawn based on this study:

1. The KK sandwich composite has the highest porosity which affected their mechanical properties because of the matrix to wetting effect on the kenaf fiber.
2. Tensile strength and modulus of GG in the SSFC shows improved properties than other sandwich specimens. The GG increased more than KK in strength and modulus by 67.7% and 42.7 % respectively.
3. Bending capacity of the hybrid face-sheet GK specimen shows improved flexural strength modulus than other specimens. The GK increased than the KK inn strength and modulus by 74% and 61.7% respectively.
4. The compressive strength of KG increased more than other specimen but the GG on the other hand shows better modulus value. KG increased in compressive strength than KK by 42.7% and modulus of GG increased by 39.3% to KK.

5. The shear strength of GG shows improved value than the other sandwich composite and more than KK 45%.
6. In general, it can be concluded that hybrid face-sheet can better perform in bending and compressive strength than GG and KK because glass fibers can possibly bear more load during testing.

In chapter nine, the thermal properties of SFC and SSFC as it relates to their mechanical properties will be discussed.

CHAPTER 9

9.0 THERMAL PROPERTIES OF SFC

In this chapter, the thermal properties (thermogravimetric analysis “TGA”) and (dynamic mechanical analysis “DMA”) of syntactic foam composite (SFC) are discussed. The thermal analysis was performed using TA Model Q 800 V20.6 instrument. The results were analyzed according to ASTM D4065 for both analyses as described earlier in chapter 3, Table **3.4,** and section **3.4.2.1.3.**

As part of the objectives for this study, the thermal analyses of the SFC were carried out to study the thermal stability and decomposition characteristics through the TGA and the viscoelastic behaviour through the DMA. The TGA helps to understand the effect of hollow glass microsphere “HGM” (heterogeneous and homogeneous) in pure epoxy resin as a function of thermal stability was analyzed by comparing the weight loss as a function of temperature. While the DMA helps to understand the effect of HGM (heterogeneous and homogeneous) on the SFCs storage modulus, loss modulus and tan delta properties.

This chapter contains one section 9.1 – thermal properties, and sub-divided into two: **9.1.1** is based on the thermal gravimetric analysis of SFCs and 9**.1.2** is on dynamic mechanical analysis of SFCs.

9.1 Thermal Properties

9.1.1 Thermal Gravimetric Analysis

The thermal gravimetric analysis of syntactic foam composites was analyzed based on the combined HGM and varied particle sizes (20-24µm designated as AA, 25-44µm designated as BB, 45-49µm designated as CC, and 50-60µm designated as DD). Five volume fractions of HGM composition in epoxy resin was considered for each of the SFCs.

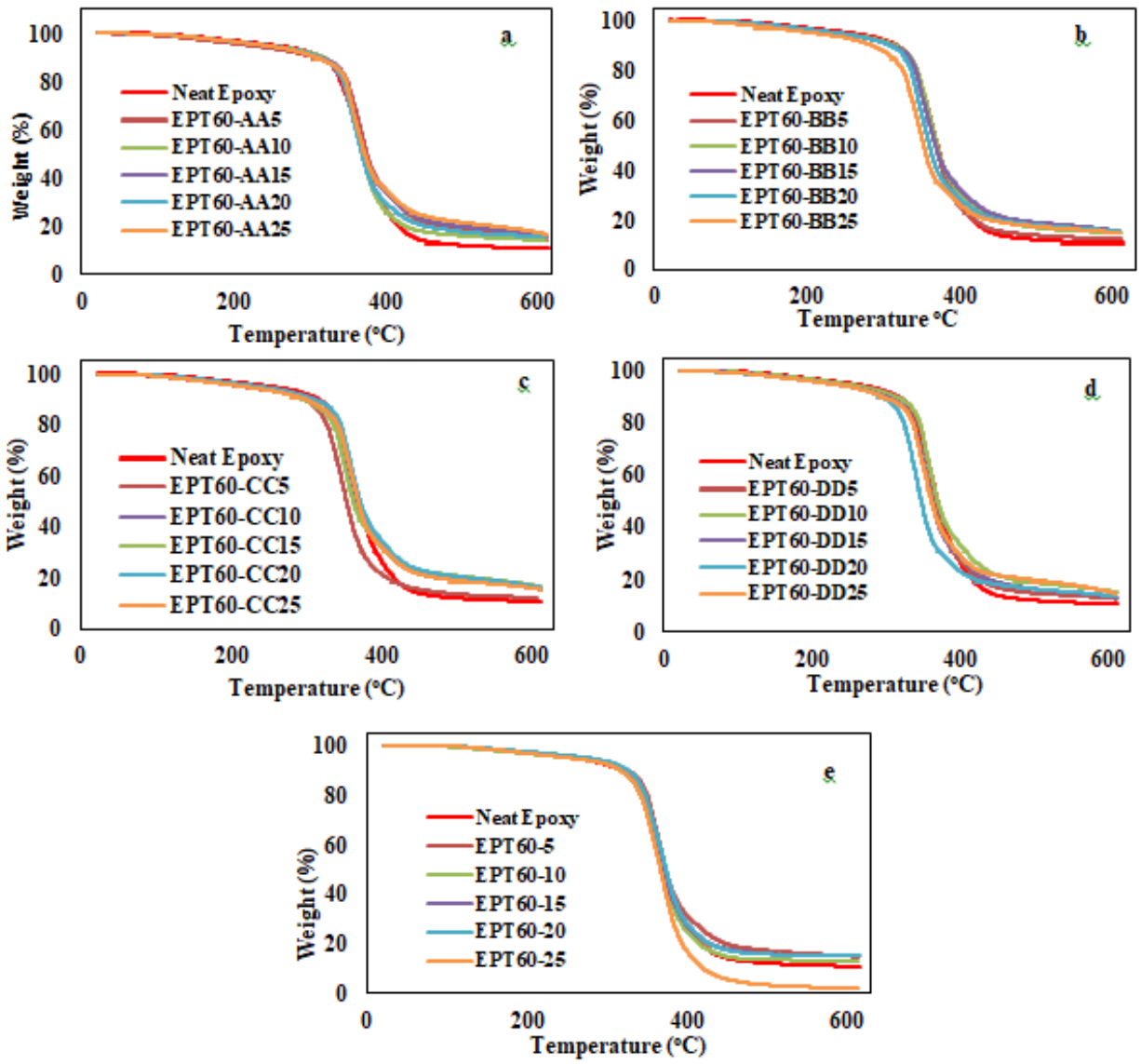

Figure 9.1: TGA analysis of syntactic foam composites and neat epoxy resin at 5-25vol% of HGM for (a) AA, (b) BB, (c) CC, (d) DD, and (e) heterogeneous particle sizes of HGM.

Figure 9.1 (a-e) shows the thermo-gravimetric analysis (TGA) for the SFC (homogeneous), SFCs (homogeneous HGM), and neat epoxy resin. The effect of hollow glass microsphere in pure epoxy resin on thermal stability was analyzed by comparing the weight loss as a function of temperature. The detailed weight loss results at 5%, 20%, and 55% degradation for SFCs and its comparison with NE are shown in Tables 9.1- 9.5. Figures 9.1 (a-d) shows that the neat

epoxy has the lowest weight% at maximum decomposition while in Figure 9.1 (e), EPT60-25 shows the lowest weight % towards maximum decomposition.

Table 9.1: Thermal properties of syntactic foam composites for heterogeneous HGM filler particle size variation at 5% weight loss, 20% weight loss, and 55% weight loss.

% Composition	Temperature at 5% weight loss (°C)	Temperature at 20% weight loss (°C)	Temperature at 55% weight loss (°C)
Neat epoxy	256	335	371
EPT60-5	277	337	375
EPT60-10	279	339	375
EPT60-15	272	341	379
EPT60-20	275	346	372
EPT60-25	257	342	369

From Table 9.1, it was experiential that the temperatures (5% loss, 20% loss, and 55% loss) of SFC has thermal stability more than the NE. This was an indication that the thermal stability of the epoxy resin can be improved by the addition of HGM. The derivatives of the thermal decomposition of the SFC for all the volume fraction compositions shows a double weight loss step between 180°C to 250°C and 300°C to 450°C and there are significant changes in the degradation stages. The addition of HGM improved the temperature of the SFC compared to the NE at 5% weight loss, 20% weight loss, and 55% weight loss. This improvement can be related to possible restriction caused by the molecules of the HGM on the motion of the NE polymer chain reaction during interaction, and thereby improve the thermal stability of SFC (Hu and Yu 2011; Cosse *et al.* 2019a). Also, good dispersion and coherency of chemical interactions between the filler and the epoxy resin can be responsible for the improvement in the thermal stability of the SFC, which enhances increased mechanical properties of the SFCs in **chapters 6&7** (Lin, Gupta and Talalayev 2009; Hu and Yu 2011; Li *et al.* 2015). Similar observation was reported by Jiao, Zhao and Chen (2016), that with the addition of HGM, the

initial decomposition temperature can be used to promote the degradation of the composite materials.

Table 9.2 Thermal properties of syntactic foam composites for homogeneous HGM filler variation (“AA” to “DD”) at 5% weight loss, 20% weight loss, and 55% weight loss.

% Composition of HGM	Temperature at 5% weight loss (°C)	Temperature at 20% weight loss (°C)	Temperature at 55% weight loss (°C)
Neat epoxy	256	335	371
EPT60-AA5	223	348	377
EPT60-AA10	250	350	379
EPT60-AA15	250	350	378
EPT60-AA20	246	346	381
EPT60-AA25	244	349	379
EPT60-BB5	241	337	379
EPT60-BB10	243	348	379
EPT60-BB15	245	350	381
EPT60-BB20	252	346	379
EPT60-BB25	227	342	383
EPT60-CC5	237	341	379
EPT60-CC10	249	348	383
EPT60-CC15	234	339	379
EPT60-CC20	243	348	379
EPT60-CC25	224	346	378
EPT60-DD5	254	350	386
EPT60-DD10	249	354	378
EPT60-DD15	236	346	381
EPT60-DD20	254	352	385
EPT60-DD25	237	349	381

Table 9.2 shows the thermal temperature compositions of SFC at homogeneous HGM filler sizes compared to neat epoxy. At 5% weight loss, the degradation temperature of neat epoxy was higher than all the SFCs at AA, BB, CC, and DD. This occurred due to possible weakness

in the cohesive force of homogeneous HGM size dispersion at 5% degradation. It can also possibly be due to poor cross-linking of the functional group of the filler molecules during covalent bonding with the matrix resulting in low molecular weight of the SFCs at 5% weight degradation. Salleh (2017b), reported an increase in the degradation of pure vinyl ester than the syntactic foam composites due to much debris or flakes from the glass microballoons. Meanwhile at 20% and 55% weight loss, the SFCs at AA, BB, CC, and DD shows higher thermal stability than the NE, this is possible because the chemistry of the epoxy resin influenced a greater interaction with inorganic filler, thereby promoting the increase in the thermal stability of the SFCs (Cosse *et al.* 2019a).

9.1.2 Dynamic Mechanical Analysis

The dynamic mechanical analysis was conducted to study the viscoelastic properties of the SFCs for the heterogeneous and homogeneous HGM size variations and to evaluate their interfacial interaction.

9.1.2.1 Storage Modulus

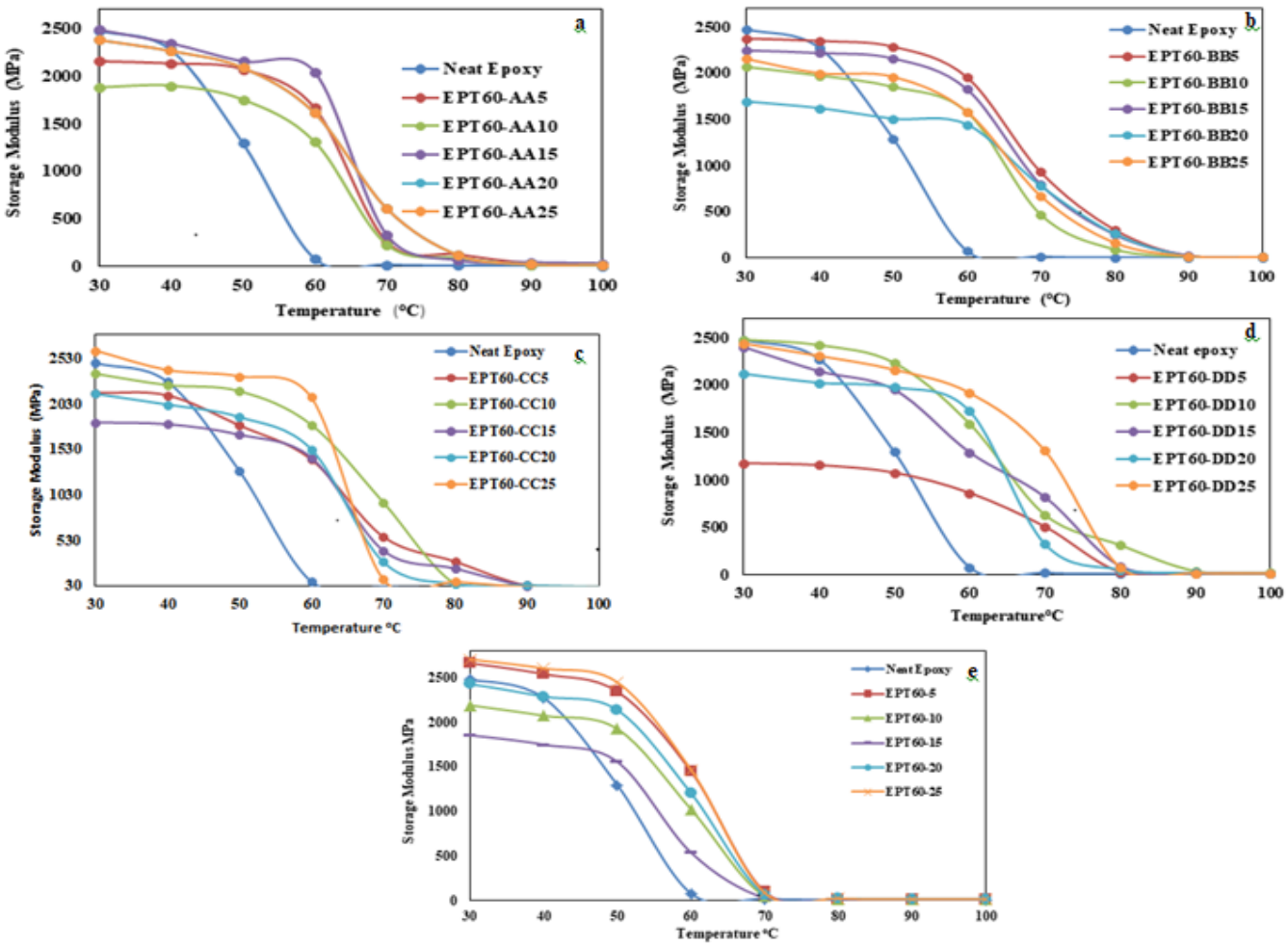

Figure 9.2: Storage modulus of SFC and neat epoxy matrix against temperature for homogeneous (a) AA, (b) BB, (c) CC, (d) DD, and (e) heterogeneous particle sizes of HGM.

The storage modulus (E'), values for the SFCs and NE were taken from three different temperatures 30^{o}C (considered as room temperature), 50^{o}C, and 60^{o}C as shown in Figure 9.2 (a-e) and Tables 9.3. The E′ of the SFCs measures the stored energy in the elastic portion of the composite. From Table 9.6, at temperature of 30^{o}C, the E' of heterogenous SFC increased compared to the NE at EPT60-5 and EPT60-25 by 185 MPa, and 227 MPa respectively, while it decrease at EPT60-10, EPT60-15, and EPT60-20 compared to the NE by -288 MPa, -624 MPa, and -52 MPa respectively. The increased values of E' could be a result of good intermolecular interaction between the epoxy resin while the decreased values could also result from poor intermolecular interaction between the epoxy and HGM during mixture (B. John 2010). For the homogeneous SFCs, the E' improved in values compare to the NE only at EPT60-AA25 and EPT60-CC25 by 79 MPa and 139MPa respectively, other SFCs experienced decreased value of E' than the neat epoxy. Huang *et al.* (2016) also reported similar decrease in storage modulus for all types of syntactic foams compared to the neat epoxy. The decline of E' is due to the incoporation of HGM, which makes the matrix more brittle.

At 50^{o}C temperature, the E' for all the SFCs samples improved compare to the NE with highest E' values at EPT60-25, EPT60-AA25, EPT60-BB5, EPT60-CC25, and EPT60-DD10 and increased by 1153 MPa, 860 MPa, 669 MPa, 1040 MPa, 875 MPa respectively. The improved low temprature E' values of the SFCs are attributed to the restricted movement of polymer chain as a result of good interaction between HGM and NE during mixing. Poveda, Achar and Gupta (2014) reported similar significant higher E' of 7.9%, 14.6%, and 400% at temperatures of -50^{o}C, 30^{o}C, and 175^{o}C respectively, compared to the NE. The improved E' is an indication that the HGM incorporation into the neat epoxy can reduce the viscosity flexibility of SFCs, leading to an increased mechanical properties of SFCs in **chapters 6 & 7.**

Moreover, at 60^{o}C temperature, the complex modulus values of SFCs also improved compared to the EPT60-0 for all the volume fractions of HGM by 1388 MPa, 1984 MPa, 1878 MPa, 2026 MPa, and 1840 MPa, at EPT60-25, EPT60-AA25, EPT60-BB5, EPT60-CC25, and EPT60-DD25 respectively. The improved E' values compared to NE at 50^{o}C and 60^{o}C can be attributed to good interaction and interfacial bonding (chapter **6&7**) between the HGM and NE molecules during mixing resulting in lowered density and void content (**chapter 5**) (Sankaran *et al.* 2006) and (Ghamsari, Zegeye and Woldesenbet 2013).

Table 9.3: The storage modulus (E') values of syntactic foam composites with heterogeneous and homogeneous HGM and neat epoxy at three representative temperatures: 30^{o}C, 50^{o}C, and 60^{o}C.

Specimen type	E' at 30°C (MPa)	E' at 50°C (MPa)	E' at 60°C (MPa)
EPT60-0	2478	1294	78
EPT60-5	2663	2343	1449
EPT60-10	2190	1924	1022
EPT60-15	1854	1555	535.4
EPT60-20	2426	2136	1203
EPT60-25	2705	2447	1466
EPT60-AA5	2157	2072	1664
EPT60-AA10	1881	1753	1309
EPT60-AA15	2487	2153	2043
EPT60-AA20	2379	2088)	1611
EPT60-AA25	2557	2154	2062
EPT60-BB5	2376	2288	1956
EPT60-BB10	2069	1854	1581
EPT60-BB15	2247	2160	1828
EPT60-BB20	1696	1509	1447
EPT60-BB25	2156	1963	1584
EPT60-CC5	2151	1794	1420
EPT60-CC10	2362	2171	1802
EPT60-CC15	1826	1692	1441
EPT60-CC20	2140	1886	1532
EPT60-CC25	2617	2334	2104
EPT60-DD5	1177	1077	863
EPT60-DD10	2479	2235	1594
EPT60-DD15	2402	1953	1291
EPT60-DD20	2119	1979	1726
EPT60-DD25	2439	2169	1918

Some of the notable trends observed for the E' are:

- At temperature of 50°C and 60°C, the percentage increase of E' improved significantly for all the SFCs than the EPT60-0 up to 47% and 96% respectively. Also, at 60°C, highest values of E' was at 25vol% of HGM except at EPT60-BB5 but has no apparent relation to particle size variation of HGM.
- The highest E' considering the volume fractions at 30°C, 50°C, and 60°C increased more than EPT60-0 for all the SFCs composition except at EPT60-BB5 with 4.3% lower.
- From heterogeneous HGM particle size variation, highest E' with respect to volume fraction at 30°C, 50°C, and 60°C, are 8.4%, 47%, and 94.7% at EPT60-25 respectively higher than EPT60-0. Also, at homogeneous HGM particle sizes variation, highest E' with respect to volume fraction at 30°C, 50°C, and 60°C improved more than the EPT60-0 with exception at EPT60-BB5 which is lower by 4.3%.
- In general, the percentage increase of SFCs E' to EPT60-0 at various volume fraction increased with increasing temperature from 30°C - 60°C. This reduction can be related to the softening of the matrix (Sankaran *et al.* 2006; Capela, Ferreira and Costa 2010). It can also imply that increase in temperature can influence the E' till it reaches maximum temperature where no significant improvement in E' can be observed again.
- Figure 9.2 (a-e) shows that the curves for different volume fraction of the same HGM particle size variation (heterogeneous and homogeneous) cross-over. The storage modulus o the neat resin decreased after the cross over. The cross-over points shift to higher temperature as the particles size variation increases. Similar cross-over was observed by Shunmugasamy, Pinisetty and Gupta (2013), where the storage modulus of neat resin became the least after the cross-over.

Table 9.4 shows the values for the maximum use of temperature T_{max} (°C), glass transition temperature T_g (°C), and percentage reduction of storage modulus of SFCs at maximum use of temperature "R" (%). T_{max} temperature (°C) is described as the temperature at which the storage modulus values of the SFCs begins to experience radical decrease in the thermograms (Sankaran *et al.* 2006; Capela, Ferreira and Costa 2010; Shunmugasamy, Pinisetty and Gupta 2013). The T_{max} values are mostly the same for all the SFCs composition and higher compared to the NE. The temperature at which the loss modulus and damping factor peak is commonly interpreted as the glass transition T_g of the material. The T_g values of the SFCs are between 70°C to 90°C and higher compared to the corresponding NE at 60°C. The percentage reduction

of storage modulus values at room temperature and at maximum use of temperature scatters across the SFCs composition but significantly higher compared to the NE.

Table 9.4: Maximum use of temperature T_{max} (ºC), glass transition temperature T_g (ºC), and percentage reduction of storage modulus of SFCs at maximum use of temperature "R" (%)

Specimen type	T_{max} (°C)	T_g (°C)	% Reduction of E' "R" (%)
EPT60-0	40	60	7.7
EPT60-5	60	70	45.6
EPT60-10	60	70	53.3
EPT60-15	50	70	16.1
EPT60-20	50	70	12
EPT60-25	50	70	9.5
EPT60-AA5	60	80	22.9
EPT60-AA10	60	80	30.4
EPT60-AA15	60	80	17.9
EPT60-AA20	60	80	32.3
EPT60-AA25	60	80	19.4
EPT60-BB5	60	80	17.7
EPT60-BB10	60	80	23.6
EPT60-BB15	60	80	18.7
EPT60-BB20	60	80	14.7
EPT60-BB25	60	90	26.5
EPT60-CC5	60	90	34
EPT60-CC10	60	80	23.7
EPT60-CC15	60	90	21.1
EPT60-CC20	60	90	28.5
EPT60-CC25	60	80	19.6
EPT60-DD5	60	90	26.7
EPT60-DD10	60	90	35.7
EPT60-DD15	60	80	46.3
EPT60-DD20	60	80	18.5
EPT60-DD25	70	80	46.3

9.2.2.2 Loss Modulus

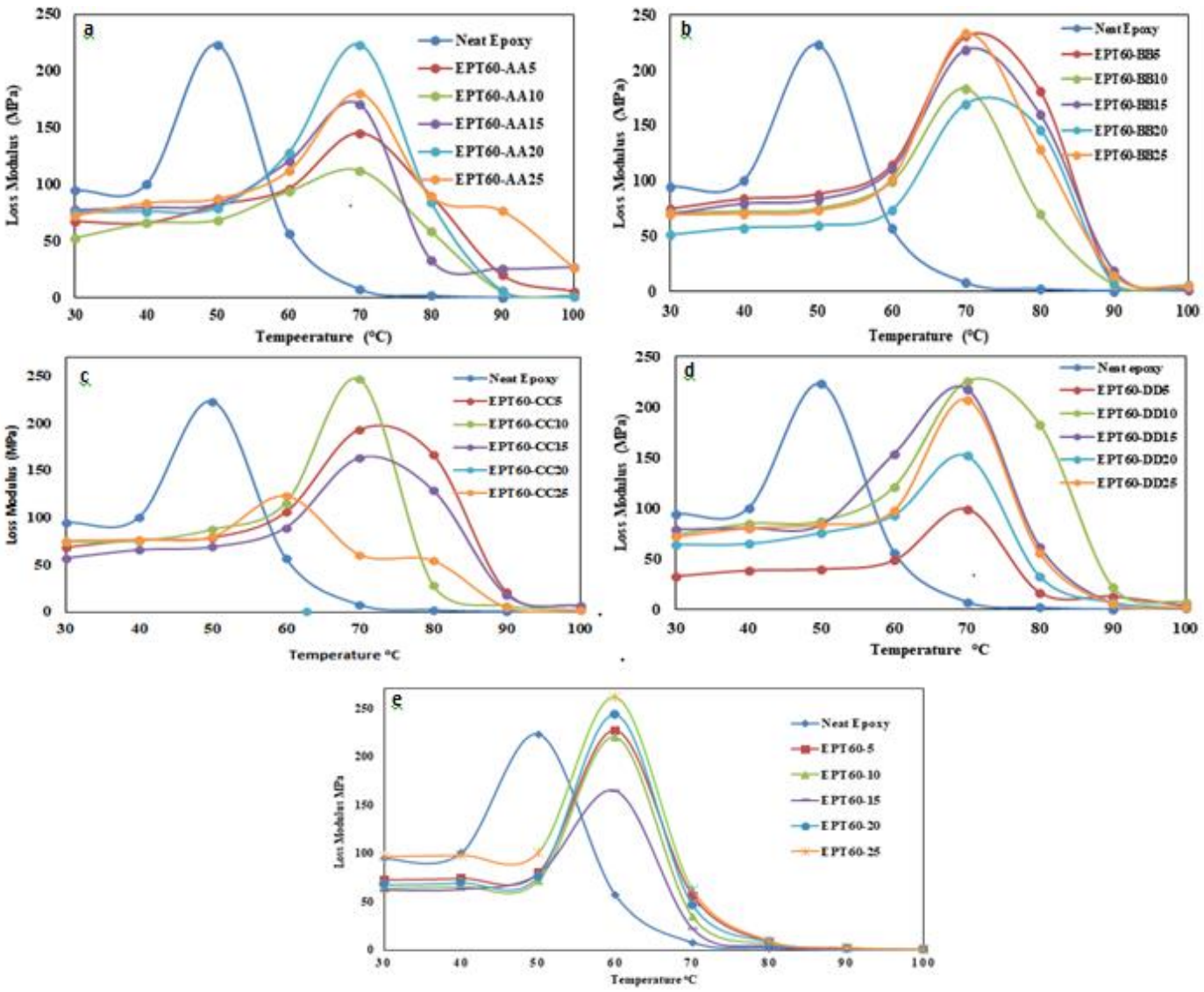

Figure 9.3: Loss modulus of SFC and neat epoxy matrix against temperature for homogeneous (a) AA, (b) BB, (c) CC, (d) DD, and (e) heterogeneous particle sizes of HGM.

Figure 9.3 (a-e) shows the loss modulus (E'') of the EPT60s which is the viscous response and a measure of the energy dissipated at heat per cycle under the deformation of the composites. From Table 9.5, at 30°C, the E'' value for SFC with heterogeneous HGM decreases compared with the EPT60-0, except at EPT60-25 which increased by 2 MPa than the EPT60-0. This shows that at room temperature, SFCs dissipate more energy to the atmosphere which affects its loss modulus.

Table 9.5: The loss modulus (E") values of syntactic foam composites with heterogeneous and homogeneous HGM and neat epoxy at three representative temperatures: 30^{o}C, 50^{o}C, and 60^{o}C

Specimen type	E" at 30°C (MPa)	E" at 50°C (MPa)	E" at 60°C (MPa)
EPT60-0	94.78	223.2	56.63
EPT60-5	72.63	79.9	227.2
EPT60-10	63.84	71.76	220.2
EPT60-15	62.09	78.63	164.6
EPT60-20	67.48	75.93	243.5
EPT60-25	96.76	101	261.5
EPT60-AA5	67.61	81.85	96.69
EPT60-AA10	53.05	68.76	94.07
EPT60-AA15	77.65	83.4	120.65
EPT60-AA20	75.71	79.68	128.28
EPT60-AA25	72.5	87.46	111.87
EPT60-BB5	74.53	88.02	114.41
EPT60-BB10	71.38	74.91	99.35
EPT60-BB15	69.85	83.02	110.67
EPT60-BB20	51.06	59.68	73.56
EPT60-BB25	69.56	72.98	102.15
EPT60-CC5	68.63	78.97	105.92
EPT60-CC10	74.42	87.56	115.56
EPT60-CC15	57.13	69.03	89.47
EPT60-CC20	62.84	73.05	84.78
EPT60-CC25	75.6	79.79	122.91
EPT60-DD5	32.97	40.07	48.07
EPT60-DD10	73.92	87.54	121.31
EPT60-DD15	79.33	83.85	154.2
EPT60-DD20	64.36	75.89	93.3
EPT60-DD25	71.82	83.87	98.1

At 50^{o}C, the E'' decreased compared with the NE for all the SFCs because of good energy dissipation in the process of forming the composites. The occurrence of reduced E'' at 30^{o}C and 50^{o}C could be related to the fact that at reduced temperature, the composites constituents tends to increased molecular mobility and thus lose their tight packing structure which progressively led to decrease E'' at the rubbery region (Sharma *et al.* 2021). Similar observation was reported by Shunmugasamy, Pinisetty and Gupta (2012) where the E"$_{max}$ of the neat resin is higher when compared to various types of the SFC. Increase in wall thickness increased the E" values of SFCs axcept at DD which does not align with this trend. This shows that the E'' of syntactic foam was noticeably affected by the particle sizes of HGM at room temperature.

At 60^{o}C, the E''values increased compared to the NE for all the SFCs samples with highest increase of 204.87 MPa, 71.66 MPa, 57.78 MPa, 66.28 MPa, and 97.37 MPa at EPT60-25, EPT60-AA20, EPT60-BB5, EPT60-CC25, and EPT60-DD15 respectively. The improved E'' values compared to NE can be attributed to good interaction and interfacial bonding between the microsphere and the matrix during mixing and also as a result of the lowered density and void content (**chapter 5**).

Table 9.6: Temperature at maximum loss modulus TE"$_{max}$ (^{o}C), and maximum loss modulus value E"$_{max}$ (MPa).

Specimen type	TE"$_{max}$ (°C)	E"$_{max}$ (MPa)
EPT60-0	50	223
EPT60-5	60	227
EPT60-10	60	220
EPT60-15	60	164
EPT60-20	60	243
EPT60-25	60	261
EPT60-AA5	70	145
EPT60-AA10	70	112
EPT60-AA15	70	170
EPT60-AA20	70	223
EPT60-AA25	70	180
EPT60-BB5	80	181
EPT60-BB10	70	183

EPT60-BB15	80	160
EPT60-BB20	80	146
EPT60-BB25	70	233
EPT60-CC5	80	167
EPT60-CC10	70	246
EPT60-CC15	80	129
EPT60-CC20	70	193
EPT60-CC25	60	122
EPT60-DD5	70	99
EPT60-DD10	80	183
EPT60-DD15	70	218
EPT60-DD20	70	152
EPT60-DD25	70	207

Table 9.6: show the temperature at maximum loss modulus TE"$_{max}$ (^{o}C), and maximum loss modulus value E"$_{max}$ (MPa) for the syntactic foam compared to the neat epoxy at the heterogeneous and homogenous HGM particle sizes. The E"$_{max}$ of neat resin increased more than the syntactic foam composites for most of the homogeneous particle sizes with some exceptions while EPT60-AA20 has the same E"$_{max}$ as the neat resin. The TE"$_{max}$ for the neat resin is lower compared to all the syntactic foam composite. Similarly, the heterogeneous TE"$_{max}$ is lower compared to the homogeneous TE"$_{max}$ of the syntactic foam composite. This suggested that particle size variation of HGM influence the temperature changes at E"$_{max}$, however, there is no significant trend on the volume fraction.

9.2.2.3 Tan Delta

The damping factor (Tan δ) is the ratio of E'' and E' and is a measure of impact and elastic characteristics or the damping capability of the SFCs, the peak height is closer to the energy dissipation of the SFC. The glass transition temperature (T_g) of the SFCs can also be evaluated from the peak temperature of Tan δ.

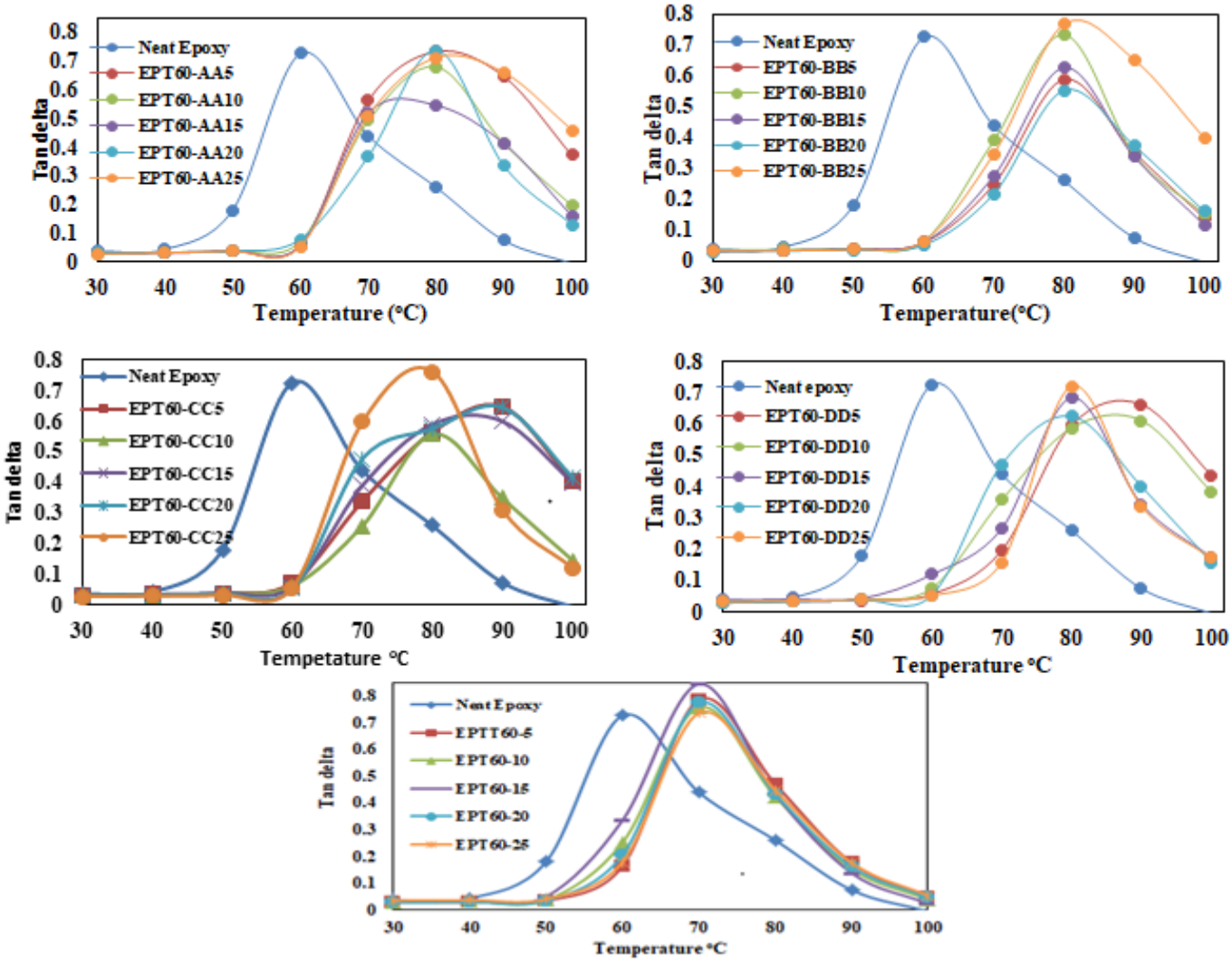

Figure 9.4 Tan delta (δ) of SFC and neat epoxy matrix against temperature for homogeneous (a) AA, (b) BB, (c) CC, (d) DD, and (e) heterogeneous particle sizes of HGM.

The tan delta (δ) of SFCs for the heterogeneous and homogeneous HGM was estimated from Figure 9.4 (a-e) and Tables 9.7. The T_g was determined from tan δ peak at temperature of 30ºC which increased compared to the NE and was observed at EPT60-25, EPT60-AA25, EPT60-BB25, EPT60-CC20, and EPT60-DD5 with values of 56 ºC, 73 ºC, 82 ºC, 81 ºC, 88 ºC, and 86 ºC respectively. It was observed that the addition of HGM into the epoxy matrix caused the peak of Tan δ to shift towards an increased temperature which could be attributed to the fact that the brittleness nature of the SFC is orchestrated the restrictions in the movement of epoxy

molecules (Sharma *et al.* 2021). The values of the tan delta which normally determines the glass transition temperature T_g, which is the ratio of the loss and storage modulus, as a function of temperature all reduced for SFCs and the e-SFCs compared with the neat epoxy resin. This is possibly due to the reduced intensity in intermolecular chain during the mixture.

At 50^{o}C, the T_g is observed to have shifted to a higher temperature with the addition of HGM, because of the restriction it gave to the movement of the epoxy polymer chain, which corresponds to an earlier report by Imran, Rahaman and Pal (2019). The values of Tan δ of the SFCs as reported in Table 9.10 shows that it reduced compared to the NE. This could possibly be due to the rigid nature of the HGM which hinders the flexibility of the chain motion in the inteface of the polymer reaction during mixture. Similar obervation was reported by (Sankaran *et al.* 2006). At 60^{o}C, the maximum value of tan δ for the neat epoxy matrix was 0.7259 and SFCs was 0.8435 at EPT60-15 as shown in Table 9.10. This shows that neat epoxy matrix resin exhibited a rubbery plateau before the SFCs which was an indication of proper dispersion of HGM in the epoxy resin. An increase in interfacial interaction between the matrix and HGM leads to an increase in the tan δ of polymer composites and also increases the damping force of the molecule motion (Hu and Yu 2011; Huang *et al.* 2016; Imran, Rahaman and Pal 2019).

Table 9.7: The tan delta (Tan δ) values of syntactic foam composites with heterogeneous and homogeneous HGM and neat epoxy at three representative temperatures: 30^{o}C, 50^{o}C, and 60^{o}C

Specimen type	Tan δ at 30°C (x10^3)	Tan δ at 50°C (x10^3)	Tan δ at 60°C (x10^3)
EPT60-0	38.2	180.7	725.9
EPT60-5	27.3	163.7	785.4
EPT60-10	29.2	251.8	756.9
EPT60-15	33.5	334.9	843.3
EPT60-20	27.1	205.5	772.7
EPT60-25	35.8	179.3	735.4
EPT60-AA5	31.4	39.5	58.1
EPT60-AA10	28.2	39.2	71.8
EPT60-AA15	31.2	38.7	59.1

EPT60-AA20	31.8	38.1	79.6
EPT60-AA25	28.4	37.8	54.3
EPT60-BB5	31.4	38.5	58.5
EPT60-BB10	34.5	40.4	62.8
EPT60-BB15	31.1	38.4	60.6
EPT60-BB20	30.1	35.7	50.8
EPT60-BB25	32.3	37.2	64.5
EPT60-CC5	31.9	39.5	74.6
EPT60-CC10	31.5	38.6	64.1
EPT60-CC15	31.3	40.8	62.1
EPT60-CC20	33.5	38.7	55.4
EPT60-CC25	28.9	34.2	58.4
EPT60-DD5	28	37.2	56.4
EPT60-DD10	29.8	39.2	76.1
EPT60-DD15	37.5	42.9	119.4
EPT60-DD20	30.4	38.3	54.1
EPT60-DD25	31.7	38.8	51.1

9.3 Conclusion.

Thermo-gravimetric analysis, and dynamic mechanical analysis were performed to understand the weight reduction capacity, the effect as regards the viscoelastic and thermal stability properties of the syntactic foam composites.

The TGA shows that temperatures at 5% weight loss, 20% weight loss, and 55% weight loss of pure epoxy and syntactic foam composites, the thermal degradation for all the volume fraction compositions show a double weight loss step between 180^{o}C to 250^{o}C and 300^{o}C to 450^{o}C. The neat epoxy has the lowest weight% at final decomposition while the SFCs slightly increased in temperature at all levels of temperature measurements (5% weight loss, 20% weight loss, and 55% weight loss). This is an indication that the thermal stability of the epoxy resin can be improved by the addition of HGM and there are significant changes in the degradation stages. It was also discovered that the thermal stability of the epoxy resin is lower than that of the syntactic foams containing HGM because of good dispersion and coherency of chemical interactions between the filler and the epoxy resin which led to an improvement in the thermal

stability of the syntactic foam composite and enhances better mechanical properties of the SFC and e-SFCs (**sections 6&7**).

At temperature of 30^{o}C, the heterogenous SFC E' increased compared to NE at EPT60-5 and EPT60-25 by 185 MPa and 227 MPa respectively. The homogeneous SFCs E' increased at EPT60-AA25 and EPT60-CC25 by 79 MPa and 139MPa respectively, other SFCs shows decreased value of E' compared neat epoxy. This can be due to the restriction of movement of polymer chains at low temperatures. At 50^{o}C temperature, E' for all the SFCs samples increased than the NE with highest E' values at EPT60-25, EPT60-AA25, EPT60-BB5, EPT60-CC25, and EPT60-DD10 and increased by 1153 MPa, 860 MPa, 669 MPa, 1040 MPa, 875 MPa respectively. Also, at 60^{o}C temperature, the E' values of SFCs for all the samples increased more than the NE for all the volume fractions of HGM. The maximum E' values 1388 MPa, 1984 MPa, 1878 MPa, 2026 MPa, and 1840 MPa, at EPT60-25, EPT60-AA25, EPT60-BB5, EPT60-CC25, and EPT60-DD25 respectively. The improved E' of SFCs can possibly resulted from good intermolecular interaction between the epoxy resin and HGM.

Loss modulus E'' of heterogeneous SFCs at 30^{o}C increased at EPT60-25 by 2 MPa than the NE while other volume fractions including the homogeneous SFCs are lower than the neat epoxy resin. At 50^{o}C temperature, the E'' decreased compared with the NE for all the SFCs because of good energy dissipation in the process of forming the composites. The occurrence of reduced E'' at 30^{o}C and 50^{o}C could be related to the fact that at reduced temperature, the composites constituents tends to increased molecular mobility and thus lose their tight packing structure which progressively led to decrease E'' at the rubbery region. At 60^{o}C, the E''values increased compared to the NE for all the SFCs samples with highest increase of 204.87 MPa, 71.66 MPa, 57.78 MPa, 66.28 MPa, and 97.37 MPa at EPT60-25, EPT60-AA20, EPT60-BB5, EPT60-CC25, and EPT60-DD15 respectively.

Tan δ determined the function of the T_g at the peak temperatures. At 30^{o}C, the tan δ increased compared to EPT60-0 and is observed at EPT60-25, EPT60-AA25, EPT60-BB25, EPT60-CC20, and EPT60-DD5 with values of 56 ^{o}C, 73 ^{o}C, 82 ^{o}C, 81 ^{o}C, 88 ^{o}C, and 86 ^{o}C respectively. It can be concluded that the addition of HGM into the epoxy matrix caused the peak of Tan δ to shift towards an increased temperature which could be attributed to the fact that the brittleness nature of the SFC is orchestrated by the restriction the restrictions in the movement of epoxy molecules by the addition of HGM. At 50^{o}C, the T_g is observed to have shifted to a higher temperature with the addition of HGM, because of the restriction it gave to the movement of the

epoxy polymer chain. The values of Tan δ of the SFCs as reported in Table 9.22 shows that it reduced compared to the NE. At 60^{o}C, the maximum value of tan δ for the neat epoxy matrix is 0.7259 at 60^{o}C and SFCs is 0.8435 at EPT60-15 as shown in Table 9.23. This shows that neat epoxy matrix resin exhibited a rubbery plateau before the SFCs which was an indication of proper dispersion of HGM in the epoxy resin.

Further, the propeties of SFCs and SSFC such as hardness, water absorption, impact and acoustic as a possible composite material for structural and aerospace applications were studied in Chapter 10.

CHAPTER 10

10.0 HARDNESS, WATER ABSORPTION, BUOYANCY, IMPACT, AND ACOUSTIC PROPERTIES OF SYNTACTIC FOAM COMPOSITE AND SANDWICH SYNTACTIC FOAM COMPOSITE

10.1 Hardness Properties of Syntactic Foam Composite and Sandwich Syntactic Foam Composite

10.1.1 Hardness Properties of Syntactic Foam Composites

In this section, the hardness properties of syntactic foam composites in comparison with the epoxy resin, the average maximum harness rate for the composites were calculated and tabulated in Table 10.1. Twenty (20) readings of indentation were taken per each sample and an average reading taken using Barcol hardness instrument.

Table 10.1: Barcol hardness properties of syntactic foam composites and epoxy resin

Hardness (Hv)	Syntactic Foam Composites					
Skimmed depth	EPT60-0	EPT60-5	EPT60-10	EPT60-15	EPT60-20	EPT60-25
1	23	30	25	28	27	25
2	25	29	24	28	27	24
3	22	28	25	26	29	24
4	21	25	23	27	29	23
5	26	27	24	27	30	23
6	20	29	26	31	25	24
7	20	28	26	29	23	25
8	21	25	27	29	23	27
9	22	26	26	28	24	26
10	20	29	25	27	22	24
11	24	25	27	28	25	23
12	22	23	28	29	24	22

13	22	24	25	28	23	24
14	24	24	26	27	26	23
15	23	26	24	28	23	22
16	24	30	25	25	25	27
17	20	29	26	26	27	26
18	22	25	23	27	27	25
19	23	23	22	26	24	24
20	26	25	23	25	23	23
Average	**22.5 ± 1.91**	**26.5 ± 2.33**	**25.0± 1.55**	**27.5 ±1.47**	**25.3 ±2.34**	**24.2 ±1.47**
Maximum	**26**	**30**	**28**	**31**	**30**	**27**
Minimum	**20**	**23**	**22**	**25**	**22**	**22**

Table 10.1 presents the average hardness result of the SFCs for the five-volume compositions of HGM (EPT60-5, EPT60-10, EPT60-15, EPT60-20, and EPT60-25) compared to the neat epoxy (EPT60-0). The SFCs increased in hardness value compared to the neat epoxy by 15.1%, 10%, 18.2%, 11.1%, and 7.0% for EPT60-5, EPT60-10, EPT60-15, EPT60-20, and EPT60-25 respectively. This was possibly because the addition of HGM into the resin increase the stiffness of the composites. Similar observation was earlier reported by Orbulov and Németh (2009), where the hardness properties of metal matrix syntactic foam (MMSF) for the Al99.5 matrix increased compared to the neat matrix material. The highest average hardness value is 27.5Hv at EPT60-15, this could imply that the SFCs at EPT60-15 were more sensitive to deformation than other composites. The increased hardness values imply that the SFCs can better withstand hardness conditions than neat epoxy when used as reinforcement in composite materials (Al-Hasani 2007; Orbulov and Németh 2009; Orbulov, Németh and Dobránszky 2010). The increased hardness properties of the SFCs can be related to their improved mechanical properties than the neat epoxy as discussed in **chapters 6&7**. Also, Anbuchezhiyan *et al.* (2017) reported that syntactic foam synthesized by the reinforcement of hollow glass microspheres and magnesium alloy matrix increased in hardness properties with a mass fraction of the HGM in the matrix alloy due to the occurrence of the reinforcement. Moreover, Manakari *et al.* (2017), reported a steady increase in the hardness value of SFC with the addition of GMB particles up to 107 Hv at 25vol% which is 127.7% more than that of the pure

Mg (47 Hv). The hardness readings of EPT60-15 are worth noticing as they have better surface toughness compared to other compositions of SFC. This contributed to their load bearing along with making the step of elastic distortion long and exceeding a critical load yielding in the composites. However, in the experimental study by Kumar (2015), he reported that the hardness value of SFC increased with an increase in volume fraction of glass microballoons up to an optimum limit of 10vol% and then decreased. The result shows that a crucial limit was reached by the clustered size of glass microballoons leading to decreasing function of the reinforcement, resulting in the decrease of the hardness value of the syntactic foam (Lam *et al.* 2005).

10.1.2 Hardness Properties of Sandwich Syntactic Foam Composites

Table 10.2 shows the hardness reading for the sandwich syntactic foam composites. Fifteen (15) readings of indentation were taken per each sample and an average reading taken using Barcol hardness instrument. Hardness test was conducted for the SSFC to examine the hardness strength of the face-sheet used for reinforcement.

Table 10.2: Barcol hardness readings for the sandwich syntactic foam composites

Hardness (Hv)	Syntactic Foam Sandwich Composites			
Skimmed depth	KK	GG	GK	KG
1	25	46	46	35
2	24	55	45	38
3	30	50	42	37
4	32	40	58	32
5	31	43	48	32
6	30	50	57	30
7	25	40	50	29
8	28	45	48	34
9	34	39	45	33
10	26	42	56	31

11	33	38	50	30
12	31	31	47	56
13	30	43	53	29
14	31	50	43	28
15	29	46	50	32
Average	**29.267±3.05**	**44.933±6.01**	**49.800±4.96**	**32.067±6.81**
Maximum	**34**	**55**	**58**	**38**
Minimum	**24**	**31**	**42**	**28**

Table 10.2 shows the Barcol hardness readings of the sandwich syntactic foam composite. Fifteen indentations were done on each sample and the readings taken. The GK sandwich structure shows the highest hardness value, 49.8 Hv, which is a 41% increase from the KK with the lowest hardness value of 29.267Hv. This is because the combination of glass and kenaf fibers can better improve the hardness of the hybrid sandwich composite structure. The order of hardness strength is GK > GG > KG > KK. The highest hardness strength by GK shows that hybrid glass/kenaf fibers can possibly enhance good hardness resistance than plain kenaf or glass fiber when used as reinforcement in sandwich composites. An increase in fiber layers and weight also contributed to the increasing hardness property which is possibly attributed to the alignment and the length of the fiber (Al-Hasani 2007). The reduced hardness strength in KK is possibly attributed to its lower mechanical properties and high porosity associated with interface and its stress concentration in the matrix.

10.2 Percentage Water Absorption of Syntactic Foam Composites and Sandwich Syntactic Foam Composites

10.2.1 Percentage Water Absorption of Syntactic Foam Composites (SFC).

Table 10.3 shows the percentage water intake of the SFC at each HGM volume fraction as compared with the neat epoxy. The water absorption of the SFC can be defined in different forms by considering the role of the internal porosity, surface, and subsurface conditions of the material. When the specimen was dipped inside the water, the actual diffusion may not have

taken place before moisture was entrapped in the surface of the SFC. Such surface entrapment was not relevant in describing the SFC water diffusion mechanism because it cannot give the actual calculation needed for the composite material diffusivity (Tagliavia, Porfiri and Gupta 2012).

From Table 10.3, the same time frame was considered for all the SFC composition, and the neat epoxy were immersed into the water at once and left throughout the stipulated time. The final time $T_{(s)}$ was considered after 720 hours and the first wet measurement $M_{(t)}$ was taken after 24 hours. The percentage of water absorption intake increased with time for all the SFC specimens because of the longer stay in the water which reflects their varying densities and void in the SFC as discussed in **chapter 5**. The percentage of water absorbed by EPT60-15 was the highest after 24 hours which was 0.27%. Subsequently, after 48 hours, EPT60-5 and EPT60-25 have almost the same percentage water intake of about 0.15%. Table 10.3 shows the raw value for the mean water absorption results for the SFC filled with HGM at 5-25vol% fraction for the period of 24 to 720 hours. Table 10.4 shows the diffusion coefficient properties as calculated from the mean water absorption values for the neat epoxy and the SFC. The value of $M_{(d)}$ for the neat epoxy was 0.572% and the ratio of $M_{(d)}/\sqrt{T_{(s)}}$ was 0.021 %/√h and by comparison was higher than the SFC samples. By observation, EPT60-20 shows the highest values of $M_{(d)}$ and $M_{(d)}/\sqrt{T_{(s)}}$ which are 0.471% and 0.018 %/√h respectively. The values of $M_{(d)}$ varies as the volume fraction of HGM increases in the SFC which correlates the relationship between the density and the specific properties of syntactic foam composites. The highest value of $M_{(d)}\ and\ M_{(d)}/\sqrt{T_{(s)}}$ observed from the neat epoxy sample was an indication that the neat epoxy resin was more porous and absorbed water than the respective SFC samples, this was further justified by the buoyancy results in **section 10.3**. Reduced water absorption rate of SFC shows that addition of HGM restricted water from entering the SFC because HGM are insoluble on water. (Gupta and Woldesenbet 2003; Tagliavia, Porfiri and Gupta 2012; Ding *et al.* 2018; Guo, Finkenstadt and Nimmagadda 2019).

Table 10.3 Mean values for the percentage water absorption of syntactic foam composites (%)

SFC	EPT60-0	EPT60-5	EPT60-10	EPT60-15	EPT60-20	EPT60-25
After 24 hours	0.0189	0.1168	0.0988	0.2696	0.0851	0.1564
STDEV	0.1276	0.0611	0.1266	0.2149	0.0878	0.1537
After 48 hours	0.0934	0.1518	0.1099	0.113	0.103	0.1547
STDEV	0.1665	0.1115	0.1505	0.1204	0.0893	0.0805
After 120 hours	0.0958	0.2055	0.2529	0.2114	0.2072	0.254
STDEV	0.0491	0.1099	0.2348	0.1232	0.0871	0.1222
After 192 hours	0.2817	0.2958	0.3061	0.3348	0.2892	0.3414
STDEV	0.1711	0.148	0.1338	0.0948	0.0803	0.1041
After 336 hours	0.4109	0.4303	0.4334	0.4292	0.4786	0.4619
STDEV	0.1019	0.1653	0.1579	0.1098	0.0516	0.0904
After 720 hours	0.5907	0.5201	0.501	0.5197	0.5565	0.5801
STDEV	0.0959	0.1343	0.221	0.1688	0.0309	0.0731

Table 10.4 Diffusion coefficient properties of syntactic foam composites

SFC	$M_{(s)}$ (%)	$M_{(t)}$ (%)	$M_{(d)}$ (%)	$\sqrt{T_{(s)}}$ (h)	$M_{(d)}/\sqrt{T_{(s)}}$ (h)
Neat epoxy	0.591	0.019	0.572	26.83	0.021
EPT60-5	0.520	0.117	0.403	26.83	0.015
EPT60-10	0.501	0.099	0.0402	26.83	0.015
EPT60-15	0.520	0.270	0.250	26.83	0.009
EPT60-20	0.556	0.085	0.417	26.83	0.018
EPT60-25	0.580	0.156	0.424	26.83	0.016
$M_{(s)}$ =final mean; $M_{(t)}$ = initial mean; $M_{(d)}$ = $M_{(s)}$ - $M_{(t)}$; $T_{(s)}$ = final time					

10.2.2 Percentage Water Absorption of Sandwich Syntactic Foam Composites

Table 10.5 and 10.6 shows the water absorption values and diffusion coefficient values for the SSFC respectively. From Table 10.5, the percentage water intake of the SSFC (KK, GG, GK, and KG) was compared and the mean values recorded. The same procedure observed for SFC was repeated for SSFC samples.

The percentage of water absorption at GG, GK, and KG increased with time while that of KK shows no trend of time increase, this can be related to the higher porosity at KK and the sandwich varying densities as described in **chapter 8.1**. The percentage of water absorbed by KK was the highest for all the time frames. From Table 10.6, KK showed the highest value of diffusion coefficient $M_{(d)}$ and the ratio $M_{(d)}/\sqrt{T_{(s)}}$ of 3.784% and 0.1410 %/√h respectively compared to GG with the lowest water absorption and diffusion coefficient of 0.593% and 0.0221%/√h respectively. The higher values of $M_{(d)}$ and $M_{(d)}/\sqrt{T_{(s)}}$ observed at KK shows that it is possibly more porous and does absorb water more than other sandwich composites. because natural reinforcement is used as face-sheets, this is also justified by the buoyancy results in **section 10.3**. The reduced water absorption rate of GG, GK, and KG shows that SSFC water absorption rate can be controlled or minimized by the combination of kenaf/glass fibers as reinforcement which implies that they can be employed for structural and marine purposes (Scudamore 2002; Ding *et al.* 2018; Guo, Finkenstadt and Nimmagadda 2019).

Table 10.5 Mean values for the percentage water absorption of sandwich syntactic foam composites

SSFC	After 24 hours	STDEV	After 120 hours	STDEV	After 192 hours	STDEV	After 336 hours	STDEV	After 720 hours	STDEV
KK	2.382	0.9041	4.135	0.5917	4.006	0.7882	7.406	1.7817	6.166	0.556
GG	0.062	0.0406	0.185	0.0040	0.327	0.1225	0.4503	0.0779	0.655	0.2184
GK	0.287	0.0293	0.762	0.0348	1.108	0.0040	1.706	0.0777	2.118	0.0297
KG	0.491	0.1092	1.307	0.5115	1.777	0.8229	2.132	0.4938	2.479	0.1574

Table 10.6 Diffusion coefficient properties of sandwich syntactic foam composites

SSFC	$M_{(s)}$ (%)	$M_{(t)}$ (%)	$M_{(d)}$ (%)	$\sqrt{T_{(s)}}$ (h)	$M_{(d)}/\sqrt{T_{(s)}}$ (h)
KK	6.166	2.382	3.784	26.83	0.1410
GG	0.655	0.062	0.593	26.83	0.0221
GK	2.118	0.287	1.831	26.83	0.0682
KG	2.479	0.491	1.988	26.83	0.0741
$M_{(s)}$ =final mean; $M_{(t)}$ = initial mean; $M_{(d)} = M_{(s)} - M_{(t)}$; $T_{(s)}$ = final time					

10.3 Buoyancy Properties of Syntactic Foam Composites and Sandwich Syntactic Foam Composite

10.3.1 Buoyancy Properties of Syntactic Foam Composites

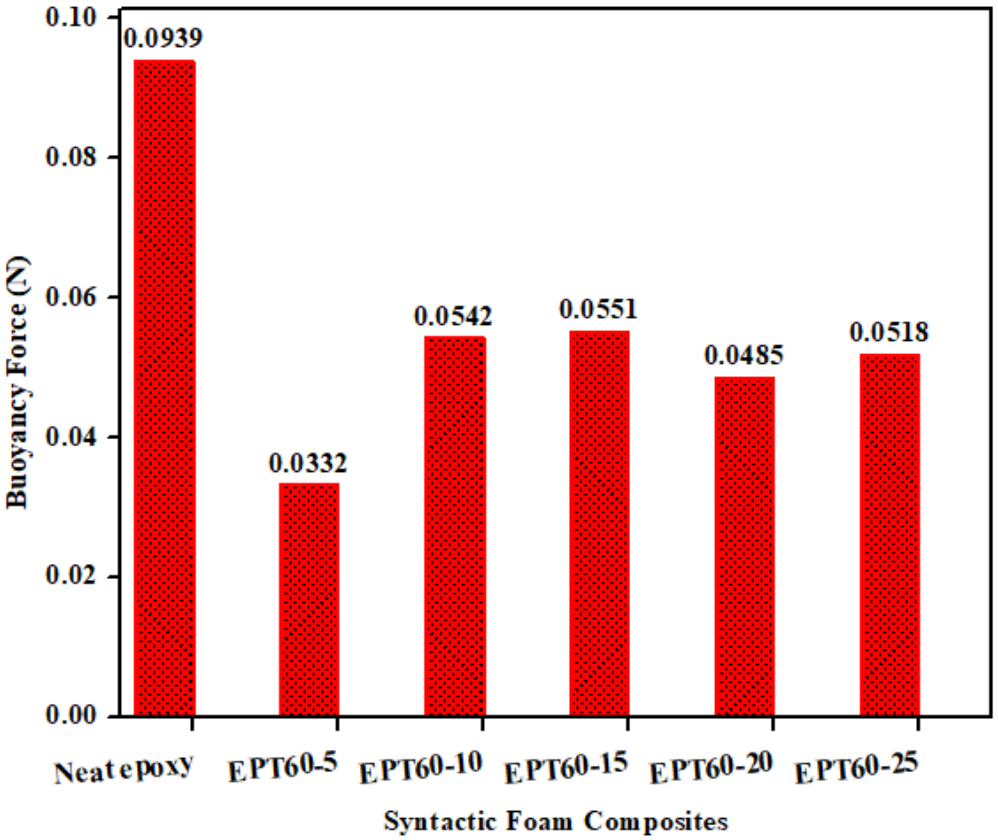

Figure 10.1: Buoyancy force (N) of Syntactic Foam Composites and the Neat Epoxy

Table 10.7: Syntactic Foam Composites Buoyancy Properties

SFC samples	The volume of displaced object "V" (m^3)	Force of gravity "F_g" (N/kg)	The density of the liquid "D" (kg/m^3)	Buoyancy force "F_b" (N)
Neat epoxy	9.57E-06	9.81	1000	0.094 ± 0.021
EPT60-5	3.38E-06	9.81	1000	0.033 ± 0.019
EPT60-10	5.53E-06	9.81	1000	0.054 ± 0.020
EPT60-15	5.62E-06	9.81	1000	0.055 ± 0.018
EPT60-20	4.94E-06	9.81	1000	0.048 ± 0.020
EPT60-25	5.28E-06	9.81	1000	0.052 ± 0.019

Figure 10.1 shows the buoyancy force (F_b) (N) of the SFC compared with the neat resin. Table 10.7 presents the detailed values of the results used in calculating the F_b. The F_b of the SFC increased with increasing volume fraction of the HGM from EPT60-5 to EPT60-15 before it decreased further at EPT60-20 and EPT60-25. The F_b of the neat epoxy was the highest at 0.0939N with ~65% more than the EPT60-5. The result shows that neat epoxy will require more energy to float in water compared to the. This may be related to water absorption results earlier discussed in **section 10.2.1** where the coefficient of diffusion of neat resin is high compared with SFC because it absorbs more water after submerging it for 720h. This means that as the neat epoxy sank in the water, the volume of the water that spills over will was equal to the volume of the resin sample. Also, the presence of HGM in the SFC enhanced it's floating capacity because it's F_b is possibly greater than the force of gravity (G) (Bess Ruff 2022), (Ren *et al.* 2017a).

10.3.2 Buoyancy Properties of Sandwich Syntactic Foam Composites

Figure 10.2 presents the buoyancy force (F_b) of the SSFC for KK, GG, GK, and KG orientations. Table 10.8 shows the detailed values of the results used in calculating the F_b. The F_b of the KK was the highest followed by the GG, then the KG and the GK, which are 0.3296N, 0.2747N, 0.2619N, and 0.2502N. The highest F_b at KK could mean that when it is submerged in the fluid, it can easily absorb water, therefore, it requires more F_b for an up-thrust to float. Following this observation, a relationship may therefore be established between the buoyancy and water

absorption results discussed earlier in **section 10.2.2** where the coefficient of diffusion of KK was more than other sandwich composites because it absorbs more water after 720h. Also, KK will sink faster when submerged because of the nature of the kenaf/kenaf fibers as reinforcement but the combination of kenaf/ glass fibers can reduce the water absorption of the SSFC (Ren *et al.* 2016; Ren *et al.* 2017a).

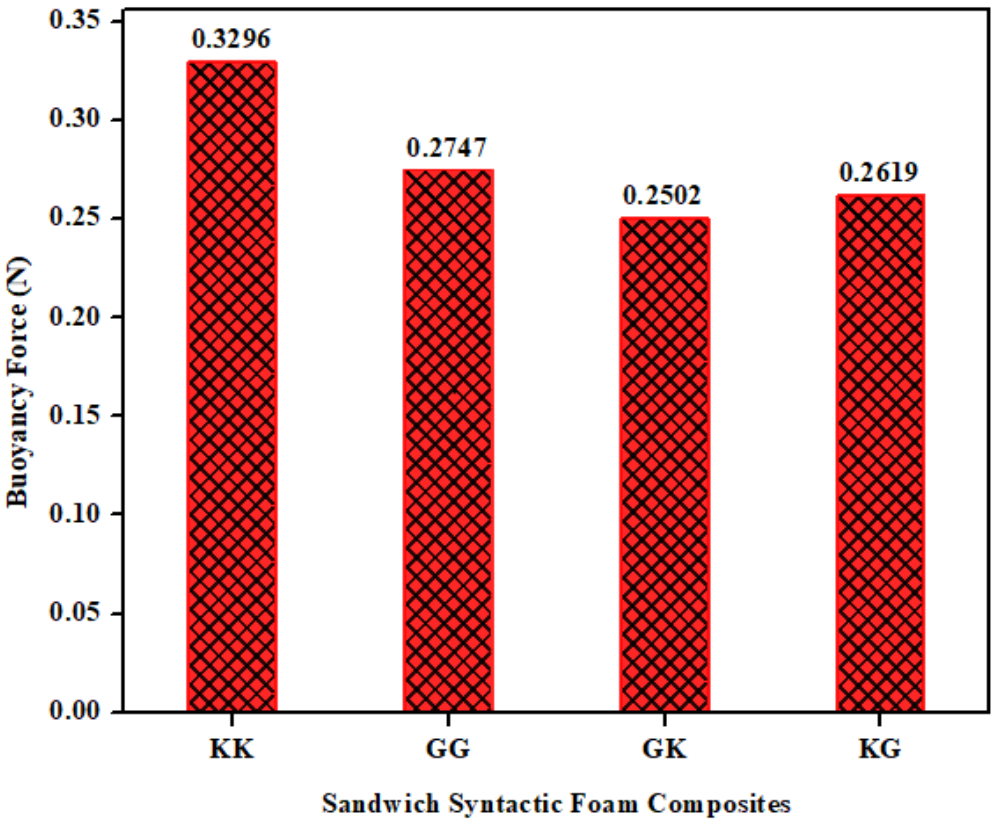

Figure 10.2: Buoyancy force (N) of Sandwich Syntactic Foam Composites for the KK, GG, GK, and KG orientations.

Table 10.8: Sandwich Syntactic Foam Composites Buoyancy Properties

SSFC samples	The volume of displaced object "V" (m^3)	Force of gravity "F_g" (N/Kg)	The density of the liquid "D" (Kg/m^3)	Buoyancy force "F_b" (N)
KK	3.36E-05	9.81	1000	0.330 ± 0.035
GG	2.80E-05	9.81	1000	0.275 ± 0.033
GK	2.55E-05	9.81	1000	0.250 ± 0.34
KG	2.67E-05	9.81	1000	0.262 ± 0.036

10.4 Impact Properties of Syntactic Foam Composites

Figure 10.3 represents the impact strength and specific impact strength of SFC. The impact strength of all the compositions of SFC is more than the neat epoxy but reduces with increasing HGM filler concentration. The impact strength of the neat epoxy is 84.57 kJ/m^2. At the addition of HGM, impact strength increased at all the varying volume fractions, with the highest impact resistance of 113.12 kJ/m^2, observed at SFCT60-5 vol% of HGM. This can be assumed that the lower percentage of HGM filler can better absorb impact strength because of reduced agglomeration and better dispersion with epoxy matrix. The percentage impact strength increases of SFC to NE from EPT60-5, EPT60-10, EPT60-15, EPT60-20, and EPT60-25vol% of HGM filler is 25.2%, 23.87%, 14.30%, 4.54%, and 1.77% respectively. This can be due to strong molecular bonding that existed in the composite during chemical interactions of the filler and the HGM. Unlike the report by Patil et al (Patil, Kubade and Kulkarni 2020) where the absorbed impact energy of hybrid syntactic foam decreased compared to the neat epoxy with the increasing composition of HGM.

The specific impact strength (SIS) of SFC on the other hand increases with increasing volume fraction of HGM filler. All compositions of SFC have higher SIS than the NE with the highest SIS of 163.36 $kJ/m^3/g$ at SFCT60-25. The net percentage increase of SIS for 5, 10, 15, 20, 25 vol% was 38.06%, 48.28, 49.73, 50.39, and 53.78% increase. This increase in the SIS can be attributed to the reduced density with increasing volume fraction of the HGM in the SFC (Olusegun A. Afolabi 2021).

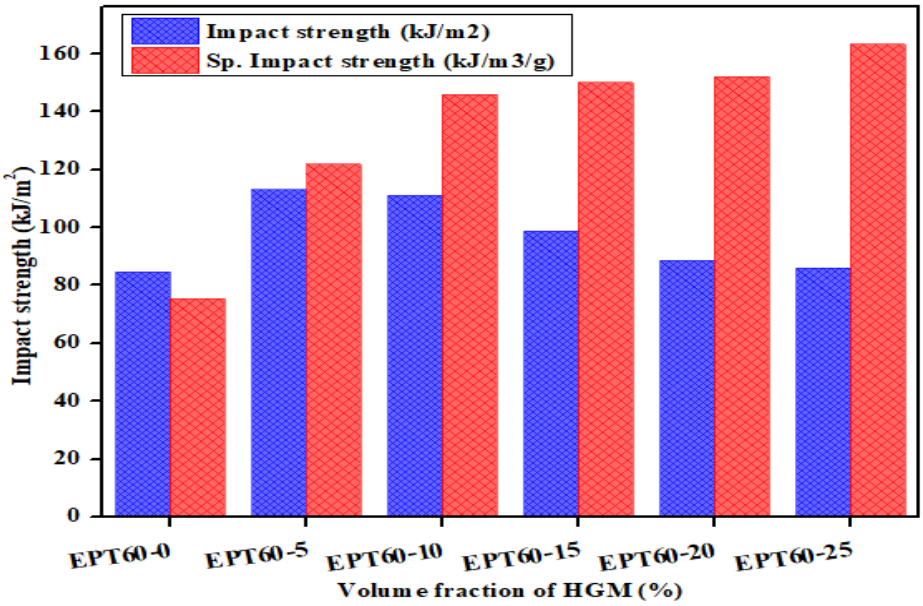

Figure 10.3: Impact strength and specific impact strength of SFC for EPT60-0, EPT60-5, EPT60-10, EPT60-15, EPT60-20 and EPT60-25

The failure surface of the fractured samples under the Charpy impact test (**appendix 13.4**) reveals a single crack failure feature generated from the tensile face of the specimen and was propagated towards the compression side.

Figure 10.4 (a -c) presents the SEM microscopic image of SFC with 5vol% and 25vol% of HGM filler and plain epoxy resin respectively under impact loading. The SFCs with the maximum and minimum impact energy are compared with the plain epoxy fractured surface. Figure 4(a) shows the fracture surface at 5vol% with HGM interface, deboned surface and matrix failure under impact test. Figure 10.4b reveals fractured surface at 25vol% HGM under impact loading showing fractured surfaces due to sudden failure leading to de-bonding of filler from the matrix. The fractured HGM can be seen to propagate the face of the EPT60-25 through Figure 4b, this can be said to be responsible for their reduced impact energy compared to other composites. The plain epoxy fracture surface is shown in Figure 4c with smooth surface structure which is responsible for their low impact resistance.

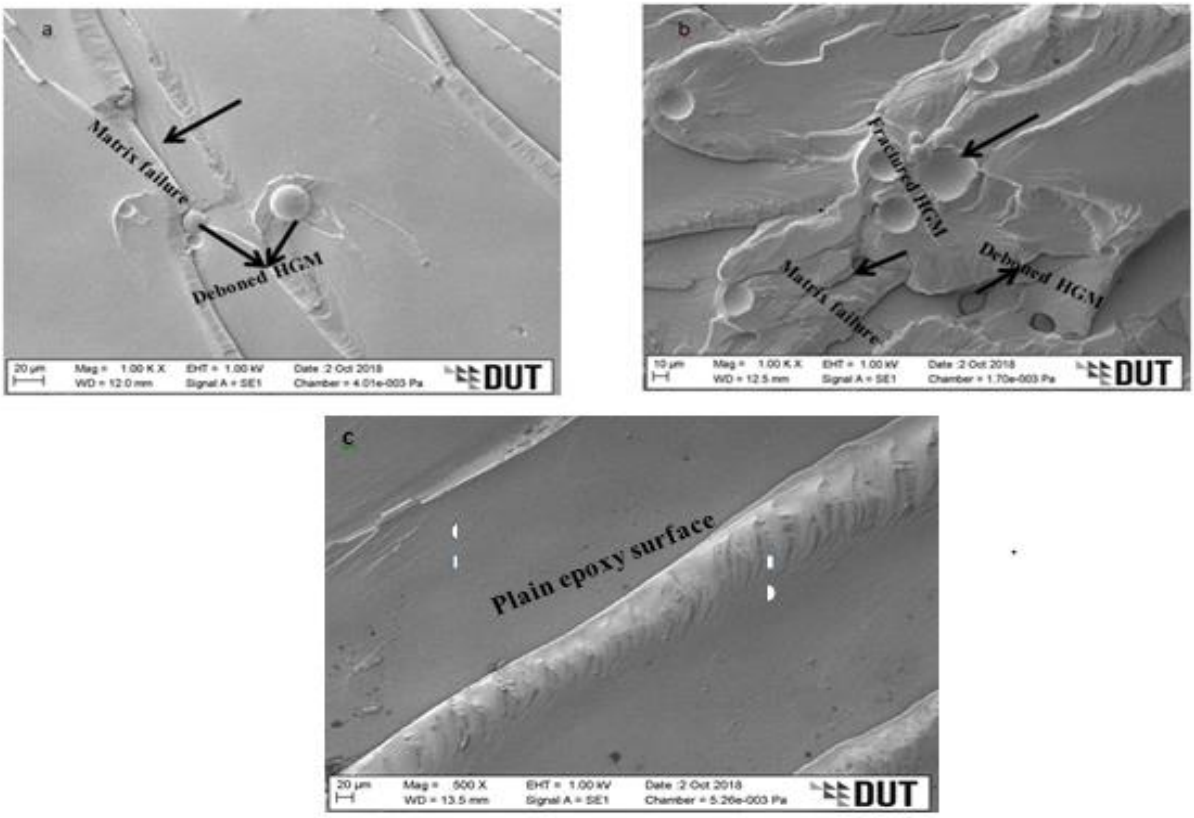

Figure 10.4 SEM images of impact SFC specimens at (a.) EPT60-5 with 5vol% HGM filler (b) EPT60-25 with 25vol%, HGM filler and (c) plain epoxy, showing the matrix failure and deboned microsphere.

10.5 Acoustic Properties of Sandwich Syntactic Foam Composites

The acoustic properties of the sandwich syntactic foam composites are presented in Table 10.9 and the mean values at Table 10.10. The sound pressure (Lp) was calculated from the sound level (P) measurement values. The sound level increased up to 61.58 dB at GG, about a 15% increase to the sound level at KG, 52.06 dB. The sound pressure of the sandwich composites does not show much appreciable difference in value for all the sequence. This is an indication that the four sequences, KK, GG, GK, and KG can be employable in the investigation of sound radiation vibration of a sandwich composite for accurate precision of sound pressure value (Hashimoto 2001).

Table 10.9: Acoustic properties of Sandwich Syntactic Foam Composites

Reading	Sound Level "P" (dB)				Sound Pressure "Lp" (dB)			
	KK	GG	GK	KG	KK	GG	GK	KG
1	60.1	56.2	49.6	49.3	129.58	128.99	127.86	127.91
2	53.9	57.2	49.8	46	129.56	129.15	127.26	127.95
3	56.4	63	57.4	51.4	128.63	129.99	128.22	129.18
4	58.6	64.6	54.8	57.8	129.03	130.20	129.24	128.77
5	60	66.9	56.8	55.8	129.36	130.51	128.93	129.09

Table 10.12 Mean values for Acoustic Properties of Sandwich Syntactic Foam Composites

Sandwich Composites	Mean Values	
	P (dB)	Lp (dB)
KK	57.80 ± 2.64	129.23 ± 0.40
GG	61.58 ± 4.68	129.77 ± 0.67
GK	53.68 ± 3.76	128.30 ± 0.80
KG	52.06 ± 4.79	128.58 ± 0.61

10.6 Conclusion:

In this chapter, the hardness, water absorption, buoyancy, impact, and acoustic properties of SFC and SSFC has been discussed. The hardness strength of SFC increased with respect to the neat epoxy for all the volume fraction of HGM with maximum of 18.2 % at EPT60-15. It was concluded that hybrid kenaf/glass fibers in GK and KG improved the strength of the sandwich composite by 41% and ~10% respectively compared to KK and GG sandwich composites.

Neat epoxy had the highest water absorption diffusion coefficient of 0.572% compared to the SFCs, and a ratio of $M_d/\sqrt{T_s}$ of 0.021 which was an indication that neat epoxy was more porous compared to the SFCs. KK sandwich composite was more porous than other orientations with diffusion coefficient of 3.784% and $M_d/\sqrt{T_s}$ of 0.1410 % because kenaf fiber was observed to

easily absorbed water when submerged. However, the combination of hybrid kenaf/glass fiber as reinforcement improved the water absorption capacity of sandwich syntactic foam composite.

Neat epoxy with buoyancy force of 0.0939N was the highest compared to the SFCs because of its porous nature as expressed in water absorption test. Thus, it required more force to float when submerged in water. Also, KK sandwich composite had the highest buoyancy force of 0.3296 N compared to other compositions reflecting from its porous nature observed in water absorption.

Impact strength of SFCs increased appreciably more than that of the neat epoxy for all the volume fractions up to 25.2 % but decreased with an increased volume fraction of HGM from 5vol% down to 25vol% of the SFCs.

Acoustic properties of the SSFC shows that the GG sound level (P), 61.58 dB is more than other orientations because of the nature of the glass fiber but there is no appreciable difference in the sound pressure (Lp) for all the sandwich orientations because of the closed gap range of their values. This is an indication that KK, GG, GK, and KG as sandwich composite can be applicable for acoustic vibration measurement for structural purposes.

CHAPTER 11

11.0 CONCLUSIONS AND RECOMMENDATIONS

11.1 Conclusions

The conclusions drawn based on each objective are presented below:

Considering the first objective, the T60 hollow glass microspheres (HGM) filler was used in its heterogeneous form and mixed with the matrix materials of epoxy resin and hardener to produce the syntactic foam composite (SFC). The HGM was varied into five (5) volume fractions of 5, 10, 15, 20, and 25 in the epoxy matrix to form the SFCs. Degassing processing method was employed for the fabrication of the SFCs to reduce the influence of void on the composite and thereby improve its strength significantly. The incorporation of the HGM into the epoxy matrix to develop the SFCs shows a better improvement in mechanical properties than the neat epoxy. This was determined by the mechanical (tensile and flexural), and the thermal (TGA, and DMA) properties. The tensile modulus and strength increased by 114% and 65% respectively, at EPT60-20 than EPT60-0. Also, flexural modulus and strength increased by 100% and 121% respectively, at EPT60-25 than EPT60-0. However, tensile, and flexural strain reduced by 56% at EPT60-25, and 32% at EPT60-15 respectively than EPt60-0. The TGA of SFC increased in degradation temperature at 5%. 20%, and 55% weight loss by 9%, 3.3%, and 2.4% respectively than the EPT60-0. The E', E'', and Tan δ increased by 9.2%, 2.1%, and 86% respectively at 30°C than EPT60-0.

Based on the second objective, following the fabrication of SFCs with the heterogeneous HGM filer, further investigation was made on the influence of different size variations of homogeneous HGM filler on the SFCs. This was actualized by separating the HGM into different particle sizes. The Retsch Magnetic Shaker (RMS) was used to separate the HGM filler into four different particle sizes of 20-24µm, 25-44µm, 45-49µm, and 50-60µm. Particle size distribution analysis (PSD) was further conducted on the varied sizes using Anton Paar PSA 1190 particle size analyzer. Each of the particle sizes was varied into five-volume fractions stated in objective one and mixed subsequently with epoxy matrix to fabricate the SFCs. The strength of the SFCs improved significantly and a positive increase in strength was noticed in the homogeneous SFCs over the heterogeneous SFCs fabricated. The improved strength was identified in their mechanical (tensile and flexural) and thermal (TGA and DMA) properties. The tensile modulus and strength increased up to 4% and 59% respectively than EPT60-0. The flexural modulus decreased while the flexural strength increased up to 66.4% than EPT60-0. SEM micrographs

show rough fractured surfaces, matrix porosity, and debonded HGM. The TGA degradation temperature reduced at 5% weight loss by 12% while at 20% and 55% weight loss, it increased by 4.5% and 2.7% respectively. The E' of SFC increased at 30°C, 50°C, and 60°C by 3.2%, 47%, and 96% respectively than EPT60-0. Increased in wall thickness "ω" increased E'' values and Tan δ increased at 60°C compared to the EPT60-0. Generally, the addition of HGM increased the thermal stability of SFCs.

Regarding objective three, the SFC fabricated was used as the core material for the sandwich syntactic foam composites (SSFC) and hybrid kenaf and glass fibers were used as the upper- and lower-layer face-sheets reinforcement. Hand lay-up method was used for the fabrication of the SSFC and thereafter vacuum bagged to remove excess matrix and reduce void fraction on the sandwich composite, thereby improving its strength. Four different orientations were employed in fabricating the SSFC, which are kenaf fiber – SFC core – kenaf fiber (KK), glass fiber – SFC core – glass fiber (GG), glass/kenaf fibers – SFC core – kenaf/glass fibers (GK), and kenaf/glass fibers – SFC core – glass/kenaf fibers. The strength of each SSFC material was determined by their mechanical (compression, tensile, flexural, and hardness) properties and discussed in objectives five and six. The SSFC tensile strength and modulus are highest at GG, 51MPa, and 2.48GPa with an increase of 67.7% and 42.7% more than KK respectively. Also. the flexural strength and modulus are highest at GK, 159.51MPa, and 7.16GPa with an increase of 74% and 61.7% more than KK, respectively. Moreover, compressive strength was highest at KG, 65.5 MPa with an increase of 42.7% more than the KK. For the shear strength, the maximum strength was at GG, 4.96MPa. It could be noted that in all the SSFC, the KK showed the lowest values due to the low ability of kenaf fibers to bear loads for a longer period during testing. However, it is worthy to note that KK can be significantly improved as reinforcement in sandwich composites when combined with glass fiber. The series model shows better comparison with the experimental results than the parallel and Hirsch's model. Generally, it can be observed that hybrid face-sheet can better perform as reinforcement in SSFC than using single plane individual face-sheet.

In objective four, the densities (measured and theoretical) of SFCs (both heterogeneous and homogeneous) HGM filler concentrations and the density of SSFC were investigated. The measured densities were calculated manually, while the theoretical density was determined by the rule of mixture and were more than the measured density. The difference was calculated in percentage as the void or porosity fraction values. The porosity of the SFCs and the SSFC was minimized because of the processing methods discussed in objectives 1-3. For the SFCs, at

5volume fraction of HGM, the heterogeneous density increased by 18% compared to the homogeneous SFCs, while at 10, 15, 20, and 25 volume fractions of HGM, the homogeneous SFCs increased in density more than the heterogeneous by 2.5%, 3.3%, 0.5%, and 3.6% respectively. Also, the density values for both heterogeneous SFCs and homogeneous SFCs decreased with increasing volume fraction of HGM filler. The wall thickness “ω” of the varied HGM increased with increasing size range while the aspect ratio “a” decreased with increasing size range. The particle size distribution volume at BB shows more uniformity with 32.01% than other size ranges. For the SSFC, the KK porosity value of 21.6% which is the highest compared to other compositions because it is less dense and more porous in terms of water absorption.

Finally, in objective five, the Barcol hardness test of heterogeneous SFCs increased up to 18.2% at a 15volume fraction of HGM more than the neat epoxy. The SSFC hardness value was highest at GK with a 41% increase than the KK with the lowest hardness. The water absorption capacity of SFCs improved more than the neat epoxy because of its high diffusion coefficient of 0.572% and the ratio of $M_{(d)}$ /$\sqrt{T_{(s)}}$ of 0.021%/$\sqrt{h}$. This shows that it is denser and absorbs more water making it require more force of buoyancy for stability on the water. The KK of SSFC also shows a more porous nature with high $M_{(d)}$ and more buoyancy force for floatation. Also, the impact strength of SFCs improved appreciably than the neat epoxy up to 25.2% but decrease with increasing volume fraction of HGM, this shows that a lower concentration of HGM filler can perform better impact resistance in structural application. Lastly, the acoustic resistance properties of SSFC have the highest sound level (P) at GG, but the sound pressure (Lp) does not show any significant difference in the sandwich composites. This implies that all the sandwich composites can be applicable for acoustic resistance in structural purposes.

11.2 Recommendations

Considering all the contributions to the body of knowledge in this study, there are still more future works to be done. Therefore, the following outlined areas can be investigated for further research works.

- The HGM used in this study is a single type varied into four size particle variations, further research can be done on the hybrid particle sizes of HGM to produce SFCs.
- This research work focused on the single SFC core and hybrid face-sheets. Future work should focus on the use of hybrid SFC core and hybrid faces-sheets for more practical application of the findings.
- Design experts can be employed for future work to validate the experimental results.
- This research work employed two existing models (Series and parallel model, and Hirsch's model) for the modeling evaluation of the sandwich composites. Future work should compare more models to validate the experimental results of the hybrid SFC sandwich composite.
- Data analysis can be employed for future work to validate the experimental results.

References.

Adel Shams, S. Z., Mauruzio Porfiri. 2017. Water Impact of Syntactic Foams. *Materials*, 10: 224-239.

Afolabi, O. A., Kanny, K. and Mohan, T. 2021a. Loading Effect of Hollow Glass Microsphere (HGM) and Foam Microstructure on the Specific Mechanical Properties and Water Absorption of Syntactic Foam Composite. *International Journal of Engineering Research in Africa*, 56: 34-50.

Afolabi, O. A., Kanny, K. and Mohan, T. P. 2021b. Processing of Hollow Glass Microspheres (HGM) filled Epoxy Syntactic Foam Composites with improved Structural Characteristics. *Science and Engineering of Composite Materials,* 28 (1): 116-127. Available: 10.1515/secm-2021-0011 (Accessed 18/08/2022).

Afolabi, O. A., Kanny, K. and Mohan, T. P. 2022. Analysis of Particle Variation Effect on Flexural Properties of Hollow Glass Microsphere Filled Epoxy Matrix Syntactic Foam Composites. *Polymers*, 14 (22).

Afolabi, O. A., Kanny, K. and Mohan, T. P. 2023. Investigation of mechanical characterization of hybrid sandwich composites with syntactic foam core for structural applications. *Composites and Advanced Materials*, 32.

Afolabi, O. A., Mohan, T. P. and Kanny, K. 2023. Processing of Low-Density HGM-Filled Epoxy–Syntactic Foam Composites with High Specific Properties for Marine Applications. *Materials (Basel)*, Article ID: 12.

Ahmadi H, L. G. H., and Hadavinia H. 2016. Investigation on Tensile Properties of Plain and Nanoclay Reinforced Syntactic Foams. *International Journal of Composite Materials*, 6 (1): 34-41.

Ahmadi, H. and Liaghat, G. 2019. Analytical and experimental investigation of high velocity impact on foam core sandwich panel. *Polymer Composites*, 40 (6): 2258-2272.

Akhtar, M. N., Sulong, A. B., Radzi, M. K. F., Ismail, N. F., Raza, M. R., Muhamad, N. and Khan, M. A. 2016. Influence of alkaline treatment and fiber loading on the physical and mechanical properties of kenaf/polypropylene composites for variety of applications. *Progress in Natural Science: Materials International*, 26 (6): 657-664.

Al-Hasani, E. S. 2007. Study of tensile strength and hardness property for epoxy reinforced with glass fiber layers. *Engineering and Technology Journal*, 25 (8): 988-997.

Alavudeen, A., Rajini, N., Karthikeyan, S., Thiruchitrambalam, M. and Venkateshwaren, N. 2015. Mechanical properties of banana/kenaf fiber-reinforced hybrid polyester composites: Effect of woven fabric and random orientation. *Materials & Design (1980-2015)*, 66: 246-257.

Alberto Corigliano, R. E., Papa Enrico 2000. Experimental Characterization and Numerical Simulations of a Syntactic Foam-Glass-fibre Composite Sandwich. *Composites Science and Technology*, 60: 2169-2180.

Altenaiji, M., Guan, Z., Cantwell, W., Zhao, Y. and Schleyer, G. 2014. Characterisation of aluminium matrix syntactic foams under drop weight impact. *Materials & Design*, 59: 296-302.

Amico, S. C., Angrizani, C. C. and Drummond, M. L. 2008. Influence of the Stacking Sequence on the Mechanical Properties of Glass/Sisal Hybrid Composites. *Journal of Reinforced Plastics and Composites*, 29 (2): 179-189.

Amran Alias., N. A. A. N., Mohd Radzai. 2007. The Behaviour of Square Sandwich Panel Part 1: Under Stactic Loading. *Journal Teknologi*, 47 (A): 1-18.

Anbuchezhiyan, G., Mohan, B., Sathianarayanan, D. and Muthuramalingam, T. 2017. Synthesis and characterization of hollow glass microspheres reinforced magnesium alloy matrix syntactic foam. *Journal of Alloys and Compounds*, 719: 125-132.

Arpitha, G. and Sanjay, M. 2014. Mechanical properties of epoxy based hybrid composites reinforced with sisal/SIC/glass fibers. Article ID.

Ashik, K. P. and Sharma, R. S. 2015. A Review on Mechanical Properties of Natural Fiber Reinforced Hybrid Polymer Composites. *Journal of Minerals and Materials Characterization and Engineering*, 03 (05): 420-426.

Ashraf, W., Ishak, M., Zuhri, M., Yidris, N., Yaacob, A. and Asyraf, M. 2019. Investigation of Different Facesheet Materials on Compression Properties of Honeycomb Sandwich Composite. *Semin. Enau Kebangs. Bahau, Negeri Sembilan, Malaysia*, Article ID: 129-132.

ASTM. 2012 *Standard terminology relating to plastics.* , PA 19428-2959. United States: 100 Barr Harbor Drive, PO Box C700, West Conshohocken, .

ASTM C271-94. Annual Book of ASTM Standards. 1994. Vol. 15.09. American Society fro Testing and Materials: West Consho-hocken, PA:

ASTM D 2583- 95 American Society for Testing and Materials. 2001. *Standard Test Method for Indentation Hardness of Rigid Plastics by Means of a Barcol Impressor,*, Article ID.

Awad, Z. K., Aravinthan, T. and Zhuge, Y. 2012. Experimental and numerical analysis of an innovative GFRP sandwich floor panel under point load. *Engineering Structures*, 41: 126-135.

Awais, H., Nawab, Y., Amjad, A., Anjang, A. and Zainol Abidin, M. S. 2020. Mechanical Properties of Hollow Glass Microspheres Filled Jute Woven Comingled Composites. *Key Engineering Materials*, 858: 41-46.

Aziz, M., Halim, Z. and Othman, M. 2018. Effect of Different Concentration of Sodium Hydroxide [NaOH] on Kenaf Sandwich Structures. In: Proceedings of *IOP Conference Series: Materials Science and Engineering*. IOP Publishing, 012080.

B. John, C. P. R. N., and K.N. Ninan. 2010. Effect of nanoclay on the mechanical, dynamic mechanical and thermal properties of cyanate ester syntactic foams. *Material Science and Engineering: A*, Vol 527: 5435-5443.

Badie, M., Mahdi, E. and Hamouda, A. 2011. An investigation into hybrid carbon/glass fiber reinforced epoxy composite automotive drive shaft. *Materials & Design*, 32 (3): 1485-1500.

Baedella Lorenzo, G. F. 2001. Elastic Design of Syntactic Foamed Sandwiches Obtained by Filling of Three-dimensional Sandwich-fabric Panels. *International Journal of Solid and Structures*, 38: 307-333.

Balıkoğlu, F., Demircioğlu, T. K., Yıldız, M., Arslan, N. and Ataş, A. 2018. Mechanical performance of marine sandwich composites subjected to flatwise compression and flexural loading: Effect of resin pins. *Journal of Sandwich Structures & Materials*, Article ID: 1099636218792671.

Bardella, L., Perini, G., Panteghini, A., Tessier, N., Gupta, N. and Porfiri, M. 2018. Failure of glass-microballoons/thermoset-matrix syntactic foams subject to hydrostatic loading. *European Journal of Mechanics-A/Solids*, 70: 58-74.

Bas, H. K., Jin, W. and Gupta, N. 2021. Chemical stability of hollow glass microspheres in cementitious syntactic foams. *Cement and Concrete Composites* 118: 103928.

Bess Ruff, M. 2022. How to Calculate Buoyancy. *https://www.wikihow.com*, Article ID.

Bharat, K., Abhishek, S. and Palanikumar, K. 2017. Mechanical Property Analysis on Sandwich Structured Hybrid Composite Made from Natural Fibre, Glass Fibre and Ceramic Fibre Wool Reinforced with Epoxy Resin. In: Proceedings of *IOP Conference Series: Materials Science and Engineering*. IOP Publishing, 012015.

Bharath Kumar, B. R., Doddamani, M., Zeltmann, S. E., Gupta, N., Ramesh, M. R. and Ramakrishna, S. 2016a. Processing of cenosphere/HDPE syntactic foams using an industrial scale polymer injection molding machine. *Materials & Design*, 92: 414-423.

Bharath Kumar, B. R., Doddamani, M., Zeltmann, S. E., Gupta, N., Uzma, Gurupadu, S. and Sailaja, R. R. N. 2016b. Effect of particle surface treatment and blending method on flexural properties of injection-molded cenosphere/HDPE syntactic foams. *Journal of Materials Science*, 51 (8): 3793-3805.

Bobkova, N. M., Trusova, E. E., Savchin, V. V., Sabadakha, E. N. and Pavlyukevich, Y. G. 2020. Obtaining Hollow Glass Microspheres and Their Use in the Production of Water-Dispersion Coatings. *Glass and Ceramics*, 76 (11-12): 401-405.

C297/C97M-04, A. 2004. *Standard test method for flatwise tensile strength of sandwich constructions.* , Article ID. USA:

C365/365M-11A, A. 2011. *Standard Test Method for Flatwise Compression Properties of Sandwich Cores.* , Article ID. Pennysylvania, USA: American Society for Testing and Materials.

Capela, C., Ferreira, J. A. M. and Costa, J. D. 2010. Viscoelastic Properties Assessment of Syntactic Foams by Dynamic Mechanical Analysis. *Materials Science Forum* 636-637: 280-286.

Carey, J. P. 2017. *Handbook of Advances in Braided Composite Materials Theory, Production, Testing and Applications*. Woodhead Publishing Series in Composites Science and Engineering.

Carrera Giovanni, C. M. R., Maria Paola Salio. 2013. GFRP Sandwich Composites : Calibration of a Numerical Model by Large Scale Tests. Article ID.

Castanie, B. B., J. J., Jaouen J.P., and Rivallant S. 2004. Combined Shear/Compression Structural Testing of Asymmetric Sandwich Structures. *Experimental Mechanics*, 44 (5): 461-472.

Chao Zhi., a. H. L. 2015. Compression properties of syntactic reinforced by with warp-knitted spacer fabric.pdf>. *Cellular Polymer*, 34 (4): 173-189.

Cheung, H.-y., Ho, M.-p., Lau, K.-t., Cardona, F. and Hui, D. 2009. Natural fibre-reinforced composites for bioengineering and environmental engineering applications. *Composites Part B: Engineering*, 40 (7): 655-663.

Colloca, M., Gupta, N. and Porfiri, M. 2013. Tensile properties of carbon nanofiber reinforced multiscale syntactic foams. *Composites Part B: Engineering*, 44 (1): 584-591.

Conta, S., Santoni, A. and Homb, A. 2020. Benchmarking the vibration velocity-based measurement methods to determine the radiated sound power from floor elements under impact excitation. *Applied Acoustics*, 169.

Cosse, R. L., Araújo, F. H., Pinto, F. A. N. C., de Carvalho, L. H., de Morais, A. C. L., Barbosa, R. and Alves, T. S. 2019a. Effects of the type of processing on thermal, morphological and acoustic properties of syntactic foams. *Composites Part B: Engineering*, 173.

Cosse, R. L., Morais, A. C. L. d., Silva, L. R. C. d., Carvalho, L. H. d., Reis Sobrinho, J. F. d., Barbosa, R. and Alves, T. S. 2019b. Preparation of Syntactic Foams made from Green Polyethylene and Glass Microspheres: Morphological and Mechanical Characterization. *Materials Research*, 22 (suppl 1).

Cunha, M. P., Grisa, A. M. C., Klein, J., Poletto, M. and Brandalise, R. N. 2018. Preparation and Characterization of Hollow Glass Microspheres- Reinforced Poly (acrylonitrile-co-butadiene-co-styrene) Composites. *Materials Research*, 21 (6).

Daniel, P., Velmurugan, R., Jayaganthan, R., Gupta, N. and Manzhirov, A. 2018. Analysis of syntactic foam – GFRP sandwich composites for flexural loads. Paper presented at the *Journal of Physics: Conf.* . 012064.

Daniel Paul., V. R., Jayaganthan., Gupta N.K., Manzhirov A.V 2018. Analysis of syntactic foam GFRP sandwich composite for flexural loads. *Journal of Physics: Conference Series*, 991.

Davies, G. A. O., Hitchings, D., Besant, T., Clarke, A. and Morgan, C. 2004. Compression after impact strength of composite sandwich panels. *Composite Structures*, 63 (1): 1-9.

Defence, D. o. 2002. *Department of Defense Handbook Composite*.

Dhar Malingam, S., Jumaat, F. A., Ng, L. F., Subramaniam, K. and Ab Ghani, A. F. 2018. Tensile and impact properties of cost-effective hybrid fiber metal laminate sandwich structures. *Advances in polymer technology*, 37 (7): 2385-2393.

Dimchev, M., Caeti, R. and Gupta, N. 2010. Effect of carbon nanofibers on tensile and compressive characteristics of hollow particle filled composites. *Materials & Design*, 31 (3): 1332-1337.

Ding, A., Wang, J., Ni, A. and Li, S. 2018. Hygroscopic ageing of nonstandard size sandwich composites with vinylester-based composite faces and PVC foam core. *Composite Structures*, 206: 194-201.

Doddamani, M., Kishore, Shunmugasamy, V. C., Gupta, N. and Vijayakumar, H. B. 2015. Compressive and flexural properties of functionally graded fly ash cenosphere-epoxy resin syntactic foams. *Polymer Composites*, 36 (4): 685-693.

Dong, C. and Davies, I. J. 2018. Effect of stacking sequence on the flexural properties of carbon and glass fibre-reinforced hybrid composites. *Advanced Composites and Hybrid Materials*, 1 (3): 530-540.

Dong, C., Ranaweera-Jayawardena, H. A. and Davies, I. J. 2012. Flexural properties of hybrid composites reinforced by S-2 glass and T700S carbon fibres. *Composites Part B: Engineering*, 43 (2): 573-581.

Elanchezhian, C., Vijaya Ramnath, B., Kaosik, R., Nellaiappan, T. K., Santhosh, K. K., Kavirajan, P. and Sughan, M. 2015. Evaluation of Mechanical Properties of Kenaf Based Hybrid Composite for Automotive Components Replacement. *ARPN Journal of Engineering and Applied Sciences*, 10: 1-6.

Elanchezhian, C. B., Vijaya Ramnath., Kaosik R., Nellaippan T.K., Santhosh Kumar K., Kavirajan P and Sughan M.U 2015. Evaluation of Mechanical Properties of Kernaf Based Hybrid Composite for Automotive Components Repalcement. *ARPN Journal ofEngineering and Applied Science*, 10 (13): 5518-5523.

Elsaid, A., Dawood, M., Seracino, R. and Bobko, C. 2011. Mechanical properties of kenaf fiber reinforced concrete. *Construction and Building Materials*, 25 (4): 1991-2001.

Erden, S. and Ho, K. 2017. Fiber reinforced composites. In: *Fiber Technology for Fiber-Reinforced Composites*. 51-79.

Erikson, R. 2002. Syntactic Metal: A survey of Current Technology. Paper presented at the *5th Aerospace Materials, Processes and Environmental Technology Conference*. Von Braun Centre, Huntsville, Alabama,

Fadhil, S. 2015. *Is the density of the same powder in macro or nano size, the same or different*.

Farid, S. 2015. *Is the density of the same powder in macro or nano size, the same or different*.

Faruk, O., Bledzki, A. K., Fink, H.-P. and Sain, M. 2012. Biocomposites reinforced with natural fibers: 2000–2010. *Progress in Polymer Science*, 37 (11): 1552-1596.

Fiore, V., Di Bella, G. and Valenza, A. 2015. The effect of alkaline treatment on mechanical properties of kenaf fibers and their epoxy composites. *Composites Part B: Engineering*, 68: 14-21.

Garay, A. C., Souza, J. A. and Amico, S. C. 2016. Evaluation of mechanical properties of sandwich structures with polyethylene terephthalate and polyvinyl chloride core. *Journal of Sandwich Structures & Materials*, 18 (2): 229-241.

Gay Daniel, H. S. V., Tsai Stephen W. 2003. *Composite Materials Design and Application*. Boca Raton London Ney York Washington, D.C: CRC Press.

Ghamsari, A. K., Zegeye, E. and Woldesenbet, E. 2013. Viscoelastic properties of syntactic foam reinforced with short sisal fibers. *Journal of Composite Materials*, 49 (1): 27-34.

Ghani, M. A. A., Salleh, Z., Hyie, K. M., Berhan, M. N., Taib, Y. M. D. and Bakri, M. A. I. 2012. Mechanical Properties of Kenaf/Fiberglass Polyester Hybrid Composite. *Procedia Engineering*, 41: 1654-1659.

Gogoi, R., Kumar, N., Mireja, S., Ravindranath, S. S., Manik, G. and Sinha, S. 2018. Effect of Hollow Glass Microspheres on the Morphology, Rheology and Crystallinity of Short Bamboo Fiber-Reinforced Hybrid Polypropylene Composite. *Jom*, 71 (2): 548-558.

Guo, G., Finkenstadt, V. L. and Nimmagadda, Y. 2019. Mechanical properties and water absorption behavior of injection-molded wood fiber/carbon fiber high-density polyethylene hybrid composites. *Advanced Composites and Hybrid Materials*, 2 (4): 690-700.

Gupta, G., Gupta, A., Dhanola, A. and Raturi, A. 2016. Mechanical behavior of glass fiber polyester hybrid composite filled with natural fillers. In: Proceedings of *IOP conference series: materials science and engineering*. IOP Publishing, 012091.

Gupta, N. 2003. Characterization of Syntactic Foams and their Sandwich Composites: Modeling and Experimental Approaches. Doctor of Philosophy, Louisiana State University and

Agricultural and Mechanical College.

Gupta, N. and Nagorny, R. 2006. Tensile properties of glass microballoon-epoxy resin syntactic foams. *Journal of applied polymer science*, 102 (2): 1254-1261.

Gupta, N., Priya, S., Islam, R. and Ricci, W. 2006. Characterization of Mechanical and Electrical Properties of Epoxy-Glass Microballoon Syntactic Composites. *Ferroelectrics*, 345 (1): 1-12.

Gupta N, W. E. 2003; . Hygrothermal studies on syntactic foams and compressive strength determination. *Compos Struct 2003;*, 61 (4): 311-320.

Gupta, N. and Woldesenbet, E. 2003. Hygrothermal studies on syntactic foams and compressive strength determination. *Composite Structures*, 61 (4): 311-320.

Gupta, N. and Woldesenbet, E. 2005. Characterization of flexural properties of syntactic foam core sandwich composites and effect of density variation. *Journal of composite materials*, 39 (24): 2197-2212.

Gupta, N., Woldesenbet, E. and Kishore. 2002. Compressive fracture features of syntactic foams-microscopic examination. *Journal of Materials Science* 37: 3199-3209.

Gupta, N., Woldesenbet, E. and Mensah, P. 2004. Compression properties of syntactic foams: effect of cenosphere radius ratio and specimen aspect ratio. *Composites Part A: Applied Science and Manufacturing*, 35 (1): 103-111.

Gupta, N., Ye, R. and Porfiri, M. 2010. Comparison of tensile and compressive characteristics of vinyl ester/glass microballoon syntactic foams. *Composites Part B: Engineering*, 41 (3): 236-245.

Gupta, N., Zeltmann, S. E., Shunmugasamy, V. C. and Pinisetty, D. 2013. Applications of Polymer Matrix Syntactic Foams. *Jom*, 66 (2): 245-254.

Gurit, A. Guide_to_Composites(1). Article ID.

Hamidon, M. H., Sultan, M. T. H., Ariffin, A. H. and Shah, A. U. M. 2019. Effects of fibre treatment on mechanical properties of kenaf fibre reinforced composites: a review. *Journal of Materials Research and Technology*, 8 (3): 3327-3337.

Hashimoto, N. 2001. Measurement of sound radiation efficiency by the discrete calculation method. *Applied Acoustics*, 62 (4): 429-446.

HILLI, A. H. M. A. 2006. Analytical and Experimental Study of High Velocity Impact on Compoiste Plates. Doctor of Philosophy, Nahran University.

Hong, Y. 2015. Processing of Expandible Thermoplastic/Thermoset Syntactic Foam. Doctor of Philosophy, Georgia Institute of Technology.

Housing, D. o. 1995. *A New Housing Policies and Strategy for South Africa*. South Africa:

Hu, G. and Yu, D. 2011. Tensile, thermal and dynamic mechanical properties of hollow polymer particle-filled epoxy syntactic foam. *Materials Science and Engineering: A*, 528 (15): 5177-5183.

Hu, Y., Li, W., An, X. and Fan, H. 2016. Fabrication and mechanical behaviors of corrugated lattice truss composite sandwich panels. *Composites Science and Technology*, 125: 114-122.

Huang, C., Huang, Z., Qin, Y., Ding, J. and Lv, X. 2016. Mechanical and dynamic mechanical properties of epoxy syntactic foams reinforced by short carbon fiber. *Polymer Composites*, 37 (7): 1960-1970.

Imran, M., Rahaman, A. and Pal, S. 2019. Effect of low concentration hollow glass microspheres on mechanical and thermomechanical properties of epoxy composites. *Polymer Composites*, 40 (9): 3493-3499.

Islam, M. M. and Kim, H. S. 2011. Sandwich composites made of syntactic foam core and paper skin: Manufacturing and mechanical behavior. *Journal of Sandwich Structures & Materials*, 14 (1): 111-127.

Jauhari, N., Mishra, R. and Thakur, H. 2015. Natural fibre reinforced composite laminates–a review. *Materials Today: Proceedings*, 2 (4-5): 2868-2877.

Jayavardhan, M. L., Bharath Kumar, B. R., Doddamani, M., Singh, A. K., Zeltmann, S. E. and Gupta, N. 2017. Development of glass microballoon/HDPE syntactic foams by compression molding. *Composites Part B: Engineering*, 130: 119-131.

Jefferson Andrew, J., Arumugam, V., Saravanakumar, K., Dhakal, H. N. and Santulli, C. 2015. Compression after impact strength of repaired GFRP composite laminates under repeated impact loading. *Composite Structures*, 133: 911-920.

Jiao, C., Zhao, L. and Chen, X. 2016. Preparation of modified hollow glass microspheres using Fe2O3 and its flame retardant properties in thermoplastic polyurethane. *Journal of Thermal Analysis and Calorimetry*, 127 (3): 2101-2112.

John, B., Nair, C. P. R., Devi, K. A. and Ninan, K. N. 2007. Effect of low-density filler on mechanical properties of syntactic foams of cyanate ester. *Journal of Materials Science*, 42 (14): 5398-5405.

John, B., Nair, C. P. R. and Ninan, K. N. 2010. Effect of nanoclay on the mechanical, dynamic mechanical and thermal properties of cyanate ester syntactic foams. *Materials Science and Engineering: A*, 527 (21-22): 5435-5443.

Kadhim Al-Sahlani, S. B., Daniel Lell, Thomas Fiedler. 2018. Effects of particle size on the microstructure and mechanical properties of expanded glass-metal syntactic foams. *Materials Science and Engineering: A*, 728: 80-87.

Kalaprasad, G. J. K., Thomas Seemon. 2014. Theoretical Modelling of Tensile Properties of Short Sisal Fiber Reinforced Low-density Polyethylene Composites. *Journal of materials science*, Article ID.

Kamal, K. K. 2017. *Composite Materials Processing Applications, Characterizations*. Heidelberger Platz 3, 14197 Berlin, Germany: Material Springer.com.

Kanny, K. and Mahfuz, H. 2005. Flexural fatigue characteristics of sandwich structures at different loading frequencies. *Composite Structures*, 67 (4): 403-410.

Karthikeyan C.S., S. S. a. K. 2000a. Comparison of Compressive Properties of Fiber-free and Fiber-bearing Syntacti Foam. *Journal of Reinforced Plastics and Composites*, 19 (09): 732-742.

Karthikeyan C.S., S. S. a. K. 2000b. Influence of chopped strand on flexural behaviour of syntactic foam.pdf>. *Polymer International*, 49: 158-162.

Karthikeyan, C. S., Sankaran, S. and Kishore. 2005. Flexural Behaviour of Fibre-Reinforced Syntactic Foams. *Macromolecular Materials and Engineering*, 290 (1): 60-65.

Karthikeyan, C. S., Sankaran, S. and Kishore. 2007. Investigation of bending modulus of fiber-reinforced syntactic foams for sandwich and structural applications. *Polymers for Advanced Technologies*, 18 (3): 254-256.

Katarzyna Greń*, P. S., Jan Chłopek. 2016. Characteristics of failure mechanism and shear strength of sandwich composite. *Composite Theory and Practice*, 16 (4): 256-259.

Khakbiz, M. 2015. *Is the density of the same powder in macro or nano size, the same or different?*

Khan, M. Z. R., Srivastava, S. K. and Gupta, M. K. 2020. A state-of-the-art review on particulate wood polymer composites: Processing, properties and applications. *Polymer Testing*, 89.

Kim Ho Sung ., M. A. K. 2001. Fracture and Impact Behaviour of Hollow Micro-sphere- Epoxy Resin Composites. *Composite Part A: Applied Science and Manufacturing*, 32: 1311-1317.

Kim, H. S. and Plubrai, P. 2004. Manufacturing and failure mechanisms of syntactic foam under compression. *Composites Part A: Applied Science and Manufacturing*, 35 (9): 1009-1015.

Kimiyoshi Naito, H. O. 2017. Tensile properties of nevel carbon/glass hybrid thermoplastic composite rod under static and fatigue loading. *Revista Material*, 22: 10.

Kumar, D. 2015. Study of Deformation and Erosion Behaviour of Epoxy-Glass Microballoon Based Syntactic Foam. Masters, National Institute of Technology Rourkela-769008, .

Kumar, N., Mireja, S., Khandelwal, V., Arun, B. and Manik, G. 2017. Light-weight high-strength hollow glass microspheres and bamboo fiber based hybrid polypropylene composite: A strength analysis and morphological study. *Composites Part B: Engineering*, 109: 277-285.

Kumar, P. K., Sekaran, H. J. A. and Pitchandi, K. 2017. Investigation on Mechanical Properties of Woven Alovera/Sisal/Kenaf Fibre and its Hybrid Composites. In.

Kumar, S. J. A. and Ahmed, K. S. 2013. Compression behavior and energy absorption capacity of stiffened syntactic foam core sandwich composites. *Journal of Reinforced Plastics and Composites*, 32 (18): 1370-1379.

Lam, C.-K., Cheung, H.-y., Lau, K.-t., Zhou, L.-m., Ho, M.-w. and Hui, D. 2005. Cluster size effect in hardness of nanoclay/epoxy composites. *Composites Part B: Engineering*, 36 (3): 263-269.

Lamanna, E., Gupta, N., Cappa, P., Strbik, O. M. and Cho, K. 2017. Evaluation of the dynamic properties of an aluminum syntactic foam core sandwich. *Journal of Alloys and Compounds*, 695: 2987-2994.

Le, V. S., Szczypinski, M. M., Hájková, P., Kovacic, V., Bakalova, T., Volesky, L., Hiep, L. C. and Louda, P. 2020. Mechanical properties of geopolymer foam at high temperature. *Science and Engineering of Composite Materials*, 27 (1): 129-138.

Lee, M. Y., Tan, J., Heng, J. Y. and Cheeseman, C. 2017. A Comparative Study of Production of Glass Microspheres by using Thermal Process. Paper presented at the *Materials Science and Engineering 205* The 2nd International Conference on Materials Engineering and Nanotechnology, 012022.

Li, B., Yuan, J., An, Z. and Zhang, J. 2011. Effect of microstructure and physical parameters of hollow glass microsphere on insulation performance. *Materials Letters*, 65 (12): 1992-1994.

Li, G. and Muthyala, V. 2008. Impact characterization of sandwich structures with an integrated orthogrid stiffened syntactic foam core. *Composites Science and Technology*, 68 (9): 2078-2084.

Li, J., Luo, X. and Lin, X. 2013. Preparation and characterization of hollow glass microsphere reinforced poly(butylene succinate) composites. *Materials & Design*, 46: 902-909.

Li, X., Zhu, M., Tang, X., Zhang, Q., Yang, X. and Sui, G. 2015. Influence of hollow carbon microspheres of micro and nano-scale on the physical and mechanical properties of epoxy syntactic foams. *RSC Advances*, 5 (63): 50919-50928.

Liang, J.-Z. 2005. Tensile and Flexural Properties of Hollow Glass Bead-filled ABS Composites. *Journal of Elastomers & Plastics*, 37 (4): 361-370.

Liang J.Z., a. L. R. K. Y. 2000. Effect of Filler Content and Surface Treatment on the Tensile Properties of Glass Bead filled Polypropylene Composites *Polymer International*, 49: 170-174.

Lin, T. C., Gupta, N. and Talalayev, A. 2009. Thermoanalytical characterization of epoxy matrix-glass microballoon syntactic foams. *Journal of Materials Science*, 44 (6): 1520-1527.

Lund, L. 2022. *Introduction to Chemistry*. Anoka-Ramsey Community College.

Mallick, P. K. 2007. *Fiber-Reinforced Composites Materials, Manufacturing, and Design*. Dekker Mechanical Engineering.

Manakari, V., Parande, G., Doddamani, M. and Gupta, M. 2017. Enhancing the Ignition, Hardness and Compressive Response of Magnesium by Reinforcing with Hollow Glass Microballoons. *Materials (Basel)*, 10 (9).

Masuelli, M. A. 2013. Introduction of fibre-reinforced polymers− Polymers and composites: Concepts, properties and processes. In: *Fiber Reinforced Polymers-The Technology Applied for Concrete Repair*. IntechOpen.

Menard, K. P. M. a. N. R. 2020. *Dynamic Mechanical Analysis*. Boca Ratton London New York: CRC press, Taylor and Francis Group.

Mohd, Y. H., Azriszul, M. A., Omar, M. F. M., Mohd, H. O., Mohd, R. M. Y. and Ng, C. H. 2017. The effect of alkali treatment under various conditions on physical properties of kenaf fiber. Paper presented at the *International Conference on Materials Physics and Mechanics* Journal of Physics: Conference Series, 012030.

Mohd Yussni Hashim, A. M. A., Omar Mohd Faizan Marwah, Mohd Hilmi Othman, Mohd Radzi Mohamed Yunus, Ng Chuan Huat. 2017. The effect of alkali treatment under various conditions on physical properties of kenaf fiber. Paper presented at the *International Conference on Materials Physics and Mechanics*. IOP Publishing,

Mortensen, A. 2007. *Concise Encyclopedia of Composite Materials,*. Amsterdam, The Netherlands: Elsevier Science.

Mutua, F. N., Lin, P., Koech, J. K. and Wang, Y. 2012. Surface Modification of Hollow Glass Microspheres. *Materials Sciences and Applications*, 03 (12): 856-860.

NALLUSAM, S. and Majumdar, G. 2016. Effect of Stacking Sequence and Hybridization on Mechanical Properties of Jute-Glass Fiber Composites. *International Journal of Performability Engineering*, 12 (3).

Nallusamy, S. and Majumdar, G. 2016. Effect of Stacking Sequence and Hybridization on Mechanical Properties of Jute-Glass Fiber Composites. *International Journal of Performability Engineering*, 12 (3): 229-239.

Nikhil Gupta and Kishore. 1999. On the Characterization of Syntactic Foam Core sandwich Composite for Compressive Properties. *Journal of Reinforced Plastics and Composites*, 19: 1347-1357.

Nikhil Gupta, D. P., Vasanth Chakravarthy Schunmugasamy. 2013. *Reinforced Polymer Matrix Syntactic Foams_ Effect of Nano and Micro-Scale Reinforcement*. New York Dordrecht London: SpringerBriefs in Materials.

Olusegun A. Afolabi, K. K., T.P Mohan. 2021. Processing of Hollow Glass Microspheres (HGM) filled Epoxy Syntactic Foam Composites with improved Structural Characteristics. *Science and Engineering of Composite Materials*, 28: 1-12.

Omar, M. Y., Xiang, C., Gupta, N., Strbik III, O. M. and Cho, K. 2015. Syntactic foam core metal matrix sandwich composite: compressive properties and strain rate effects. *Materials Science and Engineering: A*, 643: 156-168.

Orbulov, I. N. and Németh, Á. 2009. Global, depth sensing and dynamic hardness of metal matrix syntactic foams. *Periodica Polytechnica Mechanical Engineering*, 53 (2).

Orbulov, I. N., Németh, Á. and Dobránszky, J. 2010. Compressive strength and hardness of metal matrix syntactic foams. *Journal of Physics: Conference Series*, 240.

Ozkutlu, M., Dilek, C. and Bayram, G. 2018. Effects of hollow glass microsphere density and surface modification on the mechanical and thermal properties of poly(methyl methacrylate) syntactic foams. *Composite Structures*, 202: 545-550.

Paar, A. 2022. Particle Size Analysis by Laser Diffraction

Pandya, K. S., Veerraju, C. and Naik, N. K. 2011. Hybrid composites made of carbon and glass woven fabrics under quasi-static loading. *Materials & Design*, 32 (7): 4094-4099.

Pang, C., Shanks, R. A. and Daver, F. 2015. Characterization of kenaf fiber composites prepared with tributyl citrate plasticized cellulose acetate. *Composites Part A: Applied Science and Manufacturing*, 70: 52-58.

Park, S.-J., Jin, F.-L. and Lee, C. 2005. Preparation and physical properties of hollow glass microspheres-reinforced epoxy matrix resins. *Materials Science and Engineering: A*, 402 (1-2): 335-340.

Park, S.-J. and Seo, M.-K. 2011. Element and Processing. In: *Interface Science and Composites*. 431-499.

Patil, A. N., Kubade, P. R. and Kulkarni, H. B. 2020. *Effect of Composition on Impact and Flexural Properties of Hybrid Glass Microballoons/Fly Ash Cenosphere Filled Vinyl Ester Matrix Syntactic Foams*: IJRTE.

Paul, D. and Velmurugan, R. 2018. Analysis of the specific properties of glass microballoon-epoxy syntactic foams under tensile and flexural loads. *Materials Today: Proceedings*, 5 (9): 16956-16962.

Peroni, L., Scapin, M., Avalle, M., Weise, J. and Lehmhus, D. 2012. Dynamic mechanical behavior of syntactic iron foams with glass microspheres. *Materials Science and Engineering: A*, 552: 364-375.

Petrucci, R. and Torre, L. 2017. Filled Polymer Composites. In: *Modification of Polymer Properties*. 23-46.

Pickering, K. L., Efendy, M. G. A. and Le, T. M. 2016. A review of recent developments in natural fibre composites and their mechanical performance. *Composites Part A: Applied Science and Manufacturing*, 83: 98-112.

Poveda, R. L., Achar, S. and Gupta, N. 2014. Viscoelastic properties of carbon nanofiber reinforced multiscale syntactic foam. *Composites Part B: Engineering*, 58: 208-216.

Poveda, R. L., Dorogokupets, G. and Gupta, N. 2013. Carbon nanofiber reinforced syntactic foams: Degradation mechanism for long term moisture exposure and residual compressive properties. *Polymer Degradation and Stability*, 98 (10): 2041-2053.

Prabhakaran, S., Krishnaraj, V., Shankar, K., Senthilkumar, M. and Zitoune, R. 2019. Experimental investigation on impact, sound, and vibration response of natural-based composite sandwich made of flax and agglomerated cork. *Journal of Composite Materials*, Article ID: 0021998319871354.

Prof-Emeka-E-Obioha-Emeka-Obioha. 2019. *Addressing-Homelessness-Through-Public-works-Programmes-in-South-Africa.* South Africa: Walter Sisulu University.

Qiao, Y., Wang, X., Zhang, X. and Xing, Z. 2015. Thermal conductivity and compressive properties of hollow glass microsphere filled epoxy–matrix composites. *Journal of Reinforced Plastics and Composites*, 34 (17): 1413-1421.

Qiao, Y., Wang, X., Zhang, X. and Xing, Z. 2016. Investigation of flexural properties of hollow glass microsphere filled resin-matrix composites. *Pigment & Resin Technology*, 45 (6): 426-430.

Ramesh, M. 2016. Kenaf (Hibiscus cannabinus L.) fibre based bio-materials: A review on processing and properties. *Progress in Materials Science*, 78-79: 1-92.

Ramesh, M., Nijanthan, S. and Palanikumar, K. 2015. Processing and Mechanical Property Evaluation of Kenaf-Glass Fiber Reinforced Polymer Composites. *Applied Mechanics and Materials*, 766-767: 187-192.

Ramu, P., Jaya Kumar, C. V. and Palanikumar, K. 2019. Mechanical Characteristics and Terminological Behavior Study on Natural Fiber Nano reinforced Polymer Composite – A Review. *Materials Today: Proceedings*, 16: 1287-1296.

Rane, A. V., Kanny, K., Pandurangan, M. T. and Thomas, S. 2021. Density and Its Role in Predicting Interphase Characteristics and Dispersion in Poly(Lactic Acid) – Particulate Fillers Composites. *Materials Performance and Characterization*, 10 (1).

Ren, S., Guo, A., Dong, X., Tao, X., Xu, X., Zhang, J., Geng, H. and Liu, J. 2016. Preparation and characteristic of a temperature resistance buoyancy material through a gelcasting process. *Chemical Engineering Journal*, 288: 59-69.

Ren, S., Hu, X., Ren, H., Wang, M., Guo, A., Liu, J., Du, H. and Xian, L. 2017a. Development of a buoyancy material of hollow glass microspheres/SiO2 for high-temperature application. *Journal of Alloys and Compounds*, 721: 213-219.

Ren, S., Li, X., Zhang, X., Xu, X., Dong, X., Liu, J., Du, H. and Guo, A. 2017b. Mechanical properties and high-temperature resistance of the hollow glass microspheres/borosilicate glass composite with different particle size. *Journal of Alloys and Compounds*, 722: 321-329.

Report, F. H. C. 2014. *Housing Delivery - South Africa*. South Africa: Western Cape University.

Rizzi, E., Papa, E. and Corigliano, A. 2000. Mechanical behavior of a syntactic foam: experiments and modeling. *International Journal of Solids and Structures*, 37 (40): 5773-5794.

Saba, N., Jawaid, M., Alothman, O. Y., Inuwa, I. and Hassan, A. 2017. A review on potential development of flame retardant kenaf fibers reinforced polymer composites. *Polymers for Advanced Technologies*, 28 (4): 424-434.

Sadeghian, P., Hristozov, D. and Wroblewski, L. 2016. Flexural Behavior of Sandwich Panels made of FRP Composites: Synthetic and Natural Fibers. In: Proceedings of *CSCE Annual Conference 2016, London, ON, Canada*. CSCE,

Sadeghian, P., Hristozov, D. and Wroblewski, L. 2018. Experimental and analytical behavior of sandwich composite beams: Comparison of natural and synthetic materials. *Journal of Sandwich Structures & Materials*, 20 (3): 287-307.

Safari, H., Karevan, M. and Nahvi, H. 2018. Mechanical characterization of natural nano-structured zeolite/polyurethane filled 3D woven glass fiber composite sandwich panels. *Polymer Testing*, 67: 284-294.

Salleh, Z. 2017a. Characterisation of Syntactic Foams for Marine Applications. PhD, University of Southern Queensland.

Salleh, Z. 2017b. Characterisation of Syntactic Foams for Marine Applications. PhD, University of Southern Queensland.

Salleh, Z., Islam, M. M. and Epaarachchi, J. A. 2015. Compressive Behaviour of Low Density Polymeric Syntactic Foams. *Applied Mechanics and Materials*, 799-800: 135-139.

Salleh, Z., Mainul Islam, M., Ananda Epaarachchi, J. and Su, H. 2016. Mechanical properties of sandwich composite made of syntactic foam core and GFRP skins. *AIMS Materials Science*, 3 (4): 1704-1727.

Samivel, P. 2013. Mechanical Behaviour of Stacking Sequence in Kenaf and Banana fibre Reinforced-Polyester laminate. *IJSSIR*, 2.

Sankaran, S., Sekhar, K. R., Raju, G. and Kumar, M. N. J. 2006. Characterization of epoxy syntactic foams by dynamic mechanical analysis. *Journal of Materials Science*, 41 (13): 4041-4046.

Schutte, C. L. 1994. Environmental durability of glass-fiber composites. *Materials Science and Engineering,*, 13: 265-324.

Scudamore, R. J., Cantwell W.J. 2002. The Effect of Moisture and Loading Rate on the Interfacial Fracture Properties of Sandwich Structures. *Polymer Composites*, 23 (3): 406-417.

Sharba, M. J., Leman, Z., Sultan, M., Ishak, M. and Hanim, M. 2016a. Tensile and compressive properties of woven kenaf/glass sandwich hybrid composites. *International Journal of Polymer Science*, 2016.

Sharba, M. J., Leman, Z., Sultan, M. T. H., Ishak, M. R. and Hanim, M. A. A. 2016b. Tensile and Compressive Properties of Woven Kenaf/Glass Sandwich Hybrid Composites. *International Journal of Polymer Science*, 2016: 1-6.

Sharma, A., Choudhary, M., Agarwal, P., Joshi, S., Biswas, S. K. and Patnaik, A. 2021. Mechanical, Thermal and Thermomechanical Properties of Sponge Iron Slag filled Needle-Punched Nonwoven Jute Epoxy Hybrid Composites. *Fibers and Polymers*, 22 (4): 1082-1098.

Shen, S. Y., Masters, F. J., Upjohn, H. L. and Ferraro, C. C. 2013. Mechanical resistance properties of FRP/polyol–isocyanate foam sandwich panels. *Composite Structures*, 99: 419-432.

Shira, S. and Buller, C. 2015. Mixing and Dispersion of Hollow Glass Microsphere Products. Article ID: 241-271.

Shunmugasamy, V. C., Pinisetty, D. and Gupta, N. 2012. Viscoelastic properties of hollow glass particle filled vinyl ester matrix syntactic foams: effect of temperature and loading frequency. *Journal of Materials Science*, 48 (4): 1685-1701.

Shunmugasamy, V. C., Pinisetty, D. and Gupta, N. 2013. Viscoelastic properties of hollow glass particle filled vinyl ester matrix syntactic foams: effect of temperature and loading frequency. *Journal of Material and Science*, 48: 1685–1701.

Sreenivas, H. T., Krishnamurthy, N. and Arpitha, G. R. 2020. A comprehensive review on light weight kenaf fiber for automobiles. *International Journal of Lightweight Materials and Manufacture*, 3 (4): 328-337.

Stephen E Amos, B. Y. 2015. *Hollow Glass Microspheres for Plastics, Elastomers, and Adhesives Compounds*. United Kingdom: The Boulevard Langford Lane, Kidlington, Oxford, OX51GB, .

Steven Eric Zeltmann, B. C. a. N. G. 2018. Thermal expansion and dynamic mechanical analysis of epoxy matrix–borosilicate glass hollow particle syntactic foams. *Journal of Cellular Plastics*, 54 (3): 463-481.

Swain, P. T. R. a. B., S. 2014. Physical and Mechanical Behaviour of Al_2O_3 filled Jute Fibre Reinforced Composites. *International Journal of Current Engineering and Technology*, 2: 7.

Tagliavia, G., Porfiri, M. and Gupta, N. 2010. Analysis of flexural properties of hollow-particle filled composites. *Composites Part B: Engineering*, 41 (1): 86-93.

Tagliavia, G., Porfiri, M. and Gupta, N. 2012. Influence of moisture absorption on flexural properties of syntactic foams. *Composites Part B: Engineering*, 43 (2): 115-123.

Taherishargh, M., Sulong, M. A., Belova, I. V., Murch, G. E. and Fiedler, T. 2015. On the particle size effect in expanded perlite aluminium syntactic foam. *Materials & Design (1980-2015)*, 66: 294-303.

Tall, K., Krumme, A., Majak, J., Kers, J. and Aruniit, A. 2012. Influence of hollow glass microspheres on the mechanical and physical properties and cost of particle reinforced polymer composites. *Proceedings of the Estonian Academy of Sciences*, 61 (3).

Thiruchitrambalam, M., Alavudeen A, and Venkateshwaran N. 2012. Review on Kenaf Fiber Composite. *Reviews and Advanced Materials Science*, 32: 106-112.

Vitale, J. P., Francucci, G., Xiong, J. and Stocchi, A. 2017. Failure mode maps of natural and synthetic fiber reinforced composite sandwich panels. *Composites Part A: Applied Science and Manufacturing*, 94: 217-225.

Wada, O. 1992. Control of Fiber Form and Yarn and Fabric Structure. *Journal of the Textile Institute*, 83 (3): 322-347.

Wang, P., Zhong, S., Yan, K., Liao, B. and Zhang, J. 2022. Influence of a batch of hollow glass microspheres with different strength grades on the compression strength of syntactic foam. *Composites Science and Technology* 223 109442.

Watkins, I. G. and Prado, M. 2015. Mechanical Properties of Glass Microspheres. *Procedia Materials Science*, 8: 1057-1065.

Wi˛acek, J., Parafiniuk, P. and Stasiak, M. 2017. Effect of particle size ratio and contribution of particle size fractions on micromechanics of uniaxially compressed binary sphere mixtures. *Granular Matter* 19 (34).

Wiacek, J. and Stasiak, M. 2018. Effect of the particle size ratio on the structural properties of granular mixtures with discrete particle size distribution. *Granular Matter*

20 (31): 30-38.

Wiacek, J., Stasiak, M. and Kafashan, J. 2020. Structural and Micromechanical Properties of Ternary Granular Packings: Effect of Particle Size Ratio and Number Fraction of Particle Size Classes. *Materials (Basel)*, 13: 339.

Wouterson, E. M., Boey, F. Y. C., Hu, X. and Wong, S.-C. 2005. Specific properties and fracture toughness of syntactic foam: Effect of foam microstructures. *Composites Science and Technology*, 65 (11-12): 1840-1850.

Wouterson, E. M., Boey, F. Y. C., Hu, X. and Wong, S.-C. 2007. Effect of fiber reinforcement on the tensile, fracture and thermal properties of syntactic foam. *Polymer*, 48 (11): 3183-3191.

Wypych, G. 2010. *Handbook of fillers*. ChemTec Pub. Toronto.

Xu, Y., Zhu, J., Wu, Z., Cao, Y., Zhao, Y. and Zhang, W. 2018. A review on the design of laminated composite structures: constant and variable stiffness design and topology optimization. *Advanced Composites and Hybrid Materials*, 1 (3): 460-477.

Yalkin, H. E., Icten, B. M. and Alpyildiz, T. 2015. Enhanced mechanical performance of foam core sandwich composites with through the thickness reinforced core. *Composites Part B: Engineering*, 79: 383-391.

Yalkin, H. E., Icten, B. M. and Alpyildiz, T. 2017. Tensile and compressive performances of foam core sandwich composites with various core modifications. *Journal of Sandwich Structures & Materials*, 19 (1): 49-65.

Yaseer Omar, M., Xiang, C., Gupta, N., Strbik, O. M. and Cho, K. 2015. Syntactic foam core metal matrix sandwich composite: Compressive properties and strain rate effects. *Materials Science and Engineering: A*, 643: 156-168.

Yashwant S. Munde, R. B. I. 2015. Theoretical Modeling and Experimental Verication of Mechanical Properties of Natural Fiber Reinforced Thermoplastics. *Procedia Technology*, 19: 320-326.

Yiping Qiu , P. S. 1993. Micromechanical behaviour of kevlar-149/s-glass hybrid seven-fiber microcomposite: I. Tensile strength of the hybrid composite. *Composites Science and Technology*, 47: 289-301.

Young, M. P. 2007. Fracture Analysis of Glass Microsphere Filled Epoxy Resin Syntactic Foam. Masters ofEngineering, University College of New Soutj Wales.

Yousaf, Z., Smith, M., Potluri, P. and Parnell, W. 2020. Compression properties of polymeric syntactic foam composites under cyclic loading. *Composites Part B: Engineering*, 186: 107764.

Yu, M., Zhu, P. and Ma, Y. 2012. Experimental study and numerical prediction of tensile strength properties and failure modes of hollow spheres filled syntactic foams. *Computational Materials Science*, 63: 232-243.

Yung, K., Zhu, B., Yue, T. and Xie, C. 2009. Preparation and properties of hollow glass microsphere-filled epoxy-matrix composites. *Composites Science and Technology*, 69 (2): 260-264.

Zatta, A. M. A. 2009. *From Growing Kenaf to its Industrial Use*. Poznan:

Zhang, J., Chaisombat, K., He, S. and Wang, C. H. 2012. Hybrid composite laminates reinforced with glass/carbon woven fabrics for lightweight load bearing structures. *Materials & Design (1980-2015)*, 36: 75-80.

Zhia, C. and Long, H. 2015. Compressive Properties of Syntactic Foam Reinforced by Warp-knitted Spacer Fabric. *Cellular Polymers*, 34 (4): 173-188.

Zhu, B., Ma, J., Wang, J., Wu, J. and Peng, D. 2012. Thermal, dielectric and compressive properties of hollow glass microsphere filled epoxy-matrix composites. *Journal of Reinforced Plastics and Composites*, 31 (19): 1311-1326.

13. APPENDICES

Appendix 13.2:

Schematic representation for the four orientations of sandwich syntactic foam composites: (KK)-kenaf fiber-SFC-kenaf fiber; (GG)- glass fiber-SFC-glass fiber; (GK)-glass/kenaf fibers-SFC-kenaf/glass fibers and (KG)- kenaf/glass fibers-SFS-glass/kenaf fibers.

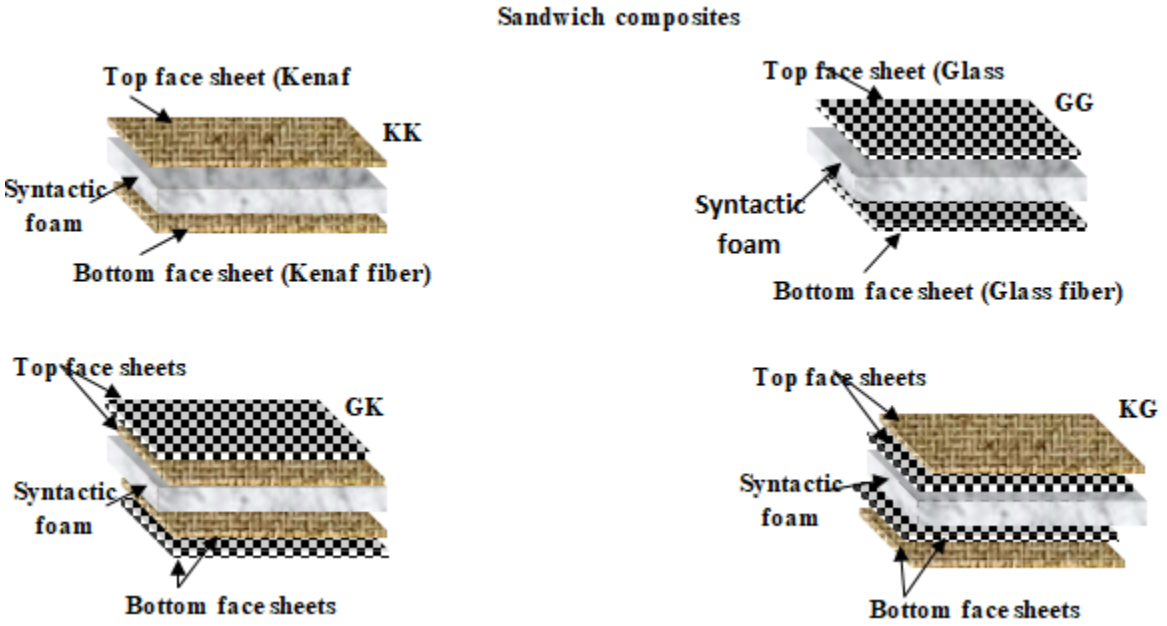

13.2 Appendix A- Published Articles

A-1: Processing of Syntactic Foam Composites by Degassing Method Published Article

Sci Eng Compos Mater 2021; 28:116–127 DE GRUYTER

Research Article

Olusegun A. Afolabi, Krishnan Kanny, and T. P Mohan*

Processing of Hollow Glass Microspheres (HGM) filled Epoxy Syntactic Foam Composites with improved Structural Characteristics

https://doi.org/10.1515/secm-2021-0011
Received Aug 10, 2020; accepted Nov 30, 2020

This HGM is embedded in a polymer material to form syntactic foam composites. The hollow particles may sometimes

Abstract:

The objective of this work is to improve the structural characteristics of hollow glass microsphere (HGM) filled epoxy syntactic foam composites with little voids content and improved HGM dispersion in the composite. A modified degassing technique has been introduced during the resin casting process of the HGM filled syntactic foam composites. The effect of HGM content volume fractions (5-25%) on the degassing techniques was examined. The syntactic foam composites were characterized by analyzing structural morphology using Scanning Electron Microscopy (SEM), Transmission Electron Microscopy (TEM), and density measurements (theoretical and experimental). Less than 5% void content has been achieved in this study. This resulted in improved tensile and dynamic mechanical properties (DMA).

Keywords:

Hollow glass microsphere (HGM), syntactic foam, tensile properties, degassing, fracture mechanism

A-2: Microstructure of Hollow Glass Microspheres towards the fabrication of Syntactic Foam Composites Published Article

International Journal of Engineering Research in Africa
ISSN: 1663-4144, Vol. 56, pp 34-50

Submitted: 2020-01-13
Revised: 2020-11-23
Accepted: 2021-01-19
Online: 2021-10-04

Loading Effect of Hollow Glass Microsphere (HGM) and Foam Microstructure on the Specific Mechanical Properties and Water Absorption of Syntactic Foam Composite

AFOLABI Olusegun Adigun[1,a*], KANNY, Krishnan[2,b], MOHAN Turup[3,c]

[1,2,3]Composite Research Group, Department of Mechanical Engineering, Durban University of Technology, Durban. 4000, South Africa.

[a]oluseguna@dut.ac.za, [b]kannyk@dut.ac.za, [c]mohanp@dut.ac.za

Abstract.

Epoxy syntactic foams (SF) filled with hollow glass microspheres (HGM) were prepared by a simple resin casting method and characterization in this study. The effect of varying the amount of HGM on the specific mechanical and water absorption properties of SF composites was investigated. Five different compositions of SF (SFT60-0.5 to SFT60-2.5) were compared with the neat epoxy matrix. The wall thickness of the microballoons differs because of their different percentile size distribution (10th, 50th, and 90th), which reflects in its density variation. The results show that the specific tensile and flexural strength increases with an increasing filler (HGM) content to about 68% and 71% respectively. The density of SF filled with HGM reduces with an increasing volume fraction of filler content. The water absorption capacity of the SF was also investigated as it relates to the HGM volume fraction variation. All the syntactic foam composition shows a better diffusion coefficient capacity (dd) than the neat epoxy resin. This makes it applicable in structural purposes and several marine application products such as Autonomous Ultimately Vehicle (AUV).

Keywords:

Hollow glass microsphere (HGM); syntactic foam; volume fraction; dynamic mechanical analysis; density; and thermal stability

A-3: Analysis of Particle Variation Effect on Flexural Properties of Hollow Glass Microsphere Filled Epoxy Matrix Syntactic Foam Composites

polymers

MDPI

Article

Analysis of Particle Variation Effect on Flexural Properties of Hollow Glass Microsphere Filled Epoxy Matrix Syntactic Foam Composites

Olusegun Adigun Afolabi *, Krishnan Kanny and Turup Pandurangan Mohan

Mechanical Engineering Department, Durban University of Technology, Durban 4000, South Africa
* Correspondence: arocrown4christ@gmail.com; Tel.: +27-625202472

Abstract:

Syntactic foam made from hollow glass microspheres (HGM) in an epoxy matrix has proven to be a good material with a strong structural strength. Understanding filler particle size variation is important in composite material formation, especially in syntactic foam, because of its numerous applications such as aerospace, marine, and structural purposes. In this present work, the effects of particle variation in different sizes (20–24 µm, 25–44 µm, 45–49 µm, and 50–60 µm) on the mechanical properties of the syntactic foam composites with a focus on flexural strength, modulus, and fracture surfaces are investigated. The particle sizes are varied into five volume fractions (5, 10, 15, 20, and 25 vol%). The results show that the highest flexural strength is 89 MPa at a 5 vol% fraction of 50–60 µm particle size variation with a 69% increase over the neat epoxy. This implies that the incorporation of HGM filler volume fraction and size variation has a strong effect on the flexural strength and bending modulus of syntactic foam. The highest particle size distribution is 31.02 at 25–44 µm. The storage modulus E' increased at 30 °C, 50 °C, and 60 °C by 3.2%, 47%, and 96%, respectively. The effects of wall thickness and aspect ratio on the size of the microstructure, the fracture surfaces, and the viscoelastic properties are determined and reported accordingly.

Keywords:

Syntactic foam; particle variation; flexural properties; volume fraction; scanning electron microscope.

A-4: **Investigation of Mechanical Characterization of Hybrid Sandwich Composites with Syntactic Foam Core for Structural Applications.**

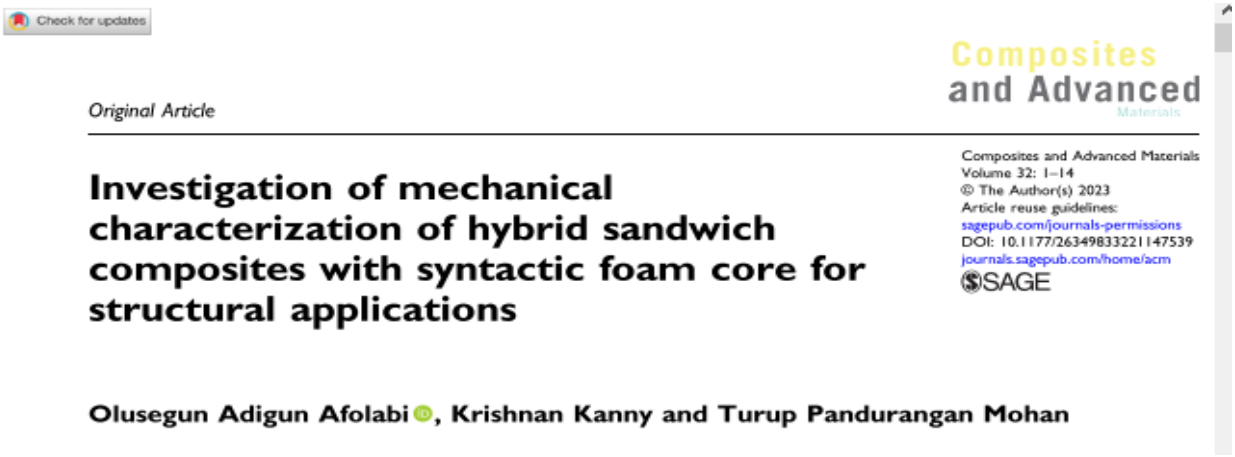

Check for updates

Original Article

Composites and Advanced Materials

Composites and Advanced Materials
Volume 32: 1–14
© The Author(s) 2023
Article reuse guidelines:
sagepub.com/journals-permissions
DOI: 10.1177/26349833221147539
journals.sagepub.com/home/acm
SAGE

Investigation of mechanical characterization of hybrid sandwich composites with syntactic foam core for structural applications

Olusegun Adigun Afolabi, Krishnan Kanny and Turup Pandurangan Mohan

Abstract.

In this work, mechanical performance on sandwich composites consisting of syntactic foam filled with hollow glass microsphere in an epoxy resin matrix as the core material and hybrid kenaf/glass fibers face-sheet based composites panel is studied. The main purpose of this work is to design a suitable lightweight composite panel material for structural application. Four different sequences of face-sheet reinforcement (e.g., kenaf-kenaf; glass-glass; glass-kenaf, and kenaf-glass) were adopted. In this study, the mechanical properties and failure modes are carefully investigated. The sandwich composites were characterized by compressive, tensile, and flexural properties. The results showed that compressive strength was highest at the "kenaf-glass" face-sheets, tensile strength was highest at "glass-glass" face-sheets, and flexural at "glass-glass" face-sheets with 52.1%, 67.6%, and 74.4% increase to "kenaf-kenaf" face-sheets, respectively. The tensile strength and modulus values with the specific strengths and modulus values showed that the mechanical properties of the sandwich composites can be influenced by hybridizing the face-sheet laminates of the composite. This shows that kenaf fiber has limited strength when used as reinforcement alone but gave an excellent performance when combined with glass fiber.

Keywords:

Sandwich composite, hybrid face-sheet, syntactic foam, density, mechanical performance

A-5: Processing of Low-Density HGM-Filled Epoxy-Syntactic Foam Composites with High Specific Properties for Marine Applications.

materials

MDPI

Article

Processing of Low-Density HGM-Filled Epoxy–Syntactic Foam Composites with High Specific Properties for Marine Applications

Olusegun Adigun Afolabi *, Turup Pandurangan Mohan and Krishnan Kanny

Composite Research Group, Department of Mechanical Engineering, Durban University of Technology, Durban 4000, South Africa
* Correspondence: arocrown4christ@gmail.com; Tel.: +27-625202472

Abstract:

A solution casting approach is used to create hollow glass microsphere (HGM)-filled epoxy–syntactic foam composites (e–SFCs) by varying the concentrations of HGM in epoxy according to different particle sizes. Density analysis is used to investigate the impact of concentration and particle size regularity on the microstructure of e-SFCs. It was observed that e–SFCs filled with an HGM of uniform particle sizes exhibit a reduction in density with increasing HGM concentration, whereas e-SFCs filled with heterogeneous sizes of HGM exhibit closeness in density values regardless of HGM concentration. The variation in e–SFC density can be related to HGM packing efficiency within e–SFCs in terms of concentration and particle size regularity. The particle size with lowest true density of 0.5529 g/cm3, experimental density of 0.949 g/cm3 and tensile strength of 55.74 MPa resulted in e-SFCs with highest specific properties of 100.81 (MPa·g/cm3), with a 35.1% increase from the lowest value of 74.64 (MPa·g/cm3) at a true density of 0.7286 g/cm3, experimental density of 0.928 g/cm3 and tensile strength of 54.38 MPa. The e–SFCs' theoretical density values were obtained. The variance in theoretical and experimental density values provides a thorough grasp of packing efficiency and inter-particle features.

Keywords:

Epoxy resin; hollow glass microspheres; syntactic foam composites; density; packing efficiency; specific tensile strength; wall thickness; aspect ratio.

Appendix 13.3: The fractured specimen under Charpy impact tests for SFC